The University of Nottingham
UNITED KINGDOM · CHINA · MALAYSIA
University of Nottingham
Faculty of Medicine and Health Sciences
School of Medicine
Division of Cancer Genetics & Stem Cell
Cancer Biology Unit

The regulation of chromatin and transmission of epigenetic information by the heterochromatin protein 1, binding protein 3 (HP1BP3) in normal and colorectal cancer cells

Shahad Kattan

(B.Sc., M.Sc.)

Under supervision of

Dr Abdolrahman S. Nateri

Thesis submitted to the University of Nottingham for the degree of

Doctor of Philosophy

November 2016

Declaration

I hereby declare that this thesis has been composed by me except where otherwise stated in the text. This thesis is based on research that was undertaken by me in Cancer Genetics & Stem Cell Group, under the supervision of Dr Abdolrahman Shams Nateri at the School of Medicine, Faculty of Medicine and Health Sciences, University of Nottingham, UK, and has not been submitted for any other degree previously.

Shahad Waddah Kattan

Student ID No: 4180968

Date 30/11/2016

Abstract

The heterochromatin-associated proteins are subject to several different post-translational modifications; hence, their level must be tightly controlled; otherwise as transcription factor co-repressor(s) complexes with these proteins, it may lead to stable silencing. An obvious mechanism to limit the expression time of a protein is to destroy it via the ubiquitin-proteasome system. FBXW7 (F-box and WD repeat domain–containing 7) is an E3-ligase targets transcriptional modulators and proto-oncogenes for degradation with crucial functions in cell-fate determination and tumorigenesis. In addition, most of current studies focused on epigenetic modifications that influence on the core histones within the euchromatin-heterochromatin transition, whereas the heterochromatin proteins and their partners' identity remained largely unclear.

Dr Nateri's lab have recently identified several proteins which are targeted by the *FBXW7* E3 ligase for the ubiquitin-mediated degradation. Among others, my study was focused on the role(s) of heterochromatin protein–binding protein 3 (HP1BP3) protein in epigenetic-reprogramming and its underlining mechanisms, including EMT and cell cycle progression, in normal and cancer cells. It's worth mentioning that apart from the single publication (Hayashihara et al., 2010a), the role of HP1BP3 was unknown when I began my project.

HP1BP3 modulates the entry/exit of nucleosomal-DNA through binding to HP1α protein. HP1α is enriched in the pericentromeric heterochromatin, and it has been reported that HP1α recruitment in this region depends on SUV39H1/2-mediated H3K9 trimethylation.

Widespread epigenomic alterations, occurs during cell differentiation, cell cycle progression and malignant transformation, but how epigenetic mechanisms contribute to the transcriptional reprogramming that accompanies EMT is still poorly understood. Furthermore, chromatin modulation events are important to control the cell-cycle-dependant gene expression during development and differentiation. Dysregulated expression of upstream cell-cycle regulators can affect DNA replication, repair, and/or division, leading to carcinogenic.

Herein, our data show that the loss of *FBXW7* mediated HP1BP3 induction alters heterochromatin states, through rescuing HP1α from its repressive function, impairing SUV39H1-mediated the methylation of histone H3 lysine 9 (H3K9me3), and stimulating the acetylation of H3K9 (H3K9ac) that lead to activation of epithelial-mesenchymal transition (EMT) pathway in Tiger skin fibroblast and HCT116 human colorectal cell lines. This induction of HP1BP3 upregulates the level of mesenchymal markers/regulators (N-cadherin, ZEB-1, Vimentin, and Snail1) in Tiger fibroblast cells while downregulating the epithelial marker (E-cadherin) and upregulating mesenchymal markers (ZEB-1, Vimentin, and Snail1) in HCT116 cells. In addition, upregulated HP1BP3 is an inducer of both G2/M cell cycle arrest

and G1 to S phase transition via downregulating Cyclin B1 and SUV39H1/H3K9me3 while upregulating H3K9ac mark, in human Tiger fibroblasts and HCT116 CRC cells.

Taken together, these findings point towards the important biological functions of HP1BP3 and its contribution in regulation of chromatin/EMT-associated genes expression which consequently can be implicated in the pathogenesis of different types of *FBXW7*-mutated cancer.

Acknowledgements

"All praise be to God, The Lord of The World"
Firstly, I thank Allah for giving me the opportunity and the ability to start and accomplish such an amazing project.

I would like to acknowledge my supervisor, Dr Abdolrahman Shams Nateri, for his continuous and constructive supervision during my thesis work and writing up. His generous guidance and engorgement enlightened me throughout my PhD studies at University of Nottingham. I am also very grateful for my kind co-supervisor, Dr Roya Babaei-Jadidi, for her valuable and constant assistance.

I wish to express my heartfelt and deepest thanks to my beloved family. Very warm thanks and respects to my parents (Waddah & Amnah) whose genuine love, continuous support and care, who believed in me, who are proud of me, who encouraged me to embrace and overcome all challenges. All of these were the source of inspiration for me. My sincerest gratitude goes to my sisters, brother (Dr Wafaa, Walaa, Ghidaa & Al-baraa), aunt (Abeer) and friends, for being in my life and giving me the hope and strength to finish my study and return home with pride. Endless gratitude to my great and wonderful Husband, Raed, for being such a patient lovely person lifting my spirits in difficult times.

I also would like to thank the Ministry of Higher Education of Saudi Arabia, the Saudi Cultural Bureau, and the University of Taibah for generously funding my PhD program at the University of Nottingham.

Finally, the friendship and teamwork spirit built in the lab affects eternity. Dear lab mates in Cancer Genetics and Stem Cells group (especially Sameerah & Federica), without you, this achievement would not have been possible. I love every one of you and I could not be more appreciative.

List of Figures

Figure 1-1: The 6 original hallmarks of cancer. 3
Figure 1-2: Emerging hallmarks and enabling characteristics. 3
Figure 1-3: The multi stages and steps of CRC that arises from the colorectal epithelium. 5
Figure 1-4: *APC*, *K-RAS*, *SMAD4* and *TP53* mutations correspond to a specific histological transformations during the CRC development starting with normal epithelium through adenomatous polyps to invasive carcinoma. 9
Figure 1-5: Schematic presentation of the SCF (Skp1-Cullin-. F-box) E3 ubiquitin-ligase complex. 12
Figure 1-6: Schematic representation of the human *FBXW7* gene organization and its isoforms 15
Figure 1-7: Schematic illustration of upstream regulatory components and downstream substrates/targets of FBXW7. 16
Figure 1-8: Schematic representation of sequential organization of findings representing the nature of CRC causes, whereas genetic alterations marked as blue and epigenetic ones as gold. 25
Figure 1-9: Organization of DNA in chromatin within the cell. 27
Figure 1-10: Schematic diagram of euchromatin and heterochromatin structure (A) and involvement of the posttranslational modifications (B).....29
Figure 1-11: Schematic clarification of chromosomal heterochromatin regions. 30
Figure 1-12: Posttranslational modifications of histone molecules. 34
Figure 1-13: Structural mapping and sequence identity of human and fission yeast heterochromatin protein 1 (HP1) proteins. 42
Figure 1-14: Amino acid alignment of HP1 proteins in humans (hHP1α, hHP1β, and hHP1γ). 43
Figure 1-15: Schematic presentation of HP1 structure and function.....46

Figure 1-16: The schematic presentation of human metaphase chromosome-associated proteins.....47
Figure 1-17: A schematic presentation of Co-transcriptional pri-miRNA processing.....60
Figure 1-18: Schematic presentation of the domain organization of human HP1BP3 protein.....63
Figure 2-1: Midiprep DNA isolation kit procedure from bacterial culture ... .80
Figure 2-2: DNA HyperLadder™ 1kb (Bioline) used for agarose gel electrophoresis.....84
Figure 2-3: DNA extraction from agarose gel using the illustra™ GFX™ PCR DNA and Gel Band Purification Kit.....85
Figure 2-4: Overlapping PCR for creating deletion mutation. 88
Figure 2-5: Overlapping PCR for creating point mutation [Threonine (ACC) and Serine (TCC) are substituted with Alanine (GCC)]. 88
Figure 2-6: The Neubauer haemocytometer slide grid layout. 93
Figure 2-7: The Precision Plus™ Dual Colour Protein ladder used for western blotting analysis. 100
Figure 3-1: Upregulation of endogenous HP1BP3 protein expression in human CRC cells lacking of *FBXW7*. 115
Figure 3-2: The pcDNA3.1 and pFLAG-GSK-3β plasmid maps, and validation analysis by restriction enzyme digestion. 117
Figure 3-3: Induced phosphorylation by GSK-3β caused significant reduction in the HP1BP3 protein level in human HCT116 cells. 120
Figure 3-4: GSK-3β inhibition could induces phosphorylation of HP1BP3 in HCT116 cells. 120
Figure 3-5: A schematic representation of the HP1BP3 protein and its predicted GSK-3β phosphorylation sites. 122
Figure 3-6: The peGFP-C2, peGFP-FLAG-MYC-FBXW7α, peGFP-FLAG-MYC-FBXW7γ, peGFP-HP1BP3-S (HP1BP3 short isoform), and peGFP-HP1BP3 (wild-type) plasmid maps and validation analysis by restriction enzyme digestion (A-F)...123

Figure 3-7: The Serine/ Threonine (T/S---T/SP) domains in HP1BP3 are responsible for its degradation by FBXW7. 125

Figure 3-8: Increasing number of co-localised HP1BP3 and HP1α nuclear foci in HCT116$^{FBXW7(-/-)}$ versus HCT116$^{FBXW7(+/+)}$ cells. 128

Figure 3-9: HP1BP3 upregulation caused by *FBXW7* loss could increases the co-localisation between HP1BP3 and HP1α nuclear foci in HCT116 cells..... 129

Figure 3-10: Inhibition and stimulation of endogenous H3K9me3 and H3K9ac, respectively, in human CRC cells lacking *FBXW7*. 133

Figure 3-11: The expression patterns and protein expression levels of endogenous HP1BP3 (red) and HP1α (green) proteins in MEF$^{Suv39h1/2(+/+)}$ and MEF$^{Suv39h1/2(-/-)}$ cell lines, examined by IF and western blotting analysis. 137

Figure 3-12: The distributions pattern of endogenous HP1BP3 and HP1α co-localisation is associated with Suv39h1/2 expression. 138

Figure 3-13: Depletion of *Suv39h1/2* abolishes endogenous H3K9me3 levels in MEF cells. 139

Figure 3-14: Endogenous H3K9me3 (green) and HP1α (red) co-localisation in (A) MEF$^{Suv39h1/2(+/+)}$ and (B) MEF$^{Suv39h1/2(-/-)}$ cell lines, examined by IF. 142

Figure 3-15: Analysis of average nuclear foci number of co-localised H3K9me3 and HP1α, not co-localised H3K9me3, and not co-localised HP1α for MEF$^{Suv39h1/2(+/+)}$ (A) and MEF$^{Suv39h1/2(-/-)}$ (B) cell lines..... 143

Figure 3-16: Western blotting analysis for endogenous HP1BP3, H3K9me3, and HP1α protein levels in DLD-1$^{FBXW7(+/+)}$ vs. DLD-1$^{FBXW7(-/-)}$ cells..... 145

Figure 3-17: FBXW7 regulation of chromatin via HP1BP3/HP1α/H3K9me3 complex in normal cells versus human colon cancer cells mutated for FBXW7. 147

Figure 4-1: The pLVX-eGFP and pLVX-eGFP-HP1BP3 plasmid maps, and validation analysis by restriction enzyme digestion. 153

Figure 4-2: Evaluation of GFP-HP1BP3 protein expression in both Tiger and HCT116 stable cell lines. 157
Figure 4-3: HP1PB3 decreases the expression/levels of SUV39H1/H3K9me3 while increases H3K9ac levels. 160
Figure 4-4: *HP1BP3* deletion leads to loss of H3K9ac in HCT116$^{FBXW7(-/-)}$. 163
Figure 4-5: HP1BP3 alters the morphology of human HCT116 CRC cells. 166
Figure 4-6: The over-expression of HP1BP3 upregulated N-cadherin, ZEB-1, Snail1, and Vimentin in Tiger cells, while upregulated ZEB-1, Vimentin, and Snail1, and inhibited E-cadherin protein expression in HCT116.....168
Figure 4-7: Loss of *HP1BP3* alters the morphology of human HCT116 CRC cells.....170
Figure 4-8: Loss of *HP1BP3* upregulates E-cadherin while downregulates ZEB-1, Vimentin, and Snail1 proteins expression in HCT116$^{FBXW7(-/-)}$. 171
Figure 4-9: FBXW7 mutation upregulates HP1BP3 expression, which leads to chromatin decondensation and consequently inappropriate activation of EMT-associated genes most likely in around 20 % of CRC cases.....177
Figure 5-1: HP1BP3 overexpression induced cell cycle progression in fibroblasts (Tiger cells). 184
Figure 5-2: HP1BP3 overexpression induced cell cycle progression in HCT116 cells.....186
Figure 5-3: HP1BP3 accumulation induced cell cycle progression in HCT116$^{FBXW7(-/-)}$ cells. 188
Figure 5-4: *HP1BP3* knockdown induced G0/G1 phase arrest in HCT116$^{FBXW7(-/-)}$ stably expressing shRNA-HP1BP3 cells..191
Figure 5-5: *HP1BP3* knockout arrested the cells at G0/G1-phase. 193
Figure 5-6: HP1BP3 overexpression increases G1 to S transitioned cells while arresting another population of cells at G2/M phase, in G1/S-arrested Tiger cells.....198

Figure 5-7: HP1BP3 upregulation delayed G2/M-G0/G1 transition but induced G0/G1 to S transition, in mitotic-arrested Tiger cells. 203

Figure 5-8: HP1BP3 modulate the expression/levels of SUV39H1/H3K9me3, H3K9ac and Cyclin B1 in specific cell cycle phases in Tiger cells.....207

Figure 5-9: FBXW7 loss arrests cells at G2/M phase and induces G1 to S transitioned cells, in HCT116 cells. 211

Figure 5-10: *HP1BP3* loss induces G2/M to G0/G1 transition and arrests cells at G0/G1 phase, in HCT116$^{FBXW7(-/-)}$ cells.....215

Figure 6-1: Schematic representations of each HP1BP3 recombinant construct sequence with amino acid start and stop numbers. 235

Figure 6-2: Validation of HP1BP3 recombinant constructs. 236

List of Tables

Table 2-1: DNA plasmids used in this thesis. 69
Table 2-2: Primary antibodies used for western blotting and immunostaining. Our laboratory has previously evaluated the specificity of many of these antibodies. 71
Table 2-3: Secondary antibodies used for western blotting and immunostaining. 72
Table 2-4: Standard PCR and overlapping PCR primers. 74
Table 2-5: Composition of common solutions and buffers used in this study. 77
Table 2-6: Restriction enzymes used in this study. 82
Table 2-7: Cycling parameters for standard PCR.....86
Table 2-8: Solutions for 8–15 % resolving gels for SDS-PAGE. 101
Table 2-9: Solutions for 5 % stacking gels for SDS-PAGE. 101

Abbreviations

Ago	Argonaute
APC	Adenomatous Polyposis Coli
BSA	Bovine Serum Albumin
C- Terminus	Carboxyl Terminus
CD	Chromodomain
CHD	Chromo Shadow Domain
CIMP	CpG Island Methylator Phenotype
CIN	Chromosomal Instability
CMV	Cytomegalovirus
CPD	CDC4-phospho-degron
CRC	Human Colorectal Cancer
CTD	C-Terminal Domain
DAPI	4',6-Diamidino-2-Phenylindole
DMEM	Dulbecco Modified Eagle Medium
DMSO	Dimethyl Sulfoxide
DNA	Deoxyribonucleic Acid
ECL	Enhanced Chemiluminescence
EDTA	Ethylenediaminetetraacetic Acid
EMT	Epithelial–Mesenchymal Transition
EtBr	Ethidium-Bromide
FACS	Fluorescence-Activated Cell Sorting
FAP	Familial Adenomatous Polyposis
FBS	Fetal Bovine Serum
FBXW7	F-Box and WD Repeat Domain–Containing 7
FRET	Fluorescence resonance energy transfer
GD	Globular Domain
GFP	Green Fluorescent Protein
GSK-3β	Glycogen Synthase Kinase-3β
H3K9ac	Acetylated Lysine 9 Residue of Histone 3
H3K9me3	Trimethylated Lysine 9 Residue of Histone H3
HAT	Histone Acetyltransferase

HCT116	Human Colon Carcinoma Cell Line
HDAC	Histone Deacetylase
HDM	Histone Demethylase
HMT	Histone Methyltransferase
HP1BP3	Heterochromatin Protein–Binding Protein 3
HP1BP3-S	Short Isoform of HP1BP3
HP1α	Heterochromatin Protein 1α
IF	Immunofluorescent
LB	Luria Broth
MCS	Multiple Cloning Site
MEF	Mouse Embryonic Fibroblast
MET	Mesenchymal–Epithelial Transition
MicroRNA	miRNA
MNase	Micrococcal Nuclease
mRNA	Messenger RNA
MSI	Microsatellite Instability
NLS	Nuclear Localisation Signal
NTD	N-Terminal Domain
N-Terminus	Amino Terminus
OD	Optical Density
PBS	Phosphate Buffered Saline
PCR	Polymerase Chain Reactions
PFA	Paraformaldehyde.
PI	Propidium Iodide
PTM	Post-Translational Modification
PVDF	Polyvinylidene Difluoride
qPCR	Quantitative PCR
RNA	Ribonucleic Acid
SCF-Complex	Skp1/Cullin1/F-Box
SDS	Sodium Dodecyl Sulphate
SDS-PAGE	Sodium Dodecyl Sulfate Polyacrylamide Gel Electrophoresis
shRNA	Small Hairpin RNA
siRNA	Small Interfering RNA

STDEV	Standard Deviation
SUV39H1/2	Suppressor of Variegation 3-9 Homolog 1/2
TBS-T	Tris-Buffered Saline-Tween 20
Tm	Melting Temperature
TMA	Tissue Microarray
UVIdoc	Ultraviolet Transilluminator Unit
WB	Western Blot

Table of Contents

CHAPTER 1 1

General Introduction 1

1.1 A brief introduction to human colorectal cancer (CRC) 2

1.1.1 The multistep nature of CRC development 4

1.1.2 Mutated genes in CRC 6

1.2 The ubiquitin-proteasome system (UPS) 10

1.3 FBXW7 12

1.3.1 FBXW7: Structure and function 12

1.3.2 FBXW7 gene and localisation of its protein isoforms 14

1.3.3 Upstream regulators and downstream substrates of FBXW7 15

1.3.4 FBXW7 mutations in human cancer, including CRC 18

1.3.5 The role of FBXW7 in invasion and metastasis 20

1.4 Epigenetic changes and EMT in CRC metastasis 22

1.5 Epigenetic alterations in CRC development 25

1.5.1 Chromatin structure 26

1.5.2 Chromatin states 28

1.5.3 Histone types 32

1.6 Histone post-translational modifications (PTMs) 33

1.6.1 Effects of acetylation and deacetylation in gene expression 35

1.6.2 Effects of methylation and demethylation on gene expression 37

1.7 Heterochromatin-associated protein structures and their roles in cancer development 39

1.7.1 HP1 39

1.7.1.1 The cross talk between HP1α and SUV39H1/2 44

1.7.2 Heterochromatin protein–binding protein 3 (HP1BP3) 46

1.7.2.1 HP1BP3 protein structure and localisation.....48
1.7.2.2 Functions of HP1BP3.....52
1.8 Rationale and objectives of this study.....61
CHAPTER 2.....66
General Materials & Methods.....66
2.1 Materials.....67
2.1.1 Cell lines.....67
2.1.2 DNA plasmids.....69
2.1.3 Antibodies.....70
2.1.4 Oligonucleotides.....73
2.2 General methods.....75
2.2.1 DNA preparation and manipulation.....75
2.2.1.1 Bacterial transformation.....75
2.2.1.2 Chemical preparation of bacterial competent cells....77
2.2.1.3 Isolation and purification of plasmid DNA, "Minipreps.....78
2.2.1.4 Isolation and purification of plasmid DNA, "Midipreps".....79
2.2.1.5 Quantification of DNA by spectrophotometry.....80
2.2.2 Gene cloning techniques.....82
2.2.2.1 Restriction enzyme digestion.....82
2.2.2.2 Agarose gel electrophoresis.....82
2.2.2.3 DNA extraction from agarose gel.....84
2.2.2.4 Polymerase chain reaction (PCR).....85
2.2.2.5 Overlapping PCR.....86
2.2.2.6 Ligation and bacterial transformation.....89
2.2.2.7 DNA nucleotide sequence verification by sequencin.....90
2.2.3 Cell culture.....91
2.2.3.1 Cell line maintenance and culture.....91

2.2.3.2 Cell counting 92
2.2.3.3 Freezing and thawing cells 94
2.2.3.4 Transient transfection 94
2.2.3.5 Generating of cell lines stably over-expressing GFP (control) and GFP-HP1BP3 proteins.....95
2.2.3.6 The drugs used for the biochemical analysis in cell culture 96
2.2.4 Immunoblotting and protein processing 97
2.2.4.1 Protein extraction and quantification.....97
2.2.4.2 Sodium dodecyl sulfate–polyacrylamide gel electrophoresis (SDS-PAGE) and western blotting 98
2.2.5 Immunofluorescence (IF) staining.....102
2.2.5.1 Cell preparation 102
2.2.5.2 Fixation and permeabilisation 102
2.2.5.3 Blocking and immunostaining.....103
2.2.5.4 Phalloidin staining 104
2.2.6 Cell cycle analysis 105
2.2.7 Double thymidine and thymidine-nocodazole synchronisatio.106
2.2.8 Statistical analysis.....107
CHAPTER 3.....108
Regulation of Chromatin by HP1BP3 via the HP1BP3/HP1α/H3K9me3 Complex in Fibroblast and CRC Cell Lines.....108
3.1 Brief introduction.....109
3.2 Results.....112
3.2.1 Loss of *FBXW7* leads to accumulation of HP1BP3 protein in human CRC HCT116 cells 112
3.2.1.1 GSK-3β–mediated HP1BP3 phosphorylation can contribute to HP1BP3 stabilisation 116

3.2.1.1.1 The consensus sequence for GSK-3β substrates in the HP1BP3 are functional.....121

3.2.2 HP1BP3 upregulation mediated by *FBXW7* loss could increases nuclear co-localisation of HP1BP3 and HP1α in HCT116 cells 126

3.2.3 Reduced level of tri-methylated H3K9 heterochromatin marker and increased level of acetylated H3K9 euchromatin marker in HCT116$^{FBXW7(-/-)}$ cells 130

3.2.4 Nuclear distribution of HP1α and HP1BP3 is associated with Suv39h1/2-mediated H3K9 trimethylation in mouse embryonic fibroblast (MEF) cells.....134

3.2.5 Further confirmation analyses of an endogenous HP1BP3/HP1α/H3K9me3 complex in CRC DLD-1 cells 144

3.3 Discussion 146

CHAPTER 4.....149

HP1BP3 Regulates Epithelial–Mesenchymal Transition (EMT), Epigenetically. 149

4.1 Brief introduction.....150

4.2 Results.....152

4.2.1 Generation and validation of stable fibroblast (Tiger) and HCT116 cell lines over-expressing GFP-HP1BP3.....152

4.2.2 Characterization and epigenetic/gene expression profiling of stable cell lines overexpressing HP1BP3 158

4.2.3 Deletion of HP1BP3 leads to SUV39H1/H3K9me3 induction and inhibition of H3K9ac in HCT116$^{FBXW7(-/-)}$ cells.....161

4.2.4 Regulation of epithelial-mesenchymal transition (EMT) through by HP1BP3 164

4.2.4.1 Ectopic HP1BP3 expression upregulates the level of mesenchymal markers in Tiger fibroblast cells while

downregulating the epithelial marker and upregulating mesenchymal markers in HCT116 cells.....164

4.2.4.2 Loss of *HP1BP3* in HCT116$^{FBXW7(-/-)}$ cells supresses EMT by inhibiting ZEB-1, Vimentin, and Snail1 and upregulating E-cadherin 169

4.3 Discussion.....172

CHAPTER 5.....178

The Epigenetic Regulation of Cell Cycle Progression by HP1BP3.....178

5.1 Brief introduction.....179

5.2 Results.....182

5.2.1 HP1BP3 expression is highly correlated with cell cycle progression in mammalian cells 182

5.2.1.1 Constitutive overexpression of HP1BP3 induces the S- and G2/M-phases transition in Tiger and HCT116 cells 182

5.2.1.2 Endogenous upregulation of HP1BP3 induces S and G2/M phases in HCT116 cells with *FBXW7* deletion 187

5.2.1.3 Inhibition and/or inactivation of HP1BP3 increases G0/G1 and consequently decreases HCT116$^{FBXW7(-/-)}$ cell populations in S phase 189

5.2.2 HP1BP3 epigenetically controls the transition between cell cycle phases in fibroblast (Tiger) cells.....194

5.2.2.1 The HP1BP3 overexpression arrests Tiger cells in G2/M while inducing G1 to S phases transition 194

5.2.2.2 Overexpression of HP1BP3 in Tiger cells, decreases SUV39H1/H3K9me3 during G1/S and G2/M, increases H3K9ac especially in G1 to S-transited cells and G2/M, and reduces Cyclin B1 during S and G2/M phase....204

5.2.3 Differential expression of HP1BP3 regulates-specific cell cycle phases in HCT116$^{FBXW7(-/-)}$ CRC cells.....208

5.2.3.1 Loss of *FBXW7*-mediated HP1BP3 upregulation may arrest HCT116 cells in G2/M while accelerating G1 to S transition.....208

5.2.3.2 Loss of *HP1BP3* in HCT116$^{FBXW7(-/-)}$ cells reversed the *FBXW7*-knockout associated cell cycle effects; induced the G2/M to G0/G1 transition, while arrested cells in G0/G1, and decreased cells in S phase.....212

5.3 Discussion.....216

CHAPTER 6.....219

General Discussion.....219

6.1 Introduction.....220

6.2 FBXW7 and SUV39H1 mediates chromatin dynamics in HP1BP3 dependant manners.....224

6.3 HP1BP3 induces EMT in HCT116 CRC cells.....226

6.4 HP1BP3 induces the transition from G1 to S phase and mitotic arrest.....228

6.5 Experimental limitations.....233

6.6 Conclusions and perspectives.....237

References.....239

Appendices.....266

Appendix 1: Site directed mutagenesis for creating point mutation [Threonine (ACC) and Serine (TCC) are substituted with Alanine (GCC)] in *HP1BP3*.....267

Appendix 2: Site directed mutagenesis for creating deletion mutations (D1 and D2) in *HP1BP3*.....269

CHAPTER 1

General Introduction

1.1 A brief introduction to human colorectal cancer (CRC)

Human colorectal cancer (CRC) is a serious and common cancer that arises sporadically in the majority of cases. CRC is the third and second most common cancer in men and women worldwide (Torre et al., 2015), respectively, and is the fourth cancer-related cause of death in the world (Labianca et al., 2013). Nevertheless, it is treatable if diagnosed in the early stages. About 75 % of CRC cases in the UK occur sporadically, whereas the remaining 25 % of cases is associated with hereditary conditions mainly caused by mutation of the adenomatous polyposis coli (*APC*) tumour suppressor gene, such as familial adenomatous polyposis (FAP) disorder (Young et al., 2011). The CRC incidence rate is statistically higher in high-income economy countries and in people older than 60 years rather than in low-income economy countries and in people younger than 40 years (Haggar and Boushey, 2009). Furthermore, the CRC mortality rate decreased by 26 % between 1975 and 2000 (Favoriti et al., 2016) due to the emphasis placed on early CRC screening and detection via improved screening tests [FOBT (faecal occult blood testing), sigmoidoscopy or colonoscopy]. However, the available treatment options often fail to cure CRC, leading to aggressive tumour with local recurrence and/or metastases and very poor survival (Stintzing, 2014).

CRC cells acquire features that render them cancerous. These features, termed the hallmarks of cancer (Hanahan and Weinberg, 2000, 2011), represent the fundamental basis of malignant transformation. The six original

key hallmarks of cancer and the recently described hallmarks and enabling characteristics are summarised in Figure 1-1 and Figure 1-2.

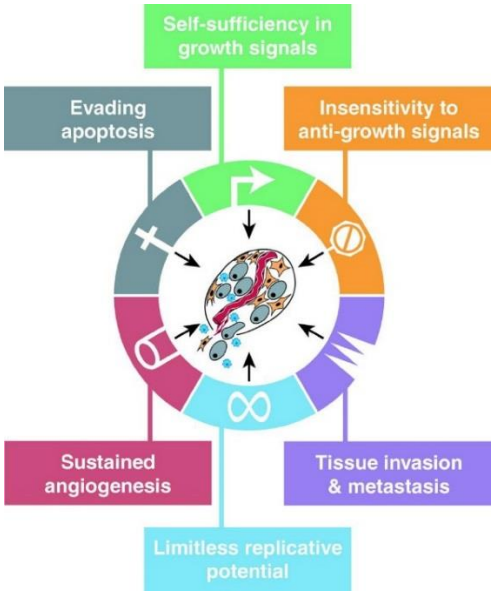


Figure 1-1: The 6 original hallmarks of cancer. Adapted from (Hanahan and Weinberg, 2000).

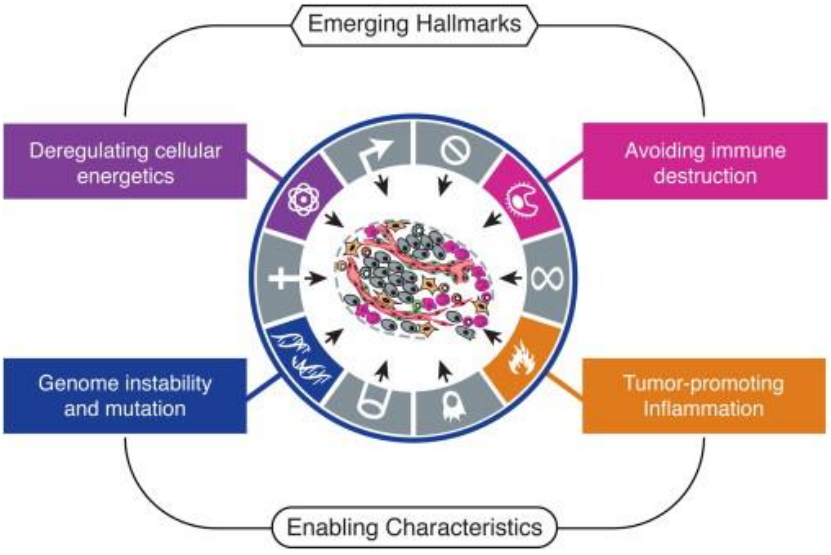


Figure 1-2: Emerging hallmarks and enabling characteristics. Adapted from (Hanahan and Weinberg, 2011).

1.1.1 The multistep nature of CRC development

The majority of CRC cases are adenocarcinomas, which arise from the colorectal epithelium (Figure 1-3). This disease is initiated by the formation of multiple adenomatous polyps, with various clinical manifestations and histological alterations, in the innermost lining of the large intestinal mucosa. These polyps grow and become cancerous after invading one or more layers of the intestine. Mucosa–adenoma–carcinoma transformation involves the accumulation of progressive mutations in oncogenes, tumour suppressor genes and DNA stability genes; a defective DNA repair system; and epigenetic alteration that contribute to the initiation and progression of CRC (Eliana et al., 2013; Grady and Carethers, 2008; Hermsen et al., 2002; Yamagishi et al., 2016; Young et al., 2011).

The estimated average progression time of adenomatous polyp to cancer is at least 10 years. During the transition of normal mucosa to polyp and subsequent cancer, it is believed that diverse mutations, dysregulation of the intracellular signalling pathways and epigenetic alterations reflect the different stages of tumour progression (Grady and Carethers, 2008; Vaiopoulos et al., 2014). Accordingly, understanding of the molecular mechanisms implicated in CRC tumorigenesis will lead to novel diagnostic and therapeutic targets against this disease.

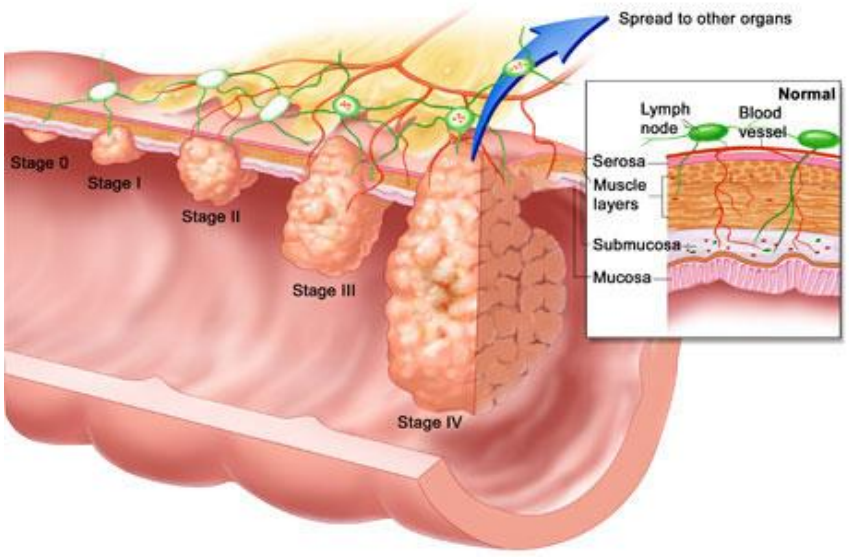


Figure 1-3: The multi stages and steps of CRC that arises from the colorectal epithelium. The process of mucosa-adenoma-carcinoma transformation requires accumulation of progressive, defective DNA repair system, and epigenetic alteration to contribute to CRC development. This cancer staged from stage 0 to IV. Stage 0 is the earliest stage and known as carcinoma in situ or intramucosal carcinoma. In stage I, the cancer has grown to the muscularis mucosa and extend to the submucosa and muscularis propria. In stage II, the cancer has grown to the outer layer (Serosa) and the wall of the colon/rectum, where its attached to or invades the adjacent tissues/organs. In stage III, the cancer has grown to 1-3 nearby lymph nodes. In stage IV, the cancer has invaded many lymph nodes and spread to adjacent organ/s (Greene et al., 2002). Adapted from (Schiessel and Metzger, 2012).

Cancer development is stimulated by the loss of genomic stability, including chromosomal instability (CIN), microsatellite instability (MSI) and the CpG island methylator phenotype (CIMP). About 85 % of sporadic CRC is associated with CIN (Dunican et al., 2002; Rao and Yamada, 2013). Although CIN is commonly found in colorectal carcinomas, its mechanism has not been clarified. CIN is characterised by extensive chromosome number imbalances (aneuploidy) and structural abnormalities that arise as a result of a variety of defects, including abnormal chromosomal segregation

and/or rearrangement, DNA damage response, telomere stability, replications, deletions, base substitutions or insertions (Dunican et al., 2002; Hermsen et al., 2002). Mutation of the *APC*, *KRAS* (Kirsten rat sarcoma viral oncogene homolog) and *TP53* genes has been linked to CIN in CRC progression (Hermsen et al., 2002). MSI account for approximately 15 % of all CRC cases and it is associated with inactivation of the DNA mismatch repair genes during DNA replication (Dunican et al., 2002; Rao and Yamada, 2013); CIMP is present in 70–80 % of sporadic MSI-positive CRC cases and in 15 % of global CRC cases, and is highly associated with *BRAF* mutation (Issa, 2004).

1.1.2 Mutated genes in CRC

In CRC, the *APC*, *TP53*, *KRAS*, *SMAD4*, transforming growth factor beta receptor 2 (*TGFBR2*), phosphatidylinositol-4,5-bisphosphate 3-kinase catalytic subunit α (*PIK3CA*), and F-box and WD repeat domain–containing 7 (*FBXW7*) are the major genes directly associated with carcinogenesis (Cai et al., 2014; Davis et al., 2014; Kuipers et al., 2015; Wood et al., 2007). The signalling pathways are deregulated as a consequence of the accumulation of such mutations, and influence many cellular processes (Cai et al., 2014; Issa, 2004; Kuipers et al., 2015; Wood et al., 2007) (Figure 1-4).

The earliest identifiable event in colorectal carcinogenesis is *APC* tumour suppressor gene mutation (Chung, 2000), which accounts for approximately 40–70 % of all CRC (Kuipers et al., 2015). *APC* is the key regulatory suppressor gene of the Wnt signalling pathway, and its biallelic mutation

results in high Wnt/β-catenin signalling activation, which in turn triggers tumour formation (Cai et al., 2014; Chung, 2000). However, additional mutations are required to develop CRC. The *KRAS* oncogene is mutated in about 40 % of patients with CRC (Kuipers et al., 2015). *KRAS* is involved in intracellular signal transduction, and its mutation results in activation of the downstream pro-proliferative signalling pathways [e.g. the mitogen-activated protein kinase (MAPK) pathway] (Cai et al., 2014; Kuipers et al., 2015). Consequently, *KRAS* mutations play a critical role in colorectal tumorigenesis. *PIK3CA* is another oncogene that is mutated in around 20 % of CRC cases. It is responsible for regulating the PI3K–AKT pathway, and its mutation disrupts several cellular processes, including proliferation, survival, apoptosis, migration and metabolism. *TP53* and *SMAD4* (tumour suppressor genes) mutations are detected in about 50 % and 25 % of CRC cases, respectively (Cai et al., 2014; Kuipers et al., 2015). *TP53* mutations actively promote tumour development by deregulating the expression of target genes involved in cell cycle progression, DNA repair and apoptosis (Kuipers et al., 2015). *SMAD4* mutations deregulate the TGFβ and bone morphogenetic protein (BMP) signalling pathways, which consequently affect several cell processes, such as proliferation, differentiation and embryogenesis, and apoptosis (Kuipers et al., 2015). In addition to *SMAD4*, *TGFBR2* is involved in regulating the TGFβ signalling pathway, and *TGFBR2* mutations are found in 20 % of CRC cases (Kuipers et al., 2015).

FBXW7 is a member of the S-phase kinase–associated protein 1 (SKP1)/Cullin1/F-box protein (SCF-complex) E3 ubiquitin ligase family that

controls diverse biological processes by targeting a wide range of proteins for degradation (Babaei-Jadidi et al., 2011a; Cheng and Li, 2012). *FBXW7* mutation may result in cancer development and progression, and is found in various human malignancies, including CRC, where *FBXW7* mutations occur in about 17–20 % of cases (Cheng and Li, 2012; Davis et al., 2014; Kuipers et al., 2015; Welcker and Clurman, 2008).

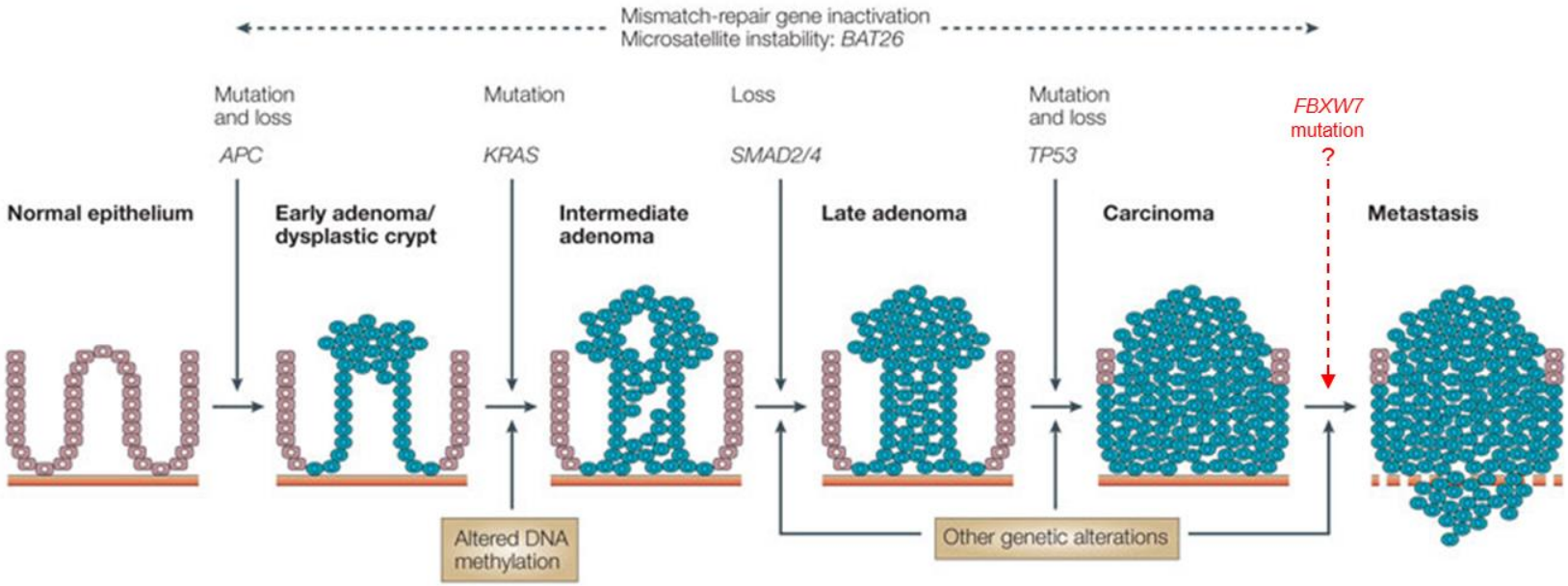


Figure 1-4: *APC, K-RAS, SMAD4* and *TP53* mutations correspond to a specific histological transformations during the CRC development starting with normal epithelium through adenomatous polyps to invasive carcinoma. Conversely, *FBXW7* position still remains unclear. Modified from (Davies et al., 2005).

1.2 The ubiquitin-proteasome system (UPS)

The UPS is a critical and highly regulated regulatory mechanism of protein homeostasis; UPS dysfunctions are present in many human pathological conditions, including many cancers (Skaar et al., 2013). The UPS comprises three major components: 1) three enzymatic components, 2) a highly-conserved ubiquitin molecule chain that is 76–amino acids long and which binds to lysine residues on substrate proteins or itself, thereby acting as a molecular label within the UPS, and 3) the 26S proteasome molecular machinery, composed of a 2.5-MDa multi-subunit complex that is responsible for degrading more than 80 % of proteins in eukaryotic cells (Lecker et al., 2006; Skaar et al., 2013). Ubiquitin molecule has seven lysine residues and each of which these residues can be further ubiquitinated to form poly-ubiquitin chain that determine the fate of the ubiquitinated protein (Ciechanover, 1998; Komander and Rape, 2012). This chain are linked via their lysine 48 (K48 linkage) and tags a protein for subsequent FBXW7-mediated degradation by the 26S proteasome (Chau et al., 1989; Davis et al., 2014; Finley, 2009; Huzil et al., 2007; Pickart, 1997; Popov et al., 2010). Three enzymatic components of the UPS, i.e. ubiquitin-activating protein (E1), ubiquitin-conjugating proteins (E2) and ubiquitin protein ligase (E3), are involved in marking a protein substrate with the ubiquitin molecule chain for degradation. First, E1 activates ubiquitin by forming a high-energy thioester bond between an ubiquitin molecule and itself in an ATP-dependent manner. Next, E2 obtains the activated ubiquitin via the conversion of one thioester to another (transthioesterification). Finally, E3 guides the transfer

of the activated ubiquitin from E2 to the targeted protein (Lecker et al., 2006; Skaar et al., 2013; Welcker and Clurman, 2008).

E3 plays a key role in this three-step chain reaction, as it recognises specific protein substrates and mediates ubiquitin transfer from E2 to the targeted substrate in a strictly controlled manner. Mammals have hundreds of E3 ligases, each with its own specificity for selecting precise host proteins (substrates) for proteasomal degradation (Wang et al., 2012b). There are two main types of E3 ubiquitin ligases: the HECT (Homologous to the E6-AP Carboxyl Terminus) domain ligase and the RING (Really Interesting New Gene) finger–containing ligase. Each comprises common subunits and one variable substrate recognition subunit; the protein targeted for degradation differs.

In mammals, there are six RING ubiquitin ligases, including the SKP1–CUL1–F-box protein (SCF) complex. SCF complex is one of the best understood group of the E3 ligases. The substrate recognition components of the SCF complex are called F-box proteins. Among 69 F-box proteins, β-TrCP, SKP2 and FBXW7 are key regulators of cellular processes that are linked to humans malignancies (Skaar et al., 2014; Welcker and Clurman, 2008). SKP2 targets negative cell cycle regulators (e.g. P27, P21, P57), whereas FBXW7 targets mostly positive cell cycle regulators (e.g. MYC, JUN, Cyclin E, Notch) (Babaei-Jadidi et al., 2011a; Bannister et al., 2001b; Bassermann et al., 2014; Cheng and Li, 2012; Skaar et al., 2014; Tu et al., 2012; Wang et al., 2012b).

1.3 FBXW7

1.3.1 FBXW7: Structure and function

SCF (Skp1–cullin/Rbx–F-box protein), is the best characterised E3 ligase complex among the E3 ubiquitin ligases (Figure 1-5). It consists of three core subunits (SKP1, Cullin1, RBX1) and a variable subunit that acts as a recruiter for specific substrates for ubiquitination by the SCF, known as the F-box protein.

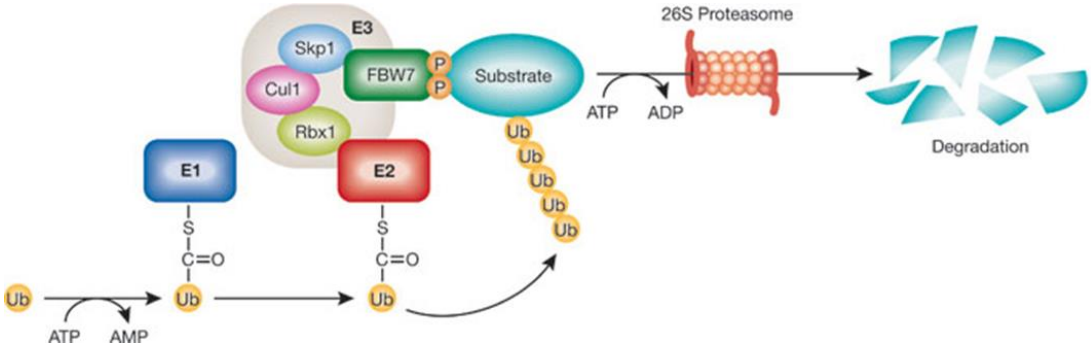


Figure 1-5: Schematic presentation of the SCF (Skp1-Cullin-. F-box) E3 ubiquitin-ligase complex. The poly-ubiquitin chain serves as the recognition marker that attached to the targeted protein, in order to be recognised and degraded by the 26S proteasome complex.

Among the 69 F-box proteins identified in humans, FBXW7 is one of the well characterized protein substrate of the SCF complex E3 ubiquitin ligase that confers substrate specificity. FBXW7 (also known as CDC4, FBW7, SeL10, Ago) is involved in a wide range of varied cellular functions such as

cell growth, cell cycle progression, differentiation and apoptosis, and metabolism (Skaar et al., 2013; Welcker and Clurman, 2008).

In humans and mice, the *FBXW7*/*Fbxw7* gene encodes a protein that encompasses three main domains: an F-box domain, a dimerisation domain (DD) and a stretch of eight WD40 repeats (Wang et al., 2012a). The F-box is a ~40–amino acid motif that selectively binds SKP1, whereas SKP1 links FBXW7 and the E2 conjugating enzyme. The DD plays a central role in FBXW7 dimerisation (Wang et al., 2012b). However, the importance of FBXW7 dimerisation in regulating ligase activity and substrate degradation is poorly understood. The WD40 repeats fold into a β-propeller structure containing multiple binding sites and that has distinct functions. The three conserved arginine residues of the WD40 repeats are required for binding FBXW7 with the downstream phosphorylated substrates. FBXW7 binding is mediated by a phosphorylated substrate motif, termed the CDC4 phosphodegron (CPD). In addition to hydrophobic residues, CPDs usually contain two critical phosphates (in the 0 and +4 positions) that are recognised by specific binding pockets within the WD40 repeats. The CPD motif is formed by (Leu)–X–pThr (or pSer)–Pro–Pro–X–pSer (or pThr, Glu or Asp) (X, any amino acid); in most cases, the central CPD threonine is phosphorylated by glycogen synthase kinase- 3β (GSK-3β) (Skaar et al., 2013; Wang et al., 2012b; Welcker and Clurman, 2008).

1.3.2 FBXW7 gene and localisation of its protein isoforms

In humans, the *FBXW7* gene (also known as *FBW7*, *HCDC4*, *SEL10* or *AGO*) spans >200 kb on locus 32q of chromosome 4 (Wang et al., 2012a). Alternative splicing of the gene generates three mRNA transcripts (FBXW7α, FBXW7β, FBXW7γ) (Figure 1-6), each of which has a unique 5′ exon joined to 10 shared exons that encode the F-box domain and WD40 repeats. Although the mRNAs and their distinct 5′ exons are responsible for determining their isoform-specific transcripts, this specificity of this characteristic is unclear. The difference at the first exon determines the different subcellular localisation and tissue distributions of the FBXW7 isoforms. A common NH2-terminal between all isoforms directs the specific localisation of each isoform. FBXW7α, FBXW7β and FBXW7γ are localised primarily in the nucleus, cytoplasm and nucleolar cellular compartments, respectively.

FBXW7α mRNA expression is much higher than that of *FBXW7β* or *FBXW7γ* and it can be detected in almost all human cell lines and primary cells (Wang et al., 2012b). It is also believed that FBXW7*α* performs most FBXW7 functions, although the roles of the other two isoforms have been determined (Bonetti et al., 2008; Davis et al., 2014; Ekholm-Reed et al., 2013; van Drogen et al., 2006). In mice, *Fbxw7β* is detected at high levels in the brain, whereas *Fbxw7α* is ubiquitously expressed and *Fbxw7γ* is restricted to the heart and skeletal muscles (Davis et al., 2014; Welcker and Clurman, 2008).

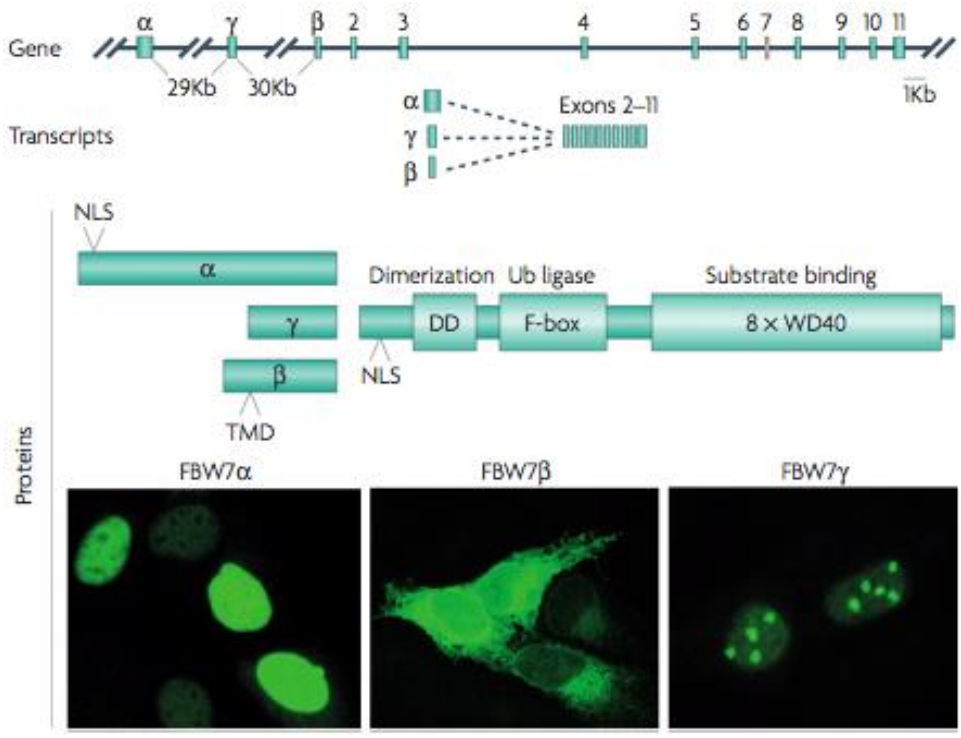


Figure 1-6: Schematic representation of the human *FBXW7* gene organization and its isoforms. *FBXW7* encodes for 3 isoforms which share 10 common exons. These isoforms differ in their first isoform-specific exon, but are functionally similar. Each isoform differs from the other in N-terminus domain that has signal to localize FBXW7α to the nucleus and FBXW7β to cytoplasmic membranes. FBXW7γ localizes to the nucleolus. Adapted from (Welcker and Clurman, 2008).

1.3.3 Upstream regulators and downstream substrates of FBXW7

SCF^{FBXW7} acts as a tumour suppressor because it negatively regulates several proteins, including oncoproteins (Cremona et al., 2016; Wang et al., 2012a; Wang et al., 2012b). Oncoproteins include Notch intracellular domain (NICD), c-Jun, mTOR, Cyclin E, c-Myc, HIF-1α, Aurora A, DEK, KLF5 and Mcl-1 among several other substrates (Figure 1-7). These substrates are involved in important biological processes such as cell cycle regulation, cell

proliferation, differentiation, survival, invasion, apoptosis and metastasis (Cremona et al., 2016; Wang et al., 2012b).

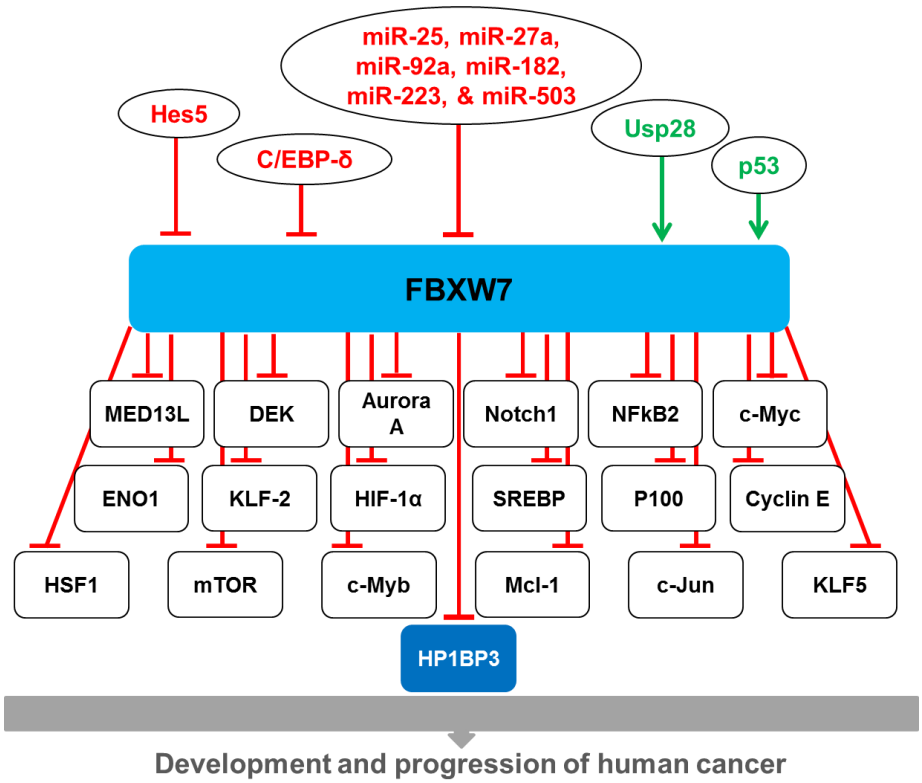


Figure 1-7: Schematic illustration of upstream regulatory components and downstream substrates/targets of FBXW7. The expression of FBXW7 is controlled by several pathways at post-transcriptional level (microRNAs), at transcriptional level (e.g. p53, C/EBP-δ and Hes5), and post-translational level (Usp28). FBXW7 targets several specific substrates for degradation including: Mediator complex subunit13-like (MED13L, a transcriptional coactivator for most RNA polymerase II-transcribed genes) (Davis et al., 2013b), DEK (proto-oncogene) (Babaei-Jadidi et al., 2011a), Aurora A (a cell cycle-regulated kinase) (Finkin et al., 2008), Notch1 (a single-pass transmembrane receptor protein) (Bannister et al., 2001b), Nuclear factor kappa B subunit 2 (NFkB2, a central activator of genes involved in inflammation and immune function) (Fukushima et al., 2012), c-Myc (an oncogenic transcription factor) (Yada et al., 2004), Enolase1 (ENO1, a glycolytic enzyme and an oncogenic protein) (Zhan et al., 2015), Kruppel-like factor 2 (KLF2, a regulator of endothelial function) (Wang et al., 2013c), Hypoxia inducible factor-1α (HIF-1α, a transcriptional regulator of the response to hypoxia) (Flügel et al., 2012), Sterol regulatory element-binding proteins (SREBP, a transcription factor and regulator of lipid homeostasis) (Sundqvist et al., 2005), P100 (transcriptional co-activator) (Busino et al., 2012), Cyclin E (a cell cycle regulator) (Ye et al., 2004), Heat-shock factor 1

(HSF1) (Kourtis et al., 2015), Mammalian target of rapamycin (mTOR, a serine/threonine kinase) (Mao et al., 2008), c-Myb (a proto-oncogenic transcription factor) (Kitagawa et al., 2009), Myeloid cell leukemia-1 (Mcl-1, an anti-apoptotic protein) (Inuzuka et al., 2011), c-Jun (a proto-oncogene) (Nateri et al., 2004), KLF5 (Krüppel-like factor, a zinc-finger transcription factor) (Bialkowska et al., 2014), and Heterochromatin Protein 1 Binding Protein 3 (HP1BP3) (Abuzinadeh et al., unpublished).

FBXW7 activity is controlled at different levels. It can be transcriptionally regulated by TP53, C/EBP-δ and HES5. Hence, the transcription factor P53 is known as the guardian of the genome; one of its important roles is positively regulating *FBXW7* expression by binding to exon 1 of the *FBXW7* gene (Kimura et al., 2003). On the contrary, Balamurugan and colleagues reported direct inhibition of *FBXW7α* by C/EBP-δ, which is involved in controlling cell differentiation, proliferation and metabolism (Balamurugan et al., 2013). The transcriptional repressor *HES5* down-regulates *FBXW7* through a positive feedback loop, leading to the accumulation of Notch protein and additionally increasing *HES5* expression (Notch target gene) (Sancho et al., 2013).

FBXW7 can also be regulated at protein level. USP28, a ubiquitin-specific protease, counteracts FBXW7 activity and stabilises c-Myc via interaction with FBXW7α or FBXW7γ (Xu et al., 2016). Furthermore, USP28 antagonises the ubiquitination of FBXW7 or its substrates, stabilising them (Xu et al., 2016). Therefore, USP28 plays a dual role, acting as both oncogenic protein and tumour suppressor depending on the tissue type involved (Xu et al., 2016).

MicroRNAs (miRNAs) are small non-coding RNAs that bind mRNA through sequence complementarities and negatively regulate the post-transcriptional expression of target genes, consequently inhibiting translation initiation and/or inducing target mRNA destruction (He and Hannon, 2004). Several miRNAs, including miR-25, miR-27a, miR-92a, miR-182, miR-223 and miR-503 (Figure 1-7), markedly down-regulate *FBXW7* expression (Wu and Pfeffer, 2016). MiRNAs function as oncogenes or tumour suppressors in the development of human tumours and affect cancer progression and prognosis (Cao et al., 2016). MiRNA expression is up-regulated in various cancers. For example, miR-27a up-regulation stabilises and elevates levels of FBXW7 substrates such as Notch1, c-Jun, Cyclin E and c-Myc, leading to enhanced proliferation of paediatric B cell acute lymphoblastic leukaemia cells, lung cancer cells and colon cancer cells (Wu and Pfeffer, 2016). MiR-223 and FBXW7 were up-regulated and down-regulated, respectively, in oesophageal squamous cell carcinoma, T cell acute lymphoblastic leukaemia (T-ALL) and gastric cancer (Cao et al., 2016).

1.3.4 FBXW7 mutations in human cancer, including CRC

FBXW7 mutation inhibits the degradation of the FBXW7 downstream substrates, leading to overexpression of the oncoprotein substrates, which consequently stimulate tumour development. Therefore, FBXW7 plays an important role in cell proliferation and tumorigenesis, where *FBXW7* mutation has been observed in various tumour types (Wang et al., 2012a; Xu et al., 2016).

FBXW7 mutations frequently occur on a single allele; in most cases, the mutations do not inactivate the encoded protein. Missense mutation is the most common *FBXW7* mutation compared to other genetic mutations; however, there is a wide spectrum of *FBXW7* mutations (deletion, missense, nonsense) in CRC (Davis et al., 2014). Frequently, the arginine residues (commonly, Arg479 and Arg482 in human and mouse, respectively) within the WD40 repeats that come into contact with the central phosphothreonine/serine of CPDs for substrate binding are substituted with (Davis et al., 2013a; Davis et al., 2011; Davis et al., 2014). Statistical analysis has shown that *FBXW7* mutations are present in about 6 % of all primary human tumours (Akhoondi et al., 2007). Also, high *FBXW7* mutation rates have been identified in CRC (17–20 %), gastric cancer (6 %), T-ALL (31 %), cholangiocarcinomas (35 %) and endometrial carcinoma (9 %) (Akhoondi et al., 2007; Kuipers et al., 2015; Welcker and Clurman, 2008). Tsunematsu and colleagues reported that *Fbxw7*-deficient mouse embryos die *in utero* as a result of vascular development abnormalities (Tsunematsu et al., 2004). Onoyama and colleagues reported that mice with liver-specific null mutations of *Fbxw7* have increased liver stem cell differentiation from the hepatocyte lineage to cholangiocytes, and increased cell proliferation (Onoyama et al, 2011). The same group had also previously reported that, in mice, conditional *Fbxw7* knockout in T cell or murine hematopoietic stem cells (HSCs) resulted in thymic lymphoma as a result of the induced proliferation (King et al., 2013; Onoyama et al., 2007). Additionally, *FBXW7* expression was significantly down-regulated in 80 % of human glioblastoma biopsies (Hagedorn et al., 2007). Conditional *Fbxw7* knockout in mouse

brain resulted in neonatal death due to Notch accumulation and consequent brain development abnormalities (Matsumoto et al., 2011).

Dr Nateri's laboratory and others have investigated the role of *Fbxw7* in mouse gut, and showed in a mouse model that *Fbxw7* plays an important role in maintaining intestinal homeostasis and induces adenoma development by controlling the proliferative activity of the stem cell compartment (Babaei-Jadidi et al., 2011a; Davis et al., 2013a; Sancho et al., 2010). In human colorectal carcinoma cell lines, *FBXW7*(-/-) alleles exhibited CIN and manifestations of nuclear abnormalities, such as micronuclei with elongated nuclei, due to Cyclin E accumulation (Rajagopalan et al., 2004; Wang et al., 2012b). In addition, conditional intestine-specific knockout mice lacking *Fbxw7* alleles showed increased cell proliferation and decreased cell differentiation as a result of intestinal epithelial cell accumulation of Notch and c-Jun. Nevertheless, *Fbxw7*-depleted mice had tumour-promoting activity at 9–10 months of age. Apc^{Min} or *Tp53* mutation combined with *Fbxw7* mutation resulted in invasive and metastatic CRC in mice (Babaei-Jadidi et al., 2011a; Grim et al., 2012; Onoyama et al., 2007; Sancho et al., 2010).

1.3.5 The role of FBXW7 in invasion and metastasis

More recent studies have implicated *FBXW7* in cancer invasion and metastasis. Heat shock factor 1 (HSF1) stabilisation upon FBXW7 down-regulation enhances the metastatic behaviour of melanoma cells (Kourtis et al., 2015). FBXW7 down-regulation activates the Notch1 pathway, which

subsequently enhances hepatocellular carcinoma cell migration and invasion (Wang et al., 2013c).

Epithelial–mesenchymal transition (EMT) promotes cell migration and invasion and correlates with poor prognosis. Generally, EMT occurs during embryonic development. Nevertheless, it also occurs in normal and pathological events, such as wound healing, organ fibrosis and tumour development. EMT is considered a major driver of cancer progression, where polarised and tightly bound epithelial cells are converted into invasive and migrating mesenchymal cells (Lamouille et al., 2014). EMT activation in adult epithelia suppresses cell adhesion molecules (E-cadherin, zona occludens 1 [ZO-1], cytokeratin) and upregulates mesenchymal markers (Vimentin, N-cadherin) and regulators (Snail1, ZEB-1). Interestingly, *FBXW7* loss was associated with the development of resistance to doxorubicin (anti-cancer drug) in hepatocellular carcinoma cells, leading to enhanced invasion capability via induction of EMT (Yu et al., 2014). EMT activation induced by FBXW7 loss significantly increased the metastatic potential of cholangiocarcinoma cells (Yang et al., 2015).

1.4 Epigenetic changes and EMT in CRC metastasis

Many studies have reported extensive gene expression reprogramming, which is mediated by epigenetic alteration during EMT, in CRC development. DNA hypomethylation and promoter region hypermethylation are associated with cancer initiation and progression. Anomalous methylation patterns have been detected in patients with CRC. For example, hypermethylation events at the CpG islands of *TP53* act equivalently to coding region mutations or deletions and influence the activity of specific signalling pathways, which in turn contributes to CRC metastasis (Kim et al., 2010; Vaiopoulos et al., 2014). *APC* and *E-cadherin* (*CDH1*) also undergo CpG island promoter hypermethylation, which mediates their inactivation in CRC and correlates with metastatic CRC (Vaiopoulos et al., 2014).

Specific chromatin remodelling complexes such as histone demethylation/methylation and deacetylation/acetylation are involved in regulating gene expression during EMT. The dysregulation of these complexes causes dramatic changes in the expression patterns of the EMT-related genes, leading to enhanced CRC cell invasive and metastatic capabilities. An *in vitro* study on a human colon carcinoma cell line (HCT116) lacking H2A.X reported increased expression of *SNAIL2*, *SLUG*, *ZEB1* and *Vimentin* (*VIM*) (key mesenchymal genes), and decreased expression of the *CDH1* epithelial gene (Weyemi et al., 2016). The same study reported the accumulation of histone H3 lysine 9 acetylation (H3K9ac), a histone marker of activated promoters, in the *SLUG* and *ZEB1* promoters on the same locus from which H2A.X had been removed (Weyemi et al.,

2016). More importantly, H3K9 hypoacetylation is representative of transcriptional repression, which has been linked to *E-cadherin* gene inactivation in CRC cell lines (Gargalionis et al., 2012; Liu et al., 2008), whereas high levels of trimethylated H3K9 (H3K9me3) have been correlated with good prognosis in early-stage CRC tissues (Benard et al., 2014).

Histone deacetylase 1 and 2 (HDAC1 and HDAC2) are overexpressed in 36.4 % and 57.9 %, respectively, of CRC patients and are considered predictors of overall survival in these patients. The inhibition of both HDAC1 and HDAC2 attenuates the growth of HCT116 and HT-29 colon cancer cells *in vitro* (Weichert et al., 2008). On the other hand, a study on valproic acid (VPA), a HDAC inhibitor, revealed that VPA is efficient in significantly increasing HCT116 and SW480 CRC cell motility *in vitro* by down-regulating E-cadherin and ZO-1 expression while up-regulating Snail1, N-cadherin and Vimentin expression (Feng et al., 2015). Another HDAC inhibitor, trichostatin A (TSA), reduced E-cadherin expression and increased Vimentin expression at mRNA and protein expression levels in two CRC cell lines (DLD-1 and HCT116) (Ji et al., 2015).

Moreover, knockdown of KDM6B, a histone lysine demethylase that activates gene expression by eliminating repressive histone H3 lysine 27 trimethylation (H3K27me3) marks from chromatin, is involved in EMT activation by promoting *SNAI1* and *ZEB-1* expression while reducing *E-cadherin* expression in SW480-ADH colon cancer cells (Pereira et al., 2011). Furthermore, knockdown of UTX, a HDM that attributes to H3K27me2/3

demethylation, considerably increases H3K27me3 mark at the *E-cadherin* promoter which consequently represses E-cadherin expression and increases migration and invasion of HCT116 cells (Zha et al., 2016). The same study also demonstrated the recruitment of CBP (a H3K27 acetyltransferase) to the *E-cadherin* promoter, where H3K27me2/3 was demethylated via UTX over-expression. This consequently up-regulated E-cadherin expression, resulting in the reduction of HCT116 cell migratory and invasive ability (Zha et al., 2016).

Although substantial development has been made in understanding the molecular networks that regulate EMT, little is known about how chromatin modifiers regulate the expression of the EMT-associated genes and/or regulators at epigenetic level.

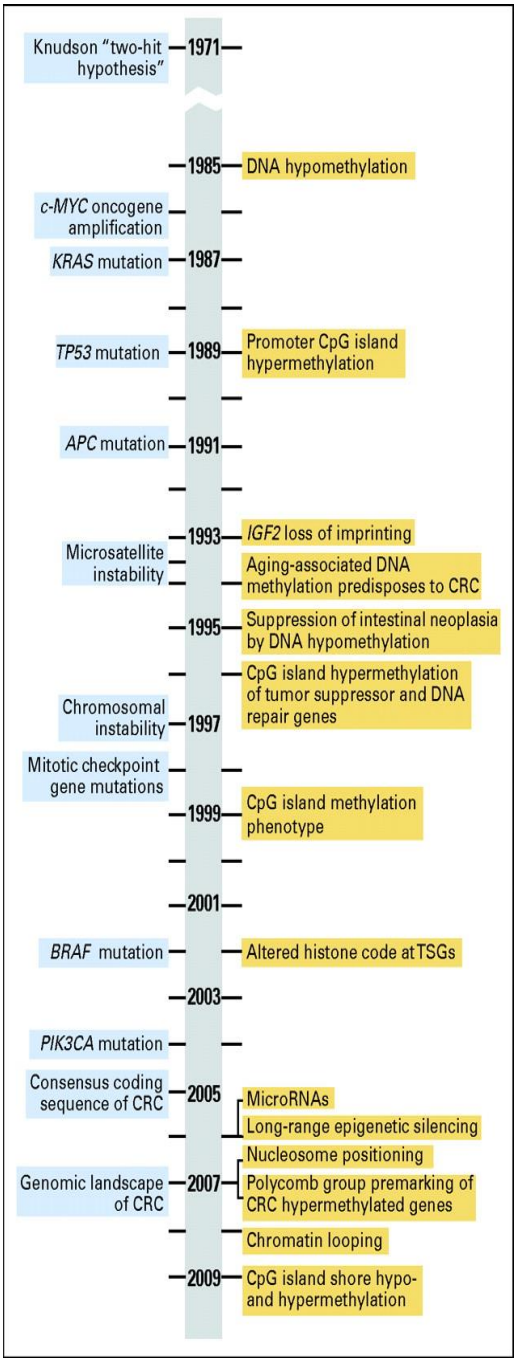


Figure 1-8: Schematic representation of sequential organization of findings representing the nature of CRC causes, whereas genetic alterations marked as blue and epigenetic ones as gold. Adapted from (van Engeland et al., 2011).

1.5 Epigenetic alterations in CRC development

In earlier studies, CRC was primarily considered a genetic disease that occurred due to sequential accumulation of genetic alterations. However, recent studies have shown that a combination of genetics and epigenetics contribute to CRC development (Figure 1-8) (Soshnev et al., 2016; Vaiopoulos et al., 2014; van Engeland et al., 2011).

Epigenetic alterations are present as inheritable changes in gene expression other than changes in the DNA sequence. The disruption of epigenetic reprogramming may influence gene expression, including DNA methylation, post-translational modification (PTM) of histones, loss of imprinting,

nucleosome positioning, chromatin looping and small non-coding RNA (Vaiopoulos et al., 2014; van Engeland et al., 2011). Epigenetic reprogramming is implicated in tumour suppressor loss of function and oncogene activation (Vaiopoulos et al., 2014). The combination of gene mutations and epigenetic changes engage signalling pathways that regulate the hallmarks of cancer activity. Consequently, it is important to understand chromatin structure and the chromatin remodelers implicated in several important biological mechanisms to study the relationship between epigenetic alteration and CRC development.

1.5.1 Chromatin structure

The 2-m long linear DNA is extensively condensed in DNA nanofibre form in the nucleus of the human cell. To achieve this condensation, the DNA associates with a set of nuclear proteins (histone and non-histone), leading to the formation of chromatin (Figure 1-9), which carries all genetic and inheritable information (Felsenfeld and Groudine, 2003). To achieve equal and appropriate segregation of genetic information to daughter cells, chromatin is further condensed to form chromosomes in metaphase during mitosis.

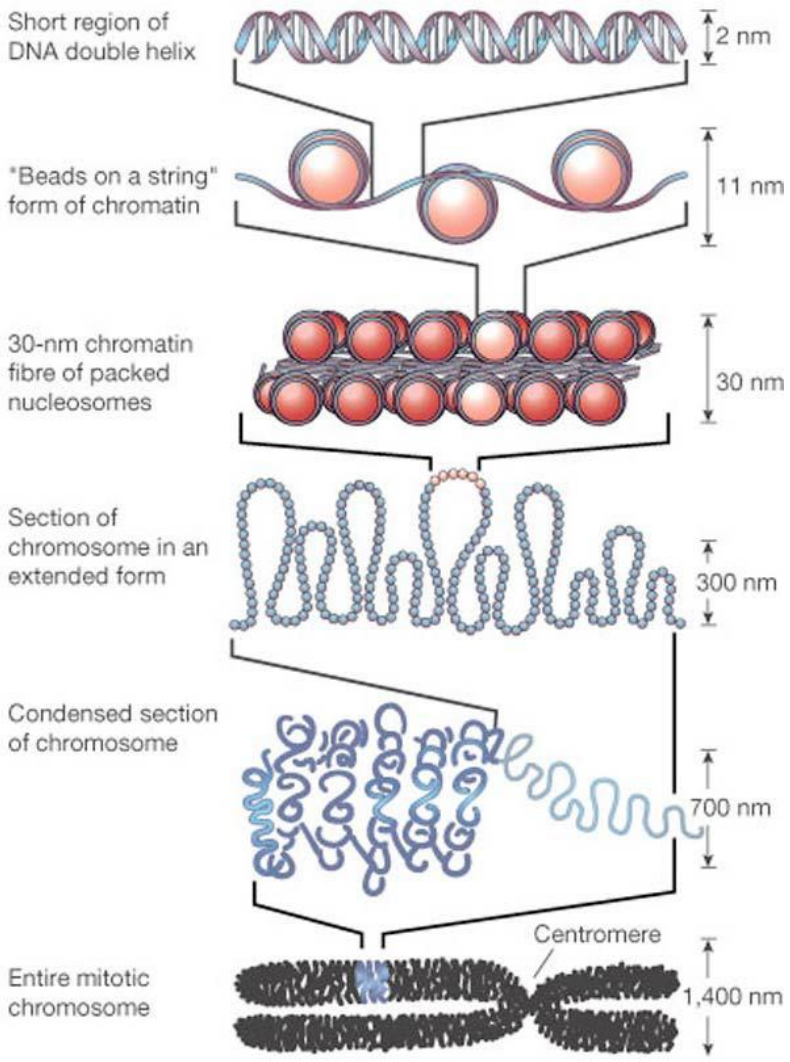


Figure 1-9: Organization of DNA in chromatin within the cell. Typically, the double helix DNA is wrapped around a histone octamer, creating nucleosomes that appear as beads on a string. These beads of nucleosome elements are then folded to form fibres of 30 nm in diameter and further coiled into higher-order structures which known as chromosomes. The total condensation of DNA in a chromosome form is more than 10,000-fold. Adapted from (Felsenfeld and Groudine, 2003).

1.5.2 Chromatin states

Early studies cytologically distinguished two states of chromatin (Heitz, 1928): Euchromatin has an open, transcriptionally active conformation, replicates early during S-phase and mainly encompasses most active genes (Alexandrow and Hamlin, 2005); conversely, heterochromatin is tightly compacted and replicates late in the cell cycle with little or no active gene expression (Cimini et al., 2003) (Figure 1-10 A).

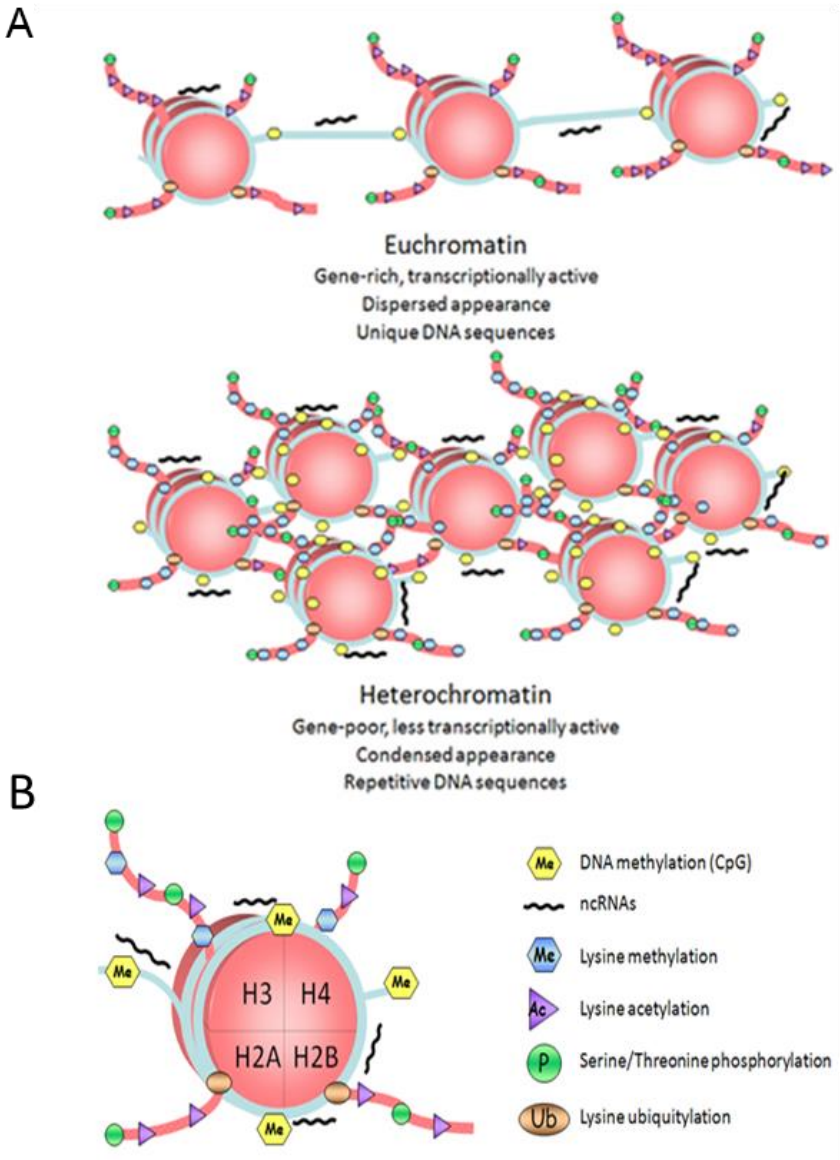


Figure 1-10: Schematic diagram of euchromatin and heterochromatin structure (A) and involvement of the posttranslational modifications (B). Adapted from *www.biochem.slu.edu*.

Epigenetic mechanisms determine the chromatin condensation or decondensation state via post-translational modifications (PTMs) (Figure 1-10 B), which take place on the histone amino-terminal tails (N-tails). Although every cell has the same genetic code, gene expression patterns differ between cells based on the influence of different sets of histone modifications on each cell (Schafer and Jung, 2005). Consequently, the condensed-state chromatin has to be reverted to its relaxed form to render the DNA accessible to the transcriptional machinery, and histone PTMs regulate this process (Elgin and Reuter, 2007; Schafer and Jung, 2005).

Some regions of the genome, such as centromeres, pericentric regions and telomeres, are maintained in the heterochromatic condensed state throughout the cell cycle in all cell types, hence is termed constitutive heterochromatin (Schafer and Jung, 2005). However, other heterochromatic regions of the genome can change their status during cell development or differentiation and are therefore known as facultative heterochromatin (Mohn and Schübeler, 2009; Schafer and Jung, 2005). Constitutive heterochromatin, mainly found at the pericentromeric regions and is organised in centromeres and telomeres, comprises various repeated non-coding DNA sequences, termed satellites (Dillon and Festenstein, 2002; Maison et al., 2011). While heterochromatin satellites are genetically inactive and cannot be transcribed or expressed, they are significant as contributors of centromeric components

in chromosomes (Figure 1-11) (Henikoff et al., 2001). Although heterochromatin function is not completely understood, heterochromatin mediates several nuclear functions, including centromere function, gene silencing and nuclear organisation (Yan et al., 2003). Centromeres are involved in two distinct heterochromatin regions: centric and pericentric. Minor satellite repeats (≈600 kb of 120-bp units) occupy the centric region, whereas major satellite repeats (6 Mb of 234-bp units) occupy the pericentric region (Henikoff et al., 2001).

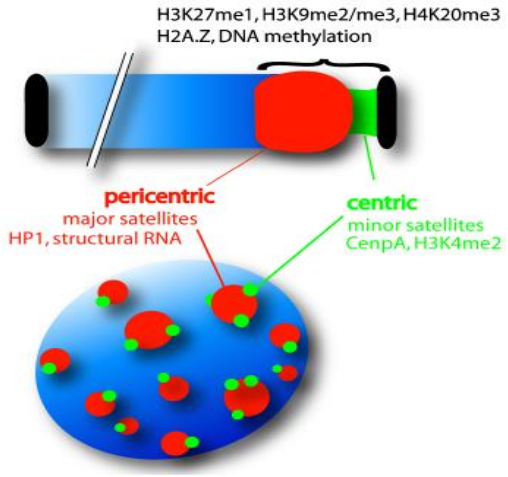


Figure 1-11: Schematic clarification of chromosomal heterochromatin regions. The heterochromatin centromere involved centric and pericentric regions which are presented by minor (green) and major (red) satellite repeats, respectively. Both centric and pericentric domains are enriched with methylation sites. Adapted from (Probst and Almouzni, 2008).

The minor satellites, along with centromeric proteins, are required for kinetochore formation (Mounia et al., 2004; Probst and Almouzni, 2008). Although H3K9me3 is enriched in both the centric and pericentric regions, distinct H3K9me3-containing dinucleosomes have been identified in the

pericentric regions only (Mounia et al., 2004), which means that each region participates in a distinctly higher order of chromatin organisation (Figure 1-11). Furthermore, when the suppressor of variegation 3-9 homolog 1/2 (SUV39H1/2) histone methyltransferase (HMTase) is absent from the cell, prolonged chromatid cohesion (that is sustained for a longer duration in major satellites compared with minor satellites) is lost only in the pericentric regions (Mounia et al., 2004). A recent study discovered that H3K9 methyltransferases and their equivalent demethylases serve as the on/off switch for pre-iPSC (induced pluripotent stem cells) fate by regulating H3K9 methylation status at pluripotency loci (Chen et al., 2013). Therefore, it is clear that SUV39H1/2 plays an important role in assembling sister chromatids together and that both the centric and pericentric regions are functionally independent (Mounia et al., 2004). HP1α (heterochromatin protein 1α) is enriched in the pericentromeric heterochromatin, and it has been suggested that HP1α recruitment in this region depends on SUV39H1/2-mediated H3K9 trimethylation (Eissenberg and Elgin, 2000; Kwon and Workman, 2011; Muchardt et al., 2002).

Chromosome condensation is a significant process that provides correct and equal segregation of genetic material among daughter cells; consequently, failure of proper segregation may lead to undesirable outcomes. Combined with the influence of centromere function, heterochromatin satellite repeat accumulation is associated with transcriptional gene silencing (Dillon and Festenstein, 2002). Recently, transcriptional gene silencing and its contribution to cancer progression became the main focus of research.

Tumour suppressor genes are genetically or epigenetically silenced in many cancers. Gene silencing via hypermethylation of the promoters of many tumour suppressor genes mediates tumorigenesis (Vaiopoulos et al., 2014).

1.5.3 Histone types

Eukaryotic DNA is packed into chromatin, which consists of a complex of DNA and histone and non-histone proteins. There are five histone isotypes: H2A, H2B, H3, H4 and H1. H1 is termed the linker histone. The core histone unit is made up of two units each of H2A, H2B, H3 and H4, forming an octomer (a H3–H4 tetramer and two H2A–H2B dimers), which is then tightly wrapped with 147 bp DNA (Bannister and Kouzarides, 2011; Thoma, 1992). This unit of core histones and the DNA is known as a nucleosome and is the basic organising unit of chromatin (Bannister and Kouzarides, 2011; Soshnev et al., 2016). Assembly of H1 and the nucleosome is known as a chromatosome, considered a basic repeat unit of chromatin fibres (Hayashihara et al., 2010a). The H1 globular domain (GD) interacts with linker DNA at the entry/exit site of nucleosomal DNA, creating higher levels of chromatin organisation and condensed structure (Maresca et al., 2005; Soshnev et al., 2016); therefore, H1 may be essential for mitotic chromosome condensation and segregation.

1.6 Histone post-translational modifications (PTMs)

Histone N-terminal tails are substrates for a number of PTMs (Figure 1-12), including acetylation, methylation, phosphorylation, ubiquitination and simulation. Each of the four core histone proteins has the same primary structure, but undergoes different chemical modifications, which results in promoted or inhibited gene transcription (Bannister and Kouzarides, 2011). PTMs act as transcriptional controllers that balance the inversion between the active euchromatin and the inactive heterochromatin. These modifications not only influence the transcription status of many genes, but also influence other molecular processes involving DNA-templated processes such as proliferation, differentiation and apoptosis (Kouzarides, 2007; Soshnev et al., 2016). Moreover, these modifications can be inherited by daughter cells following cell division. Consequently, epigenetic modifications can repair altered gene expression patterns produced as a result of environmental reasons such as radiation and chemical exposure, and nutrition. Consequently, epigenetic modifications may act as an epigenetic memory for gene expression patterns (Bannister and Kouzarides, 2011; Soshnev et al., 2016).

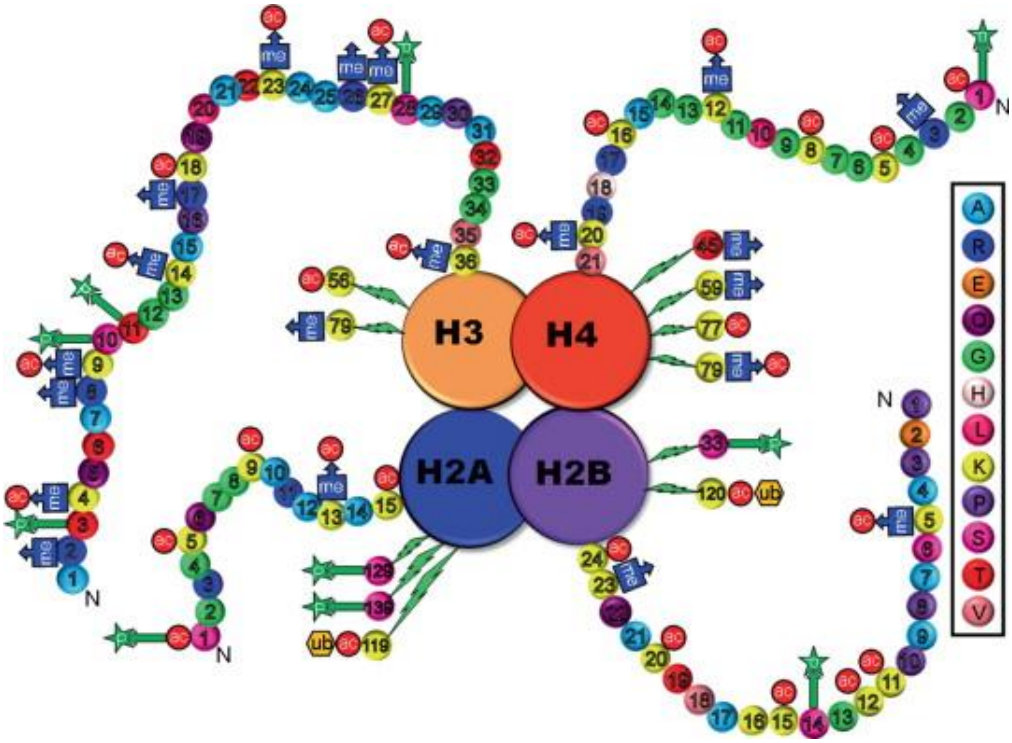


Figure 1-12: Posttranslational modifications of histone molecules. The protruding out N-terminals tails of histone are subjected to a great range of posttranslational modifications. These protruding tails consist of amino acid residues that have been numbered according to their positions in human histones and the respective modifications have been shown on the residues. The column in the right-hand sides shows different colour-coded amino acids. A, alanine; R, arginine; E, glutamic acid; Q, glutamine; G, glycine; H, histidine; L, leucine; K, lysine; P, proline; S, serine; T, threonine; V, valine, me, methylation; ac, acetylation; P, phosphorylation; Ub, ubiquitination; and N, N-terminal end of the histones. Note that lysine residues can be mono-, di-, or tri-methylated and arginine residues can be mono- and di-methylated. Adapted from (Jayani et al., 2010).

The involvement of a range of enzymes catalysing PTMs is crucial for initiating the function of the PTM regulatory machinery, which is responsible for controlling transcriptional activity. Deregulation of enzymatic interactions or expression can alter the flow of normal physiological processes and induce incorrect transcription patterns by silencing or down-regulating tumour suppressor expression or enhancing oncogene expression (Schafer and Jung, 2005; Vaiopoulos et al., 2014).

1.6.1 Effects of acetylation and deacetylation in gene expression

More than four decades ago, Allfrey and collaborators discovered a strong correlation between histone acetylation and transcriptional activation (Allfrey et al., 1964; Brownell et al., 1996), but the molecular mechanism involved has only been described in recent years (Davie, 1998; Gregory et al., 2001). This finding spurred an important wave of interest in the role of histone modifications in regulating DNA-dependent processes. Histone acetylation is tightly regulated by the activity of two enzyme families: histone acetyltransferases (HATs) and HDACs (Dawson and Kouzarides, 2012; Gargalionis et al., 2012; Kuo and Allis, 1998; Vaiopoulos et al., 2014). HATs, such as PCAF, GCN5 and HAT1, promote histone acetylation and hence transcriptional activation (Hebbes et al., 1988; Kuo and Allis, 1998). HATs add acetyl groups acquired from acetyl coenzyme A to the epsilon amino group of lysine residues in the N-termini histones, resulting in neutralisation of the positive charge of the lysine residue on the histone tails and reducing the electrostatic interaction between the positive-charge histones and negative-charge DNA (Davie, 1998). This renders the DNA promoters and enhancers more accessible to RNA polymerase and leads to activation of the transcription of certain genes. This transcriptionally active chromatin state is known as euchromatin (Grunstein et al., 1995). Regions of active DNA are marked with H3 and/or H4 acetylation (Vaiopoulos et al., 2014; van Engeland et al., 2011).

HDACs have antagonistic properties to HATs, stimulating the removal of acetyl groups from histone lysine residues, leading to chromatin compression and transcriptionally repressing genes by enabling interaction between DNA and histones (Davie and Spencer, 1999). This chromatin state is termed heterochromatin. Typically, HATs and HDACs regularly add and remove acetyl groups to and from lysine in the histone N-termini, respectively (Kuo and Allis, 1998; Vaiopoulos et al., 2014). However, HATs and HDACs demonstrate activity towards non-histone protein substrates such as P53, which stimulates or inhibits its transcription machinery (Barlev et al., 2001; Murphy et al., 1999). These substrates are involved in regulating gene expression and cell death, proliferation and migration (Chen et al., 2015; Gargalionis et al., 2012; Luo et al., 2000; Marks, 2010; Peserico and Simone, 2010).

HAT and HDAC activities are well-described and their role in tumorigenesis has been broadly studied (Marks, 2010). HAT and HDAC imbalances may induce tumorigenesis. Many anomalous histone acetylation patterns have been detected in CRC (Gargalionis et al., 2012). It was recently found that GCN5, a HAT, is up-regulated in human colon adenocarcinoma tissues (Yin et al., 2015). Among 18 HDACs, HDAC1–3, HDAC5 and HDAC7 are also elevated in CRC. HDAC2 up-regulation was detected in early-stage CRC (Stypula-Cyrus et al., 2013; Vaiopoulos et al., 2014). Histone PTM activates several oncogenes and represses numerous tumour suppressor genes. In CRC, for example, transcriptional repression of the *E-cadherin* tumour

suppressor gene is linked to H3K9 deacetylation (Gargalionis et al., 2012; Liu et al., 2008).

1.6.2 Effects of methylation and demethylation on gene expression

Another histone PTM that occurs at both the lysine and arginine residues of the histone N-terminal tails is methylation. Similar to acetylation, methylation is reversible and is regulated by the activities of two groups of mutually antagonistic enzymes: HMTases (also known as K-methyltransferase, KMT) and HDMs (also known as K-demethylase, KDM). HMTases and HDMs add and remove methyl groups from and to specific histone lysine or arginine residues, respectively (Vaiopoulos et al., 2014). To date, more than 20 HMTases have been identified, including SUV39H1/2, G9a, EZH2, NSD1 and SET1. Many HDMs have been identified and classified into either the lysine-specific demethylase (LSD) family or the Jumonji C (JMJC/KDM) family based on their homology and catalytic domains. LSD family members likely do not act on trimethylated lysine residues, whereas JMJC/KDM enzymes demethylate mono-, di- and trimethylated lysine (García-Giménez, 2015). Histone H3 undergoes methylation at multiple lysine sites, including K4, K9, K27, K36 and K79, and a lysine residue can be unmethylated (me0), monomethylated (me1), dimethylated (me2) or trimethylated (me3). H4 is also methylated mostly at lysine 20 and less commonly at lysine 79 and 59. H3K4 trimethylation is associated with transcriptional activation, whereas trimethylated H3K27, H3K9 and H4K20 are associated with transcriptional repression (Bártová et

al., 2008; Benard et al., 2014; García-Giménez, 2015; Vaiopoulos et al., 2014).

Colon adenocarcinomas undergo epigenetic alterations that mediate tumour progression (Enroth et al., 2011). A study that mapped genome-wide H3K4me3 and H3K27me3 binding in both normal and tumour samples from the colon found that, in the tumour samples, H3K4me3-positive genes developed hyperactivity while H3K27me3-positive genes became hyper-silenced as compared to the expression levels in normal colon mucosa (Enroth et al., 2011). H3K9me3 was decreased in patients with CRC when compared to healthy controls (Gezer et al., 2013). In contrast, despite the association between H3K9me3 and transcriptional repression, and the subsequent involvement in the abnormal silencing of tumour suppressor genes (i.e. *DCC* (Derks et al., 2009)), SUV39H1/H3K9me3 was increased in the invasive and lymph node metastatic regions of CRC tissues (Yokoyama et al., 2013). Bernad and colleagues also reported elevated H3K9me3 in patients with early-stage CRC, which correlated with good prognosis (Benard et al., 2014). Consistent with H3K9me3 elevation, induced levels of *SUV39H1* mRNA (a H3K9 methyltransferase) were detected in primary CRC tissues (Kang et al., 2007), suggesting SUV39H1 involvement in mediating the repression of the EMT-related genes. It appears that altered SUV39H/H3K9me3 expression/levels and the involvement of other histone modifiers may play a central role in human CRC development and metastasis through mechanisms that are currently unclear.

1.7 Heterochromatin-associated protein structures and their roles in cancer development

1.7.1 HP1

Accurate DNA packaging in nucleosomes results in mitotic chromosome condensation, which is essential for correct chromosome segregation (Eissenberg and Elgin, 2000). Not only are histone proteins that interact with nucleosomes involved in maintaining the condensed chromatin state; non-histone proteins also participate in this process and can influence the function of the transcriptional machinery. Nevertheless, the mechanisms involved in chromatin structural rearrangement from mitosis through interphase and in chromosome assembly during mitosis remain unclear.

Heterochromatin Protein 1 (HP1) is a non-histone protein that directly localises to constitutive heterochromatin (Canzio et al., 2014; Chevillard et al., 1993; Mateescu et al., 2008) and represents a family of small (~21 kDa) protein substrates originally discovered in *D. melanogaster* (James et al., 1989; Vermaak et al., 2005). HP1 proteins are a highly conserved family of proteins that consist of 184–192 amino acids. HP1 isoforms have been reported in many organisms, from fission yeast (Swi6, Chp2, Chp1) to human (HP1α, HP1β, HP1γ). The percentage of sequence similarity among human HP1 (HP1α, HP1β, and HP1γ), Swi6, and Chp2 and their domain mapping are illustrated in Figure 1-13, whereas the alignment of the human HP1 proteins is demonstrated in Figure 1-14. In mammals, all three HP1 isoforms have similar amino acid sequences and structural organisation, but their

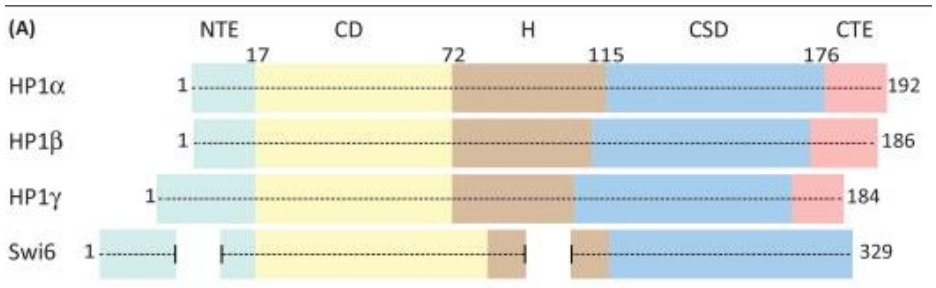
subcellular localisation differs; therefore, the isoforms have distinct functions. HP1α localises to both the metaphase centromeres and telomeres, whereas HP1β is found in interphase centromeres (Canzio et al., 2014; Hayakawa et al., 2003). Interestingly, HP1β dissociates from the centromeric regions; instead, HP1α accumulates there (Hayakawa et al., 2003). Both isoforms are generally associated with more compacted chromatin structure and are involved in transcriptional gene silencing (Canzio et al., 2014; Dialynas et al., 2006). However, emerging evidence shows that HP1α in *Drosophila* chromosomes is found at many euchromatic/gene active sites (Kwon and Workman, 2011; Piacentini et al., 2009; Sdek et al., 2013) and can open the chromatin (Cryderman et al., 2011) and stimulate highly expressed euchromatic genes via its association with their transcription start sites in silkworm genome (Shoji et al., 2014). Conversely, HP1γ localises largely in euchromatin and is distributed in multiple small foci outside the nucleoli and mediates transcriptional activation and RNA processing (Canzio et al., 2014; Minc et al., 1999; Vakoc et al., 2005). Consequently, the differing localisation determines distinct functions.

All HP1 proteins have a specific domain structure that includes a highly conserved terminal chromodomain (CD) that recognises H3K9, and a well-conserved C-terminal chromo shadow domain (CHD) that interacts with SUV39H1/2 (Bannister et al., 2001b; Lachner et al., 2001; Smothers and Henikoff, 2000; Yamamoto and Sonoda, 2003). The CD and CHD are connected to each other through a less conserved hinge region that binds DNA and RNA (Maison et al., 2011) and stimulates specific HP1α targeting

and accumulation at pericentric heterochromatin (Muchardt et al., 2002) (Figure 1-13 and Figure 1-15). In human cells, the HP1α CHD is essential for HP1α localisation to the metaphase centromere, whereas the N-terminal HP1β CD is essential for HP1β localisation to the interphase centromere. This shows that the HP1α and HP1β domains determine the localisation of the respective proteins to the metaphase and interphase centromeric chromosome regions, leading to the association of several HP1 isoforms with the centromeres at different cell cycle phases (Hayakawa et al., 2003).

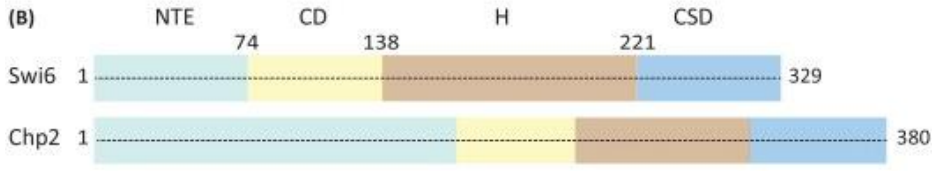
The homozygous loss of *Drosophila HP1* is fatal, highlighting the significance of HP1 in normal development (Lu et al., 2000). In addition, *D. melanogaster* die at the late third instar larval stage, i.e. when the maternal HP1 becomes depleted, perhaps because of the failure of HP1-null cells to segregate their chromosomes faithfully (Lu et al., 2000). It was recently reported that HP1 is a key chromatin factor that controls stem cell function (Zeng et al., 2013). However, the epigenetic mechanism orchestration of stem cell responses remains to be elucidated. In humans, reduced HP1 has been associated with cancer progression in many tumours (Dialynas et al., 2008; Lee and Ann, 2015; Lieberthal et al., 2009; Tretiakova et al., 2014). In contrast, the role of HP1 in colon cancer has not been fully elucidated, but De Lange and colleagues reported down-regulated HP1α expression in metastatic CRC cells (De Lange et al., 2000). Recent data suggest that aberrant expression of gastrin-releasing peptide (GRP) and its receptor (GRPR) down-regulates HP1β, which consequently increases invasion of CACO-2 human colon adenocarcinoma cells *in vitro* (Tell et al., 2011). A

more recent study on 178 CRC tissue specimens from different patients reported significantly increased HP1γ expression, which was correlated with short survival when compared to the matched adjacent non-tumour tissues (Liu et al., 2015).



Percentage sequence identity compared to HP1α

	NTE	CD	H	CSD	CTE
HP1β	35%	82%	33%	82%	38%
HP1γ	15%	71%	36%	87%	19%
Swi6	11%	42%	10%	23%	



Percentage sequence identity compared to Swi6

	NTE	CD	H	CSD	CTE
Chp2	12%	38%	13%	38%	

Figure 1-13: Structural mapping and sequence identity of human and fission yeast heterochromatin protein 1 (HP1) proteins. (A) Top: Mapping of human HP1α, HP1β, HP1γ, and fission yeast Swi6 domains. Bottom: Percentage sequence identity relative to human HP1α. (B) Top: Mapping of fission yeast Swi6 and Chp2 domains. Bottom: Percentage of identity for sequence alignment relative to Swi6. In (A) and (B), light green specifies the N-terminal domain (NTE), yellow the chromodomain (CD), light brown the hinge (H) region, blue the chromoshadow domain (CSD), and pink the C-terminal extension (CTE). Adapted from (Canzio et al., 2014).

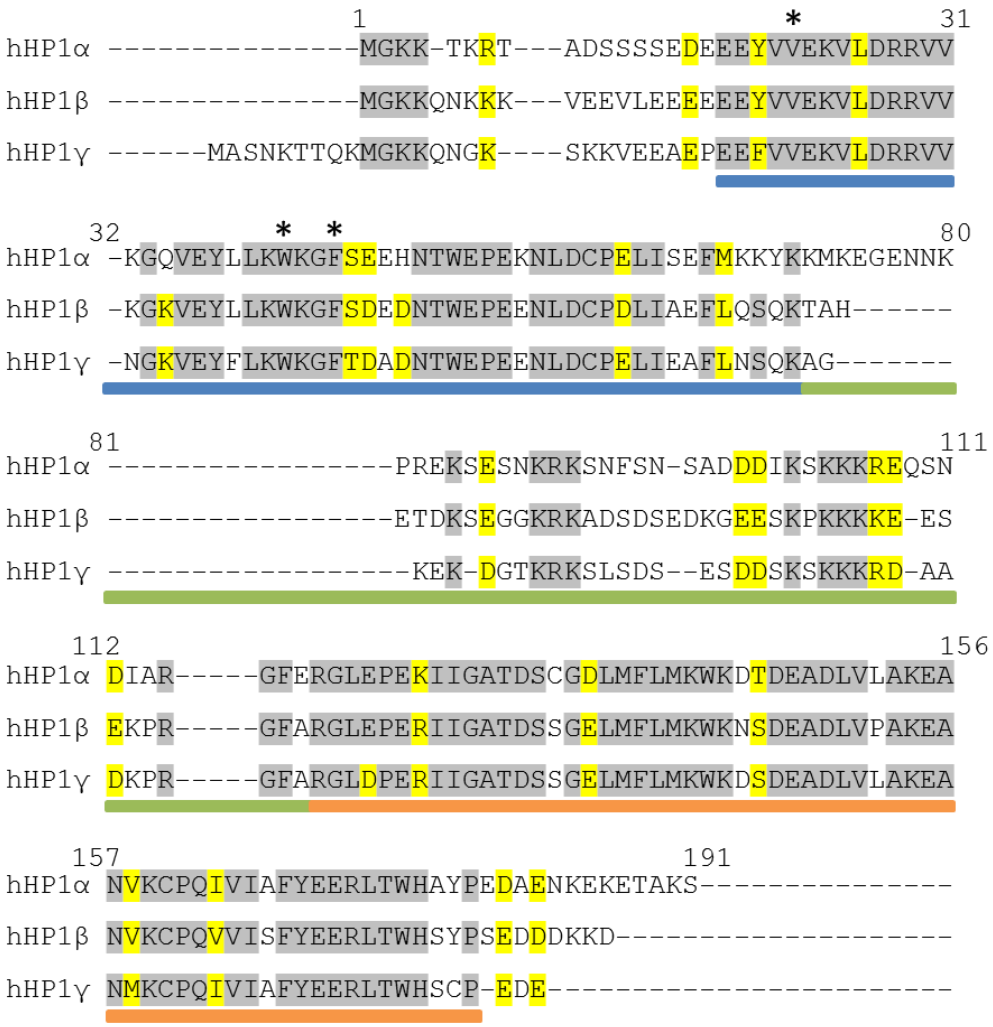


Figure 1-14: Amino acid alignment of HP1 proteins in humans (hHP1α, hHP1β, and hHP1γ). The CD and CSD domains are highly conserved, whereas there is less conservation of the H region. Identical residues and similar residues are highlighted in grey and yellow, respectively. The CD is underlined in blue, the H region in green, and the CSD domain in orange. Black asterisks designate amino acids participating in the aromatic binding cage. Numbers above the aligned hHP1 proteins refer to residue numbers. The multiple alignments of sequence identities were made using protein BLAST (*http://www.ebi.ac.uk/services*).

1.7.1.1 The cross talk between HP1α and SUV39H1/2

Among the multiple mammalian HMTases, SUV39H1 and SUV39H2 play an important role in heterochromatin formation. They are encoded by *SUV39H1* and *SUV39H2* and consist of two conserved domains: a C-terminal SET domain crucial for the catalytic activity of most lysine methyltransferases, and an N-terminal CD that binds lysine 9 of H3 and other proteins. SUV39H1 and SUV39H2 both target H3K9, but with a distinct degree of methylation (Maison et al., 2011; Schuhmacher et al., 2015). For example, SUV39H1 generates H3K9me3 by favouring unmethylated H3K9 and monomethylated H3K9 (H3K9me1) as substrates over dimethylated H3K9 (H3K9me2) (Chin et al., 2006). By contrast, SUV39H2 prefers un-methylated H3K9 as a substrate over methylated H3K9 (Schuhmacher et al., 2015). However, H3K9me2 conversion to H3K9me3 is slower than that of unmethylated H3K9 to H3K9me1 and H3K9me1 to H3K9me2 in both enzymes (Schuhmacher et al., 2015). The N-terminal of both enzymes binds to the HP1α CHD to create H3K9me3 that contributes to heterochromatin stability (Figure 1-15) (Yamamoto and Sonoda, 2003). Subsequently, H3K9me3 directly interacts with the HP1α CD and serves as a histone modification pattern (Bannister et al., 2001a). This pattern determines the condensed state of chromatin and serves as an essential marker of epigenetic silencing (Nakayama et al., 2001; Rea, 2000).

A study conducted on *Suv39h1/2*-deficient mice reported chromosomal instabilities and severely impaired viability (Peters et al., 2001), whereas SUV39H1 overexpression in mice promoted both migration and

tumorigenesis and resulted in significantly decreased survival rates (Yokoyama et al., 2013). These findings indicate the role of SUV39H1/2 as a central epigenetic regulator of mammalian development. Other than histone modification, non-histone modification is also required for maintaining constitutive heterochromatin compaction, spread and silencing activity (García-Giménez, 2015). A recent study revealed that SET7/9 (a lysine methyltransferase) attenuates SUV39H1 activity in response to adriamycin treatment (a DNA damage inducer), leading to heterochromatin decompaction, genomic instability, and inhibited cell proliferation (Wang et al., 2013a). Moreover, the phosphorylation on the serine residues (S11–S14) of the HP1α N-terminal enhances the binding capacity of HP1α to H3K9me3, particularly during metaphase, which is essential for proper HP1α localisation to heterochromatin (Hiragami-Hamada et al., 2011). Additionally, it is strongly indicated that HP1α SUMOylation enhances HP1α binding activity towards DNA, consequently mediating transcriptional repression (Maison et al., 2011). Altogether, these data indicate the significance of SUV39H1/2 and HP1α interaction and the upstream modification of H3K9me3-mediated heterochromatin establishment/spread in normal development and cell cycle progression (Singh, 2010).

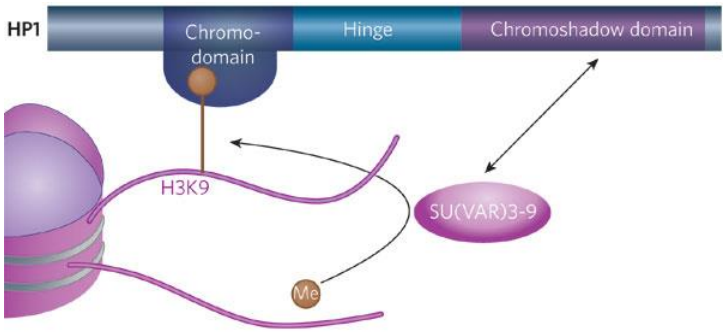


Figure 1-15: Schematic presentation of HP1 structure and function. The methyltransferase that is encoded by *Drosophila melanogaster SU(VAR)3-9* binds to chromo shadow domain of HP1, leading to methylated lysine 9 of histone H3 (H3K9me3). Then, H3K9me3 binds to chromo domain of HP1 to provide a foundation for heterochromatin spreading and epigenetic inheritance. Adapted from (Grewal and Elgin, 2007).

1.7.2 Heterochromatin protein–binding protein 3 (HP1BP3)

Hayashihara and colleagues have recently reported a novel chromatin-interacting protein that interacts with HP1α: HP1BP3 (also known as HP1-BP74) (Hayashihara et al., 2010a). The authors reported HP1BP3 in isolated and highly purified human metaphase chromosomes extracted from HeLa S3 cells in high-salt solutions using salt stripping. At the start of my study, apart from this single publication (Hayashihara et al., 2010a) very little was known about the HP1BP3 protein.

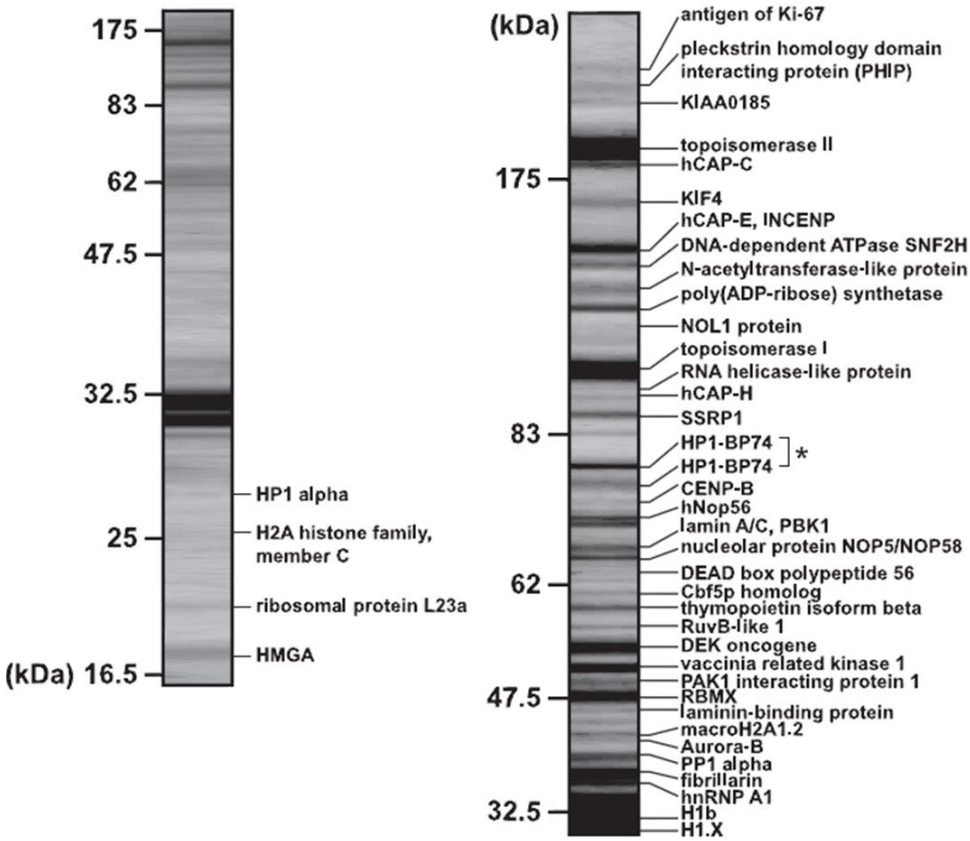


Figure 1-16: The schematic presentation of human metaphase chromosome-associated proteins. Dissociation and identification of proteins was achieved by using 0.4 M NaCL and mass spectrometry, respectively. The * represents the expression of two separate bands corresponded to HP1BP3 (HP1BP74), as demonstrated. Adapted from (Hayashihara et al., 2010a).

The human *HP1BP3* gene encodes a highly conserved protein with a remarkable degree of sequence and functional similarity to the murine HP1BP3 protein (Garfinkel et al., 2015b). The *HP1BP3* gene contains 12 exons spanning 1.662 kb of chromosome 1 (chromosomal position: 1p36.12) in humans and 13 exons spanning 1.665 kb of mouse chromosome 4 (chromosomal position: 4 D3; 4). Additionally, it encodes two endogenously expressed bands termed HP1BP3a and HP1BP3b, corresponding to the long

and short isoforms, respectively (Garfinkel et al., 2015b; Hayashihara et al., 2010a). The latter arises from alternative splicing in the 5′ terminal region of human *HP1BP3* mRNA, resulting in exon skipping at exon 2 and an alternative transcript starting at exon 3. Consequently, the splice variant is characterised by a 38–amino acid deletion at the N-terminal of the long HP1BP3 protein (Garfinkel et al., 2015b). In humans, the a and b HP1BP3 isoforms consist of 553 and 515 amino acids, respectively, whereas the long and short mouse Hp1bp3 isoforms consist of 500 and 462 amino acids, respectively. Sequence alignment of the long and short transcripts of humans and mice has detected more than 84 % homology between the two species. Moreover, expression of the mRNAs of the two splice variants and their protein products are present in the majority of human and mouse tissues. Interestingly, all studied samples expressed at least HP1BP3a isoform (Garfinkel et al., 2015b).

1.7.2.1 HP1BP3 protein structure and localisation

HP1BP3 is a novel nuclear protein that contains different domains responsible for distinct interactions (Garfinkel et al., 2015b; Hayashihara et al., 2010a). Recently, it was revealed that HP1BP3 is a ubiquitously expressed protein with remarkably close structural resemblance to linker histones of the H1 family that has high binding affinity to nucleosomes. Members of the H1 family are mainly involved in global chromatin compaction and affect chromatin organisation and function by interacting with the linker DNA between nucleosomes (Thoma and Koller, 1977). H1 is required for proper chromosome segregation by the mitotic spindle (Maresca

et al., 2005), gene expression regulation (Fan et al., 2005), mammalian development (Fan et al., 2003) and stem cell differentiation (Pan and Fan, 2016; Zhang et al., 2012). The middle portion of HP1BP3 (Lysine 97– Lysine 274) has a H1 globular domain (GD) (Methionine 153– Threonine 237) with sequences identical to that in the linker histone H1, and associates with linker DNA at the entry/exit site of nucleosomal DNA (Hayashihara et al., 2010a). Another structural study reported that HP1BP3 has three GDs and a positively charged C-terminal that exhibit identical and high sequence similarity, respectively, with that of H1 family members (Garfinkel et al., 2015b). These domains increase H1 affinity to chromatin in live cells. The three GDs (designated GD1, GD2 and GD3) are located downstream of a glutamine-rich, unstructured N-terminal domain (NTD) comprising 100 amino acids. A 20–amino acid polyaspartate/glutamate tract (DE) is located upstream of GD3, which is adjacent to a highly positively charged C-terminal domain.

The remarkable sequence conservation (98 % identity) of the three HP1BP3 GDs, which been found among mice and humans, is highly prominent. Like H1 subtypes, both N- and C-terminal domains are essential for the chromatin-binding characteristic of HP1BP3, which is affected by cell cycle progression and PTMs (Garfinkel et al., 2015b). Indeed, recent experimental evidence has shown significantly reduced HP1BP3 interaction with chromatin following C-terminal region deletion (Garfinkel et al., 2015b). N-terminal domain deletion also reduced HP1BP3 affinity for chromatin and reduced nuclear HP1BP3 localisation to the nucleoli. These data suggest that the triple

GD region, along with the C- and N-terminal domains, act cooperatively towards the chromatin-binding properties of HP1BP3 (Garfinkel et al., 2015b).

Apart from its similarity with H1 family members, HP1BP3 has its own structural characteristics. HP1BP3 interacts with HP1α CHD through a novel PXVXL-binding motif at proline 255–leucine 259 (Hayashihara et al., 2010a), which is close to the middle of the second HP1BP3 GD identified by Garfinkel and colleagues (Garfinkel et al., 2015b). A valine (V257) to glutamic acid substitution using site-directed mutagenesis led to complete abolishment of HP1BP3 interaction with heterochromatic regions, strongly suggesting HP1α-dependent heterochromatin enrichment of HP1BP3 (Garfinkel et al., 2015b). HP1BP3 showed strong co-localisation with both HP1α and H3K9me3 (heterochromatin markers), whereas there was significantly reduced co-localisation between HP1BP3 and HP1γ (euchromatin marker), more strong evidence for HP1α-dependent HP1BP3 involvement in heterochromatin (Garfinkel et al., 2015b). The DE domain is a unique structural property of HP1BP3 and the *H1* gene family. Generally, the main role of the negative-charge DE (a 20 amino acid poly aspartate/glutamate tract) domain is directed towards interaction with core histones and/or regulating DNA binding dynamics. DE sequence deletion noticeably increased HP1BP3–chromatin residence times (Garfinkel et al., 2015b).

The structure of HP1BP3 governs its cellular localisation. Consequently, the presence of histone H1–like domains confers DNA-binding properties on HP1BP3, while the HP1α binding motif stabilises its interaction with heterochromatin. Altogether, this indicates the intranuclear localisation characteristic of HP1BP3. Indeed, the current evidence shows that the HP1BP3 nuclear expression pattern is predominant in all investigated cell lines and tissues (Garfinkel et al., 2015b). Although HP1BP3 is ubiquitously expressed in all vertebrates, its distribution varies between cell type (Garfinkel et al., 2015b). HP1BP3 is highly expressed in the brain compared to other observed tissues. Interestingly, germ cells are null for HP1BP3 expression. High amounts of HP1BP3 have been detected in embryonic tissue but not in trophoblast placental regions. Furthermore, HP1BP3 expression intensity differs within the same tissue type. Renal proximal tubules exhibited strong HP1BP3 expression signals as compared with the distal tubules. Similarly, HP1BP3 intranuclear expression patterns differ based on cell type. HP1BP3 expression in Purkinje cells was presented by enrichment in the perinucleolar heterochromatic foci, while neuronal cells of the cerebellum showed diffuse distribution of HP1BP3 (Garfinkel et al., 2015b). A study on primary cultures of cerebral cortical neurons demonstrated a clone with an identical sequence to HP1BP3. HP1BP3 up-regulation was observed and linked to neuronal maturation (Li et al., 2002), suggesting the possible contribution of HP1BP3 to neuronal development processes including proliferation, differentiation and/or migration.

1.7.2.2 Functions of HP1BP3

Several studies have attempted to address questions concerning the role of HP1BP3 in chromatin biology, pathobiology and cellular biology (Dutta et al., 2014a; Dutta et al., 2014b; Garfinkel et al., 2015a; Garfinkel et al., 2016; Garfinkel et al., 2015b; Hadac et al., 2016; Liu et al., 2016a; Neuner et al., 2016). Initially, HP1BP3 was identified as a novel heterochromatin-associated protein (Hayashihara et al., 2010a); accordingly, additional research was directed towards how HP1BP3 is involved in heterochromatin architecture. Recent evidence has shown that *HP1BP3*-null HEK293T cells presented chromatin unfolding activity (Dutta et al., 2014a). Hence, these data reveal a novel regulatory role for HP1BP3 in maintaining higher-order chromatin assembly and heterochromatin integrity. Dutta and colleagues recently reported on the contribution of HP1BP3 to chromosome dynamics via a chromatin proteomics strategy (Dutta et al., 2014a). The strategy revealed the dynamic association of histone proteins and multiple non-histone proteins with DNA. Hence, the applied proteomic approaches showed the association between the non-histone HP1BP3 protein and chromatin remodelling during the different stages of cell cycle progression (Dutta et al., 2014a).

A typical eukaryotic cell cycle is divided into two basic parts: mitosis (division of the nucleus) and interphase (distribution of identical genetic material, i.e. DNA, to two daughter cells). Generally, human cells spend about 95 % of their time in interphase (the phase between two successive mitoses). Interphase encompasses the G1 phase (the first gap phase between

mitosis and the onset of DNA replication where cells grow), the S phase (occurrence of DNA synthesis) followed by the G2 phase (the second gap phase of cell growth and preparation for mitosis) (Cooper, 2000; Ma et al., 2014). Interestingly, two studies had strong evidence that HP1BP3 localises in the nuclei but is excluded from the nucleoli and chromosomes in interphase and mitosis, respectively (Garfinkel et al., 2015b; Hayashihara et al., 2010a). Such localisation patterns have also been found for proteins associated with high-order chromatin structure formation (Cherukuri et al., 2008). Moreover, HP1BP3–chromatin association is increased during G1–S transition to control cell proliferation (Dutta et al., 2014a). Maintenance of the proper duration of each cell cycle phase is important; dysregulation of the duration of any cell cycle phase can lead to uncontrolled cell proliferation and therefore cancer development. As cell cycle progression is regulated by protein kinases [known as cyclin-dependent kinases (CDKs)], checkpoint regulatory proteins and chromatin-associated proteins, these proteins must be expressed properly at the correct interval. Accurate G1–S transition plays a pivotal role in regulating cell proliferative capacity (Bertoli et al., 2013; Liu et al., 2016b; Nielsen et al., 1999; Wang et al., 2014). *HP1BP3*-null mice exhibited partial post-natal lethality and adult growth retardation (Garfinkel et al., 2015a; Garfinkel et al., 2015b), thereby underlining the physiological significance of HP1BP3 activity in growth and viability and highlighting the impact of HP1BP3 in regulating G1–S transition and cell proliferation.

Dutta and colleagues reported that *HP1BP3*-deficient HEK293T cells were more susceptible to micrococcal nuclease (MNase) digestion and had

reduced chromatin compaction compared with mock cells. These findings point to the possible role of HP1BP3 in modulating chromatin structure by interconverting euchromatin and heterochromatin and consequently activating or silencing the transcription of many genes (Dutta et al., 2014a). Garfinkel and colleagues reported that HP1BP3 does not influence global chromatin structure (Garfinkel et al., 2015b). Despite the discordant findings, the two groups reported that abolishing HP1BP3 altered the expression of many genes (Dutta et al., 2014a; Garfinkel et al., 2015b). Any changes in the compaction state of chromatin affects access of the transcriptional machinery to genes, thereby modulating gene expression and subsequently key cellular events such as proliferation, differentiation and apoptosis. Microarray analysis of HeLa cells revealed that HP1BP3 loss affected the transcription of 383 genes, where the transcription of 271 genes was up-regulated and that of the remaining genes was down-regulated (Garfinkel et al., 2015b). Mass spectrometry–based quantitative proteomic analysis identified 384 proteins with differential expression in *HP1BP3*-deficient HEK293T cells than in the experimental control, where 176 and 208 proteins were up- and down-regulated, respectively. More importantly, the altered expression of nuclear transport proteins resulted in induced net flux into the nucleus, consequently enlarging nuclear size (Dutta et al., 2014a). Accordingly, the experimental data indicated not only the involvement of HP1BP3 in heterochromatin structure stability, but also its role in regulating gene transcription and consequently protein expression (Dutta et al., 2014a).

The dynamic of chromatin compaction and decompaction during cell cycle progression is very important for the correct procession of basic cellular events (Ma et al., 2014). The maintenance of chromatin integrity is accomplished by chromatin–protein interaction that regulates key cellular functions during interphase (Alexandrow and Hamlin, 2005; Bhaskara et al., 2013; Hayakawa et al., 2003; Ma et al., 2014; Park et al., 2011; Park et al., 2014; Probst and Almouzni, 2008).

There are two constantly interchanging chromatin in interphase: euchromatin provides transcription factors access to DNA in the nucleosomes, which is necessary for normal cell function, while heterochromatin encompasses the chromosome structure, containing genes that are differentially expressed through development and/or differentiation and which are then silenced, preventing aberrant recombination between densely packed arrays of DNA repeats and thereby preserving genome stability. Hence, a highly dynamic state of chromatin is vital for proper DNA replication and the transfer of genetic and epigenetic material to progeny cells (Bannister and Kouzarides, 2011; Richards and Elgin, 2002). Dysregulation of chromatin-associated proteins can lead to cell cycle dysregulation and the subsequent expression of several cellular function–associated proteins, consequently promoting carcinogenesis (Czvitkovich et al., 2001; Di Paola et al., 2012; Ji et al., 2015; Kogure et al., 2013; Petti et al., 2015; Ramadoss et al., 2012; Stypula-Cyrus et al., 2013). As HP1BP3 contributes to chromatin dynamics, it might act as a critical driving force behind tumour initiation and/or progression via cell

cycle deregulation and therefore lead to uncontrolled cell proliferation, the hallmark of cancer.

There is strong evidence that the heterochromatin association of HP1BP3 is boosted under hypoxic conditions to induce alterations in epigenetic modification and gene expression (Dutta et al., 2014b). Hypoxia is one of the main determining factors of oncogenesis that promotes tumour initiation, progression and resistance to radio/chemotherapy (Ghattass et al., 2013). Hypoxia-induced alterations in the chromatin-dependent processes represent a key driving factor of tumorigenesis. The effect of HP1BP3 loss in an oxygen-depleted environment has been examined both *in vitro* and *in vivo* (Dutta et al., 2014b). Human tumour xenografts were used to determine the biological role of HP1BP3 in tumour growth. Subcutaneous injections of *HP1BP3*-null A431 cells produced tumour growth in three of six mice, whereas mock-null A431 cells produced tumours in six of six mice (Dutta et al., 2014b). These data reveal that HP1BP3 mediates hetero-chromatinisation in hypoxic conditions, promoting cancer cell survivability, and therefore define HP1BP3 as a regulator of cancer progression. Following exposure to 10 Gy ionising radiation, HP1BP3 abolishment in *HP1BP3*-null A431 cells attenuated cell viability by 18 %; the IC_{50} value of doxorubicin in the cells was markedly reduced from 670.2 ± 62 ng/ml to 503.2 ± 36 ng/ml as compared to the control (Dutta et al., 2014b). Another study identified HP1BP3 as a candidate of 5-fluorouracil (5-FU) resistance. In comparison to 5-FU–sensitive tumours, the *HP1BP3* gene was overexpressed in 5-FU–resistant colon tumours (Hadac et al., 2016). These data shed the light on the

contribution of HP1BP3 to tumour resistance against radiotherapy and chemotherapy.

More recently, it was discovered that HP1BP3 is a chromatin retention factor for co-transcriptional microRNA (miRNA) processing (Figure 1-17). miRNAs constitute a family of RNA-interference system and consist of short (~22 nucleotides) single-stranded RNA, and are involved in various pathological and physiological processes (He and Hannon, 2004). MiRNA biogenesis is mediated by the activity of two RNase III enzymes: Drosha and Dicer. The first step occurs in the nucleus where Drosha and the double-stranded RNA (dsRNA)-binding protein DGCR8 cooperate to cleave primary RNA (pri-miRNA; ~100 nucleotides) transcripts into ~70-nucleotide stem–loop precursor miRNA (pre-miRNA) and detach the two single-stranded RNA tails in the pri-miRNA (He and Hannon, 2004). The second step occurs in the cytoplasm, where the Dicer–TRBP/PACT complex further cleaves pre-miRNAs to generate mature miRNAs. The mature miRNAs are then assembled and loaded into the miRNA-induced silencing complexes (miRISCs) that contain Argonaute (AGO) and other associated proteins to mediate gene silencing via both translational repression and mRNA degradation (He and Hannon, 2004). Artificial pri-miRNA transcript retention at the chromatin significantly increases miRNA processing and expression (He and Hannon, 2004). RNA polymerase II (Pol II) activity intensely boosted the efficiency of pri-miRNA processing in the nuclear extract of HeLa cells during miRNA transcription (He and Hannon, 2004). Quantitative real-time PCR conducted on *HP1BP3*-depleted HeLa and

human osteosarcoma (U2OS) cell lines revealed marked decreases in the ratio of mature miR-21 and let-7a relative to pri-miR-21 and pri-let-7a, respectively, suggesting the involvement of HP1BP3 in human miRNA processing (Liu et al., 2016a). Co-transfection coupled with co-immunoprecipitation (co-IP) experiments on HeLa cells revealed the association of the three HP1BP3 GDs with the Drosha–DGCR8 microprocessor complex, indicating the importance of these GDs in mediating HP1BP3 interaction with the microprocessor *in vivo* (Liu et al., 2016a). Furthermore, HP1BP3 depletion in HeLa cells reduced the expression of 148 of 164 miRNAs tested; of the 148 miRNAs, the expression of 68 miRNAs was significantly reduced by more than 2-fold when compared with the control (Liu et al., 2016a). These data indicate the role of HP1BP3 in global human miRNA biogenesis.

In addition, chromatin immunoprecipitation sequencing (ChIP-seq) revealed that HP1BP3 favours the binding of actively transcribed miRNA loci, which is consistent with Drosha binding to active miRNA loci (Liu et al., 2016a). Furthermore, ChIP-seq and ChIP analysis showed HP1BP3 and Drosha co-binding to 42 highly transcribed miRNA loci (Liu et al., 2016a). Moreover, *HP1BP3*-deficient HeLa cells exhibited remarkably down-regulated Drosha ChIP signals at all examined active miRNA loci (Liu et al., 2016a). These findings indicate the importance of HP1BP3 in the co-transcriptional processes of virtually all pri-miRNA transcripts by its co-localisation with Drosha in chromatin and/or its possible recruitment of Drosha at the actively transcribed miRNA loci for co-transcriptional pri-miRNA processing

(Figure 1-17) (Liu et al., 2016a). A competition experiment using non-radiolabelled pri-miRNA or dsDNA revealed that HP1BP3 can bind pri-miRNA and dsDNA concurrently via diverse mechanisms (Liu et al., 2016a). HP1BP3 deficiency substantially decreased Drosha binding to all examined endogenous pri-miRNAs, indicating that HP1BP3 facilitates the association of Drosha to pri-miRNA *in vivo* (Figure 1-17) (Liu et al., 2016a). Moreover, HP1BP3 diminution in HeLa cells did not alter the expression of the examined pri-miRNA transcripts, nevertheless it down-regulated the production of the corresponding mature miRNAs (Liu et al., 2016a). These results suggest that HP1BP3 stimulates chromatin retention of pri-miRNA transcripts to increase pri-miRNA processing co-transcriptionally by providing more opportunities for the microprocessor complex to bind pri-miRNA on the chromatin (Figure 1-17) (Liu et al., 2016a).

In addition, *HP1BP3*-depleted HeLa cells had significantly decreased and increased examined pri-miRNA from the chromatin and the nucleoplasm, respectively, suggesting that HP1BP3 loss leads to the premature release of pri-miRNA transcripts from chromatin (Liu et al., 2016a). The above observations all point to a possible explanation for the lethality and growth retardation of *Hp1bp3*$^{-/-}$ mice observed by Garfinkel *et al*., in that it could have occurred as a consequence of defects in global miRNA processing associated with HP1BP3 loss rather than chromatin architectural defects (Liu et al., 2016a).

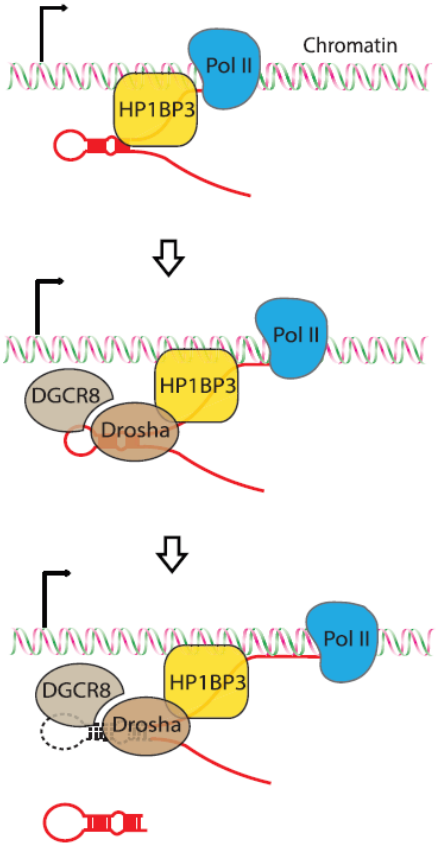


Figure 1-17: A schematic presentation of Co-transcriptional pri-miRNA processing. The schematic illustrates that HP1BP3 enhances pri-miRNA processing co-transcriptionally via retaining premature pri-miRNA transcript on chromatin. Adapted from (Liu et al., 2016a).

All obtained findings point towards the vital role of HP1BP3 in cancer progression and its possible implementation as a novel biomarker and potential therapeutic target in human cancer. As outlined above, at the start of this study, apart from a single publication (Hayashihara et al., 2010a) very little was known about the HP1BP3 protein.

1.8 Rationale and objectives of this study

Epigenetic mechanism regulation such as DNA methylation, histone modification and nucleosome remodelling is crucial for biological processes such as replication, recombination, DNA repair and transcription. The epigenetic regulatory machinery, which operates through association with a wide-range of histone and non-histone proteins and modifier enzymes, must be tightly controlled because, if unchecked, it may cause cancer via incorrect transcription patterns by silencing or down-regulating tumour suppressor expression or enhancing oncogene expression. An obvious mechanism for limiting the expression time of a protein is to destroy it via the UPS. Ideally, chromatin/heterochromatin-associated protein turnover should be tied to its efficiency in driving transcription.

Using a modified yeast 2-hybrid reverse Ras recruitment system (rRRS) (Nateri et al., 2004), previous studies in Dr Nateri's laboratory identified HP1BP3 as a downstream target of the E3 ubiquitin ligase FBXW7 for degradation (Li et al, submitted & Abuzinadeh et al., in preparation). Apart from above few published articles, very little is known about HP1BP3, including its regulatory machinery, function and its roles in colorectal cancer cells.

HP1BP3 is a nuclear protein with 553 amino acids with different domains; it is involved in distinct DNA and protein–protein interactions (Figure 1-18) HP1BP3 consists of linker histone 1 and histone 5 domains that associate with the entry/exit site of nucleosomal DNA by binding to HP1α

(Hayashihara et al., 2010a). As such, HP1BP3 is a chromosomal protein that exists as a component of heterochromatin and is involved in chromatin function and structure. Recent study in Dr Nateri's lab has also indicated that HP1BP3 degradation by FBXW7 regulates mouse HSC cell cycle entry and the transcriptional signature associated with the self-renewing HSC phenotype and leukemic status (Abuzinadah et al., in preparation).

To further investigate the molecular mechanisms underpinning HP1BP3 activity regulation that is translated into biological response, we investigated the HP1BP3 structural features and phosphorylation site regions using web-based computational analysis programmes (Figure 1-18). Our computing analysis determined that HP1BP3 has several important domains, including ATM/ATR phosphorylation SQ/TQ sites, GSK-3β (T/SXXXS/TP) phosphorylation sites, three H15 (linker histone H1/H5 globular) domains, a HP1α binding site, a lysine-rich domain (ubiquitin-binding domain), and several nuclear localisation signal (NLS) (Figure 1-18).

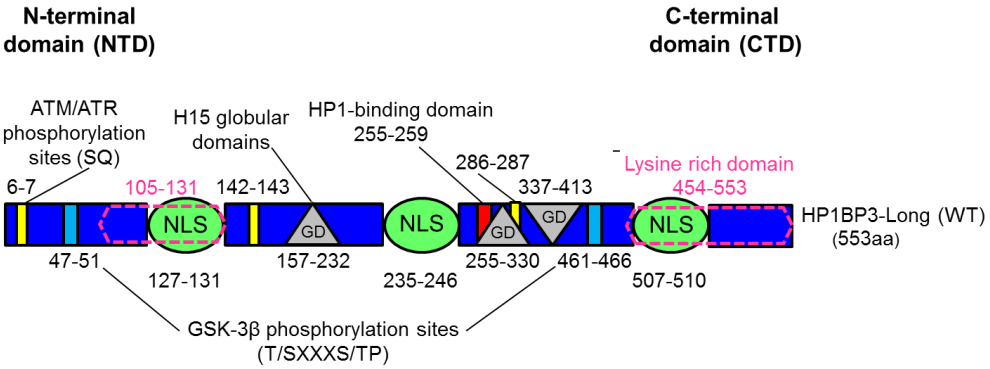


Figure 1-18: Schematic presentation of the domain organization of human HP1BP3 protein. Pink dashed boxes represent lysine-rich domain (ubiquitin-binding domain). Green ovals represent nuclear localisation signals (NLS). Grey triangles represent H1/H5 globular domains (GD). Red box represents HP1α-binding domain. Light blue box represents GSK-3β phosphorylation sites. Yellow boxes represent ATM/ATR phosphorylation sites. Numbers refer to amino acid positions.

HP1BP3 binds directly to HP1α, where H3K9me3 binds to recruit HP1α. HP1α modulation between heterochromatin and euchromatin is important in normal homeostasis and cancer, therefore we examined whether up-regulated HP1BP3 disrupts HP1α targeting of the heterochromatin region through competition with SUV39H1/2, which can affect major cellular events. The function of HP1BP3 remains to be explored; hence, the aims and objectives of the present study were as follows:

i. Revalidating the SCF^{FBXW7} E3 ligase mediated control of HP1BP3 abundance. The level of HP1BP3 protein was assessed in two human CRC cell lines (HCT116 and DLD-1) with and without *FBXW7* deletion mutations, using the western blotting (WB) and Immunofluorescence assays.

ii. Examining the GSK-3β-phosphorylation dependency of HP1BP3 protein stability. HCT116 cells either overexpressing the constitutive active GSK-3β kinase or treated with GSK-3β inhibitor were examined for by WB assays.

iii. Exploring whether loss of FBXW7 in HCT116 influences the co-localisation between HP1BP3 and HP1α/H3K9me3 and/or their protein levels, using IF and WB.

iv. Investigating if the HP1BP3 and HP1α co-localisation is dependent on the presence or absence of methyltransferases, SUV39H1/2 genes. This was examined using IF and WB assays in mouse embryonic fibroblast (MEF) cells derived from *Suv39h1/2* double-null mice, in which HP1α was no longer enriched at the pericentric heterochromatin.

v. Examining the changes in expression levels of EMT-associated proteins caused by ectopic expression of HP1BP3 and epigenetic markers alteration.

vi. Characterising the cell cycle function of HP1BP3 in human normal and cancer cell lines with and without deletion of *FBXW7* and *HP1BP3* genes. The cell cycle progression was analysed using PI staining followed by fluorescence-activated cell sorting (FACS) on Tiger (normal human embryonic fibroblast cells) and HCT116 cell lines stably over-expressing HP1BP3, along HCT116$^{FBXW7(-/-)}$ cells with high level of endogenous HP1BP3 protein expressions.

vii. Furthermore, to confirm the specificity of HP1BP3 regulating the cell cycle progression and phases transition, HP1BP3 expression was

either stably downregulated by lenti-shRNA and/or knockout CRISPR/Cas9-mediated strategies in HCT116$^{FBXW7(-/-)}$ cell lines. Moreover, we analysed the epigenetic markers alteration caused by HP1BP3 in distinct cell cycle phases by treating cells with double-thymidine or thymidine-nocodazole block (synchronising drugs) to synchronise the cells in G1/S or G2/M phase, respectively.

CHAPTER 2

General Materials & Methods

2.1 Materials

All reagents and chemicals used for biochemical, molecular and cellular experiments were purchased from Sigma-Aldrich unless otherwise stated.

2.1.1 Cell lines

The human colorectal cancer (CRC) cell lines HCT116 (adherent, derived from the colon of a male patient; with β-catenin mutation at Ser-45) and DLD-1 [adherent, derived from the colon of a male patient; with APC (adenomatous polyposis coli) mutation] were initially purchased from American Type Culture Collection. Both cell lines, with either wild-type *FBXW7* (+/+) or *FBXW7* gene deletions (-/-), were kind gifts from Professor A. Balmain (University of California, San Francisco, CA) and Dr B. Vogelstein (Ludwig Center, Johns Hopkins University, Baltimore, MD) (Mao et al., 2004; Rajagopalan et al., 2004). These cell lines have been used and extensively characterised in Dr Nateri's laboratory (Babaei-Jadidi et al., 2011a; Li et al., 2015; Lorenzi et al., 2016). HCT116$^{FBXW7(-/-)}$ and DLD-1$^{FBXW7(-/-)}$ cells were initially generated via the homologous recombination strategy to excise the exon 5 of *FBXW7* (Rajagopalan et al., 2004). Mouse embryonic fibroblasts (MEFs) with (-/-) and without (+/+) deletion of the *Suv39h1* and *Suv39h2* alleles (kindly provided by Professor T. Jenuwein, Max Planck Institute, Freiburg, Germany) were also used in the present study (Peters et al., 2001). *Suv39h1* and *Suv39h2* loci were independently disrupted by homologous recombination to produce in-frame fusion proteins of the first 40 amino acids of Suv39h1 or of the first 113 amino acids of Suv39h2 with

lacZ (Peters et al., 2001). The human skin fibroblast cell line Tiger was a kind gift from Professor G. Peters (Molecular Oncology Lab, CRUK, London Research Institute) and has been characterised in Dr Nateri's laboratory (Ibrahim et al., 2012; Nateri et al., 2005). All cell lines were authenticated in Dr Nateri's laboratory by genetic profiling using polymorphic short tandem repeat (STR) loci.

2.1.2 DNA plasmids

The plasmids used in this study are summarised in Table 2-1. These plasmids were constructed, fully validated (by double restriction enzymes digestion and DNA sequencing) and extensively used in Dr Nateri's laboratory.

Table 2-1: DNA plasmids used in this thesis.

Plasmid	Supplier	Cat. No.	Backbone vector	Bacterial selection
pcDNA3.1	Invitrogen	V790-20	NA	Ampicillin
pFLAG-GSK-3β	Dr Nateri's lab	NA	pcDNA	Kanamycin
peGFP-C2	Clontech	6083-1	NA	Kanamycin
peGFP-FLAG-MYC-FBXW7α	Dr Nateri's lab	NA	peGFP-C2	Kanamycin
peGFP-FLAG-MYC-FBXW7γ	Dr Nateri's lab	NA	peGFP-C2	Kanamycin
peGFP-FLAG-MYC-FBXW7β	Dr Nateri's lab	NA	peGFP-C2	Kanamycin
peGFP-C2-HP1BP3-S	Dr Nateri's lab	NA	peGFP-C2	Kanamycin
peGFP-C2-HP1BP3	Dr Nateri's lab	NA	peGFP-C2	Kanamycin
pLVX-eGFP	Dr Nateri's lab	NA	pLVX-Puro	Ampicillin
pLVX-eGFP-HP1BP3	Dr Nateri's lab	NA	pLVX-eGFP	Ampicillin

"NA" refers to not applicable.

2.1.3 Antibodies

The primary and secondary antibodies used for western blotting and immunostaining are listed in Table 2-2 and Table 2-3. The specificity of HP1 (α isoform) antibody has been validated commercially (Millipore, 05-689) and by other studies (Ayyanathan et al., 2003; Dawson et al., 2009; Liu et al., 2014). Moreover, Xiao et al. has validated the specificity of SUV39H1 antibody (Sigma-Aldrich, S8316) used in this study (Xiao et al., 2016). Furthermore, the specificity of both H3K9me3 (Millipore, 07-442) and H3K9ac (Sigma-Aldrich, H0913) antibodies was commercially validated.

Table 2-2: <u>Primary antibodies used for western blotting and immunostaining.</u> Our laboratory has previously evaluated the specificity of many of these antibodies.

Primary Antibody	Supplier	Cat. No	Source	Dilution Factor	
				WB	IF
HP1BP3	Sigma-Aldrich	HPA028215	Rabbit	1:1000	1:100
HP1α	Millipore	05-689	Mouse	1:1000	1:100
FLAG (tag)	Sigma-Aldrich	F1804	Mouse	1:2000	NA
GSK-3β	Cell Signaling	9315	Rabbit	1:2000	NA
P-GSK-3β (Ser21/9)	Cell Signaling	9331	Rabbit	1:1000	NA
GFP (tag)	Santa-Cruz	sc-9996	Mouse	1:1000	NA
SUV39H1	Sigma-Aldrich	S8316	Mouse	1:1000	1:100
H3K9me3	Millipore	07-442	Rabbit	1:1000	1:500
H3K9ac	Sigma-Aldrich	H0913	Mouse	1:1000	NA
H3	GeneTex	GTX122148	Rabbit	1:2000	NA
N-cadherin	BD Transduction	610920	Mouse	1:1000	NA
ZEB1	Santa-Cruz	sc-25388	Rabbit	1:500	NA
Vimentin	Santa-Cruz	sc-32322	Mouse	1:1000	NA
E-cadherin	BD Transduction	610181	Mouse	1:4000	NA
Snail1	Cell Signaling	3879S	Rabbit	1:1000	NA
Cyclin B1	Santa-Cruz	sc-3245	Mouse	1:1000	NA
β-Actin	Abcam	Ab6276	Mouse	1:10000	NA

"NA" refers to not applicable.

Table 2-3: Secondary antibodies used for western blotting and immunostaining.

Secondary Antibody	Supplier	Cat. No	Source	Dilution Factor	
				WB	IF
Anti-rabbit-HRP	Santa-Cruz	sc-2004	Goat	1:5000	NA
Anti-mouse-HRP	Santa-Cruz	sc-2005	Goat	1:5000	NA
Alexa Fluor® 488 anti-mouse	Invitrogen	A-21202	Donkey	NA	1:500
Alexa Fluor® 594 anti-rabbit	Invitrogen	A11037	Goat	NA	1:500
Alexa Fluor® 488 anti-rabbit	Invitrogen	A-21206	Donkey	NA	1:500
Alexa Fluor® 594 anti-mouse	Invitrogen	A-11005	Goat	NA	1:500

"NA" refers to not applicable.

2.1.4 Oligonucleotides

The oligonucleotides/primers utilised in this study (Table 2-4) was designed by the Primer3 web-based primer design tool (Version 0.4.0, available at *http://frodo.wi.mit.edu/primer3/*) for standard real-time polymerase chain reaction (PCR) (Section 2.2.2.4) and/or manually for overlapping PCR (Section 2.2.2.5). The NCBI Primer-BLAST tool used to check primer specificity by blasting the primer sequences against the NCBI human transcript database (*http://www.ncbi.nlm.nih.gov/tools/primer-blast/*). All primers purchased from Sigma-Aldrich and were spun down and resuspended in DNase/RNase-free water (Sigma-Aldrich, 4502) in the appropriate volume to a final concentration of 100 µM stock solution and stored at −20°C until used.

Table 2-4: Standard PCR and overlapping PCR primers. The external primers highlighted with green and the internal primers with, red colours.

Primer Name	Sequence
Standard PCR primers	
HP1BP3-Fwd	5′-ATCTCGAGCATGGCGACTGATACGTC-3′
HP1BP3-Rev	5′-ACCGTCGACTTACTTTTTCACTCTGAAAGACTTCTTCA-3′
Overlapping PCR primers (GSK-3β Point mutation- AA)	
HP1BP3-Fwd	5′-ATCTCGAGCATGGCGACTGATACGTC-3′
HP1BP3-AA-Rev	5′-CCCTGGGGCCTTGGCTGGGGCTTTCTTCTG-3′
HP1BP3-AA-Fwd	5′-AAGCCCCAGCCAAGGCCCCAGGGA-3′
HP1BP3-Rev	5′-ACCGTCGACTTACTTTTTCACTCTGAAAGACTTCTTCA-3′
Overlapping PCR primers (GSK-3β deletion- D1)	
HP1BP3-Fwd	5′-ATCTCGAGCATGGCGACTGATACGTC-3′
HP1BP3-D1-Rev	5′-ATTCACAGTTCGACGAATCGGCATGGTG-3′
HP1BP3-D1-Fwd	5′-ATTCGTCGAACTGTGAATCCCAAAAGCAAGCTTGCTGAAGG-3′
HP1BP3-Rev	5′-ACCGTCGACTTACTTTTTCACTCTGAAAGACTTCTTCA-3′
Overlapping PCR primers (GSK-3β deletion- D2)	
HP1BP3-Fwd	5′-ATCTCGAGCATGGCGACTGATACGTC-3′
HP1BP3-D2-Rev	5′-TTTCTTCTGCAACCTTCTCTTAGGTG-3′
HP1BP3-D2-Fwd	5′-AGAAGGTTGCAGAAGAAACCAGGGAAGGCCGCATCTGTGAAG-3′
HP1BP3-Rev	5′-ACCGTCGACTTACTTTTTCACTCTGAAAGACTTCTTCA-3′

2.2 General methods

2.2.1 DNA preparation and manipulation

2.2.1.1 Bacterial transformation

Bacterial transformation used to introduce DNA plasmids into bacterial cells for amplification. In this study, chemically prepared DH5α competent cells (Section 2.2.1.2) were used for DNA plasmid transformation (Table 2-1). To enhance the ability of the bacterial cells to uptake the DNA plasmids efficiently, *Escherichia coli* DH5α cells underwent a set of chemical treatments and consequently acquired competent properties. About 100–500 ng DNA plasmid was mixed with 50 µl competent cells and incubated on ice for 30 min. The mixture was subjected to heat shock at 42°C for 45 sec and then reincubated on ice for 5 min. Then, 500 µl Luria broth (LB) medium (Table 2-5) was added to the mixture and incubated at 37°C for 1 h with 230-rpm shaking on a Thermomixer. Next, 40–50 µl of the mixture was plated on an LB/agar plate containing an appropriate antibiotic [kanamycin (30 µg/ml) or ampicillin (50 µg/ml)] and incubated overnight at 37°C to yield single colonies. The next morning, raised single colonies were picked, cultured in 2 ml LB medium containing an appropriate antibiotic as outlined above, and reincubated for 5 h in a shaking incubator at 37°C and 230 rpm. Then, the DNA was extracted and amplified with miniprep (Section 2.2.1.3) or midiprep (Section 2.2.1.4) and confirmed by enzymatic digestion.

Small amounts of the transformed plasmid bacterial culture were stored for longer periods using glycerol stock (Sigma-Aldrich, G5516). The mixture

contained 20 % sterile glycerol in bacterial broth, and was vortexed and stored at −80°C.

To prepared the LB agar plates, 1 g bacteriological agar (Sigma-Aldrich, A5306) was added to 100 ml LB medium and microwaved until it became liquid. Next, the appropriate antibiotic was resuspended in the homogenised agar when its temperature had decreased to 50–60°C. Then, the mixture was poured into 10 cm^2 plates (15 ml each) and left to solidify at room temperature. The solidified agar plates were immediately used for bacterial culture or stored for 2–3 weeks at 4°C until used. By providing essential nutrients at the necessary concentrations, the culture medium enables efficient bacterial growth and division.

Table 2-5: Composition of common solutions and buffers used in this study.

Material	Composition	Experiment	Stock conc.	Working conc.	Storage temp
LB Medium	10 g Trypton, 5 g yeast extract and 10 g NaCl dissolved in 1 L distilled water (dH_2O) and autoclave before usage.	Bacterial transformation	1X	1X	4°C
RF1 buffer	12 g Rubidium-chloride, 9 g Manganese-chloride x $2H_2O$, 2.94 g Potassium acetate, 1.5 g Calcium-chloride x $2H_2O$, 150 g Glycerol in 900 ml dH_2O, adjust pH to 5.8, then complete to 1 L with dH_2O.	Competent cell preparation	1X	1X	4°C
RF2 buffer	2.09 g MOPS, 1.2 g Rubidium-chloride, 11 g Calcium-chloride x $2H_2O$, 150 g Glycerol in 900 ml dH_2O, adjust pH to 6.8, in 1 L dH_2O.	Competent cell preparation	1X	1X	4°C
RIPA buffer	150 mM NaCl, 25 mM Tris-HCl, 1% Triton X-100, 1% Sodium deoxycholate, 1% NP-40 , 0.1% SDS in dH_2O	Protein extraction	1X	1X	4°C
5X loading buffer	0.2 M Tris-HCl pH 6.8, 10% w/v sodium dodecyl sulfate, 20% glycerol 0.05% bromophenol blue, 10 mM beta-mercaptoethanol, in dH_2O	Western blotting	5X	1X	-20°C
Semi-dry Transfer buffer	30.3 g Tris HCL, 14.4 g glycine, 200 ml methanol in 1 L dH_2O	Western blotting	10X	1X	RT
TBS buffer	20 mM Tris, 13.7 mM NaCl in dH_2O, pH was adjusted to 7.6	Western blotting	10X	1X	RT

2.2.1.2 Chemical preparation of bacterial competent cells

To prepare the competent cells, 5 µl DH5α bacterial cells was cultured in 5 ml LB medium and incubated overnight at 37°C in a shaking incubator. This

pre-culture (2 ml) was transferred to 500 ml antibiotic-free LB medium and reincubated at 37°C with 230-rpm shaking for 2–3 h. The optical density (OD) of the culture was measured at regular intervals by spectrophotometer (Scientific Laboratory Supplies) until the OD was about 0.5–0.6. Then, the culture was divided into two sterile centrifuge bottles and incubated on ice for 30 min. The bacterial cells were then spun down at 2500 rpm for 12 min and the supernatant was discarded; the pellet in each bottle was resuspended in 20 ml RF1 buffer (Table 2-5), incubated on ice for 15 min and spun down for 9 min at 2500 rpm. Finally, each bacterial cell pellet was resuspended in 7 ml RF2 buffer (Table 2-5), aliquoted into sterile Eppendorf tubes and stored immediately at −80°C.

2.2.1.3 Isolation and purification of plasmid DNA, "Minipreps"

A GenElute™ Plasmid Miniprep Kit (Sigma-Aldrich, PLN350-1KT) was used according to the manufacturer's instructions to extract the DNA from the transformed bacterial cells. As described in Section 2.2.1.1, single colonies were picked from the agar plate culture, inoculated in a tube containing 5 ml LB medium supplemented with antibiotic appropriate for the vector used, and then incubated overnight. In the morning, the bacterial culture was spun down at 3800 rpm for 10 min and the pellet was resuspended in 200 µl ice-cold resuspension solution containing RNase. The tube was vortexed until the cell suspension was completely resuspended. Then, 200 µl alkaline lysis solution was added and the tube was gently inverted 5–6 times

and incubated for 4–5 min on ice to clear. Prolonged exposure to alkaline conditions can permanently denature the DNA plasmid, which might affect subsequent applications. Then, 350 µl neutralisation buffer was added and the tube was gently inverted 6–8 times to neutralise the alkaline pH of the lysis solution. The tube was centrifuged at 13000 rpm for 10 min to precipitate cellular debris. The separation column provided in the kit was equilibrated by adding 500 µl column preparation solution and then spun down at 13000 rpm for 1 min. Then, the supernatant was loaded onto the equilibrated column and centrifuged at 13000 rpm for 1 min. The DNA-containing column was washed with 750 µl washing solution and centrifuged twice at 13000 rpm for 1 min per spin to dry the column. Lastly, 100 µl DNase/RNase-free water was added to the column and centrifuged at 13000 rpm for 1 min to elute the DNA in to a new collection tube, and the eluted DNA was stored at −20°C. Typically, a Miniprep kit yielded 20–30 µg high-purity plasmid.

2.2.1.4 Isolation and purification of plasmid DNA, "Midipreps"

A Genopure Plasmid Midi Kit (Roche, 03143414001) was used according to the manufacturer's recommendations to extract large amounts of DNA (100–200 µg) from the transformed bacterial cells. The pre-culture obtained as described in Section 2.2.1.1 was transferred to 100 ml antibiotic-containing LB medium and incubated overnight at 37°C in a shaking incubator. The bacterial culture was then spun down and the DNA was extracted according to the protocol illustrated in Figure 2-1.

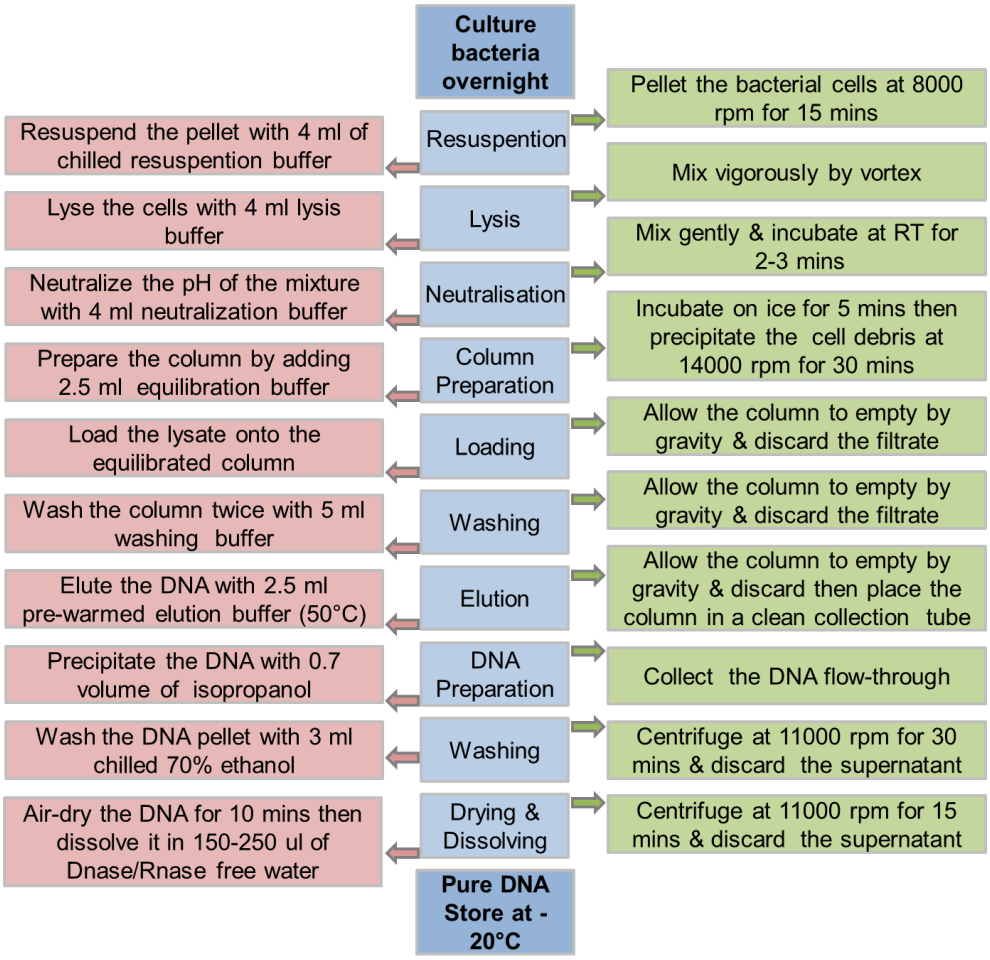


Figure 2-1: Midiprep DNA isolation kit procedure from bacterial culture. The centrifugation in all steps was performed at 4°C.

2.2.1.5 Quantification of DNA by spectrophotometry

DNA concentrations were measured using a NanoDrop ND-1000 UV-Vis spectrophotometer (LabTech International Ltd., Ringmer, UK). To measure the DNA concentration, the NanoDrop first blanked with 1.5–2 µl DNA elution buffer. Then, 1.5–2 µl of extracted DNA was pipetted onto the NanoDrop to determine its concentration and purity. Generally, the absorbance of nucleic acid and its contaminants detected during extraction is between 230 nm and 320 nm. Therefore, the NanoDrop measures the

absorbance at 230 nm, 260 nm and 280 nm. DNA absorbance peaks at 260 nm (A_{260}) and each A_{260} unit corresponds to 50 µg DNA per ml water. The A_{260}/A_{280} ratio is measured to determine the purity of samples comprising nucleic acid, and ratios of >1.8 or >2 are commonly accepted as 'pure' for DNA. A lower A_{260}/A_{280} ratio may indicate the presence of protein or organic contaminants (such as phenol). The A_{260}/A_{230} ratio can be used as a secondary measure of nucleic acid purity, and is generally higher than the A_{260}/A_{280} ratio (range, 1.8–2.2). A lower A_{260}/A_{230} ratio can also indicate the presence of impurities in the extracted DNA.

2.2.2 Gene cloning techniques

2.2.2.1 Restriction enzyme digestion

To validate the DNA plasmids outlined in Table 2-1, specific restriction enzymes were used according to the recognition sites. Restriction endonucleases isolated from bacteria can cut DNA at specific sequences. All restriction enzymes were purchased from New England Biolabs (NEB) and were used according to the manufacturer's instructions with the appropriate buffers at the optimal temperature. The restriction enzymes, buffers and appropriate conditions used are listed in Table 2-6**.** To digest DNA, an enzymatic mixture containing 0.5–1 µl DNA (1 µg/µl), 10 % 10× NEB buffer and 1 µl restriction enzyme was prepared and topped up to a final volume of 20 µl with Sigma water. Then, the digested DNA samples were run in ethidium bromide (EtBr)-stained gels.

Table 2-6: Restriction enzymes used in this study.

Restriction Enzyme	Cat. No.	Matching Buffer	Reaction Conditions
EcoR1	#R0101S	NEBuffer 3	37°C
BglII	#R0144S	NEBuffer 3	37°C

2.2.2.2 Agarose gel electrophoresis

Agarose gel electrophoresis was performed to visualise the DNA bands. Agarose gel (1 % [w/v]) was prepared by adding 1 g agarose powder (Eurogenetec, EP-0010-05) to 100 ml 1× Tris-acetate-EDTA (TAE) buffer

(Sigma-Aldrich, T9650), and microwave-heated for 1–2 min. The gel was cooled at room temperature until it was 40–50°C. To detect DNA bands in the gel, about 10 µl EtBr (Sigma-Aldrich, E1385) (final concentration, 0.05 µg/µl), an intercalating agent that binds to DNA bands and releases fluorescence when exposed to ultraviolet (UV) light, was added to the dissolved agarose mixture before solidification. The gel was then poured into a gel-casting tray containing an appropriate comb and allowed to solidify at room temperature. DNA samples containing 1–2 µl 10× gel loading buffer (final concentration, 1×; 30 % glycerol and 0.25 % bromophenol blue in distilled water) were loaded into the gel. DNA HyperLadder™ 1kb (Bioline, BIO-33025) was used to estimate the size of the DNA bands (Figure 2-2). A Bio-Rad power supply was used for the electrophoresis; the power source programme was set to 90–120 V for 50 min, with 1× TAE buffer as the running buffer. When the electrophoresis had been completed, the DNA bands were visualised and images were captured using a UV transilluminator (UVidoc). If further band separation was required, the electrophoresis was continued for another 10–20 min.

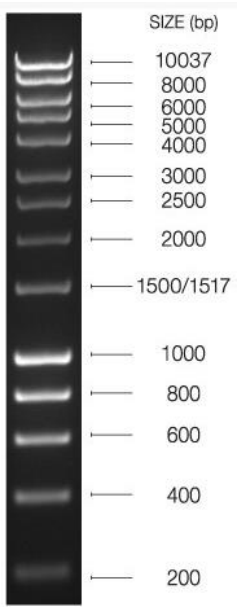


Figure 2-2: DNA HyperLadder™ 1kb (Bioline) used for agarose gel electrophoresis.

2.2.2.3 DNA extraction from agarose gel

Agarose gel sections containing the DNA bands of interest were excised under UV light, cut into small pieces, and placed in clean Eppendorf tubes. As prolonged UV exposure damages DNA and consequently reduces cloning efficiency, short exposure durations ranging from 20 sec up to 60 sec were used. An illustra™ GFX™ PCR DNA and Gel Band purification kit (GE Healthcare, 28-9034-70) was used to purify DNA from agarose gels or soluble PCR mixtures as outlined in Figure 2-3. The same protocol was used to extract the PCR product. The only difference is that 500 µl capture buffer was added to the PCR and the protocol described in Figure 2-3 was followed. Then, the NanoDrop unit was used to measure the concentration of the purified DNA as described in Section 2.2.1.5.

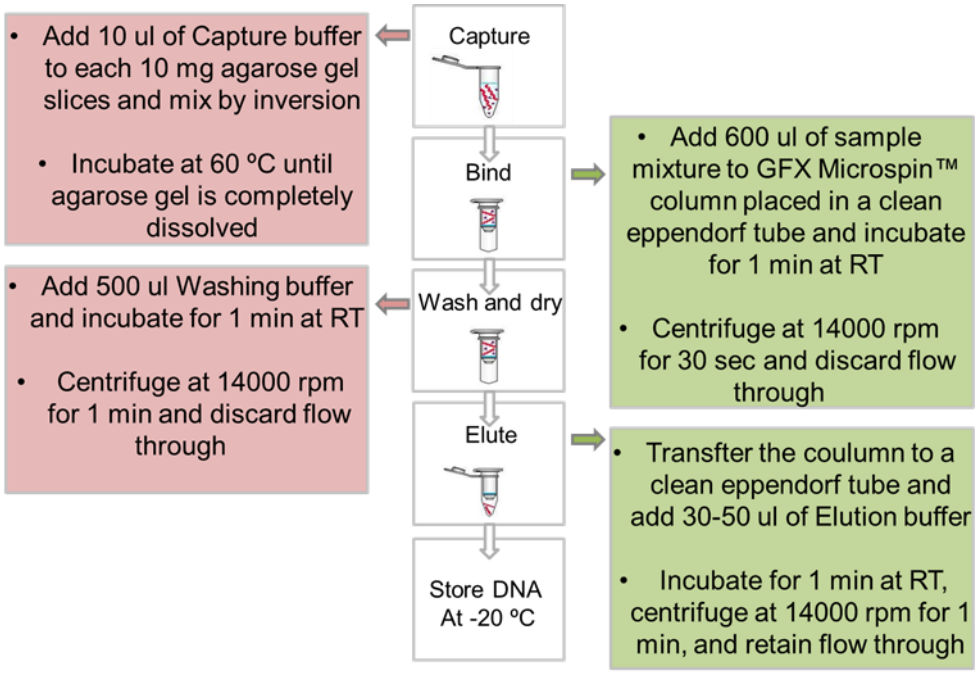


Figure 2-3: DNA extraction from agarose gel using the illustra™ GFX™ PCR DNA and Gel Band Purification Kit. All centrifugation was performed at room temperature.

2.2.2.4 Polymerase chain reaction (PCR)

All standard PCR were performed using a thermal cycler (Applied Biosystems). PCR was performed in a 50-µl reaction system containing 1 µl DNA template (0.5 µg), 1 µl *Taq* DNA polymerase (Qiagen #201205), 10 µl 10× reaction buffer (Qiagen), 1 µl 0.25 mM dNTPs (Qiagen #201913), 1 µl forward and reverse primer (final concentration, 1 µM) and 34 µl sterile PCR-grade water (Sigma-Aldrich, W1754). DNA sequences containing digestion sites for the restriction endonucleases *Xho*I and *Sal*I were designed for the external forward (HP1BP3-Fwd) and reverse primers (HP1BP3-Rev), respectively.

The typical PCR cycling conditions are outlined in Table 2-7. Briefly, the annealing temperature was changed according to the purpose of the reaction and the melting temperature (Tm) of the primers, and was 5°C below the lowest primer Tm. The extension time was determined according to the length of the target gene (amplicon), typically 1 min per kb DNA.

Table 2-7: Cycling parameters for standard PCR.

Cycle Steps	Temperature (°C)	Time	Number of cycles
Initial Denaturation	94	4.0 minutes	1
Denaturation	94	40 seconds	39
Annealing	52-62	40 seconds	39
Elongation	72	1.5 minute	39
Final Elongation	72	10.0 minutes	1
Cooling	4	∞	–

2.2.2.5 Overlapping PCR

In this study, the overlapping PCR (Heckman and Pease, 2007) was used to create a specific point mutation (AA) or internal deletions (D1 or D2) in the *HP1BP3* gene sequence corresponding to the predicted GSK-3β phosphorylation site/s (*Appendix* 1 and 2). An overlapping PCR consists of two main steps: 1) Two separate PCR (PCR1 and PCR2) to amplify two

separate DNA fragments (A and B); 2) Fusion of Fragment A and B and PCR (PCR3) for elongation resulting in Fragment C with either a point mutation (Figure 2-5) or deletion (Figure 2-4).

The PCR conditions used are described in Table 2-7. The annealing temperature of 58°C was used in PCR1 and PCR2, whereas temperatures between 52°C and 62°C were used in PCR3. The primers stated here are examples for describing the overlapping PCR method. The primer sequences used in this method to amplify Fragment A, B or C are described in Section 2.1.4. Generally, specific external and internal primers were used for each modification made (point mutation or deletion). A forward external primer (OL1-F) and reverse internal primer (OL4-R) were used to amplify Fragment A (N-terminal fragment). Another reverse external primer (OL2-R) and forward internal primer (OL3-F) were used to amplify Fragment B (C-terminal fragment). The internal primers (OL3-F and OL4-R) containing the desired mutation share complementary ends and hybridise to the region to be modified. These primers facilitate the recombination of the amplified fragments (A and B), where the ends of the fragments have complementary sequences generated by OL3-F and OL4-R, allowing the hybridisation of A to B during PCR3 and producing the final product (Fragment C) with the desired point mutation (Figure 2-5) or creating a deletion (Figure 2-4). The appropriate restriction sites (*Xho*I and *Sal*I) were also added to the 5′- end of the external primers to facilitate the cloning of the final PCR product (Fragment C) into the peGFP-C_2 vector.

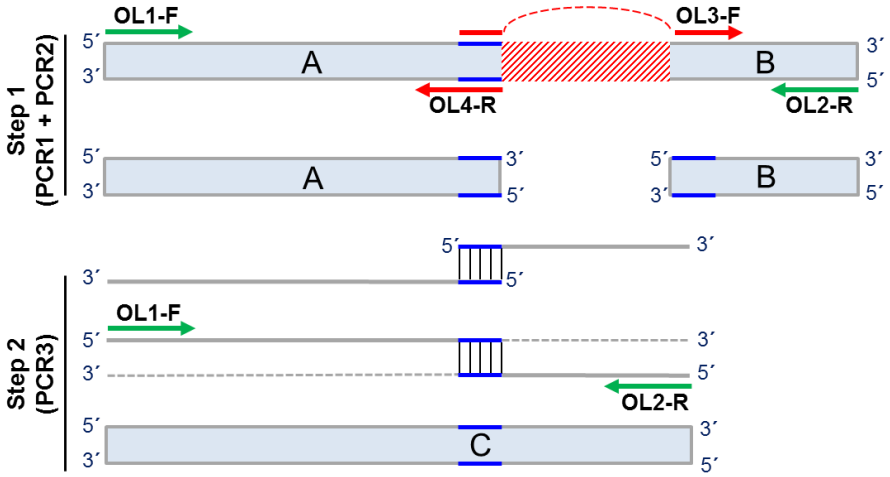


Figure 2-4: Overlapping PCR for creating deletion mutation. A representation of the overlapping PCR method: in Step 1, Fragment A and B (N- and C-terminal domains) are amplified by PCR1 and PCR2, respectively. These PCR products were then used as a template in Step 2, i.e. PCR3, to create a mutated DNA fragment (Fragment C) with a distinct deleted sequence (box with red diagonal lines). Green arrows, external primers; red arrows, internal primers.

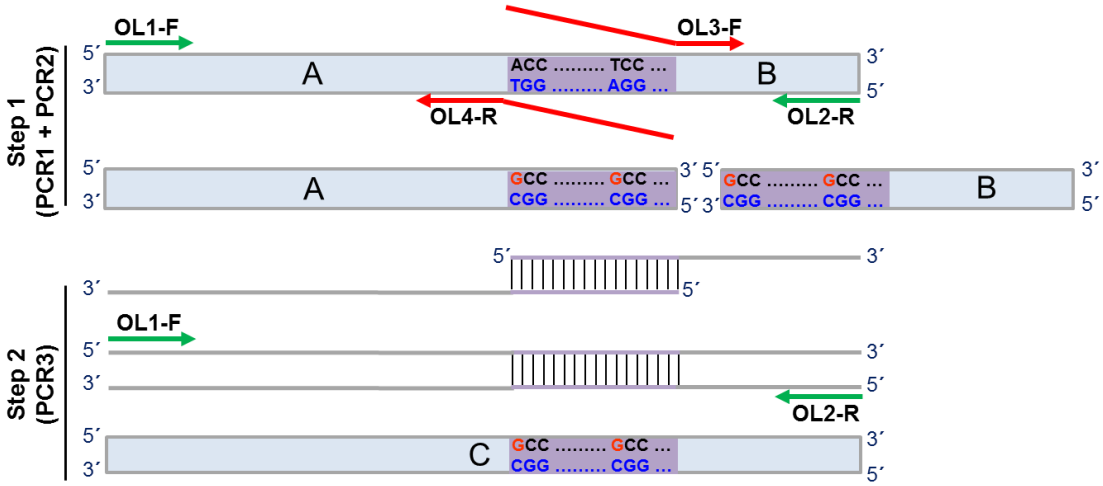


Figure 2-5: Overlapping PCR for creating point mutation [Threonine (ACC) and Serine (TCC) are substituted with Alanine (GCC)]. A representation of overlapping PCR technique: in Step 1, Fragment A and B (N- and C-terminal domains) are amplified by PCR1 and PCR2, respectively, and used as a template for Step 2, i.e. PCR3, to create the mutated DNA fragment (Fragment C) with a distinct point mutation (purple box). Green arrows, external primers; red arrows, internal primers.

Fragments A and B were electrophoresed on 1 % agarose gel (Section 2.2.2.2) and the expected DNA bands were extracted and purified as described in Section 2.2.2.3 (*Appendix* 1 and 2). Small amounts of the gel-purified Fragment A and B were used as a template for PCR3. Finally, 2–3 µl of the Fragment C was run on 1 % agarose gel to authenticate the amplification of the recombinant DNA (*Appendix* 1 and 2). The remaining amount of the fragment C was digested by *Xho*I and *Sal*I, (Section 2.2.2.1) and then extracted from the enzymatic digestion reaction as described in Section 2.2.2.3. Then, the purified recombinant product was cloned into the peGFP-C_2 vector as described in Section 2.2.2.6.

2.2.2.6 Ligation and bacterial transformation

Sticky- (cohesive-) end ligation was used throughout this study. Digested DNA purified from the agarose gel was ligated to a linearised vector with T4 DNA ligase (NEB, #M0202S). For ligation, pre-digested DNAs for both plasmid backbones and inserts (usually 1:7 ratio) were combined in a sterile 1.5 ml Eppendorf tube containing 1× T4 DNA ligase buffer (NEB, #B0202S) and 2 µl T4 DNA ligase. Sigma water was added to obtain a final volume of 20 µl per reaction and the tubes were incubated overnight at 4°C. The ligated/recombinant DNA was then introduced into bacterial cells by transformation (Section 2.2.1.1) to amplify the new recombinant plasmid DNA. A volume of 10 µl was transformed into 100 µl chemically competent cells according to the procedure outlined in Section 2.2.1.1. Following transformation, the bacterial culture was poured and spread over the surface of LB agar plates containing relevant selective antibiotic [kanamycin (30

µg/ml) or ampicillin (50 µg/ml)]. The plates were covered and left at room temperature for 10 min (to allow absorption of the liquid by the agar), then incubated at 37°C overnight. To check self-ligation of backbone vector or uncut vector, a double restriction enzymes digested DNA vector-only reaction (negative control), as outlined above. Following incubation, 10–15 colonies were picked and regrown overnight at 37°C in LB medium. Finally, the ligated plasmid DNA was extracted and amplified using the Miniprep (Section 2.2.1.3) or Midiprep (Section 2.2.1.4) and finally confirmed by enzymatic digestion (Section 2.2.2.1) and sequencing analysis.

2.2.2.7 DNA nucleotide sequence verification by sequencing

Following confirmation by enzymatic digestion, the DNA sequence of the recombinant constructs and/or purified PCR products was reconfirmed by automated DNA sequencing. About 10 µl DNA (50 ng/µl) and 15 µl forward and/or reverse primers (10 µM) were sent to the Queen's Medical Centre (QMC) DNA sequencing facility (University of Nottingham). The sequencing results were analysed using Chromas Lite v2.01 software (*http://www.softpedia.com/get/Science-CAD/Chromas-Lite.shtml*).

Furthermore, the protein expression of all plasmid clones were validated by the western blotting analysis as described in Section 2.2.4.

2.2.3 Cell culture

All cell culture work was performed in a class II biological safety cabinet to maintain aseptic conditions. In Dr Nateri's lab, we regularly check cells for mycoplasma contamination with MycoAlert™ Mycoplasma Detection Kit from Lonza, according to the manufacturer's protocol.

2.2.3.1 Cell line maintenance and culture

HCT116 and DLD-1 cell lines [with FBXW7 deletion (-/-) and *FBXW7* wild-type (+/+) alleles], and Tiger cell lines were grown in T75 flasks (Costar) in complete RPMI 1640 medium (Sigma-Aldrich, R0883) supplemented with 10 % fetal bovine serum (FBS, Sigma-Aldrich, F7524), 2.0 mM L-glutamine (Invitrogen, 25030-081) and 100 units/ml penicillin/streptomycin (Invitrogen, 15140-122). MEFs were also cultured in T75 flasks in Dulbecco's modified Eagle's medium (DMEM, Sigma-Aldrich, D5671) supplemented with 10 % FBS, 2.0 mM L-glutamine, 100 units/ml penicillin/streptomycin, 0.1 mM 2-mercaptoethanol (Invitrogen, 31350-010), 1 % MEM non-essential amino acids (Invitrogen, 11140) and 1 mM sodium pyruvate (Invitrogen, 11360). $MEF^{wild\text{-}type}$ differed from MEFs with deletion (-/-) of *Suv39h1* and *Suv39h2* alleles in that the flasks of the latter were coated with 1 % gelatine (Sigma-Aldrich, G7765) to maintain the MEFs in good condition. The MEFs with deletion alleles were culture in DMEM (Sigma-Aldrich, D5671) supplemented with 10 % FBS, 2.0 mM L-glutamine, 100 units/ml penicillin/streptomycin, 0.1 mM 2-mercaptoethanol (Invitrogen, 31350-010), 1 % MEM non-essential amino acids (Invitrogen, 11140) and 1 mM sodium pyruvate (Invitrogen, 11360).

All cell lines were maintained at 37°C in a humidified incubator (Sanyo) supplied with 5 % CO_2. The cell monolayer confluence was checked and the colour of the medium was observed to determine the cell growth state; confluence was maintained at ~70–80 %. Old medium was replaced with the fresh complete medium every other day for subconfluent flasks, whereas subculturing (passaging) was performed for any cell line that reached high confluence, i.e. ~80–90 %. Cells were detached from the surface of the flask by aspirating the consumed medium, then rinsing the cells with 4 ml sterile phosphate-buffered saline (PBS, Sigma-Aldrich, D8537), and then 2 ml 1× trypsin/EDTA (ethylenediaminetetraacetic acid, Sigma-Aldrich, T3924) was added to the flask. After 5–10-min incubation at 37°C in a CO_2 incubator, 10 ml fresh complete medium was added to the cells to stop the trypsinisation. Next, the cells were pelleted by centrifugation for 5 min at 1500 rpm. Then, 10 ml fresh medium was added to the cell pellet and 1.5–3 ml resuspended cells was maintained in a T75 flask containing 8–10 ml fresh complete growth medium for further experiments. The trypsinised cells were diluted to the preferred concentration in complete medium based on the cell type and culture confluence, and subcultured into sterile tissue culture flasks.

2.2.3.2 Cell counting

The cell concentration/number was counted using a Neubauer haemocytometer (Marienfeld-Superior, Germany) with trypan blue viability dye (Sigma-Aldrich, T8154), which is not absorbed by healthy viable cells. Trypsinised cells were pipetted up and down to disrupt any cell clumps present. Then, 50 µl cell suspension was transferred to a new Eppendorf tube

containing 50 µl trypan blue. After mixing, about 10 µl cell/trypan blue mixture was loaded to the haemocytometer slide and the cells were counted in the four large corner squares of the slide (each large square is divided into 16 smaller squares) (Figure 2-6) under ×10 objective magnification. The principle of haemocytometer counting is that the total cell concentration per ml is equal to the number of cells in one large square multiplied by 10^4 per ml. The cell concentration was calculated using the following equation:

$$\text{Cell concentration (cell/ml)} = \frac{Xt}{4} * 2 * 10^4$$

Where;
Xt is the total number of cells counted,
4 is the number of squares counted,
2 is the dilution factor.

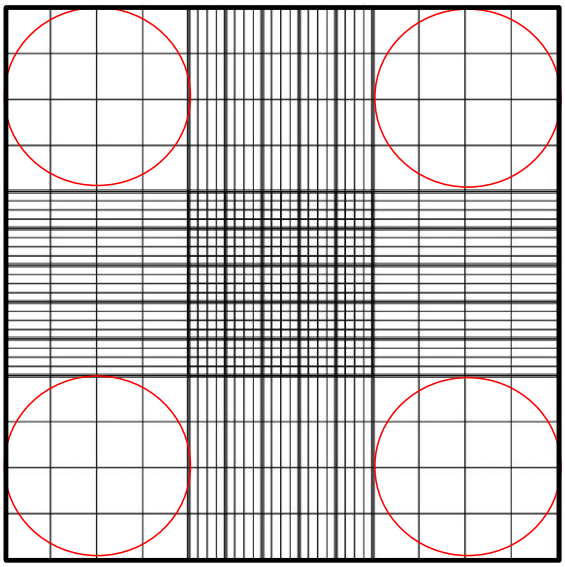


Figure 2-6: The Neubauer haemocytometer slide grid layout. Red circles indicate the four corner squares in which the cells were counted.

2.2.3.3 Freezing and thawing cells

Cells were frozen in 10 % dimethyl sulfoxide (DMSO, Sigma-Aldrich, D4540) + 90 % FBS for storing. First, the cells were trypsinised as described in Section 2.2.3.1, pelleted by centrifugation at 1500 rpm for 5 min and then resuspended in 90 % FBS containing 10 % DMSO. The mixture transferred into the cryotube, and it was stored overnight at −80°C, and then placed in the liquid nitrogen tank for long-term storage.

To thaw cells from frozen stocks, cells defrosted quickly in a 37°C water bath, and transferred to 10 ml pre-warmed complete medium. Following centrifugation at 1500 rpm for 5 min the freezing medium removed and cells were resuspended in 10 ml fresh medium, seeded in T75 flasks and incubated at 37°C in a 5 % CO_2 incubator.

2.2.3.4 Transient transfection

Mammalian cell line transfection with DNA plasmids (Table 2-1) was carried out using Lipofectamine 2000 transfection reagent (Invitrogen, 11668-019) in accordance with the manufacturer's instructions. Depending on the nature of the experiment, cells were seeded in either 6-well or 10 cm^2 plates and incubated overnight in complete growth medium at 37°C to 60–70 % confluence. As soon as cells had reached the desired confluence (40–70 %), 4–10 µg plasmid DNA (depending on the plate size) was added to 250 µl Opti-MEM® Reduced-Serum Medium (Invitrogen, 31985-047). In another sterile Eppendorf tube, 10–20 µl transfection reagent was diluted in 250 µl Opti-MEM and incubated for 5 min at room temperature. Then, the contents

of the two Eppendorf tubes were combined, mixed gently and incubated for 15 min at room temperature to form transfection complexes. In the meantime, the complete growth medium of the cultured cells was aspirated and the cells were carefully rinsed with Opti-MEM to remove any remaining serum-containing medium that might interfere with efficient transfection. Then, the transfection mixture was added gently to the cells and incubated at 37°C for 6–7 h before being replaced with complete fresh medium. The transfected cells were incubated for 36 h before use.

2.2.3.5 Generating of cell lines stably over-expressing GFP (control) and GFP-HP1BP3 proteins

Two stable cell lines were generated in this study. The *HP1BP3* gene was permanently integrated into the cell genome by using eGFP or eGFP-HP1BP3 DNA plasmids expressing a Puromycin resistance gene to generate HCT116$^{FBXW7(+/+)}$ and Tiger cell lines stably expressing HP1BP3 (Chapter 4; Section 4.2.1).

About 18 h prior to the start of the procedure, 5×10^5 cells in fresh complete medium were plated in three wells on a 6-well plate. Furthermore, duplicate wells were used for each plasmid construct. The third well contained untransfected cells that served as the control for Puromycin selection. After overnight incubation, the cells at 60–70 % confluent, were transfected with eGFP or eGFP-HP1BP3 plasmids as outlined in Section 2.2.3.4. After 36-h transfection, the transfection medium was replaced with the fresh complete medium containing 3 μg/ml Puromycin (Sigma-Aldrich, P8833). The 3

μg/ml concentration was selected because it was sufficient for killing all of the untransfected cells (in the control well). Puromycin-containing medium for the plated cell lines was replaced every other day for 2 weeks or until resistant colonies were observed.

After Puromycin-resistant colonies appeared, single Puromycin-resistant cells were plated in 96-well plates and maintained in complete medium containing 3 μg/ml Puromycin for 3–4 days to ensure that only Puromycin-resistant cells were plated. Then, the medium was replaced with fresh complete medium and the cells were maintained in culture to expand and mark Puromycin-resistant clones. Proteins extracted from the Puromycin-resistant clones (3 clones) were prepared for western blot analysis to validate the single cell-derived colonies are over-expressing of eGFP or eGFP-HP1BP3 proteins respectively.

2.2.3.6 The drugs used for the biochemical analysis in cell culture

To test the influence of GSK-3β inhibition on HP1BP3 phosphorylation, SB-216763 (a selective GSK-3β inhibitor; Sigma-Aldrich, S3442) was prepared according to the manufacturer's instructions and incubated with the culture (at a final concentration of 10 μM) for 6 h at 37°C. Then, western blotting was performed as described in Section 2.2.4.

2.2.4 Immunoblotting and protein processing

2.2.4.1 Protein extraction and quantification

To lyse the cells and extract the cellular protein, the cells were initially washed with ice-cold PBS in the 10 cm^2 culture dishes or 6-well plates. Then, 250–750 µl RIPA buffer supplemented with 1× protease inhibitor cocktail (Sigma-Aldrich, P8340) was added to the wells after the PBS had been discarded. The cells were agitated for 20 min at 4°C to ensure complete lysis. The lysate was then purified and collected in fresh, sterile Eppendorf tubes following centrifugation at ≥13000 rpm for 10 min at 4°C. The supernatant (protein extract) was aspirated and placed in a set of new tubes and stored at −80°C.

Total protein concentrations were measured using a Bradford Assay Kit for Protein Quantification (Sigma-Aldrich, B6916) in accordance with the manufacturer's instructions. All available samples were diluted in distilled water (1:20 or 1:40, depending on the expected protein concentration) in a new set of Eppendorf tubes. Diluted samples (20 µl) were placed separately in triplicate in 96-well microplates (Scientific Laboratory Supplies). A protein standard series was prepared using bovine serum albumin (BSA, Sigma-Aldrich, 4503) diluted with distilled water to final concentrations of 0 (blank), 100, 300, 500, 800 and 1000 µg/ml. Each BSA standard (20 µl) was added to the microplate wells. Subsequently, 200 µl diluted Bradford reagent (1:5) was added to all wells containing standard or sample. The microplate was incubated for 5 min at room temperature and then shaken for 10 sec before the protein concentration was measured.

The spectrophotometer was adjusted to the microplate reader (Bio-Rad) to measure the absorbance of the standard solutions and the unknown samples at 595 nm (absorbance values = A_{595}). The average concentration of extracted protein per sample was calculated using a standard curve in which the A_{595} values of the standard solutions were presented on the Y-axis while their concentrations were presented on the X-axis. Then, the isolated proteins were stored at −80°C prior to use.

2.2.4.2 Sodium dodecyl sulfate–polyacrylamide gel electrophoresis (SDS-PAGE) and western blotting

Mini-PROTEAN Tetra Cell® (Bio-Rad, 1658004), a vertical mini gel electrophoresis system, was used for western blot analysis. According to the guidelines in Table 2-8, 8 %, 10 % or 15 % resolving gel (10 ml), comprising the bottom portion of the SDS-PAGE system, and 5 % stacking gel (4 ml), which comprised the upper portion of the system, were assembled from the reagents listed in Table 2-9. Gels were cast between two 7 × 8.5 cm glass plates in a gel casting frame and allowed to solidify for 20–30 min. Meanwhile 100–250 µg total protein from the samples was mixed with 5× loading buffer containing SDS (Table 2-5) and denatured at 95°C for 4 min. Eppendorf tubes containing denatured proteins were cooled on ice for 5 min and then loaded into the SDS-PAGE wells created using a Teflon comb. To determine the molecular mass of the protein bands, 5 µl Precision Plus™ Dual Color Protein ladder, Broad Range (10–250 kDa) (Bio-Rad, 1610374) was run beside the samples (Figure 2-7).

Electrophoresis was performed at 100 V for 2 h in 1× Tris/glycine/SDS (TGS) running buffer (Bio-Rad, 161-0772) to allow proteins to move through the gels. After the SDS-PAGE was completed, a polyvinylidene difluoride (PVDF) membrane (GE Healthcare, RPN303F) was activated by 100 % methanol for 30 sec. Then, the gel was carefully removed from the glass plates and placed in a semi-dry electrophoretic transfer cell (Bio-Rad) at 15 V for 30 min, where the electrophoretically separated proteins were transferred to the PVDF membrane. The membrane and filter papers were incubated in transfer buffer (Table 2-5) for 15 min before the semi-dry transfer. The transfer cell, comprising filter paper, gel, membrane and a second piece of filter paper, was sandwiched together and air bubbles were removed by gently rolling a rolling pin on the surface of the filter paper on the platform of the transfer cell. Subsequently, the membrane was removed and blocked with 3 % dried milk (GE Healthcare, CPK1075) or 3 % BSA (for phosphorylated proteins), dissolved in Tris-buffered saline (TBS) (Table 2-5) containing 0.1 % Tween 20 (Sigma-Aldrich, 1379) (TBS-T) for 1 h at room temperature, and then incubated with the primary antibodies (Table 2-2) overnight at 4°C. The next day, the membrane was washed with 5 ml TBS-T buffer three times at 7 min per wash, and incubated with the secondary antibody (Table 2-3) for 1 h at room temperature. The immunostained cells were then washed four times with the washing buffer for 10 mins each. Lastly, bands corresponding to protein–antibody complexes were detected using enhanced chemiluminescence (ECL) detection reagent (GE Healthcare, RPN2135). The chemiluminescent signal was visualised by an Odyssey Fc Imaging System (LI-COR Biosciences, UK) according to the

manufacturer's guidelines. Then, the membrane washed and reprobed with anti- β-actin or H3 primary antibodies as loading controls.

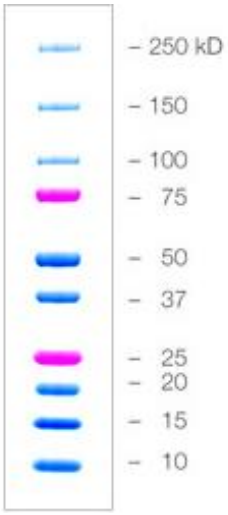


Figure 2-7: The Precision Plus™ Dual Colour Protein ladder used for western blotting analysis. Broad Range (10–250 kDa).

Table 2-8: Solutions for 8–15 % resolving gels for SDS-PAGE.

Solution components	Component volumes per gel mold volume of			Cat. No.
	10 ml	15 ml	20 ml	
8%				
Distilled H_2O	4.6	6.9	9.3	-
30% acrylamide mix	2.7	4.0	5.3	A3699
1.5 M Tris, pH 8.8	2.5	3.8	5.0	T9650
10% SDS	0.1	0.15	0.2	L3771
10% Ammonium persulfate	0.1	0.15	0.2	A9164
TEMED	0.006	0.009	0.012	T7024
10%				
Distilled H_2O	4	5.9	7.9	-
30% acrylamide mix	3.3	5.0	6.7	A3699
1.5 M Tris, pH 8.8	2.5	3.8	5.0	T9650
10% SDS	0.1	0.15	0.2	L3771
10% Ammonium persulfate	0.1	0.15	0.2	A9164
TEMED	0.004	0.006	0.008	T7024
15%				
Distilled H_2O	2.3	3.4	4.6	-
30% acrylamide mix	5.0	7.5	10.0	A3699
1.5 M Tris, pH 8.8	2.5	3.8	5.0	T9650
10% SDS	0.1	0.15	0.2	L3771
10% Ammonium persulfate	0.1	0.15	0.2	A9164
TEMED	0.004	0.006	0.008	T7024

Note: All chemicals were purchased from Sigma-Aldrich.

Table 2-9: Solutions for 5 % stacking gels for SDS-PAGE.

Solution components	Component volumes per gel mold volume of		
	4 ml	6 ml	8 ml
Distilled H_2O	2.7	4.1	5.5
30% acrylamide mix	0.67	1.0	1.3
1.5 M Tris, pH 6.8	0.5	0.75	1.0
10% SDS	0.04	0.06	0.08
10% Ammonium persulfate	0.04	0.06	0.08
TEMED	0.004	0.006	0.008

Note: All chemicals were purchased from Sigma-Aldrich.

2.2.5 Immunofluorescence (IF) staining

IF is used to detect and visualise the expression pattern and distribution of a specific protein within the cell compartment (Weber et al., 1975). The main principle is to visualise the antigen–antibody complex. In this study, indirect IF labelling was used. According to the IF protocol, a primary antibody specific to the protein of interest is applied, followed by the addition of a fluorescent dye–labelled secondary antibody directed against the immunoglobulin of the host species in which the primary antibody was raised. The IF staining protocol comprises several steps, as detailed below:

2.2.5.1 Cell preparation

Cells were trypsinised and counted as described in Section 2.2.3.1 and 2.2.3.2. Depending on the experiment, ≈60,000 or 120,000 cells per well were selected and cultured on coverslips in 6-well plates and incubated at 37°C. Initially, the coverslip was sterilised with 70 % ethanol and washed three times with PBS. Subsequently, the PBS was discarded and the well was washed with complete growth medium before the cells were seeded in the plate.

2.2.5.2 Fixation and permeabilisation

The growth medium was aspirated and the cells were washed twice in PBS and fixed by 30-min incubation with 4 % paraformaldehyde (PFA) (Avocado, 043368) (diluted from 16 % stock solution with PBS) at room temperature. Fixation is required to prevent further degradation of the cellular

proteins. Then, the PFA was aspirated and the cells were washed twice in PBS at 5 min per wash. Subsequently, the cells were incubated in 800 µl permeabilisation solution (0.1 % Triton X-100 diluted in PBS) for 30 min (to generate pores in the cell membrane to allow antibodies to be delivered to the cell interior) and washed twice with PBS at 5 min per wash.

2.2.5.3 Blocking and immunostaining

To prevent non-specific antibody interactions, the permeabilised cells were blocked by 1-h incubation in 500 µl blocking solution containing 3 % BSA in PBS at room temperature. Following this, the cells were washed once with PBS for 5 min and incubated overnight at 4°C with 300 µl primary antibody (prepared in 2 % BSA) at the dilution outlined in Table 2-2. The negative control was incubated with 2 % BSA only. After overnight incubation, the cells were washed four times with washing buffer containing 1 % BSA and 0.1 % Tween 20 in PBS at 10 min per wash. Then, 300 µl secondary antibody (prepared in 2 % BSA) was added at the dilution outlined in Table 2-3, for 1 h at room temperature. As the secondary antibodies were fluorescently labelled and hence light-sensitive, their addition and subsequent procedures were performed in a dark room and the 6-well plate was wrapped in aluminium foil immediately after the secondary antibody had been added. Then, the cells were washed five times with washing buffer at 10 min per wash. Subsequently, the coverslips were removed gently from the 6-well plate using forceps and placed on a sterilised slide with ~15 µl ProLong® Gold Antifade Reagent with DAPI (Invitrogen, P-36931). Then, the edges of the coverslips were sealed using clear nail varnish, and incubated at room

temperature overnight before images were captured with a DMI3000 B inverted microscope (Leica Microsystems).

2.2.5.4 Phalloidin staining

Phalloidin is a commonly used dye for the morphological analysis. It can bind F-actin and display the shape and structure of the cell. The initial step of Phalloidin staining is similar to the IF protocol in which the cells were grown on coverslips, fixed, and permeabilised with 0.1 % Triton X-100 (Section 2.2.5.1 - 2.2.5.3). After permeabilisation, cells were incubated with diluted (50 µg/ml, in PBS) fluorescent Phalloidin conjugate solution (Sigma-Aldrich, 1951) for 40 min in dark. The stained cells were washed 2-3 times in PBS for 5 min at room temperature then the coverslips were removed, mounted and analysed with the Leica microscope as described above (Section 2.2.5.3).

2.2.6 Cell cycle analysis

Cell cycle analysis for the mouse and human cell lines was performed using Propidium iodide (PI, Sigma-Aldrich, P4864) staining to enable the assessment of their cell cycle phase distribution (Chapter 5) and as described previously (Babaei-Jadidi et al., 2011a). PI is fluorescent molecule with a molecular mass of 668.4-Da (g/mol) intercalating agent that stains double-stranded DNA. The cells were washed, trypsinised, and collected by centrifugation at 1200 rpm for 5 min. After washing twice in 2 ml cold PBS, the cells were transferred to fluorescence-activated cell sorting (FACS) tubes. Prior to the assay, the cells were counted and sufficient cells were added to the FACS tubes (3×10^4 to 7×10^4 cells/tube). Then, the cells were pelleted by centrifugation at 1500 rpm for 5 min and the cell-free supernatant was decanted carefully, and the pelleted cells were fixed in 1 ml cold 70 % ethanol added dropwise to the tube while vortexing gently, and incubated at −20°C for 15 min. Then, the cells were spun down by centrifugation at 1200 rpm for 5 min, washed twice with cold PBS, stained with 300 µl of PI solution (50 µg/ml), treated with 100 µg/ml RNase (Sigma-Aldrich, R4875) for 30 min and analysed by FACS. RNase was added to the PI–cell mixture to avoid PI binding to RNA. The FACS tubes were kept on ice and cell cycle distribution was assessed using a FC500 Flow Cytometer. Then, the obtained data were analysed using WEASEL software version 1 (*http://www.frankbattye.com.au/Weasel/*).

2.2.7 Double thymidine and thymidine-nocodazole synchronisation

To determine the influence of HP1BP3 on cell cycle progression, normal and CRC cells were synchronised at the G1/S border or mitosis using double thymidine (DNA synthesis inhibitor) (Whitfield et al., 2000) or thymidine-nocodazole (Stoeber et al., 2001; Whitfield et al., 2002), respectively (Chapter 5). Initially, two sets of cells (flow cytometry and western blot analysis) were cultured in 10 cm^2 plates and incubated overnight in complete growth medium at the 35–40 % confluence. The experiment was controlled by designating one 10 cm^2 plate as the untreated (asynchronous) control in parallel. The old medium in the experimental plates was replaced with fresh complete medium containing 2 mM thymidine (Sigma-Aldrich, T1865) and were then incubated at 37°C for 18 h (double thymidine experiment) or 24 h (thymidine-nocodazole experiment).

Next, we washed the cells twice with PBS and released in standard growth medium by incubation for 9 h (double thymidine experiment) or 3 h (thymidine-nocodazole experiment). After that, the growth medium was replaced with medium containing 2 mM thymidine (double thymidine experiment) or 100 ng/ml nocodazole (Sigma-Aldrich, M1404, thymidine-nocodazole experiment). The cells were then incubated for 15 h in thymidine or 12 h in nocodazole. The cells were later released from the treatment by PBS washing and collected over 0 h, 4 h, 8 h, 12 h and 24 h. The first set of cells was fixed and stained for cell cycle analysis as described in Section 2.2.6 while the second set was lysed for western blotting analysis to

explore the expression changes occurred for mitotic and epigenetic-related proteins.

2.2.8 Statistical analysis

The statistical analysis carried out by the Student's *t*-test using Microsoft Office Excel. All experiments were carried out in triplicate, repeated at least 2-3 independent times and results are presented as the mean ± standard deviation (STDEV), unless stated otherwise. *P* value ≤ 0.05 (*) was considered statistically significant, P ≤ 0.01 (**) highly significant and P ≤ 0.001 (***) very highly significant.

CHAPTER 3

Regulation of Chromatin by HP1BP3 via the HP1BP3/HP1α/H3K9me3 Complex in Fibroblast and CRC Cell Lines

3.1 Brief introduction

Currently, most studies are focused on epigenetic post-translational histone modifications (methylation, acetylation, sumoylation, phosphorylation etc.), which create an epigenetic mechanism for regulating a variety of normal and tumour-related processes (Carlberg and Molnár, 2014; Soshnev et al., 2016). These modifications may influence the core histones in euchromatin/heterochromatin transition, but the identity of the heterochromatin proteins and their partners has remained largely unclear. Moreover, the heterochromatin-associated proteins are also exposed to post-translational modifications that modulate their activity (Carlberg and Molnár, 2014; Hiragami-Hamada et al., 2011; Soshnev et al., 2016). Therefore, their levels must be closely controlled; otherwise, they may act as transcription modifiers through co-repressor(s) complexes and lead to stable gene silencing.

One of the most common means of limiting the expression of many proteins is to destroy them via the ubiquitin/proteasome pathway (Lecker et al., 2006; Tu et al., 2012). FBXW7 is an E3 ligase that targets several proto-oncogenes and transcriptional modulators for degradation, and it plays crucial roles in tumorigenesis (Babaei-Jadidi et al., 2011a; Cremona et al., 2016; Wang et al., 2012a; Welcker and Clurman, 2008). We identified HP1BP3 as substrate that is targeted by the *FBXW7* tumour-suppressor gene for ubiquitin-mediated degradation [(Babaei-Jadidi et al., 2011b); Li et al., in publication]. HP1BP3 is a heterochromatin-associated nuclear protein (Dutta et al., 2014a; Garfinkel et al., 2015b; Hayashihara et al., 2010a) that contains several

important domains, including glycogen synthase kinase-3β (GSK-3β) (T/SXXXS/TP) phosphorylation sites, three H15 (linker histone H1/H5 globular) domains, HP1α binding site, lysine rich-domain: Ubiquitin-binding domain, and nuclear localisation signal (NLS) (Chapter 1; Figure 1-17).

HP1BP3 binds directly to the heterochromatin protein HP1α (Garfinkel et al., 2015b; Hayashihara et al., 2010a), where trimethylated histone H3 lysine 9 (H3K9me3) recruits HP1α (Lachner et al., 2001). H3K9 trimethylation is mediated by SUV39H1/2 histone methyltransferases (Bártová et al., 2008; Lachner et al., 2001; Rea, 2000), and this complex is enriched in the establishment of constitutive heterochromatin (Maison et al., 2002; Maison et al., 2011; Schuhmacher et al., 2015). Moreover, H3K9me3 protects cells from genome instability (Peters et al., 2001), and HP1α modulation at chromatin inversion plays a significant role in normal homeostasis and cancer (De Koning et al., 2009; Kwon and Workman, 2011; Maison et al., 2002; Thomsen et al., 2011; Vad-Nielsen and Nielsen, 2015). More importantly, HP1BP3 binding to HP1α might be involved in the higher order of chromatin organisation. However, very little is known about HP1BP3, particularly the chromatin regulatory machinery and the function of the *HP1BP3* gene in normal and cancer cells; therefore, its function remains to be explored.

Herein, we show the HP1BP3 protein accumulation in colorectal cancer (CRC) cells lacking of *FBXW7* gene. Furthermore, our data indicates that the FBXW7 mediates the HP1BP3 degradation in a phosphorylation-dependent

manner through GSK-3β kinase activity. We also show that HP1BP3 upregulation caused by *FBXW7* loss, alters the heterochromatin states, by impairing the H3K9me3 methylation, rescuing the repression activity of HP1α in which it consequently leads to more transcriptional active chromatin structure by further stimulating the acetylated form of the same lysine 9 residue in histone H3 (H3K9ac).

3.2 Results

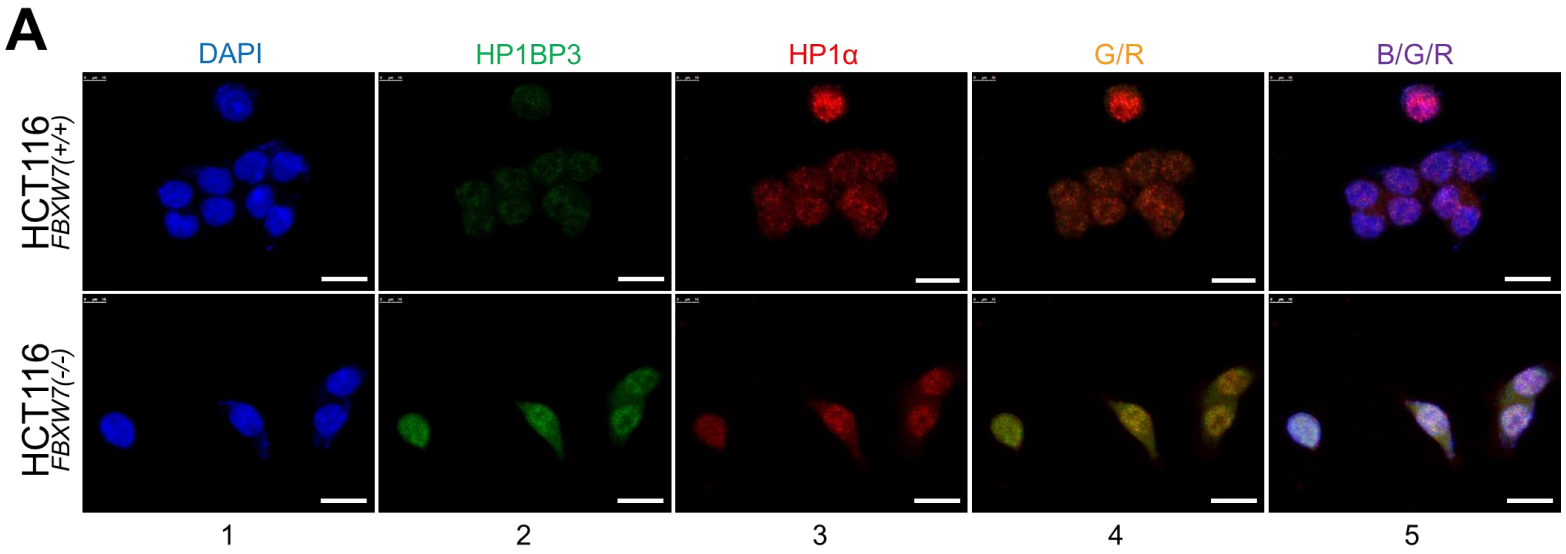
3.2.1 Loss of *FBXW7* leads to accumulation of HP1BP3 protein in human CRC HCT116 cells

The globular domain of HP1BP3 interacts with HP1α (Garfinkel et al., 2015b; Hayashihara et al., 2010a), and this complex interaction could play a role in the formation and/or maintenance of the compact chromatin structure. In addition, recent work from our laboratory suggested that, in murine systems, Hp1bp3 is targeted for degradation by SCF^{FBXW7}-ubiquitin proteasome activity, while *Hp1bp3* mRNA level unchanged. Accordingly, the initial experiment aimed at re-evaluating and confirming the accumulation of human HP1BP3 protein in human CRC cells lacking *FBXW7* alleles. To do this, we used HCT116 human colon cancer cells with the deletion and the wild-type *FBXW7* alleles, i.e. $HCT116^{FBXW7(-/-)}$ and $HCT116^{FBXW7(+/+)}$ cells, respectively (Babaei-Jadidi et al., 2011a). HP1BP3 and HP1α endogenous expression and co-localisation were examined by immunofluorescence as described in the Materials and Methods (Section 2.2.5).

Due to the lack of a commercially available antibody specifically cross-reacting and detecting the endogenous FBXW7 protein, validation of $HCT116^{FBXW7(-/-)}$ cells was carried out by reverse transcription PCR (RT-PCR) [performed by Dr F. Lorenzi in Dr Nateri's laboratory; (Lorenzi et al., 2016)]. We found that $HCT116^{FBXW7(-/-)}$ cells had upregulated HP1BP3 levels when compared to $HCT116^{FBXW7(+/+)}$ cells (Figure 3-1 A; Column 2). Despite

the reported interaction between HP1α and HP1BP3 (Garfinkel et al., 2015b; Hayashihara et al., 2010a), there was no change in HP1α levels and no effect on HP1α distribution between both cell lines (Figure 3-1 A; Column 3).

To further confirm the immunofluorescence data, HP1BP3 and HP1α expression levels were investigated using western blotting (Materials & Methods; Section 2.2.4). The western blotting also showed increased HP1BP3 expression levels in the HCT116$^{FBXW7(-/-)}$ cells (Figure 3-1 B), but HP1α expression levels were unchanged between the HCT116$^{FBXW7(-/-)}$ and HCT116$^{FBXW7(+/+)}$ cells (Figure 3-1 B). These findings suggest that increased levels of HP1BP3 expression do not affect HP1α levels and further confirms that the SCF^{FBXW7} activity can specifically target HP1BP3 for degradation.


A
DAPI
HP1BP3
HP1α
G/R
B/G/R
HCT116 FBXW7(+/+)
HCT116 FBXW7(-/-)
1
2
3
4
5

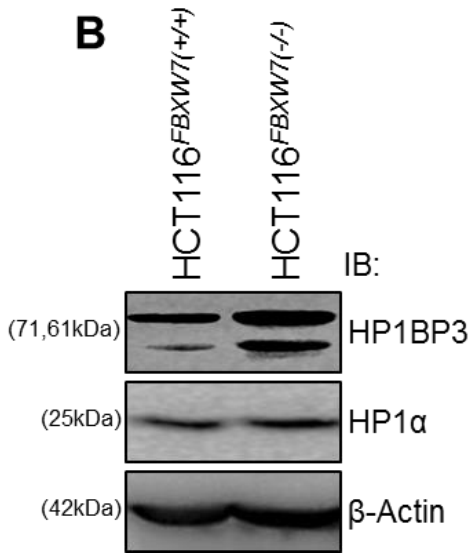


Figure 3-1: Upregulation of endogenous HP1BP3 protein expression in human CRC cells lacking of *FBXW7*. (A) HP1BP3 (green) and HP1α (red) proteins expression in HCT116$^{FBXW7(+/+)}$ and HCT116$^{FBXW7(-/-)}$ cell lines, examined by immunofluorescence technique. Scale bar is 20 μm. (B) Western blotting analysis for endogenous HP1BP3 and HP1α expression levels in HCT116$^{FBXW7(+/+)}$, and HCT116$^{FBXW7(-/-)}$. Cell lysate was extracted and total protein of 100 μg was run on 10 % SDS-PAGE and transferred to PVDF membranes. Anti-HP1BP3 and -HP1α antibodies were used to detect endogenous level of HP1BP3 and HP1α. β-Actin is used as a loading control in western blotting analysis. The level of HP1BP3 was increased in HCT116$^{FBXW7(-/-)}$ cells which confirm that HP1BP3 is targeted for degradation by FBXW7, but HP1α expression level was unchanged among HCT116$^{FBXW7(+/+)}$ and HCT116$^{FBXW7(-/-)}$ cell lines. Immunofluorescence and western blotting experiments were repeated in three different occasions. Control without primary showed no staining.

3.2.1.1 GSK-3β–mediated HP1BP3 phosphorylation can contribute to HP1BP3 stabilisation

GSK-3β phosphorylates the target substrates of FBXW7 (Cremona et al., 2016; Welcker and Clurman, 2008), which boosts the substrate binding to FBXW7 and stimulates target degradation by SCF^{FBXW7}-ubiquitin proteasome activity (Babaei-Jadidi et al., 2011a). Therefore, we wondered whether overexpressing the activated form of GSK-3β (Sundqvist et al., 2005) to potentially stimulate HP1BP3 phosphorylation would alter HP1BP3 levels as detected by western blotting (Figure 3-1 B).

To answer this question, HCT116 cells were transiently transfected with activated pFLAG-GSK-3β or pcDNA plasmid (Materials & Methods; Section 2.2.3.4) (Babaei-Jadidi et al., 2011a). pFLAG-GSK-3β plasmid was constructed and fully validated (by double restriction enzymes digestion and DNA sequencing) in Dr Nateri's lab. Both plasmids contained an *Eco*RI restriction site in their multiple cloning site (MCS) (Figure 3-2 A + B). Accordingly, *Eco*RI was used for plasmid validation and digestion (Materials & Methods; Section 2.2.2.1). *Eco*RI digestion produced DNA fragments corresponding to the control vector pcDNA (5.4 kb) and pFLAG-GSK-3β (6.6 kb) (Figure 3-2 C). The digested DNAs were run on 1 % agarose gel to confirm the linearization of the indicated DNA constructs (Materials & Methods; Section 2.2.2.2).

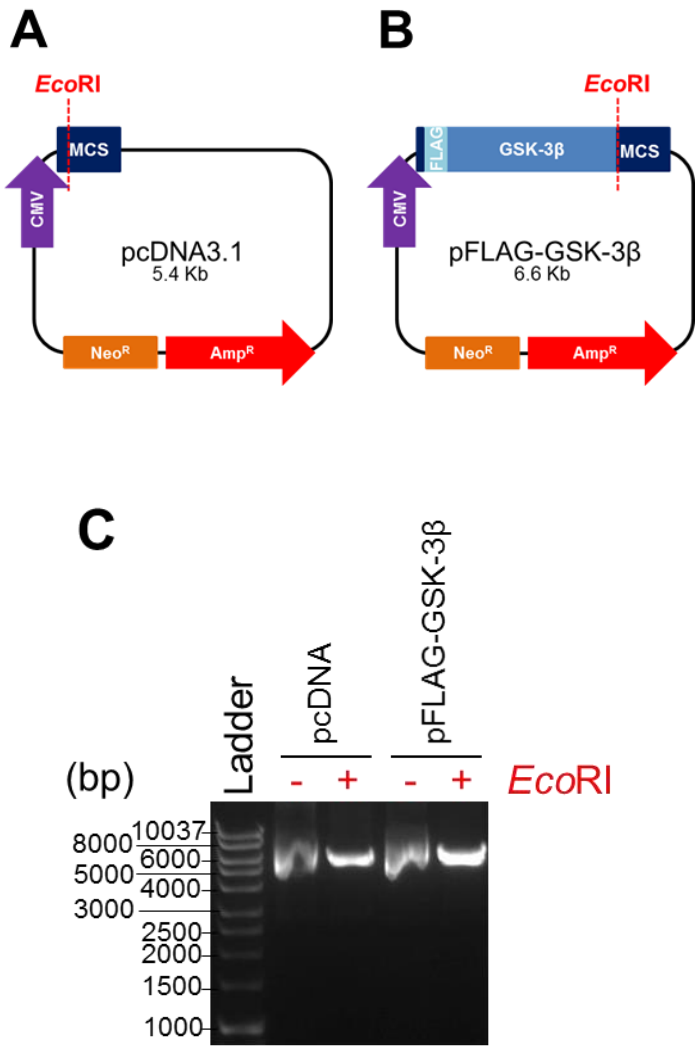


Figure 3-2: The pcDNA3.1 and pFLAG-GSK-3β plasmid maps, and validation analysis by restriction enzyme digestion. (A and B) Schematic presentation showing the control vector pcDNA3.1 and pFLAG-GSK-3β plasmid with *Eco*RI restriction enzyme sites. (C) The digested DNAs were run on 1 % agarose gel to confirm the linearisation of the plasmids.

The pcDNA plasmid was transfected in to HCT116 cells to serve as the control. After transfection, immunoblotting with anti-FLAG antibody was used to identify the expression of exogenous GSK-3β, and anti–GSK-3β antibody was used to detect the expression of both endogenous and

exogenous GSK-3β (Figure 3-3). Anti-HP1BP3 antibody was used to detect changes in endogenous HP1BP3 expression caused by GSK-3β overexpression (Figure 3-3). Interestingly, we found that the overexpression of activated (non-phosphorylated) GSK-3β decreased HP1BP3 expression (a and b isoforms) (Figure 3-3).

To further confirm that HP1BP3 is a potential substrate of GSK-3β, HCT116 cells were treated with the GSK-3β inhibitor SB-216763 (10 μM) or vehicle control dimethyl sulfoxide (DMSO) for 6 h (Materials & Methods; Section 2.2.3.6), and cell lysates were extracted for western blot detection of phosphorylated (P)-GSK-3β (inactive form) and HP1BP3. It is worth mentioning that phospho-specific HP1BP3 is still commercially unavailable for use, while the top band of HP1BP3, which was detected by anti-HP1BP3, could be the phosphorylated form of HP1BP3 protein (Figure 3-4), however further studies required to verify this. Previous studies have reported that SB-216763 causes upregulation in the phosphorylation of GSK-3β on Serine 9 which inhibits its activity (Dash et al., 2011; Guha et al., 2011; Park et al., 2009). Mechanistically, SB-216763 inhibits p90-RSK (Smith et al., 2001) and phosphatidylinositol 3-kinase (PI 3-kinase)/protein kinase B (PKB) (Cross et al., 2001), which inactivates GSK-3β by phosphorylating its serine 9 (De Mesquita et al., 2001; Sutherland et al., 1993). Consistent with these studies, the western blotting using an anti–(P)-GSK-3β antibody confirmed the SB-216763–mediated inhibition of GSK-3β activity (Figure 3-4). As expected, (P)-GSK-3β expression was upregulated (Figure 3-4). Excitingly, our results showed that GSK-3β suppression by SB-216763 treatment led to

significant and moderate accumulation of HP1BP3 a and b isoforms, respectively, in the HCT116 cells (Figure 3-4). Consequently, our results reveal possible HP1BP3 phosphorylation mediated by GSK-3β activity. However, this possibility requires additional evaluation and further examination using the site-directed mutagenesis based on overlapping PCR (Materials & Methods; Section 2.2.2.5), which was failed despite of many attempts in the last PCR step (*Appendix* 1 and 2), and kinase assay, to confirm the existence of amino acid residues in HP1BP3 that could be phosphorylated by GSK-3β.

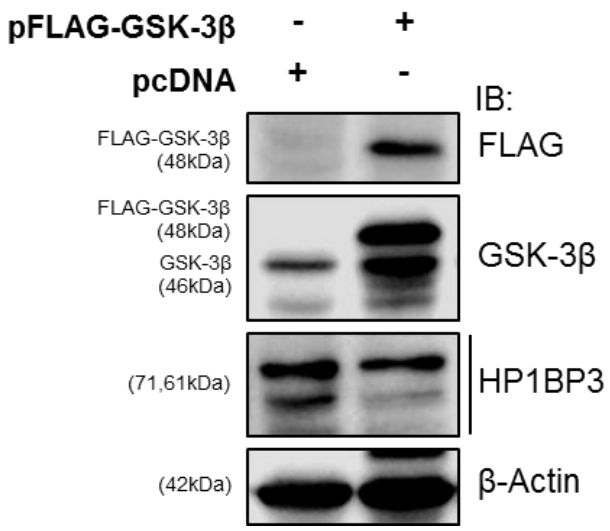


Figure 3-3: Induced phosphorylation by GSK-3β caused significant reduction in the HP1BP3 protein level in human HCT116 cells. Transient transfection of GSK-3β using pFLAG-GSK-3β in human HCT116 cells resulted in reduction HP1BP3 protein level compared to control cells which are not overexpressed with GSK-3β. Control cells were transfected with pcDNA backbone plasmid. Cell lysate was extracted and total protein of 50 µg (for anti-FLAG) or 100 µg (for anti- GSK-3β, -HP1BP3) was run on 10 % SDS-PAGE and transferred to PVDF membranes. Anti-FLAG, -GSK-3β, and -HP1BP3 antibodies were used to detect exogenous and/or endogenous level of FLAG, GSK-3β, and HP1BP3. β-Actin is used as a loading control in western blotting analysis. This experiment was repeated in two different occasions.

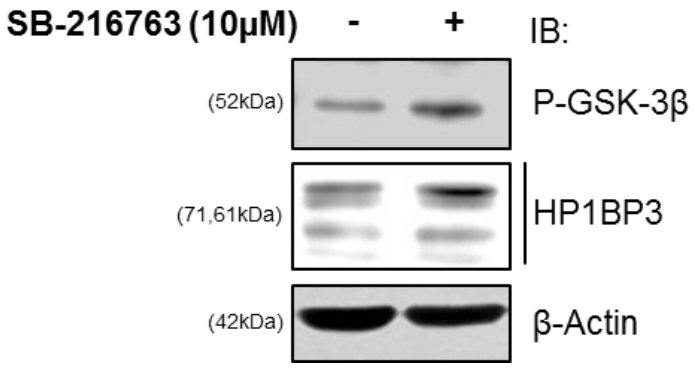


Figure 3-4: GSK-3β inhibition could induces phosphorylation of HP1BP3 in HCT116 cells. Cells were treated with the GSK-3β inhibitor SB-216763 (10 µM) or vehicle control DMSO for 6 h and cell lysate was extracted and examined for (P)-GSK-3β (inactive form) and HP1BP3 by western blotting. Total protein of 100 µg was run on 10 % SDS-PAGE and transferred to PVDF membranes. β-Actin is used as a loading control in western blotting analysis. This experiment was repeated in two different occasions.

3.2.1.1.1 The consensus sequence for GSK-3β substrates in the HP1BP3 are functional

GSK-3β is a serine/threonine kinase that phosphorylates T/S---T/SP in the CDC4-phospho-degron (CPD) motifs of several FBXW7 substrates (Cremona et al., 2016; Welcker and Clurman, 2008). Moreover, our above data revealed that GSK-3β might phosphorylate HP1BP3. Consequently, we were interested in identifying the CPD motif in HP1BP3. Sequence comparison revealed that HP1BP3 might have two GSK-3β phosphorylation motifs similar to the CPD motifs described in other FBXW7 target proteins (Cremona et al., 2016; Welcker and Clurman, 2008) (Figure 3-5). One motif is located at the N-terminus (S47 and Thr51) and the other is located at the C-terminus (Thr461 and S466) (Figure 3-5). Moreover, Dr Nateri's lab has indicated that, in the presence of GSK-3β, HP1BP3 is targeted by FBXW7γ and less so by FBXW7α (Abuzinadah et al., in preparation). Therefore, to identify which motif is functional in HP1BP3, peGFP-FLAG-MYC-FBXW7α, peGFP-FLAG-MYC-FBXW7γ and peGFP-HP1BP3-S (short HP1BP3 isoform lacking the N-terminus motif) or peGFP-HP1BP3 (long HP1BP3 isoform containing the N-terminus and C-terminus motifs) plasmids were co-transfected in to HCT116 cells (Figure 3-6). These plasmids, has been constructed and fully validated (by double restriction enzymes digestion and DNA sequencing) in Dr Nateri's lab. To avoid differences in transfection efficiency, transfected cells were divided into two 10 cm^2 plates and treated with SB-216763 (10 μM) or vehicle control DMSO for 6 h and cell lysates were extracted and examined for FLAG, (P)-GSK-3β and green fluorescent protein (GFP) by western blotting (Figure 3-7).

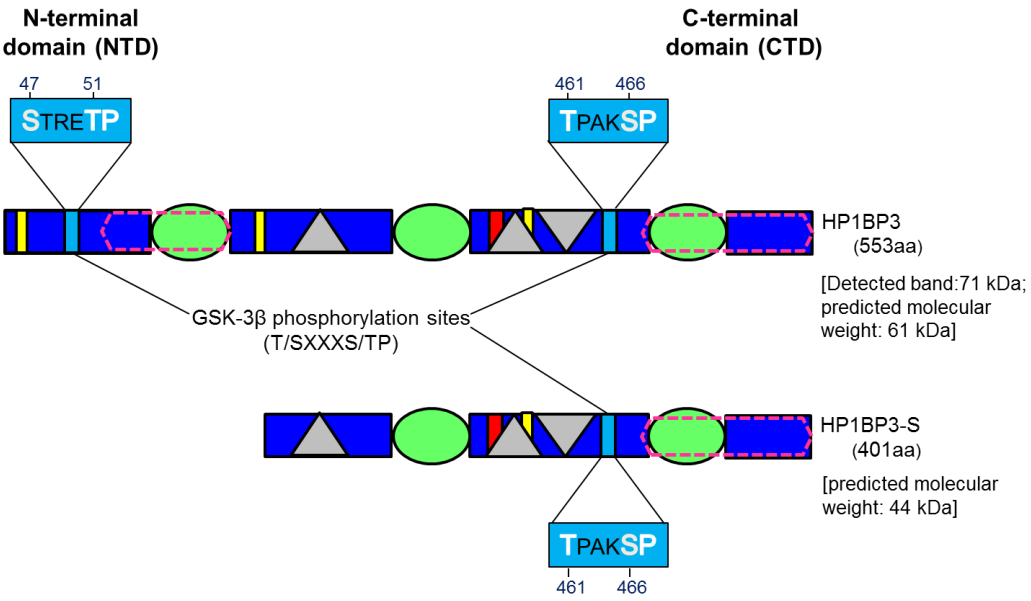


Figure 3-5: A schematic representation of the HP1BP3 protein and its predicted GSK-3β phosphorylation sites. Schematic shows the presence of two putative GSK-3β consensus phosphorylation motifs (T/S---T/SP) in the wild type isoform, whereas HP1BP3-S (short isoform) has one predicted motif.

Prior to transfection, the above mentioned plasmids (Figure 3-6 A–E) were validated by digestion using *Eco*RI or *Bgl*II restriction enzymes. The digested DNAs were run on 1 % agarose gel to confirm the release of the indicated DNA fragment/s and the control vector (peGFP-C2) linearisation. The digestion confirmed the existence of the estimated DNA fragment presented in Figure 3-6 F.

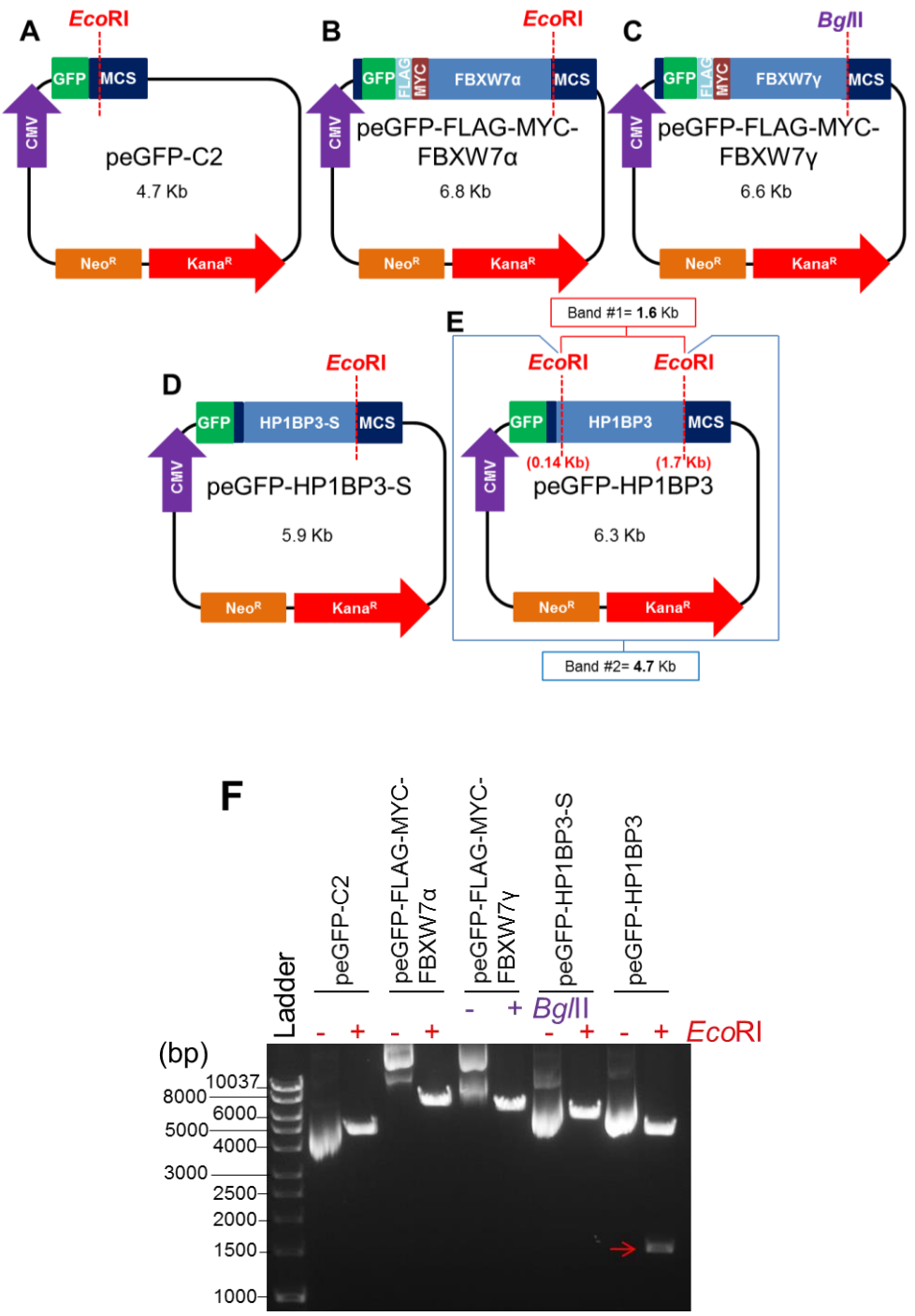


Figure 3-6: The peGFP-C2, peGFP-FLAG-MYC-FBXW7α, peGFP-FLAG-MYC-FBXW7γ, peGFP-HP1BP3-S (HP1BP3 short isoform), and peGFP-HP1BP3 (wild-type) plasmid maps and validation analysis by restriction enzyme digestion (A-F). Schematic presentation shows the backbone vector (A) peGFP-C2, (B) peGFP-FLAG-MYC-FBXW7α, (D) peGFP-HP1BP3-S, and (E) peGFP-HP1BP3 plasmids with *Eco*RI restriction enzyme site/s. (C) Schematic presentation showing the peGFP-FLAG-MYC-FBXW7γ plasmid with *Bgl*II restriction enzyme site. (F) The digested DNAs were run on 1 % agarose gel to confirm the linearization of the vector or the release of the expected DNA fragment/s out from the backbone vector.

Our data reveal that the expression level of the long HP1BP3 isoform was increased more than the short HP1BP3 isoform in the SB-216763–treated HCT116 cells (Figure 3-7 A; lane 2 vs. 4) but that DMSO decreased the level of HP1BP3 (Figure 3-7 A; lane 1 vs. 3). As the stability of the short HP1BP3 isoform was less increased in the presence of SB-216763 (Figure 3-7 A and B; lane 2) in comparison to the long HP1BP3 isoform (Figure 3-7 A and B; lane 4), it appears that both N-terminus phosphorylation (Thr51 and Ser47) and C-terminus phosphorylation (Thr461 and Ser466), contribute to the recognition of HP1BP3 by SCF^{FBXW7} for degradation. Altogether, the data further suggest that the E3 ligase SCF^{FBXW7} degrades (P)-HP1BP3 in a GSK-3β–dependent manner. Consistent with this, the expression of endogenous HP1BP3 was upregulated in $HCT116^{FBXW7(-/-)}$ cells (Figure 3-1 B) and as well as that the FBXW7 directly interacted with HP1BP3 protein (Abuzinadeh et al., in submission), we can conclude that the SCF^{FBXW7} activity modulate the HP1BP3 protein for degradation in GSK-3β-dependent manner. However, these findings need to be supported by an additional experiment, using specific siRNA against GSK-3β.

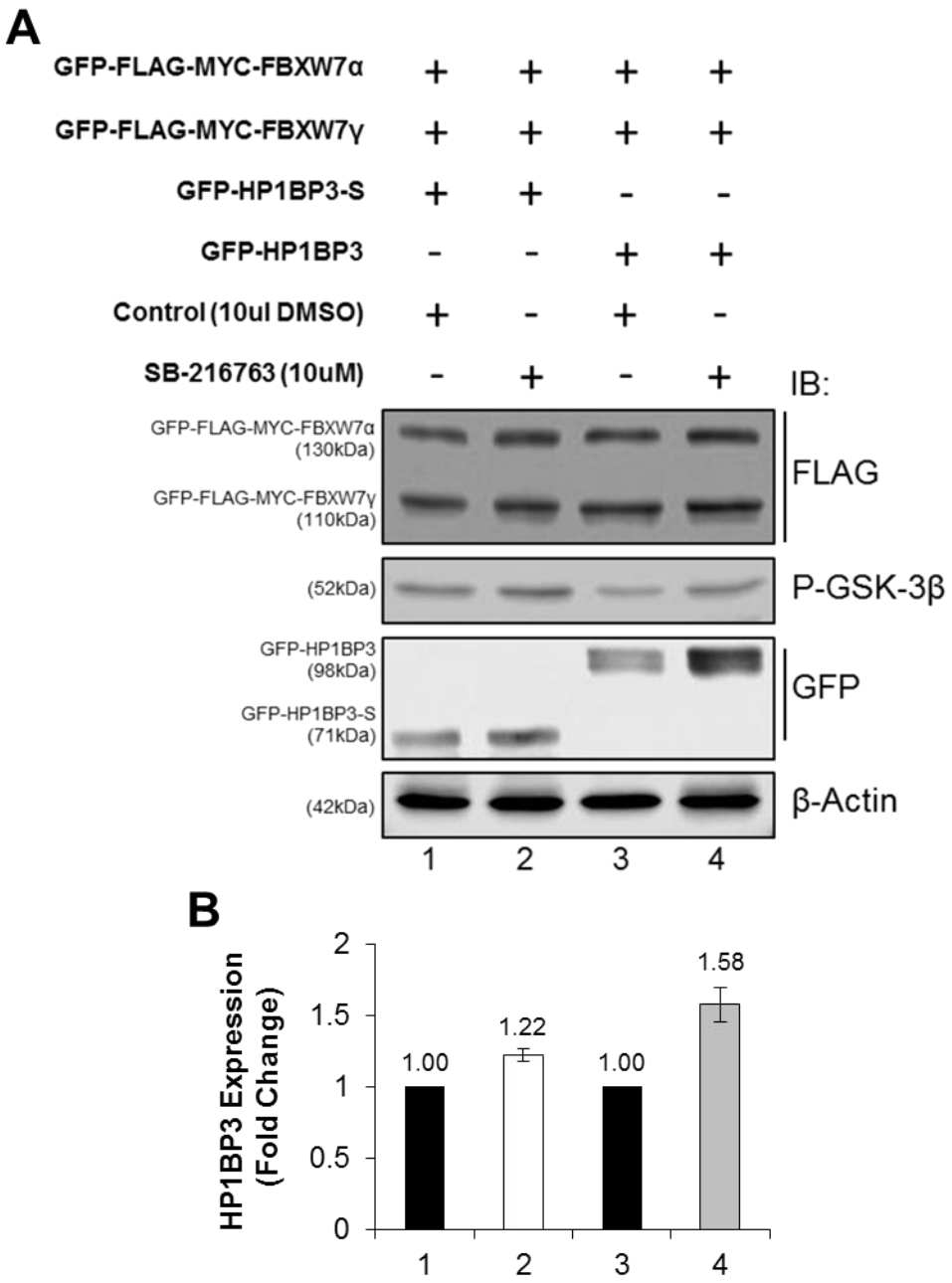


Figure 3-7: The Serine/ Threonine (T/S---T/SP) domains in HP1BP3 are responsible for its degradation by FBXW7. (A) FLAG/GFP-tagged versions of the indicated proteins were co-expressed in HCT116 cells, treated with the GSK-3β inhibitor SB-216763 (10 μM) or vehicle control DMSO for 6 h. Cell lysate was extracted and total protein of 50 μg was run on 8 % or 10 % SDS-PAGE, transferred to PVDF, and subjected to western blotting for FLAG, (P)-GSK-3β (inactive form), and GFP antibodies. β-Actin is used as a loading control in western blotting analysis. (B) Band intensities of HP1BP3 long isoform and HP1BP3 short isoform in GFP blots were normalised to β-Actin and calculated using ImageJ. Values are represented as fold change. Error bars show the STDEV of two independent experiments.

3.2.2 HP1BP3 upregulation mediated by *FBXW7* loss could increases nuclear co-localisation of HP1BP3 and HP1α in HCT116 cells

As outlined above, HP1α is an essential heterochromatin-associated protein typically involved in the epigenetic regulation of gene silencing (Canzio et al., 2014; Lachner et al., 2001; Maison et al., 2011; Yamamoto and Sonoda, 2003). Others have demonstrated that HP1α can also activate gene expression in certain contexts (Cryderman et al., 2011; Kwon and Workman, 2011; Piacentini et al., 2009; Sdek et al., 2013; Shoji et al., 2014). As mentioned earlier, although recently reported that HP1BP3 binds to HP1α and has been associated with chromatin condensation (Garfinkel et al., 2015b; Hayashihara et al., 2010a), but the biochemical/biological mechanisms and consequences of this interaction remain largely unclear. As FBXW7 deletion had no effect on HP1α levels and/or distribution (Figure 3-1 A; Column 3 and Figure 3-1 B), whereas HP1BP3 was accumulated in HCT116$^{FBXW7(-/-)}$ cells (Figure 3-1 A; Column 2 and Figure 3-1 B), we aimed to explore the role of HP1BP3 via the significance of the HP1BP3/HP1α complex in regulating carcinogenesis.

Previous reports have stated that knowledge of the biological system can sometimes be derived indirectly from quantitative co-localisation (Costes et al., 2004); therefore, we first quantified HP1BP3 and HP1α co-localisation using immunofluorescence images of HCT116$^{FBXW7(-/-)}$ cells versus HCT116$^{FBXW7(+/+)}$ cells (Figure 3-8). To achieve this, fluorescence images for HP1BP3 were manually enhanced to HP1α level in order to visualise the

nuclear foci regardless of the actual protein expression level. The number of foci with HP1BP3 and HP1α co-localisation (yellow-orange), non–co-localised HP1BP3 (green) and non–co-localised HP1α (red) were counted separately in more than 16 cells per cell line (Figure 3-8 A + B) using ImageJ software. Then, the average number of nuclear foci in each cell line was estimated and compared (Figure 3-9 A–C). The merged images suggests a higher co-localisation between HP1BP3 and HP1α in the HCT116$^{FBXW7(-/-)}$ cells (Figure 3-8 B) compared to the HCT116$^{FBXW7(+/+)}$ cells (Figure 3-8 A). Moreover, HP1BP3 and HP1α co-localised foci in the HCT116$^{FBXW7(-/-)}$ cells were significantly increased versus the HCT116$^{FBXW7(+/+)}$ cells (Figure 3-9 C). However, the number of HP1BP3 foci that were not co-localised with HP1α, and vice versa, was higher in the HCT116$^{FBXW7(+/+)}$ cells. The quantitative co-localisation data may support our hypothesis that HP1BP3 upregulation and consequent additional binding of HP1BP3 to HP1α may rescue the repression activity of HP1α. This could be due to the competitive interaction between HP1BP3 and other heterochromatin components such as SUV39H1, as reported previously (Maison et al., 2011). Obviously, further studies are required for functional analyses of the HP1BP3/HP1α complex. Moreover, further experiment, such as fluorescence resonance energy transfer (FRET), is required to further support our observation.

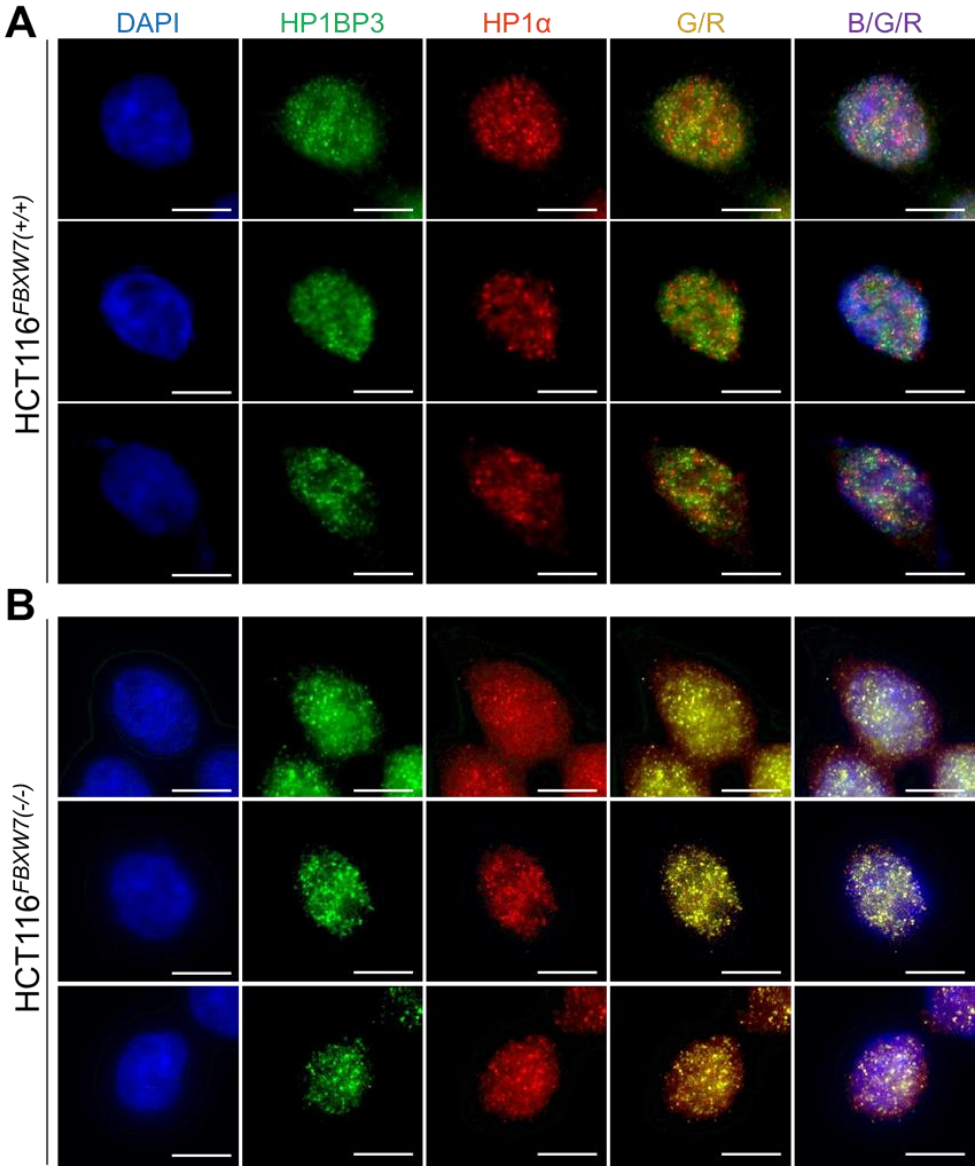


Figure 3-8: Increasing number of co-localised HP1BP3 and HP1α nuclear foci in HCT116$^{FBXW7(-/-)}$ versus HCT116$^{FBXW7(+/+)}$ cells. HP1BP3 (green) and HP1α (red) endogenous proteins expression in HCT116$^{FBXW7(+/+)}$ (A) and HCT116$^{FBXW7(-/-)}$ (B) cell lines, examined by immunofluorescence technique. For counting foci, HP1BP3 fluorescent images were enhanced to the HP1α level regardless their actual protein level, to visualise nuclear foci by ImageJ software. Scale bar is 10μm.

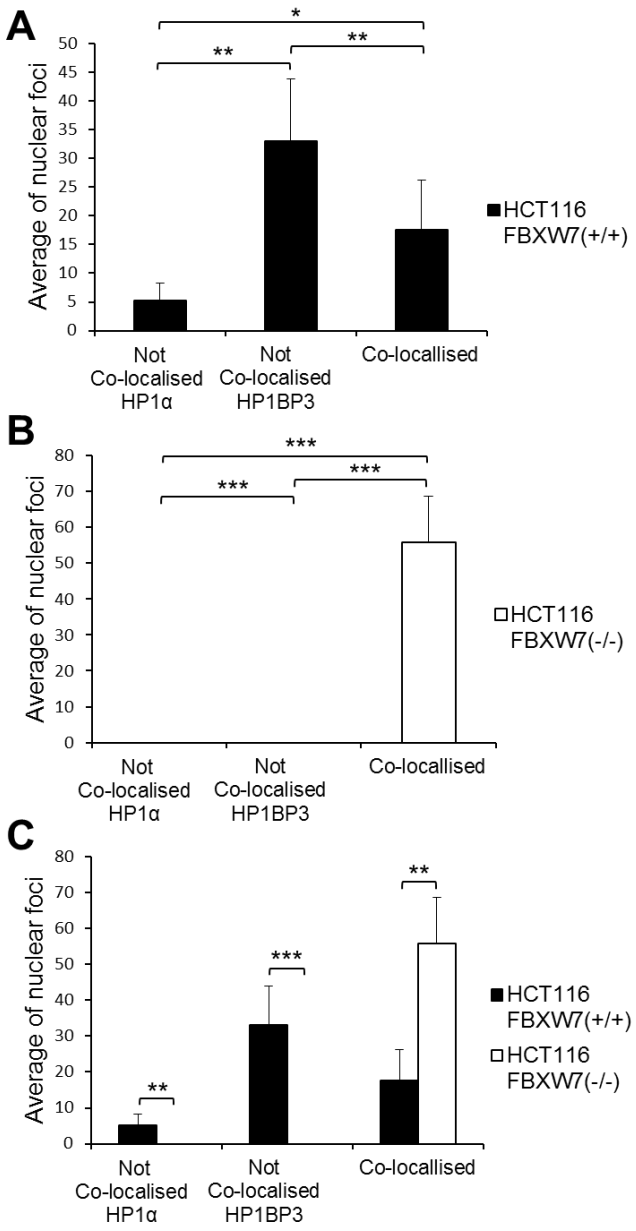


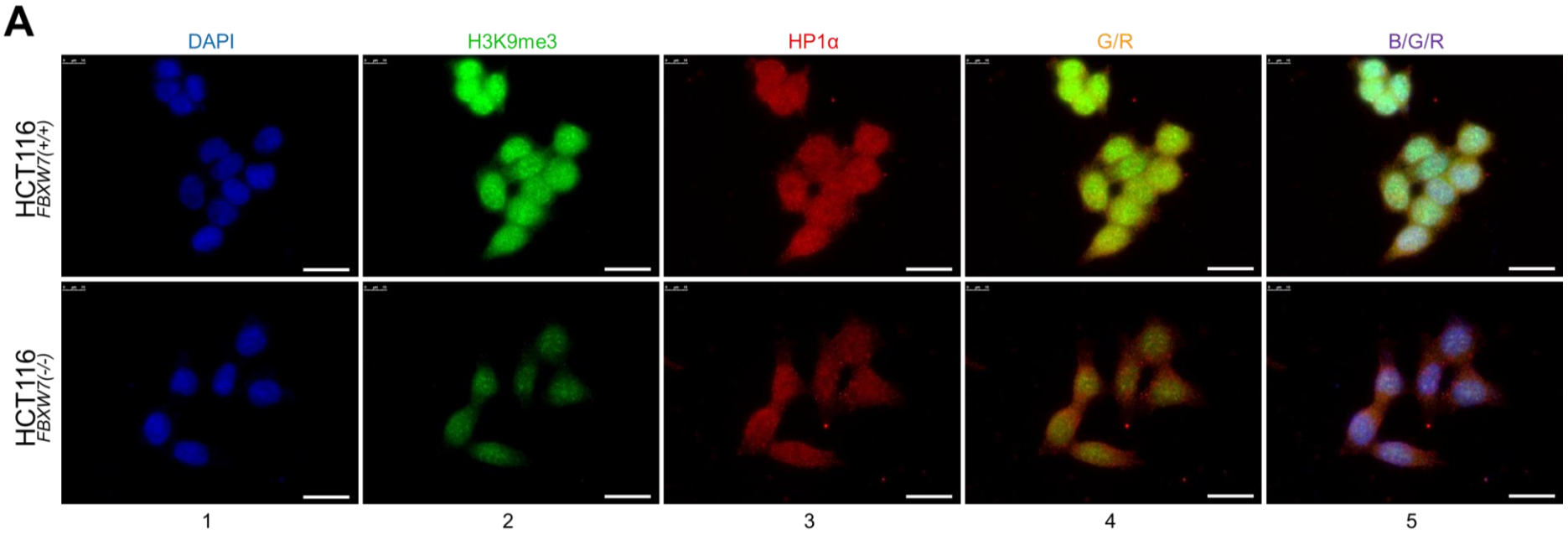
Figure 3-9: HP1BP3 upregulation caused by *FBXW7* loss could increases the co-localisation between HP1BP3 and HP1α nuclear foci in HCT116 cells. (A-C) Statistical analysis of average number of co-localised HP1α and HP1BP3, not co-localised HP1BP3, and not co-localised HP1α nuclear foci between HCT116$^{FBXW7(+/+)}$ and HCT116$^{FBXW7(-/-)}$ cell lines. IF were performed for endogenous HP1BP3 and HP1α in the indicated cell lines; HCT116$^{FBXW7(+/+)}$ (A) and HCT116$^{FBXW7(-/-)}$ (B) cell lines. HP1BP3-images were manually enhanced to the level of HP1α, to visualise nuclear foci of 16 individual cells from each cell lines, using ImageJ software. Then, the average of nuclear foci indicated in each cell line, were compared in (C). Nuclear foci were manually counted which shows significant increase in interaction between HP1BP3 and HP1α in HCT116$^{FBXW7(-/-)}$ compared to control cells; *HCT116*$^{FBXW7(+/+)}$. Moreover, free not co-localised HP1BP3 and HP1α nuclear foci are higher in *HCT116*$^{FBXW7(+/+)}$ than HCT116$^{FBXW7(-/-)}$. Statistical significant values were calculated using student's *t* test. *P= 0.01 to 0.05, **p= 0.001 to 0.01, ***p<0.001.

3.2.3 Reduced level of tri-methylated H3K9 heterochromatin marker and increased level of acetylated H3K9 euchromatin marker in HCT116$^{FBXW7(-/-)}$ cells

It is well established that high tri-methylated H3K9 (H3K9me3) level is associated with action of the histone methyltransferase SUV39H1/2 (Bártová et al., 2008; Rea, 2000), which facilitates H3K9me3 binding to HP1α (Bannister et al., 2001b; Canzio et al., 2014; Lachner et al., 2001; Maison et al., 2011). In this manner, both SUV39H1/2 and HP1α contribute to the propagation of heterochromatic domains through H3K9me3 and consequently lead to the maintenance of the silenced loci (Bannister et al., 2001b; Lachner et al., 2001; Maison et al., 2011; Yamamoto and Sonoda, 2003). On the other hand, as our data suggested a high degree of co-localisation between HP1α and HP1BP3, we subsequently investigated the H3K9me3 heterochromatin marker profile and cellular distribution in HCT116$^{FBXW7(-/-)}$ and HCT116$^{FBXW7(+/+)}$ cells. The H3K9 residue can be methylated and/or acetylated, leading to the formation of heterochromatin and/or euchromatin, respectively (Park et al., 2011). Therefore, we postulated that *FBXW7* loss could mediate changes to these chromatin markers.

The HP1BP3 and H3K9me3 primary antibodies available in our laboratory are produced in rabbits, hence their cross-reactivity renders the establishment and immunofluorescence examination of endogenous HP1BP3 and H3K9me3 co-localisation in HCT116$^{FBXW7(+/+)}$ and HCT116$^{FBXW7(-/-)}$ cells are difficult. Therefore, the co-localisation study was performed for H3K9me3 and HP1α using anti-H3K9me3 (green) and anti-HP1α (red) antibodies

(Figure 3-10 A) instead. The fluorescence co-localisation study revealed no changes in the distribution of both proteins, while H3K9me3 levels were markedly reduced in the HCT116$^{FBXW7(-/-)}$ cells compared to the HCT116$^{FBXW7(+/+)}$ cells (Figure 3-10 A; Column 2). Western blotting confirmed that H3K9me3 levels were reduced in the HCT116$^{FBXW7(-/-)}$ cells compared to the HCT116$^{FBXW7(+/+)}$ cells (Figure 3-10 B). However, HP1α expression was unchanged between the HCT116$^{FBXW7(+/+)}$ and HCT116$^{FBXW7(-/-)}$ cells (Figure 3-10 B). Moreover, increased H3K9ac was detected in the HCT116$^{FBXW7(-/-)}$ cells versus the HCT116$^{FBXW7(+/+)}$ cells (Figure 3-10 B). The data suggest that the loss of *FBXW7*-mediated HP1BP3 accumulation may lead to the loss of H3K9me3 and consequent H3K9ac upregulation in CRC cells. However, further studies need to be performed to dissect the cross talk between HP1BP3/HP1α co-localisation and the H3K9 methylation in HCT116$^{FBXW7(-/-)}$ cells versus the HCT116$^{FBXW7(+/+)}$ cells.


A
DAPI
H3K9me3
HP1α
G/R
B/G/R
HCT116 FBXW7(+/+)
HCT116 FBXW7(-/-)
1
2
3
4
5

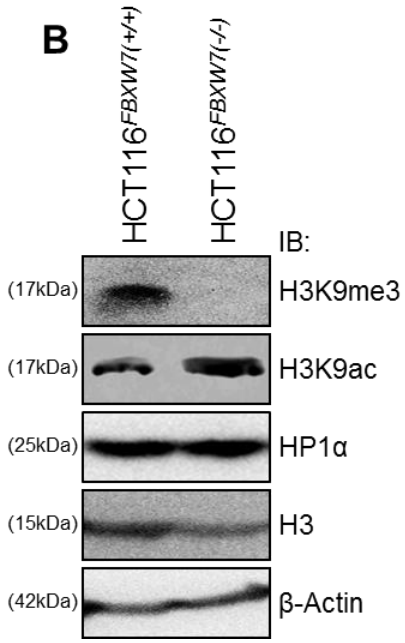


Figure 3-10: Inhibition and stimulation of endogenous H3K9me3 and H3K9ac, respectively, in human CRC cells lacking *FBXW7*. The expression levels of (A) H3K9me3 marker (green) and HP1α (red) protein in HCT116$^{FBXW7(+/+)}$ and HCT116$^{FBXW7(-/-)}$ cell lines, examined by immunofluorescence technique. Scale bar is 20 μm. (B) Western blotting analysis for endogenous H3K9me3, H3K9ac, and HP1α expression levels in HCT116$^{FBXW7(+/+)}$ and HCT116$^{FBXW7(-/-)}$. Total protein of 100 μg was run on 10 % (for anti- HP1α) or 15 % (for ant- H3K9me3, -H3K9ac) SDS-PAGE and transferred to PVDF membranes. Anti-H3K9me3, -H3K9ac, and -HP1α antibodies were used to detect endogenous expression/level of H3K9me3, H3K9ac, and HP1α. The level of H3K9me3 was reduced, whereas H3K9ac level was increased, in HCT116$^{FBXW7(-/-)}$ cells compared to HCT116$^{FBXW7(+/+)}$ cells. β-Actin and H3 are used as a loading control in western blotting analysis. IF and WB experiments were repeated in two different occasions.

3.2.4 Nuclear distribution of HP1α and HP1BP3 is associated with Suv39h1/2-mediated H3K9 trimethylation in mouse embryonic fibroblast (MEF) cells

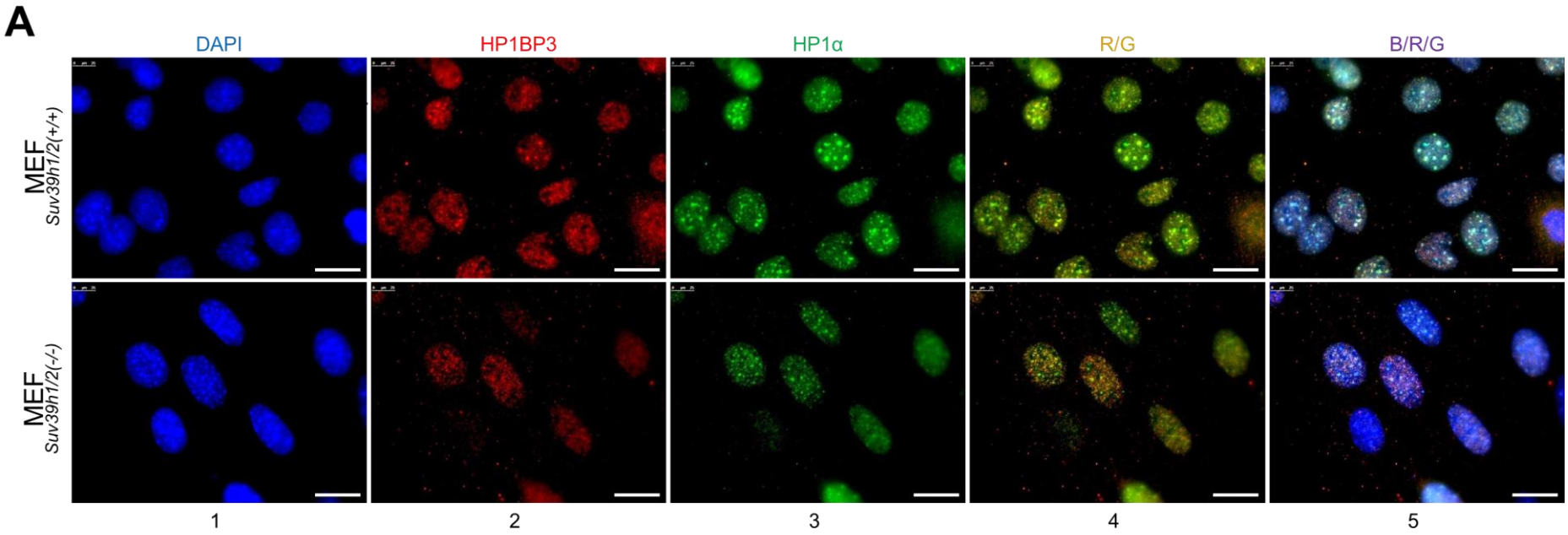
As outlined above, SUV39H1/2 binds to HP1α, where it functions as a histone methyltransferase that methylates lysine 9 of histone H3, i.e. H3K9 (Lachner et al., 2001; Yamamoto and Sonoda, 2003). SUV39H1/2 plays an essential role in ensuring faithful chromosome segregation through its modulation at pericentric/paracentric chromatin inversion, which is vital in normal homeostasis and in cancer (Peters et al., 2001; Petti et al., 2015). Accordingly, we examined whether SUV39H1/2 activity via possible H3K9 trimethylation is required for HP1BP3 binding to HP1α.

To do this, we used MEF cells derived from *Suv39h1/2* double null mice ($MEF^{Suv39h1/2(-/-)}$) (Peters et al., 2001), in which HP1α is no longer enriched at the pericentric heterochromatin (Maison et al., 2011), and control MEF cells with wild-type of *Suv39h1/2* alleles ($MEF^{Suv39h1/2(+/+)}$). HP1BP3 and HP1α endogenous expression and co-localisation were examined by immunofluorescence. Interestingly, HP1BP3 and HP1α levels were not affected in the $MEF^{Suv39h1/2(-/-)}$ cells (Figure 3-11 B), but the distribution patterns of both proteins was altered in the $MEF^{Suv39h1/2(-/-)}$ cells versus $MEF^{Suv39h1/2(+/+)}$ cells (Figure 3-11 A and Figure 3-12 B vs. A). In the $MEF^{Suv39h1/2(-/-)}$ cells, HP1BP3 and HP1α were distributed at the nuclear periphery around the nucleoli but were also distributed throughout the nucleoplasm (Figure 3-12 B). Moreover, there was diffuse immunofluorescence staining throughout the euchromatic regions of the

MEF$^{Suv39h1/2(-/-)}$ cells (Figure 3-12 B). Conversely, in the MEF$^{Suv39h1/2(+/+)}$ cells, both HP1BP3 and HP1α had more defined distribution patterns, fewer foci and larger foci (Figure 3-12 A vs. B). The observed foci in the MEF$^{Suv39h1/2(+/+)}$ cells corresponded to the accumulation of HP1α in major satellite repeats reported previously by Maison *et al*. (Maison et al., 2011). However, Immuno-DNA fluorescence in situ hybridization (FISH) with anti-HP1α/HP1BP3 and major/minor satellite DNA probes is required to further confirm the accumulation of both proteins in major or minor satellite repeats in MEF$^{Suv39h1/2(+/+)}$ or MEF$^{Suv39h1/2(-/-)}$ cells, respectively.

Additionally, HP1BP3 and HP1α distribution patterns resembled diaminophenylindole (DAPI)-staining patterns in the MEF$^{Suv39h1/2(+/+)}$ cells (Figure 3-12 A), where DAPI stains the pericentromeric heterochromatin domains strongly. Furthermore, there appeared to be no observable differences in HP1α and HP1BP3 co-localisation between the MEF$^{Suv39h1/2(-/-)}$ and MEF$^{Suv39h1/2(+/+)}$ cells (Figure 3-12 A + B). Western blotting confirmed that there were no changes in HP1BP3 and HP1α levels in the MEF$^{Suv39h1/2(+/+)}$ cells versus MEF$^{Suv39h1/2(-/-)}$ cells (Figure 3-11 B).

Together with other previously published data (Maison et al., 2011), our findings suggest that the heterochromatin association of HP1α and HP1BP3 in MEF$^{Suv39h1/2(+/+)}$ cells is lost in MEF$^{Suv39h1/2(-/-)}$ cells via alteration of the HP1α and HP1BP3 foci distribution within the nucleus.


A
DAPI
HP1BP3
HP1α
R/G
B/R/G
MEF Suv39h1/2(+/+)
MEF Suv39h1/2(-/-)
1
2
3
4
5

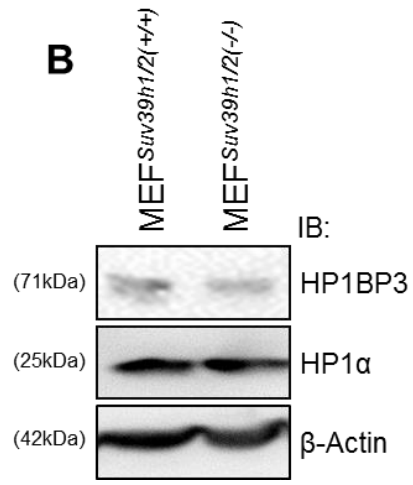


Figure 3-11: The expression patterns and protein expression levels of endogenous HP1BP3 (red) and HP1α (green) proteins in MEF$^{Suv39h1/2(+/+)}$ and MEF$^{Suv39h1/2(-/-)}$ cell lines, examined by IF and western blotting analysis. (A) IF analyses of endogenous HP1BP3 (red) and HP1α (green) proteins in MEF$^{Suv39h1/2(+/+)}$ and MEF$^{Suv39h1/2(-/-)}$ cell lines. Scale bar is 50 μm. (B) Western blotting analysis for endogenous HP1BP3 and HP1α expression levels in MEF$^{Suv39h1/2(+/+)}$ and MEF$^{Suv39h1/2(-/-)}$. Total protein of 100 μg was run on 10 % SDS-PAGE and transferred to PVDF membranes. Anti-HP1BP3 and -HP1α antibodies were used to detect endogenous level of HP1BP3 and HP1α. β-Actin is used as a loading control in western blotting analysis. The level of HP1BP3 and HP1α expression was not affected by *Suv39h1/2*-knockout, but the distributions pattern of both proteins was significantly different between these cell lines. IF and WB experiments were repeated in two different occasions.

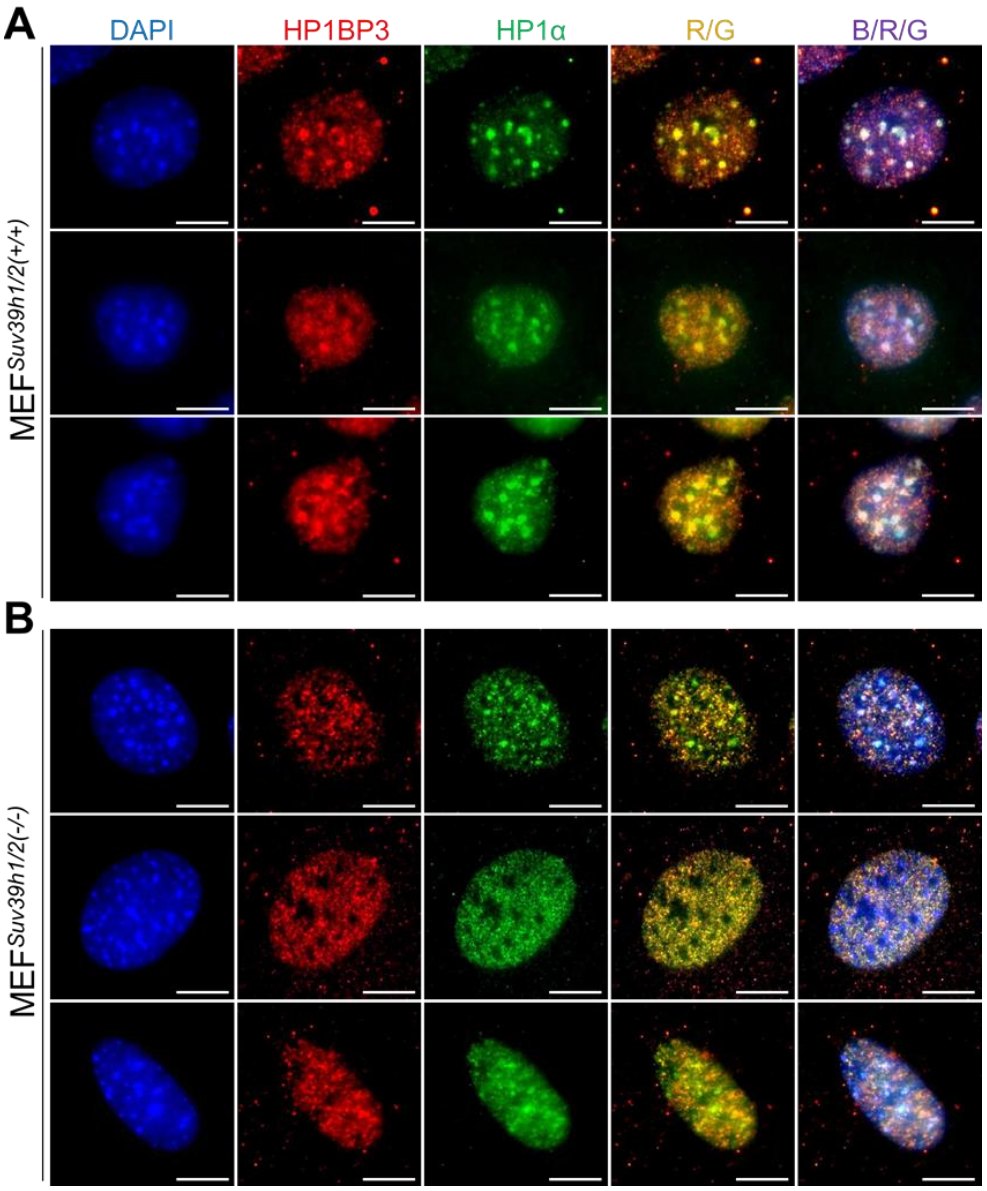


Figure 3-12: The distributions pattern of endogenous HP1BP3 and HP1α co-localisation is associated with Suv39h1/2 expression. (A) Endogenous HP1BP3 (red) and HP1α (green) in MEF$^{Suv39h1/2(+/+)}$ (A) and MEF$^{Suv39h1/2(-/-)}$ (B), examined by IF assays. Images were enhanced by ImageJ software to visualise nuclear foci. HP1BP3 fluorescent images were enhanced to the HP1α level regardless their actual protein level, to visualise nuclear foci by ImageJ software. The distribution pattern of HP1BP3 and HP1α proteins was altered between both cell lines. IF experiment was repeated in two different occasions. Scale bar is 25 μm.

After examining HP1BP3 and HP1α levels and their expression patterns in MEF$^{Suv39h1/2(+/+)}$ and MEF$^{Suv39h1/2(-/-)}$ cells, we examined the H3K9me3 and HP1α levels and expression patterns in the cells under the assumption that the HP1BP3 and HP1α distribution patterns in MEF$^{Suv39h1/2(-/-)}$ cells might be associated with H3K9me3 status. First, H3K9me3 levels were examined by western blotting. As expected, H3K9me3 was abolished in the MEF$^{Suv39h1/2(-/-)}$ cells (Figure 3-13).

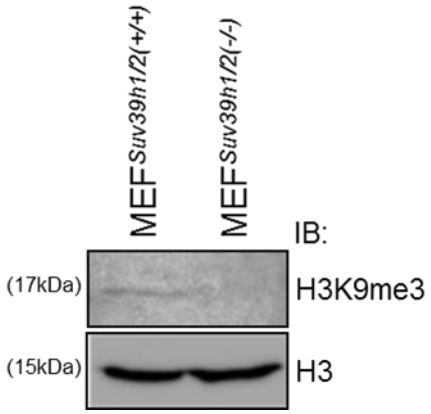


Figure 3-13: Depletion of *Suv39h1/2* abolishes endogenous H3K9me3 levels in MEF cells. Total protein of 250 µg was run on 15 % SDS-PAGE and transferred to PVDF membranes. Anti-H3K9me3 antibody was used to detect endogenous level of H3K9me3 in MEF$^{Suv39h1/2(+/+)}$ and MEF$^{Suv39h1/2(-/-)}$ cell lines. H3 is used as a loading control in western blotting analysis. WB experiment was repeated in three different occasions.

Next, the co-localisation of the endogenous HP1α and H3K9me3 in the MEF$^{Suv39h1/2(+/+)}$ cells versus MEF$^{Suv39h1/2(-/-)}$ cells was examined by immunofluorescence (Figure 3-14 A vs. B). The H3K9me3 distribution pattern in the MEF$^{Suv39h1/2(+/+)}$ cells differed from that in the MEF$^{Suv39h1/2(-/-)}$

cells (Figure 3-14 A + B). Upon examination of the cellular distribution of each foci, the immunofluorescence images suggested less H3K9me3 and HP1α co-localisation in the MEF$^{Suv39h1/2(-/-)}$ cells versus the MEF$^{Suv39h1/2(+/+)}$ cells (Figure 3-14 B vs. A and Figure 3-15 C). Moreover, the H3K9me3 and HP1α distribution patterns were less defined in the MEF$^{Suv39h1/2(-/-)}$ cells versus the MEF$^{Suv39h1/2(+/+)}$ cells (Figure 3-14 B vs. A). Additionally, there were more and smaller H3K9me3 and HP1α foci in the MEF$^{Suv39h1/2(-/-)}$ cells than in the MEF$^{Suv39h1/2(+/+)}$ cells (Figure 3-14 B vs. A). Furthermore, as SUV39H1/2 trimethylates H3K9 (Bártová et al., 2008; Rea, 2000), the H3K9me3 immunofluorescence staining patterns in both cell lines resembled that of SUV39H1, as expected and as reported previously (Krouwels et al., 2005). Moreover, although the western blot in Figure 1-13 showed abolishment of H3K9me3 levels in MEF$^{Suv39h1/2(-/-)}$ cells, residual staining was detected in these cells (Figure 3-14). It has been reported that the level of H3K9me3 is slightly detectable in MEF$^{Suv39h1/2(-/-)}$ cells, in compression to the control cell line (Peters et al., 2001). However, the observed staining pattern is in agreement with previous immunocytochemical study that used a specific anti-H3K9me3 antibody in MEF$^{Suv39h1/2(-/-)}$ cells and detected the presence of slight trim ethylated H3K9 (Krouwels et al., 2005). In figure 3-13, it could be that 250 µg of protein lysate was insufficient to detect the minimal expression of H3K9me3 which might be expressed as a result of other methyl transferases in these cells.

In addition, the number of foci for H3K9me3 and HP1α co-localisation, non–co-localised H3K9me3 and non–co-localised HP1α were counted in 16 cells

per cell line after ImageJ enhancing (Figure 3-14 and Figure 3-15). Then, the average nuclear foci in the indicated cell lines (Figure 3-15) were compared (Figure 3-15 C). The H3K9me3 and HP1α co-localisation foci in the MEF$^{Suv39h1/2(-/-)}$ cells were significantly decreased compared to the MEF$^{Suv39h1/2(+/+)}$ cells (Figure 3-15 C). The MEF$^{Suv39h1/2(+/+)}$ cells had larger and fewer H3K9me3 foci compared to the MEF$^{Suv39h1/2(-/-)}$ cells, confirming that H3K9me3 is built up by SUV39H1/2 and associates with heterochromatin-silenced foci, as previously reported (Maison et al., 2011). However, three-dimensional imaging, using a confocal z-stack images, is required to further support our observation.

Considering all the data together, we may conclude that the H3K9me3 status is negatively correlated with the increasing binding between HP1BP3 and HP1α and their para- and pericentric inversions/ distribution within both HCT116$^{FBXW7(-/-)}$ and MEF$^{Suv39h1/2(-/-)}$ cells.

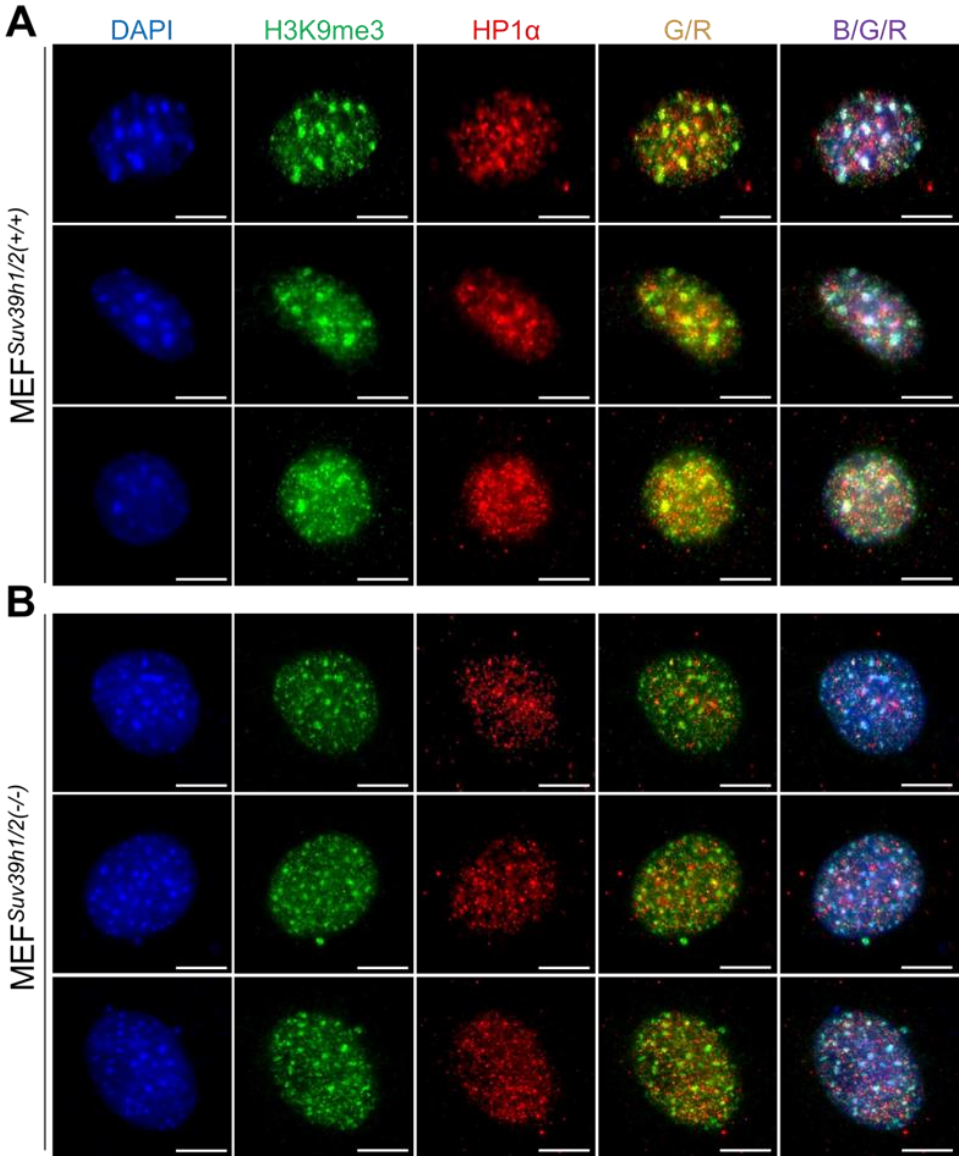


Figure 3-14: Endogenous H3K9me3 (green) and HP1α (red) co-localisation in (A) MEF$^{Suv39h1/2(+/+)}$ and (B) MEF$^{Suv39h1/2(-/-)}$ cell lines, examined by IF. Images were manually enhanced by ImageJ software to visualise and count nuclear foci. For counting foci, H3K9me3 fluorescent images were enhanced to the HP1α level regardless their actual protein level, to visualise nuclear foci by Image software. Co-localised foci of H3K9me3 and HP1α was decreased in MEF$^{Suv39h1/2(-/-)}$ compared to MEF$^{Suv39h1/2(+/+)}$. IF experiment was repeated in two different occasions. Scale bar is 25 µm.

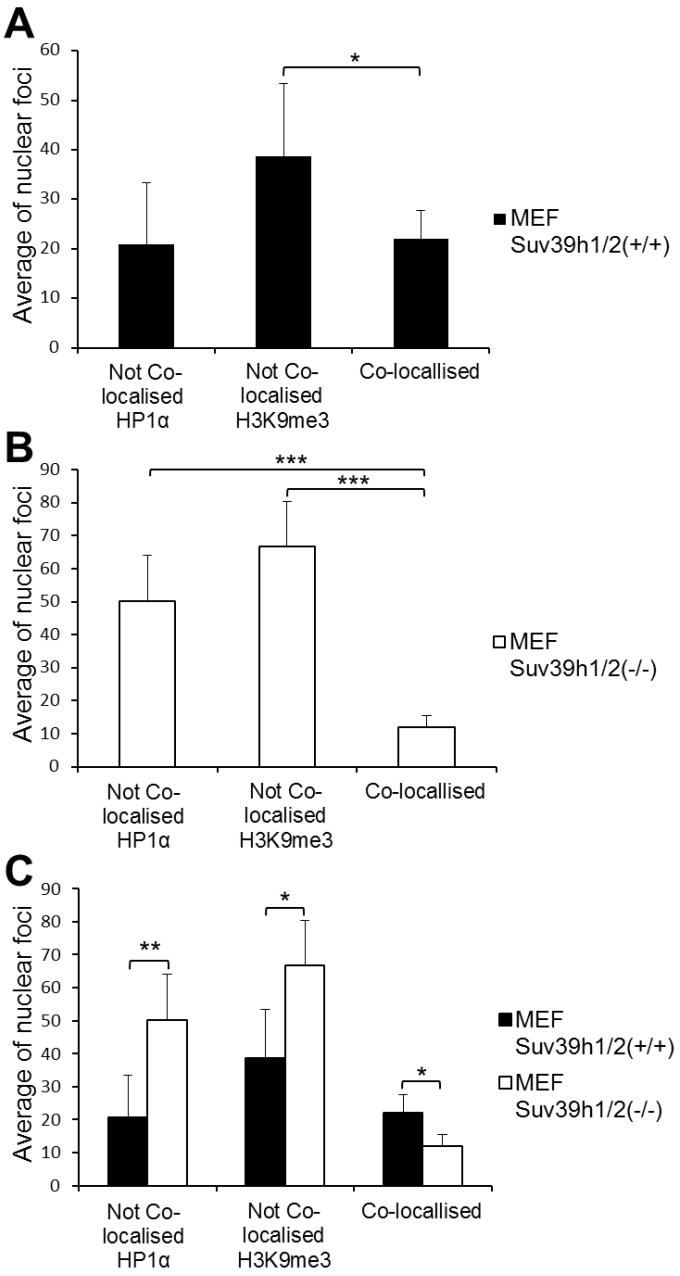


Figure 3-15: Analysis of average nuclear foci number of co-localised H3K9me3 and HP1α, not co-localised H3K9me3, and not co-localised HP1α for MEF$^{Suv39h1/2(+/+)}$ (A) and MEF$^{Suv39h1/2(-/-)}$ (B) cell lines. IF were performed for endogenous H3K9me3 and HP1α in the indicated cell lines. Images were enhanced to visualise nuclear foci of 16 individual cells from each cell lines, using ImageJ software. Then, the average of nuclear foci in the indicated cell lines, were compared in (C). Nuclear foci were manually counted which suggests decreased co-localisation between H3K9me3 and HP1α in MEF$^{Suv39h1/2(-/-)}$ compared to control cells (MEF$^{Suv39h1/2(+/+)}$). Significant values were calculated using student's t test. *P= 0.01 to 0.05, **p= 0.001 to 0.01, ***p<0.001.

3.2.5 Further confirmation analyses of an endogenous HP1BP3/HP1α/H3K9me3 complex in CRC DLD-1 cells

To avoid context dependence from the use of a single human CRC cell line (HCT116), western blotting was repeated to examine HP1BP3 and HP1α expression levels and H3K9me3 levels in another CRC cell line (DLD-1) with and without *FBXW7* deletion mutation, i.e. DLD-1$^{FBXW7(-/-)}$ versus DLD-1$^{FBXW7(+/+)}$, respectively (Babaei-Jadidi et al., 2011a; Rajagopalan et al., 2004). Briefly, consistent with the earlier observations in HCT116$^{FBXW7(-/-)}$ (Figure 3-1 B and Figure 3-10 B), H3K9me3 was undetectable, while HP1BP3 was highly accumulated in DLD-1$^{FBXW7(-/-)}$ versus DLD-1$^{FBXW7(+/+)}$ cells (Figure 3-16).

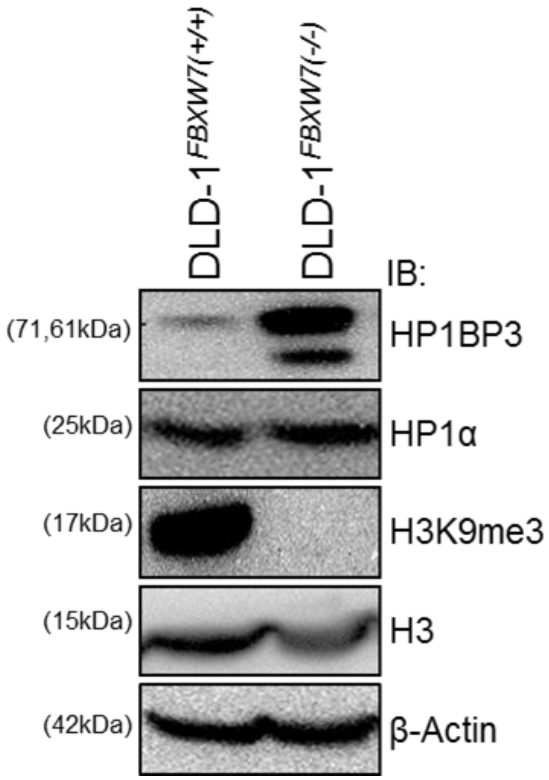


Figure 3-16: Western blotting analysis for endogenous HP1BP3, H3K9me3, and HP1α protein levels in DLD-1$^{FBXW7(+/+)}$ vs. DLD-1$^{FBXW7(-/-)}$ cells. Total protein of 100 µg was run on 10 % or 15 % SDS-PAGE and transferred to PVDF membranes. Anti-HP1BP3, -HP1α, and -H3K9me3 antibodies were used to detect endogenous level of HP1BP3, HP1α, and H3K9me3. H3 and β-Actin are used as a loading control in western blot analysis. WB experiment was repeated in two different occasions.

3.3 Discussion

As euchromatin and heterochromatin can be distinguished by specific histone tail modifications, epigenetic modifications such as H3K9 tri-methylation, have been well characterised as a mark of transcriptional repression. However, acetylation of the same residue has been correlated with transcriptional activation. Deregulation of enzyme activity and other non-histone cofactor molecules responsible for tri-methylating or acetylating H3K9 may associate in carcinogenesis (Hayami et al., 2011; Hu et al., 2014; Khanal et al., 2013; Kogure et al., 2013; Wang et al., 2013b; Yin et al., 2015). Consequently, the dysregulation of H3K9me3/H3K9ac levels is a hallmark of many cancers (Benard et al., 2014; Benard et al., 2013; Deligezer et al., 2010; Hamamoto et al., 2015; Leszinski et al., 2012). Moreover, low H3K9me3 levels contribute to elevated self-renewal capability of differentiated melanoma cells (Tan et al., 2014). In CRC, the genetic cause of the disease is well understood, but the underlying epigenetic modification requires more investigation.

According to our results, it appears that *FBXW7*, which is mutated in 17–20 % of CRC cases (Davis et al., 2014; Kuipers et al., 2015), participates in the degradation of HP1BP3 in a phosphorylation-dependent manner via GSK-3β activity (Figure 3-3 and Figure 3-4) and in maintaining a high H3K9me3 ratio in human CRC cells. High HP1BP3 expression in HCT116 cells with the *FBXW7* alleles deletion may result in decreased H3K9me3 and increased H3K9ac (Figure 3-1 B, Figure 3-10, and Figure 3-16) (Figure 3-17), leading to aberrant activation of gene expression and/or genomic instability.

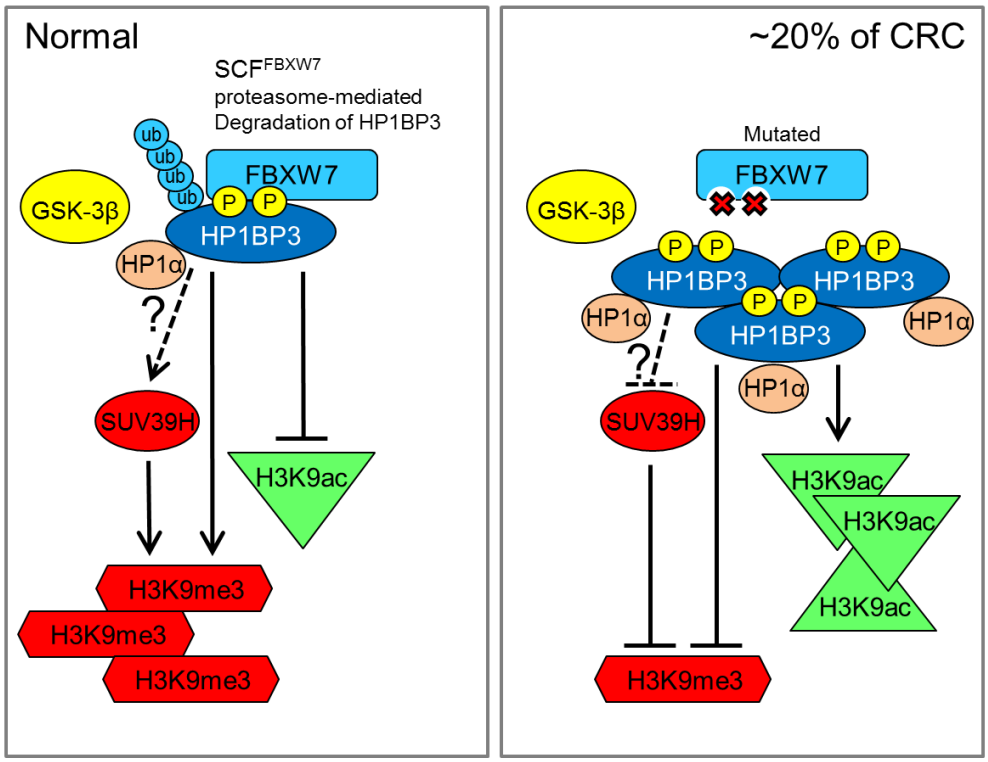


Figure 3-17: FBXW7 regulation of chromatin via HP1BP3/HP1α/H3K9me3 complex in normal cells versus human colon cancer cells mutated for FBXW7.

Nevertheless, the HP1BP3-induced alteration between trimethylated and acetylated H3K9 can consequently be mediated by blocking the activity of SUV39H1/2 histone methyltransferase or other histone methyltransferases and/or histone deacetylases, or stimulating histone acetyltransferases or histone demethylases but further studies are required to verify this in CRC cells. Despite the involvement of HP1α in transcriptional gene silencing (Canzio et al., 2014; Dialynas et al., 2006), it was reported that HP1α (located in *Drosophila*'s chromosomes) is found at many euchromatic/gene active sites (Kwon and Workman, 2011; Piacentini et al., 2009; Sdek et al., 2013) with an ability in opening the chromatin (Cryderman et al., 2011). It is

possible that the loss of the H3K9me3/HP1α complex or interaction/co-localisation in MEF$^{Suv39h1/2(-/-)}$ cells (Figure 3-11 A, Figure 3-14 B and Figure 3-15 B) can induces the HP1BP3/HP1α complex/co-localisation observed in human colorectal cancer HCT116$^{FBXW7(-/-)}$ cells (Figure 3-8 B and Figure 3-9 B) (Figure 3-17). Therefore, the subsequent chapters will focus on exploring the mechanisms by which *FBXW7* is mutated, leading to HP1BP3 accumulation, H3K9me3 repression and H3K9ac stimulation in CRC cells, as well as the possible oncogenic activity of HP1BP3. However, it would be interesting to explore the levels and the patterns of H3K9 mono- and di-methylation in the tested cell lines. Hopefully, future experiments reveal more about the underlying mechanisms, i.e. how FBXW7 inhibits H3K9me3 accumulation via HP1BP3 or possibly a histone methyltransferase such as SUV39H1, and their biological significance in carcinogenesis

CHAPTER 4

HP1BP3 Regulates Epithelial–Mesenchymal Transition (EMT), Epigenetically

4.1 Brief introduction

Apart from the few recent publications regarding HP1BP3 (Dutta et al., 2014a; Garfinkel et al., 2015a; Garfinkel et al., 2015b; Hadac et al., 2016; Hayashihara et al., 2010a), little is known about the function and role of HP1BP3 in normal and cancer cells via the epigenetic programming. Tumour cells respond to transcriptional- and epigenetic-changes and undergo epithelial-to-mesenchymal transition (EMT) (Bedi et al., 2014; Lamouille et al., 2014; Wu et al., 2012). Moreover, we and other groups have recently demonstrated that there is an intimate correlation between the FBXW7, EMT and drug resistance (Du and Shim, 2016; Li et al., 2015; Lorenzi et al., 2016; Mao et al., 2008; Wang et al., 2013d; Yu et al., 2014). Here, therefore we investigated the possible role of HP1BP3 as the FBXW7 target, mediated epigenetic reprograming the EMT in fibroblast and HCT116 CRC cell lines.

EMT is proof of cell plasticity that is critical to normal development and malignant progression (Lamouille et al., 2014; Mani et al., 2008; Nieto and Cano, 2012). This process is generally accompanied by enhanced cell migration and metastasis via acquiring mesenchymal characteristics (such as up-regulation of Vimentin, N-cadherin, Snail1, ZEB-1) and loss of expression of epithelial markers (such as E-cadherin) (Lamouille et al., 2014; Mani et al., 2008). In EMT, migrating tumour cells acquire “stem cell-like” properties and exhibit drug resistance, explaining the eradication of cancer cells by chemotherapy (Bedi et al., 2014; Du and Shim, 2016). Despite their close correlation, the deep insight into EMT, cancer stem cells (CSC), and drug resistance remains largely unexplored. Moreover, although extensive

epigenetic reprogramming (Tam and Weinberg, 2013; Wu et al., 2012) occurs during cell differentiation and malignant transformation (Meissner, 2010; Mohn and Schübeler, 2009), how epigenetics regulate EMT via heterochromatin-associated protein(s) remains unknown. Consequently, we examined the level of heterochromatin-, euchromatin-, and EMT-related proteins using loss- and gain-of-function in a human skin fibroblast cell line (Tiger) and a colorectal cancer cell line (HCT116) to explore the biological importance of HP1BP3 in linking between the epigenetics and EMT process.

Consistent with the results presented in the previous chapter, we found a negative correlation between HP1BP3 and H3K9me3 via downregulation of the SUV39H1 expression, while HP1BP3 positively correlated with the H3K9ac. Ectopic expression of HP1BP3 was involved in EMT induction by upregulating ZEB-1 and Snail1 transcription factors and consequently the level of N-cadherin and Vimentin mesenchymal markers and, inhibiting of E-cadherin epithelial marker. Interestingly, we also found that depletion of HP1BP3 could reverse the EMT process through suppressing the ZEB-1, Snail1, Vimentin, and upregulating of E-cadherin levels.

4.2 Results

4.2.1 Generation and validation of stable fibroblast (Tiger) and HCT116 cell lines over-expressing GFP-HP1BP3

Stable integration and long-term expression of a gene of interest is a common gain-of-function approach that allow efficient alteration of gene function (Büssow, 2015). Stably transfected cell lines are used in a wide range of research applications (Chaudhary et al., 2012; Lai et al., 2013). The generation of a stable cell line is important in structural and functional biology. Therefore, to investigate the role of HP1BP3 in regulating chromatin structure and gene transcription, we initially generated the human fibroblast and colorectal cancer cell lines that stably expressing the long HP1BP3 isoform (Material & Methods; Section 2.2.3.5).

To this end, we over-expressed pLVX-eGFP or pLVX-eGFP-HP1BP3 (from Dr M. Abuzinada in Dr Nateri's laboratory) in Tiger and HCT116 cell lines. These plasmid was constructed and fully validated (by double restriction enzymes digestion and DNA sequencing) in Dr Nateri's lab. Both plasmids contained an *EcoR*I restriction site in their multiple cloning site (MCS). Accordingly, *EcoR*I was used for validating the given plasmids and digesting the pLVX-eGFP-HP1BP3 and the pLVX-eGFP backbone vectors (Figure 4-1 A and B), as outlined in the Material and Methods (Section 2.2.2.1). *EcoR*I has an additional restriction site near to the 5′ end of HP1BP3 DNA sequence in the pLVX-eGFP-HP1BP3 plasmid. This digestion should then result in two DNA fragments corresponding to HP1BP3 (1.6 kb) and the

backbone vector pLVX-eGFP (8.8 kb). Digested DNAs were run on 1 % agarose gel (Materials & Methods; Section 2.2.2.2) to confirm the release of the indicated DNA fragments and the backbone vector linearisation (Figure 4-1 C). The digestion confirmed the presence of the two expected DNA fragments (Figure 4-1 C).

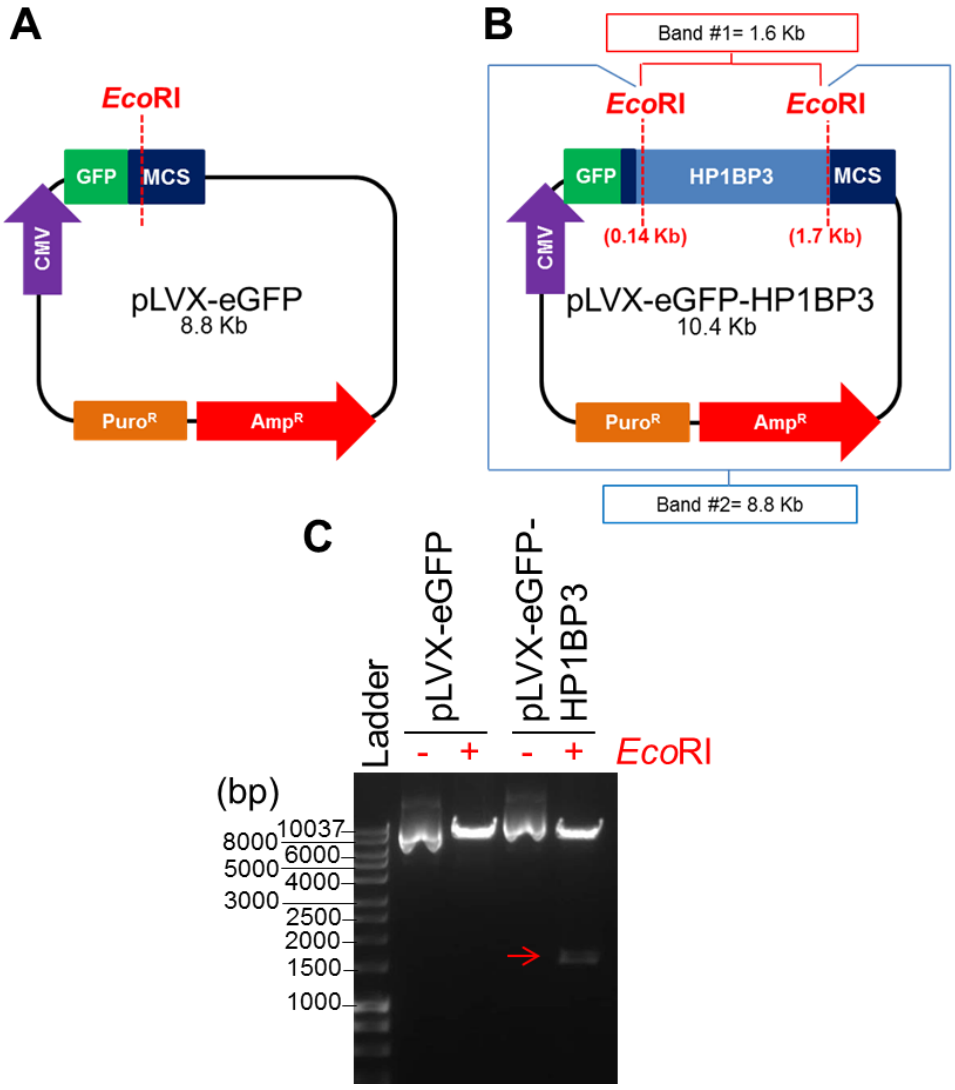
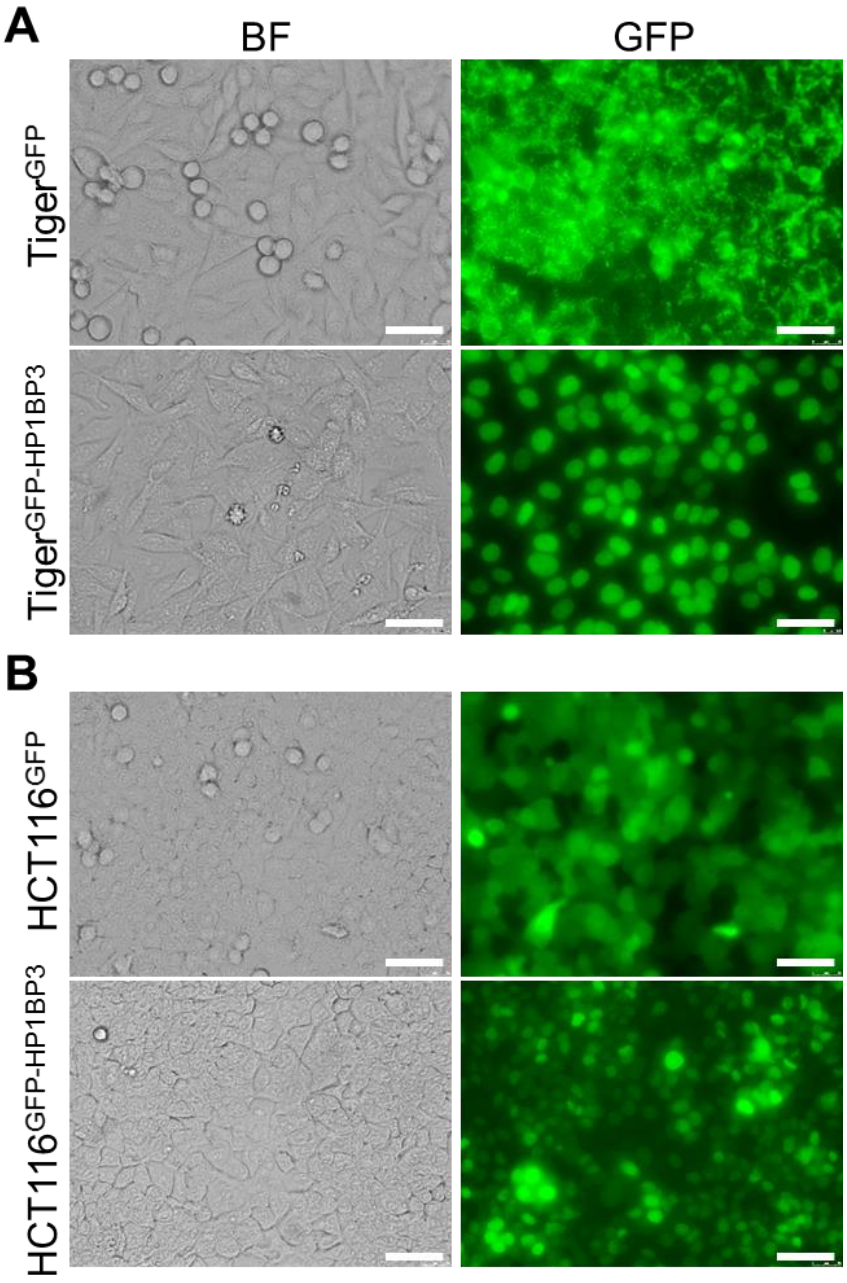


Figure 4-1: The pLVX-eGFP and pLVX-eGFP-HP1BP3 plasmid maps, and validation analysis by restriction enzyme digestion. (A and B) Schematic presentation showing the backbone vector pLVX-eGFP and pLVX-eGFP-HP1BP3 plasmid with *Eco*RI restriction enzyme sites. (C) The digested DNAs (pLVX-eGFP and pLVX-eGFP-HP1BP3) were run on 1 % agarose gel to confirm the linearisation of the vector (8.8 kb) and the release of the two expected DNA fragments (1.6 kb and 8.8 kb length) out from pLVX-eGFP-HP1BP3 plasmid.

To validate GFP-HP1BP3 expression, the pLVX-eGFP-HP1BP3 and the control pLVX-eGFP plasmids were transfected into the cells. These plasmids express a Puromycin-resistant gene that acts as an antibiotic selection marker. Briefly, cells seeded in 6-well plates until 50-60 % confluent, followed by plasmid transfection as illustrated in Materials and Methods (Section 2.2.3.4). The transfected cells were maintained for 3 days in culture, prior to selection. Subsequently, the Puromycin selection was carried out every 2 days for 10 days, during which all green fluorescent protein (GFP)– Puromycin-negative cells had died; the remaining cells contained plasmids emitting GFP fluorescence. Single cells were transferred to 96-well plates and grown until they formed colony-like structures and reached high confluence (Materials & Methods; Section 2.2.3.5), following which they were amplified and inspected for GFP or GFP-HP1BP3 expression.

Prior to western blotting verification of HP1BP3 expression by the generated stable cell lines, we observed HP1BP3 expression via fluorescence microscopy. The fluorescence microscopy analysis of the cells expressing enhanced GFP (eGFP, as a control for transfection efficiency) or eGFP-HP1BP3 confirmed eGFP or eGFP-HP1BP3 expression, respectively, in all generated cell lines (Figure 4-2 A and B). As shown in Figure 4-2 A and B, HP1BP3 was expressed in spotty nuclear localisation similar to the expression pattern of the endogenously expressed HP1BP3 (Chapter 3; Figure 3-8 and Figure 3-12). In the eGFP-expressing cells (control), the eGFP was expressed in both nuclear and cytoplasmic subcellular compartments (Figure 4-2 A and B).

Western blotting (Material & Methods; Section 2.2.4) of whole cell lysates confirmed the eGFP-HP1BP3 and eGFP expression (Figure 4-2 C). Moreover, as shown in Figure 4-2 C, the expression of HP1BP3 fused to eGFP in the pLVX-eGFP-HP1BP3 construct yielded the expected size of around 98 kDa [71 kDa (HP1BP3) + 27 kDa (eGFP)]. Frequently, non-specific bands were observed when using the anti-eGFP antibody. These can easily be distinguished from GFP in Figure 4-2 C for both cell lines stably expressing the eGFP. These non-specific bands were detected in a molecular weight range of 17–19 kDa, and the intensity of the non-specific bands were usually distinct from the eGFP bands. Together, these data suggest that the eGFP and eGFP-HP1BP3 DNA fragments were incorporated in the genome of transfected cell lines.


A
BF
GFP
Tiger^GFP
Tiger^GFP-HP1BP3
B
HCT116^GFP
HCT116^GFP-HP1BP3

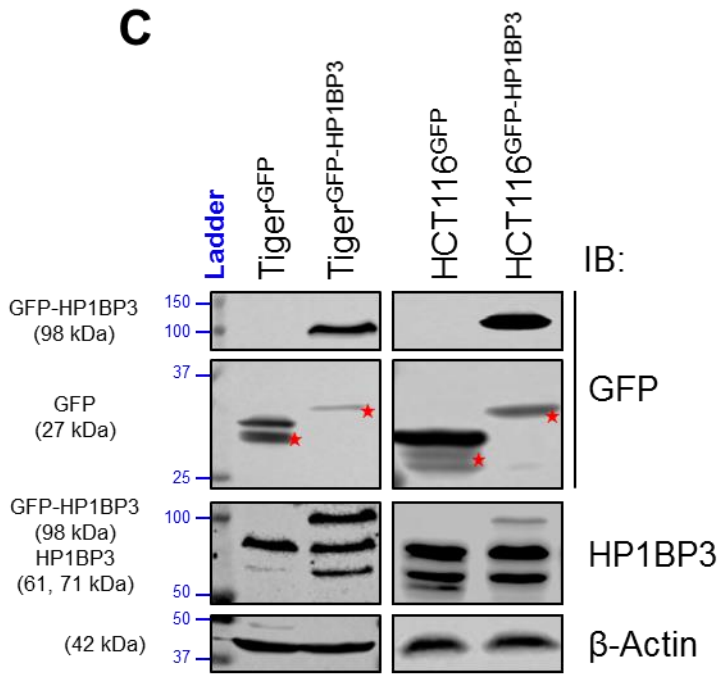


Figure 4-2: Evaluation of GFP-HP1BP3 protein expression in both Tiger and HCT116 stable cell lines. (A) Fluorescence microscopy of transfected Tiger cells with pLVX-eGFP (top) and pLVX-eGFP-HP1BP3 (bottom). (B) Fluorescence microscopy of transfected HCT116 cells with pLVX-eGFP (top) and pLVX-eGFP-HP1BP3 (bottom). Scale bare is 50 µm. (C) Western blotting analysis shows the expression of GFP-HP1BP3 in Tiger and HCT116 stable cell lines with anti-GFP, -HP1BP3, and -β-Actin (as a loading control) antibodies. Total protein of 100 µg was run on 10 % SDS-PAGE and transferred to PVDF membranes. Cells stably expressing pLVX-eGFP plasmid used as a control for transfection efficiency. The red stars indicate unspecific bands and western blotting analysis experiments were repeated at least in three different occasions.

4.2.2 Characterization and epigenetic/gene expression profiling of stable cell lines overexpressing HP1BP3

As outlined in chapter 3, the SUV39H1 binds to HP1α, which functions as a histone methyltransferase to methylate Lys-9 of histone H3 (Lachner et al., 2001; Yamamoto and Sonoda, 2003). SUV39H1 plays an essential role in ensuring faithful chromosome segregation through HP1α modulation at pericentric/paracentric chromatin inversion, which is vital in normal homeostasis and in cancer (De Koning et al., 2009; Kwon and Workman, 2011; Maison et al., 2002; Peters et al., 2001; Thomsen et al., 2011; Vad-Nielsen and Nielsen, 2015). H3K9me3 is a well-known transcriptional heterochromatin repressive marker; H3K9ac is a well-known epigenetic marker enriched in the euchromatic promoter region of activated genes (Bannister and Kouzarides, 2011; Bártová et al., 2008; Wang et al., 2008). Therefore, we examined whether the stably overexpressed HP1BP3 protein could affect H3K9ac and/or SUV39H1/H3K9me3 expression/levels.

To further testing the possibility of the deregulated HP1BP3 altering the heterochromatin–euchromatin inversion of mammalian cells, we used Tiger and HCT116 cell lines that stably expressed GFP or GFP-HP1BP3 proteins. Western blotting showed that ectopic HP1BP3 expression decreased SUV39H1 and H3K9me3 while has increased the H3K9ac levels in both cell lines (Figure 4-3). Note that the SUV39H1 expression was undetectable or very low in CRC HCT116 cells (Figure 4-3). Moreover, consistent with our earlier finding (Chapter 3; Figure 3-1 B and Figure 3-10 B), HP1α protein levels were unaltered (Figure 4-3). This finding suggests that HP1BP3 might

act as an important regulator of the transcription of many genes by altering the levels of two common markers of heterochromatin–euchromatin inversion: H3K9me3 and H3K9ac. However, further work is needed to assess the expression of other histone modifying enzymes involved in H3K9 acetylation and methylation. Also, it will be interesting in future to define genes, which are involved in the regulation of cancer progression, associated with the HP1BP3.

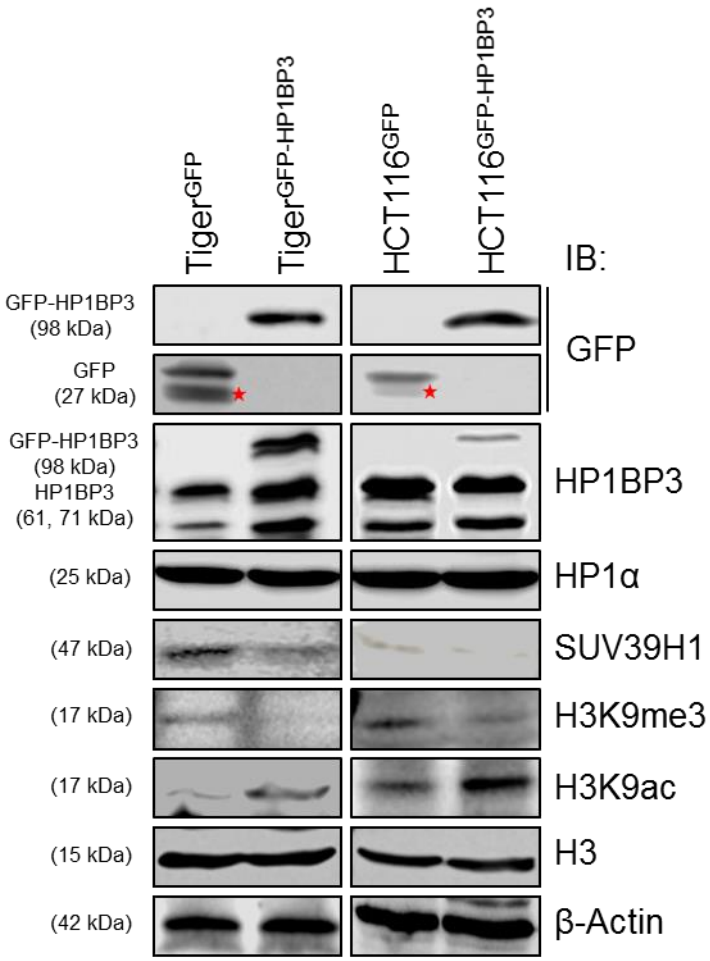


Figure 4-3: HP1PB3 decreases the expression/levels of SUV39H1/H3K9me3 while increases H3K9ac levels. Western blot analysis for GFP, HP1BP3, SUV39H1, H3K9me3, or H3K9ac was performed in both Tiger and HCT116 stably expressing GFP or GFP-HP1BP3. Total protein of 100 µg (for anti-GFP, -HP1BP3, -HP1α, -H3K9me3, -H3K9ac, -H3) or 250 µg (for anti-SUV39H1) was run on 10 % (for anti-GFP, -HP1BP3, -HP1α, -SUV39H1, -β-Actin) or 15 % (for anti-H3K9me3, -H3K9ac, -H3) SDS-PAGE and transferred to PVDF membranes. Anti-β-Actin and -H3 were served as loading control. The red stars indicate unspecific bands and western blotting analysis experiments were repeated at least in two different occasions.

4.2.3 Deletion of HP1BP3 leads to SUV39H1/H3K9me3 induction and inhibition of H3K9ac in HCT116$^{FBXW7(-/-)}$ cells

As outlined earlier, Dr Nateri's laboratory have identified a number of new FBXW7-associated proteins including HP1BP3, and by using a wide range of experimental models showed that FBXW7 targets HP1BP3 for degradation (Abuzinada M. et al., in submission). Our earlier results (Chapter 3; Figure 3-1 B) further confirmed the accumulation of HP1BP3 protein when *FBXW7* deleted in HCT116 cells. Furthermore, in *FBXW7*-deleted HCT116 cells H3K9ac (euchromatin marker) was upregulated, whereas the H3K9me3 (heterochromatin marker) downregulated (Chapter 3; Figure 3-10 B). Moreover, a stable overexpression of HP1BP3 in HCT116 cells and fibroblasts downregulated H3K9me3 and upregulated H3K9ac levels (Figure 4-3).

Herein, we aimed to explore the specificity of the HP1BP3 by loss-of-function (*HP1BP3* knockout alleles) strategy. Mice homozygous for a knockout *Hp1bp*3 allele exhibit postnatal lethality and reduced body size (Garfinkel et al., 2015a; Garfinkel et al., 2015b). While, I was working on this project, Dr M. Normatova in Dr Nateri's laboratory has generated the *HP1BP3*-deficient CRC cell lines using the CRISPR/Cas9 system (Normatova M. et al., 2016, in submission). The CRISPR/Cas9 system provides a highly accessible and amendable genome-editing tool that researchers implemented to manipulate the genome sequence precisely and to elucidate the function of a gene in biology and human diseases (Cho et al.,

2013; Ran et al., 2013). Subsequently, I have also used the HCT116$^{FBXW7(-/-):HP1BP3(+/+)}$ cells (wild-type control, with accumulated levels of endogenous HP1BP3) and *HP1BP3*-deficient HCT116$^{FBXW7(-/-):HP1BP3(-/-)}$ cells to confirm the role of HP1BP3 in regulating heterochromatin–euchromatin inversion.

In our laboratory, the *HP1BP3* knockout cell lines are characterized in details, and I have further validated the HP1BP3 protein expression of the given cell lines. The western blotting assays showed the complete absence of both a and b HP1BP3 isoforms (71 and 61 kDa, respectively) in the *HP1BP3* knockout HCT116$^{FBXW7(-/-)}$ cells compared to the control HCT116$^{FBXW7(-/-):HP1BP3(+/+)}$ cells (Figure 4-4; Lane 2 and 3 vs. 1). Furthermore, western blotting data showed the upregulation of H3K9me3 and H3K9ac reduction, while HP1α protein expression levels were not affected in the *HP1BP3* knockout cells (Figure 4-4; Lane 2 and 3 vs.). This confirms the specificity of HP1BP3 in chromatin remodelling via alteration of H3K9me3 and H3K9ac levels regardless of HP1α expression level. However, it would be interesting to examine whether up-regulated HP1BP3 influences the levels of H3K9me1 and H3K9me2.

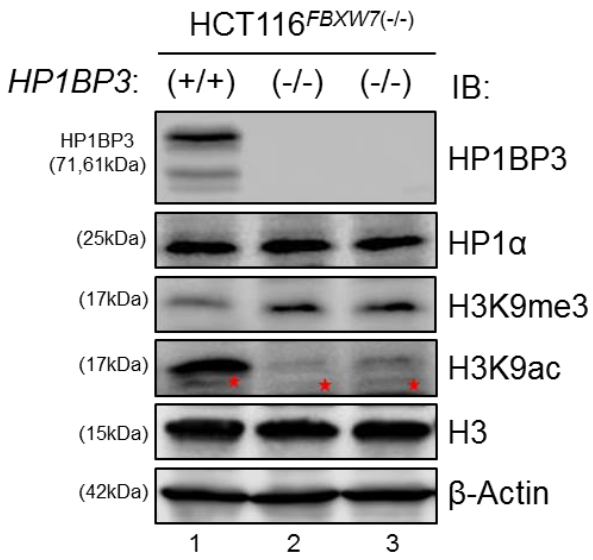


Figure 4-4: *HP1BP3* deletion leads to loss of H3K9ac in HCT116$^{FBXW7(-/-)}$. Western blot analysis for HP1BP3, HP1α, H3K9me3, or H3K9ac in HCT116$^{FBXW7(-/-):HP1BP3(+/+)}$ (control cell line) and HCT116 $^{FBXW7(-/-):HP1BP3(-/-)}$. Lane 2 and 3 represent different *HP1BP3*-knockout cells raised from two different CRISPR/Cas9 clones during bacterial transformation. Total protein of 100 µg was run on 10 % (for anti-HP1BP3, -HP1α, -β-Actin) or 15 % (for anti- H3K9me3, -H3K9ac, -H3) SDS-PAGE and transferred to PVDF membranes. Anti-β-Actin and -H3 were served as loading control. The red stars indicate unspecific bands. This experiment was repeated at least in two different occasions.

4.2.4 Regulation of epithelial-mesenchymal transition (EMT) by HP1BP3

4.2.4.1 Ectopic HP1BP3 expression upregulates the level of mesenchymal markers in Tiger fibroblast cells while downregulating the epithelial marker and upregulating mesenchymal markers in HCT116 cells

Upon the initial microscopic observations, we observed cell morphological changes of fibroblastic mesenchymal phenotypes in CRC HCT116 cells that are over-expressing HP1BP3 (Figure 4-5). Changes in cell morphology and cytoskeletal architecture are often associated with EMT (Lamouille et al., 2014; Moreno-Bueno et al., 2009). Additionally, changes in cytoskeleton actin from cortical actin filaments to stress fiber (filopodia formation) was documented as another hallmark of EMT which is involved in cell migration and invasion (Lamouille et al., 2014; Li et al., 2010; Vignjevic et al., 2006). Phalloidin staining is a valuable imaging tool used to observe the distribution of the filamentous structure of F-actin and F-actin stress fiber formation which shows the disorganization of adherens junctions, consequent weakened cell-cell association and induction of cell motility (Cooper, 1987; Lamouille et al., 2014; Li et al., 2010).

In HCT116, the effects of HP1BP3-over-expression on morphological changes and possible EMT association was initially inspected using tetramethylrhodamine B isothiocyanate (TRICT)-conjugated Phalloidin that presented the morphological alterations (Materials & Methods; Section

2.2.5.4) of HCT116$^{GFP\text{-}HP1BP3}$ versus the parental HCT116 cells (Figure 4-5; row 3, B vs. A). Branched and elongated phenotypes with protruding actin fibres were observed in HCT116$^{GFP\text{-}HP1BP3}$ cells (Figure 4-5; row 3, B). In opposition to HCT116$^{GFP\text{-}HP1BP3}$, HCT116 cells maintained the circular epithelial-like morphology with a cortical distribution of F-actin at the edge of the cells (Figure 4-5, row 3, A). These data suggest that HP1BP3 may involve in cell morphology via EMT alterations.

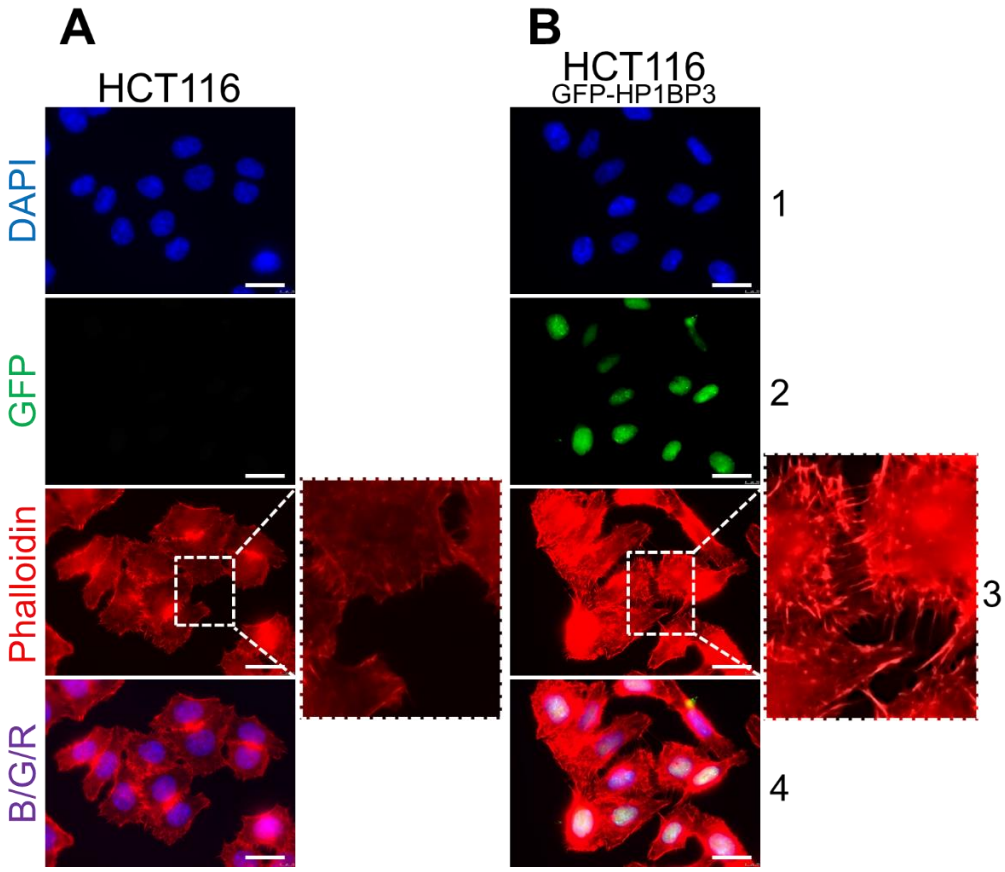


Figure 4-5: HP1BP3 alters the morphology of human HCT116 CRC cells. (A) HCT116 and (B) HCT116$^{GFP\text{-}HP1BP3}$ cells were examined by using tetramethylrhodamine B isothiocyanate (TRICT)-conjugated Phalloidin and stained for DAPI (blue, row 1) and Phalloidin (red, row 3). GFP represents the exogenous stable expression of HP1BP3 (row 2). The junction between HP1BP3 expressing cells or control cells is boxed and magnified (row 3) as indicated. HP1BP3-over-expressing HCT116 cells show gain of fibroblast-like pattern. This pattern has been seen in at least three different fields. This experiment was repeated in two different occasions. Scale bars is 20 μm.

Additionally, as ectopic expression of HP1BP3 downregulated H3K9me3, while the H3K9ac was upregulated (Figure 4-3), we have therefore hypothesised that HP1BP3 could be involved in chromatin relaxation, and leading to transcriptional activation of EMT-related genes. To test this, we used the HP1BP3–over-expressing Tiger and HCT116 cell lines to examine the expression level of the well-known EMT-associated markers and regulators such as the N-cadherin, Vimentin, E-cadherin, ZEB-1, and Snail1 (Batlle et al., 2000; Lamouille et al., 2014; Maeda et al., 2005; Romero-Pérez et al., 2013).

Western blotting indicated that ectopic HP1BP3 expression in the Tiger cells upregulated N-cadherin, ZEB-1, Snail1, and Vimentin expression (Figure 4-6). We also examined the expression of these EMT-related markers in GFP– or HP1BP3–over-expressing HCT116 cell lines and found that the mesenchymal markers Vimentin, N-cadherin, ZEB-1, and Snail1 were upregulated in $HCT116^{GFP\text{-}HP1BP3}$ cells compared with the control cells ($HCT116^{GFP}$) (Figure 4-6). Additionally, the epithelial marker E-cadherin was downregulated in $HCT116^{GFP\text{-}HP1BP3}$ cells (Figure 4-6). Taken together, these data suggest the involvement of HP1BP3 in the EMT activation of HCT116 cells, while the E-cadherin expression was still undetectable in fibroblasts.

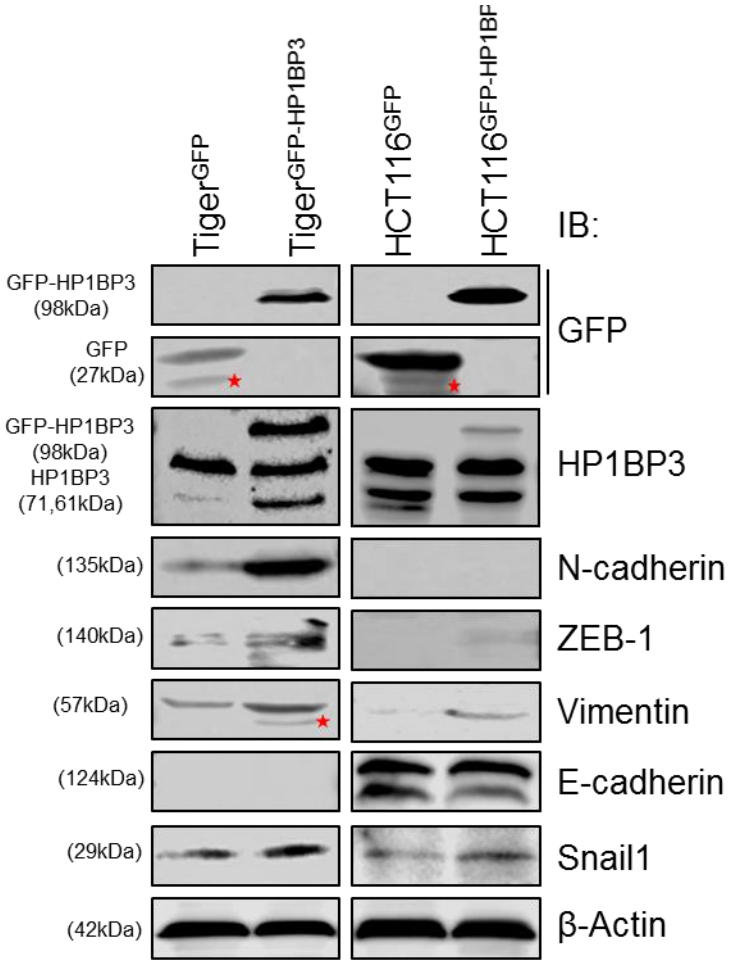


Figure 4-6: The over-expression of HP1BP3 upregulated N-cadherin, ZEB-1, Snail1, and Vimentin in Tiger cells, while upregulated ZEB-1, Vimentin, and Snail1, and inhibited E-cadherin protein expression in HCT116. Total protein of 50 µg (for anti-E-cadherin), 100 µg (for anti-GFP, -HP1BP3, -N-cadherin, -Vimentin, -Snail1) or 250 µg (for anti-N-cadherin, -ZEB-1, -Vimentin, -E-cadherin) was run on 8 % (for anti-N-cadherin, -ZEB-1, -E-cadherin) or 10 % (for anti-GFP, -HP1BP3, -Snail1, -β-Actin) SDS-PAGE and transferred to PVDF membranes. Membranes were probed with primary antibodies against GFP, HP1BP3, N-cadherin, ZEB-1, Vimentin, E-cadherin, and Snail1. Anti-β-Actin was served as loading control. The red stars indicate unspecific bands and western blotting analysis experiments were repeated at least in two different occasions.

4.2.4.2 Loss of *HP1BP3* in HCT116$^{FBXW7(-/-)}$ cells supresses EMT by inhibiting ZEB-1, Vimentin, and Snail1 and upregulating E-cadherin

To confirm the involvement of endogenous HP1BP3 in regulating EMT activity, we performed *HP1BP3* loss-of-function experiments using *HP1BP3*-deficient HCT116 cells with *FBXW7* allele deletions. Western blotting confirmed the loss of HP1BP3 expression in the HCT116$^{FBXW7(-/-):HP1BP3(-/-)}$ cells (Figure 4-8) when compared to the control HCT116$^{FBXW7(-/-):HP1BP3(+/+)}$ cells.

It has been shown that *FBXW7*- depleted cells undergo dramatic activation of EMT *in vitro* and/or *in vivo* [(Wang et al., 2013d; Yang et al., 2015; Yu et al., 2014); Li N & Babaei-Jadidi R., et al., Cancer Cell, 2016 under revision]. As expected, the microscopic examination and Phalloidin staining displayed morphological alteration in HCT116$^{FBXW7(-/-):HP1BP3(-/-)}$ (Figure 4-7; row 2, B) when compared to the control cells [HCT116$^{FBXW7(-/-):HP1BP3(+/+)}$] (Figure 4-7; row 2, A). It was obvious that loss of HP1BP3 in *FBXW7*-null cells attenuated the branched and elongated phenotypes observed in both HCT116$^{FBXW7(-/-):HP1BP3(+/+)}$ (Figure 4-7; row 2, A) and HCT116$^{GFP\text{-}HP1BP3}$ (Figure 4-5; row 3, B) which further suggests the role of HP1BP3 in activating EMT pathway.

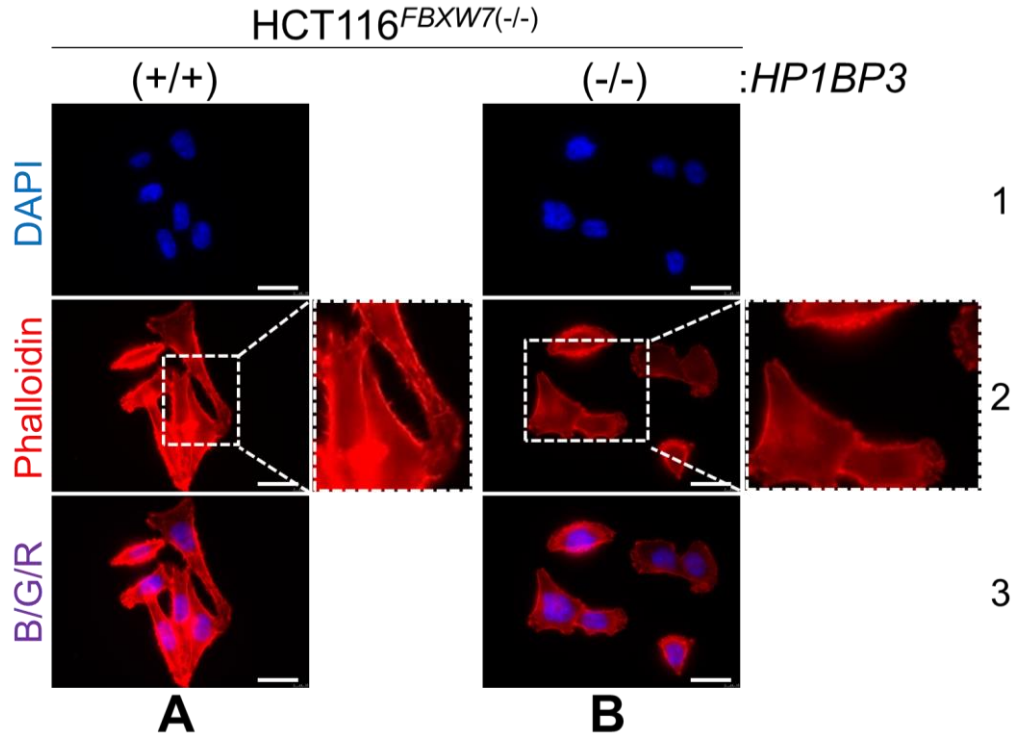


Figure 4-7: Loss of *HP1BP3* alters the morphology of human HCT116 CRC cells. (A) HCT116$^{FBXW7(-/-):HP1BP3(+/+)}$ (control cell line) and (B) HCT116 $^{FBXW7(-/-):HP1BP(-/-)}$ cell lines were examined by using tetramethylrhodamine B isothiocyanate (TRICT)-conjugated Phalloidin stained for DAPI (blue, row 1) and Phalloidin (red, row 2). The junction between HP1BP3 null cells or control cells is boxed and magnified (row 2) as indicated. HP1BP3 loss in HCT116$^{FBXW7(-/-)}$ cells show loss of fibroblast-like pattern. This pattern has been seen in at least three different fields. This experiment was repeated in three different occasions. Scale bars is 20 μm.

Additionally, HP1BP3 knockout caused a modest reduction in ZEB-1 and Vimentin expression levels and decreased significantly the Snail1 expression level in the *HP1BP3*-deficient cells when compared to the control HCT116$^{FBXW7(-/-):HP1BP3(+/+)}$ cells (Figure 4-8). On the other hand, E-cadherin was upregulated in HCT116$^{FBXW7(-/-):HP1BP3(-/-)}$ cells compared to the control cells (Figure 4-8). These findings suggest that the loss of HP1BP3 can reverse EMT.

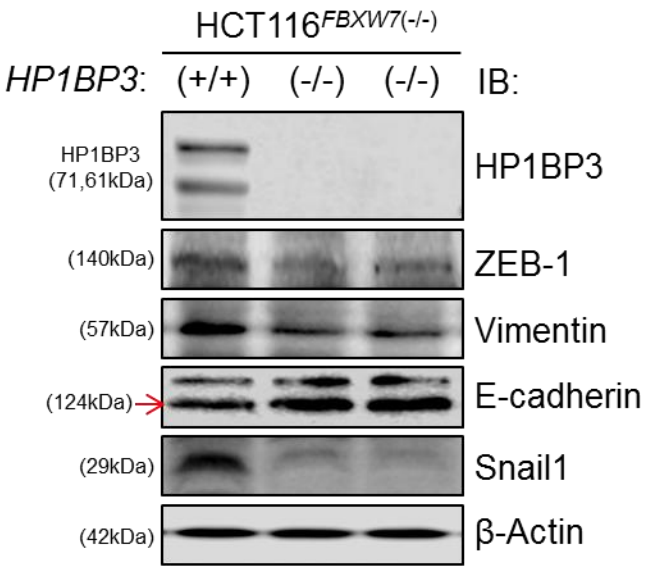


Figure 4-8: Loss of *HP1BP3* upregulates E-cadherin while downregulates ZEB-1, Vimentin, and Snail1 proteins expression in HCT116$^{FBXW7(-/-)}$. Western blot analysis for HP1BP3, ZEB-1, Vimentin, E-cadherin, or Snail1 in HCT116$^{FBXW7(-/-):HP1BP3(+/+)}$ and HCT116 $^{FBXW7(-/-):HP1BP3(-/-)}$. Lane 2 and 3 represent different HP1BP3-knockout cells raised from two different CRISPR/Cas9 clones during bacterial transformation. Total protein of 50 µg (for anti-E-cadherin), 100µg (for anti-HP1BP3, -Snail1), or 250µg was run (for anti-ZEB-1, -Vimentin) on 8 % (for anti-E-cadherin, -ZEB-1) or 10 % (for anti-HP1BP3, -Vimentin, -Snail1, -β-Actin) SDS-PAGE and transferred to PVDF membranes. Anti-β-Actin was served as loading control. This experiment was repeated in two different occasions.

4.3 Discussion

EMT and its reverse process MET (mesenchymal-epithelial transition) and their regulatory mechanisms play critical roles in carcinogenesis and metastasis (Lamouille et al., 2014; Nieto and Cano, 2012). In addition, recent reports suggest that the epigenetic changes such as histone modifications and DNA methylation are involved in EMT/MET regulation and reprogramming (Bedi et al., 2014; Kiesslich et al., 2013; Le Bras et al., 2012). Previously, we showed HP1BP3 upregulation and H3K9me3 reduction in DLD-1 and HCT116 cells lacking *FBXW7* alleles regardless of their differing genetic backgrounds (Chapter3; Figure 3-1 B, Figure 3-10 B, and Figure 3-16). Nevertheless, there was no variation in HP1α protein level (Chapter 3; Figure 3-1 and Figure 3-16) and no effect on HP1α distribution among the HCT116$^{FBXW7(+/+)}$ and HCT116$^{FBXW7(-/-)}$ cell lines regardless of HP1α and HP1BP3 localisation (Chapter 3; Figure 3-8 and Figure 3-9 C). Moreover, statistical analysis suggested a significant increase in HP1BP3 and HP1α co-localisation in HCT116$^{FBXW7(-/-)}$ versus HCT116$^{FBXW7(+/+)}$ cells (Chapter 3; Figure 3-9 C). Therefore we assume that binding HP1BP3 may rescue the repressive activity of HP1α via competitive inhibition between HP1α/SUV39H1 and H3K9me3 as reported previously (Maison et al., 2011). We found that there were no changes in the distribution of both HP1α and H3K9me3 although H3K9me3 levels were reduced significantly in HCT116$^{FBXW7(-/-)}$ cells compared to HCT116$^{FBXW7(+/+)}$ cells (Chapter 3; Figure 3-10 A and B). The data suggest that the loss of FBXW7-mediated HP1BP3 accumulation may lead to chromatin modulation via H3K9me3 loss in cancer cells. However, we wonder how HP1BP3, via possible

interaction/inhibition with/of histone-modifying enzymes such as the SUV39H1 methyltransferases, obstructs the build-up of H3K9me3 and what the biological implications behind HP1BP3 in cancer development are.

It is well-known that highly active genes show strong H3K9ac enrichment at their promoters while silenced genes are strongly correlated with H3K9me3 enrichment (Barski et al., 2007; Wang et al., 2008). To maintain the repressive heterochromatin state, the N-terminus of SUV39H1 recruits and interacts with HDAC1, 2, or 3 (histone deacetylases) (Vaute et al., 2002) (Figure 4-9). Additionally, a histone deacetylase called SIRT1 regulates SUV39H1, deacetylating H3K9ac (at promoters of several tumour suppressors genes) and SUV39H1, and leading to elevated levels of SUV39H1 and H3K9me3 and to heterochromatin formation and tumour suppressors genes go silent (Liu and McCall, 2013; Vaquero et al., 2007) (Figure 4-9). Conversely, many proteins/enzymes participate to promote and maintain euchromatin structure. It has been reported that Prolyl Isomerase Pin1 interacts with SUV39H1 in a phosphorylation-dependent manner and stimulates the ubiquitination-mediated degradation of SUV39H1 via MDM2 E3 ubiquitin ligase, causing reduced H3K9me3 levels (Khanal et al., 2013; Mungamuri et al., 2012; Zhou and Lu, 2016). Moreover, Wang et al. revealed that SET domain-containing protein 7 (SET7/9), a protein methyltransferase, plays role in methylating SUV39H1, inhibiting the methyltransferase activity of SUV39H1, and leading to decreased H3K9me3 levels (Wang et al., 2013a). Furthermore, the enzymes PCAF/GCN5 (H3K9 acetyltransferase) and JMJC/KDM or LSD-1 (H3K9 demethylases) (Hamamoto et al., 2015;

Kouzarides, 2007) are involved in maintaining an active chromatin state, where their activity is specific to H3K9 residues.

Thus, to gain insight into the influence of HP1BP3 in modulating the heterochromatin state in mammalian cells, the HP1BP3 loss- and gain-of-function approaches were applied. HP1BP3 gain-of-function confirmed the negative correlation between HP1BP3 and SUV39H1/H3K9me3 (Figure 4-3), which in turn correlated with the increased H3K9ac (euchromatin marker) in the Tiger and HCT116 cell lines (Figure 4-3). However, HP1α protein expression was not affected by the ectopic upregulation of HP1BP3 (Figure 4-3). It was difficult to detect SUV39H1 expression in HCT116^{GFP} cells in comparison to Tiger^{GFP} cells (Figure 4-3). This reduction of SUV39H1 and consequent transcriptional activation could further support the fact that cancer cells have more tumour suppressor or/and oncogene transcription activity than normal cells. Regardless of the low expression of SUV39H1 in HCT116 cells, its expression was further reduced by the ectopic expression of HP1BP3 (Figure 4-3). HP1BP3 loss-of-function in the HCT116$^{FBXW7(-/-)}$ cells confirmed this finding (Figure 4-4), suggesting that the upregulation of endogenous HP1BP3 in HCT116$^{FBXW7(-/-)}$ cells is involved in inhibiting the SUV39H1/H3K9me3-mediated silencing of euchromatic genes and may also be associated with inducing the acetylated state of H3K9 (euchromatin marker). In fact, it is possible that HP1BP3 contributes to SUV39H1 inhibition, may be by competing between SIRT1 and SUV39H1 interaction sites or by supressing SIRT1 activity (Figure 4-9). Additionally, induced expression of HP1BP3 could block the transcriptional

repression of SUV39H1 by inhibiting HDAC1, 2, or 3 recruitment or by promoting SET7/9 expression (Figure 4-9). Another possibility is that HP1BP3 upregulation mediates SUV39H1 inhibition and degradation by upregulating Pin1 expression. However, these possibilities require further investigation.

Taking into account that HP1BP3–over-expressing cells showed morphological changes (Figure 4-5), we postulated that the HP1BP3 accumulation caused by *FBXW7* loss could be involved in transcriptionally activating EMT-related genes by inducing chromatin relaxation through H3K9ac. It is well-known that the switch from E-cadherin to N-cadherin is an important indicator of EMT in many cancers, including colorectal cancer (Kiesslich et al., 2013; Lamouille et al., 2014; Maeda et al., 2005). Our data showed N-cadherin upregulation in HP1BP3–over-expressing Tiger cells (Figure 4-6). However, Tiger cells are mesenchymal, therefore E-cadherin expression was not detectable, as expected. Consequently, we were unable to determine whether HP1BP3 represses E-cadherin in fibroblasts. On the other hand, Snail1 is a transcription factor family member highly expressed in mesenchymal cells and that mediates E-cadherin repression by binding to its promoter (Batlle et al., 2000; Lin et al., 2010). Snail1 expression was slightly higher in $Tiger^{GFP\text{-}HP1BP3}$ in compression to $Tiger^{GFP}$ (control) cell lines (Figure 4-6). We also showed the upregulation of Vimentin, a mesenchymal cell migration regulator (Batlle et al., 2000; Lamouille et al., 2014), in HP1BP3–over-expressing Tiger when compared to the control cells (Figure 4-6). The expression of ZEB-1, a well-known transcriptional

suppressor of E-cadherin epithelial marker in many cancers (Bedi et al., 2014; Lamouille et al., 2014; Romero-Pérez et al., 2013; Sanchez-Tillo et al., 2010; Vaiopoulos et al., 2014), was also higher in Tiger$^{GFP\text{-}HP1BP3}$ cells in compared to the control (Figure 4-6). Taken together, our data suggest that HP1BP3 can upregulates the expression of N-cadherin, ZEB-1, Snail1, and Vimentin in Tiger fibroblast cells, where it induces the euchromatic state and consequently affects the transcription of these EMT-related genes.

In CRC, HCT116 cells, the ectopic expression of HP1BP3 upregulated Snail1 expression and repressed E-cadherin (Figure 4-6). Western blotting did not reveal N-cadherin upregulation in HCT116$^{GFP\text{-}HP1BP3}$ cells, although Vimentin and ZEB-1 expression was very low in HCT116 cells, but the upregulation of their expression levels was observed in the HCT116 cells expressing HP1BP3 ectopically. Additionally, the loss-of-function study highly supports our finding of HP1BP3-mediated EMT activation (Figure 4-8).

In summary, HP1BP3 might be an upstream regulator of SUV39H1 activity and subsequent chromatin remodelling cause changing cell morphologies via activating EMT pathway. Furthermore, HP1BP3 could be a potential target for reversing EMT and intervention in the progression of about 20 % of colorectal cancer cases that acquire *FBXW7* mutation (Figure 4-9). However, further work is required to measure the mRNA levels of EMT-related genes, using quantitative PCR (qPCR). This could elucidate potential mechanisms by which HP1PB3 induces EMT in normal and/or CRC.

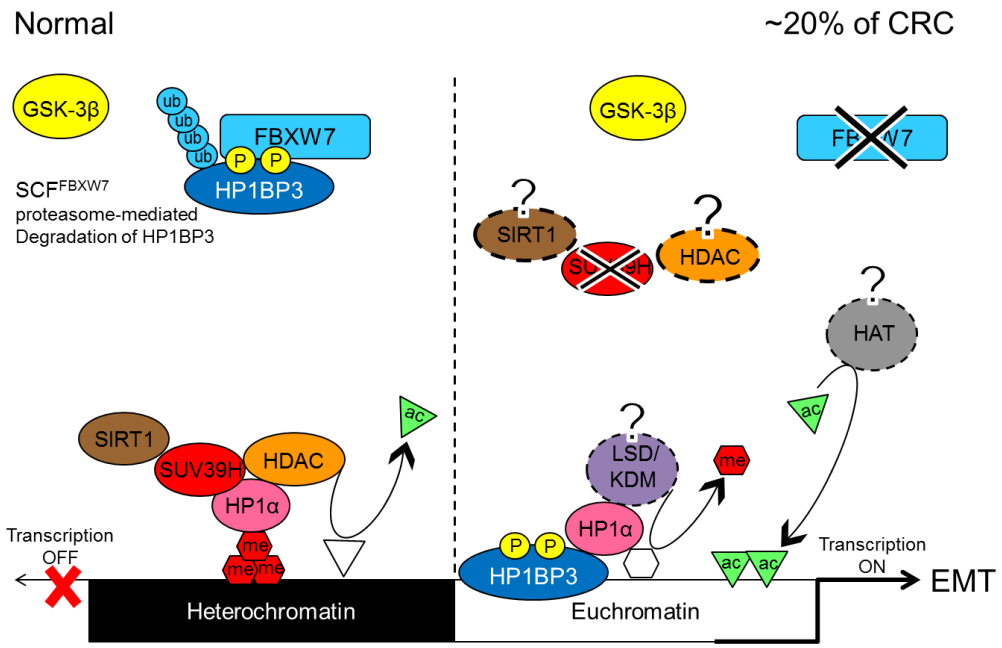


Figure 4-9: FBXW7 mutation upregulates HP1BP3 expression, which leads to chromatin decondensation and consequently inappropriate activation of EMT-associated genes most likely in around 20 % of CRC cases.

CHAPTER 5

The Epigenetic Regulation of Cell Cycle Progression by HP1BP3

5.1 Brief introduction

The accurate expression and transmission of genetic information requires chromatin rearrangement from a decondensed to a highly condensed structure. This rearrangement mechanism enables cell division (Antonin and Neumann, 2016). DNA is wrapped around histones, in which histone tails are subjected to numerous post-translational modifications that dictate its level of compaction (Soshnev et al., 2016). The access of transcription factors to the designated regulatory sites is highly regulated through the packaging of DNA and chromatin configuration. These modifications affect structural changes in chromatin condensation during the cell cycle (Ma et al., 2014; Park et al., 2011).

During the cell cycle progression, the chromatin is de-condensed in the S phase to enable replication (Alexandrow and Hamlin, 2005). However, chromosome recondensation is a vital process that regulates the separation of sister chromatids in mitosis and maintains the genomic stability (Cimini et al., 2003). The H3K9me3 is a marker of heterochromatic status which it is highly expressed in G2 to M transition while the H3K9ac, a marker of euchromatic status, is highly expressed during the S phase (Park et al., 2011). Therefore, an irregular chromatin remodelling-dependent regulatory system results in cell cycle deregulation. Deregulation of the cell cycle can lead to unfaithful chromosome segregation, aberrant proliferation, and cancer development.

In addition to the histone modification, the expression of non-histone proteins is required for cell cycle progression, whereas the contribution of non-histone proteins and in particular HP1BP3 protein to cell cycle progression and chromatin rearrangement remain poorly understood. In Chapter 3, we found that, the loss of *FBXW7* in HCT116 and DLD-1 colorectal cancer cells led to the accumulation of nuclear HP1BP3 and H3K9me3 reduction, whereas HP1α levels were unchanged. Moreover, *FBXW7* loss–mediated HP1BP3 induction decreased H3K9me3 levels in the cells. Furthermore, there were fewer co-localisation foci between HP1α and HP1BP3 in $FBXW7^{(+/+)}$ colorectal cancer cells than in $FBXW7^{(-/-)}$ cells. Accordingly, we suggested that *FBXW7* loss–mediated HP1BP3 induction can rescue the repression activity of HP1α via competitive inhibition between HP1α/SUV39H1 and H3K9me3 as reported by Maison *et al.* (Maison et al., 2011). Furthermore, we reported in Chapter 4 that HP1BP3 alters heterochromatin states, inhibits SUV39H1, impairs H3K9 methylation, and enhances the acetylation of the same lysine residue, which activates EMT. Additionally, a study conducted on HP1BP3 reported early postnatal lethality in $Hp1bp3^{(-/-)}$ mice (Garfinkel et al., 2015b). Taken these data together, we hypothesised that the upregulation of HP1BP3, a heterochromatin component, could cause global defects in chromatin compaction during cell cycle progression.

To address the influence of HP1BP3 upregulation or its loss on cell cycle progression, we used HP1BP3–over-expressing Tiger (human skin fibroblasts) and HCT116 cells, $HCT116^{FBXW7(-/-):HP1BP3(-/-)}$ cells, and $HCT116^{FBXW7(-/-)}$ shRNA-HP1BP3 (*HP1BP3* knockdown) cells. We also

used HCT116$^{FBXW7(+/+)}$ versus HCT116$^{FBXW7(-/-)}$ cells, in which *FBXW7* loss causes endogenously induced HP1BP3 expression. Then, the cell cycle in each cell line was examined and analysed, and compared to the appropriate control.

Moreover, to investigate the effect of HP1BP3 upregulation on specific cell cycle phases, Tiger^{GFP} versus Tiger$^{GFP\text{-}HP1BP3}$ cells and HCT116$^{FBXW7(+/+)}$ versus HCT116$^{FBXW7(-/-)}$ cells were treated with double thymidine (arrests cells at G1/S) and/or thymidine/nocodazole (arrests cells at G2/M) treatments (Materials & Methods; Section 2.2.7) (Stoeber et al., 2001; Whitfield et al., 2002; Whitfield et al., 2000). We have then focused on mechanisms that regulate the timing specific cell cycle phases in these cells using western blotting for anti- HP1BP3, -SUV39H1/H3K9me3, -H3K9ac, and Cyclin B1 antibodies.

In brief, we found that the HP1BP3 overexpression alter the cell cycle progression by induction of the early S phase entry, while cause delays in mitotic entry and its exit. However, *HP1BP3* loss accelerated the exit from mitosis and delayed S phase entry.

5.2 Results

5.2.1 HP1BP3 expression is highly correlated with cell cycle progression in mammalian cells

5.2.1.1 Constitutive overexpression of HP1BP3 induces the S- and G2/M-phases transition in Tiger and HCT116 cells

Many histone and non-histone proteins participate in chromatin remodelling regulation during the cell cycle progression. As our previously obtained data revealed that HP1BP3 regulates chromatin structure, it was of interest to explore the influence of HP1BP3 expression on cell cycle progression in Tiger and HCT116 cells stably overexpressing HP1BP3 protein.

Western blotting (Material & Methods; Section 2.2.4) of Tiger and HCT116 cell lysates confirmed the eGFP-HP1BP3 or eGFP expression (Figure 5-1 A and Figure 5-2 A). We used the Propidium iodide (PI) staining and the fluorescence-activated cell sorting (FACS) -based analysis (Materials & Methods; Section 2.2.6 and 2.2.8) to study the cell cycle distribution of cells stably over-expressing HP1BP3. The WEASEL software was used to generate both the cell cycle histograms and statistics (Figure 5-1 B and C and Figure 5-2 B and C). Importantly, ectopic expression of HP1BP3 noticeably decreased the percentage of cells in G0/G1, which was compensated by the increased percentage of Tiger$^{GFP\text{-}HP1BP3}$ and HCT116$^{GFP\text{-}HP1BP3}$ cells in S and G2/M phases as compared with the respective control cells expressing only GFP (Tiger^{GFP} and HCT116^{GFP}) (Figure 5-1 C and Figure 5-2 C).

Compared to the control, the ratio of G1 to G0 phase cells in the Tiger$^{GFP\text{-}HP1BP3}$ population was significantly lower than control cells (from 40.5 % to 27.8 %), while the Tiger$^{GFP\text{-}HP1BP3}$ cells in S- phase was significantly higher; from 41.4 % to 47.1 % (Figure 5-1 C). In addition, the G2/M population of Tiger$^{GFP\text{-}HP1BP3}$ cells increased significantly from 15.5 % to 18.9 % (Figure 5-1 C).

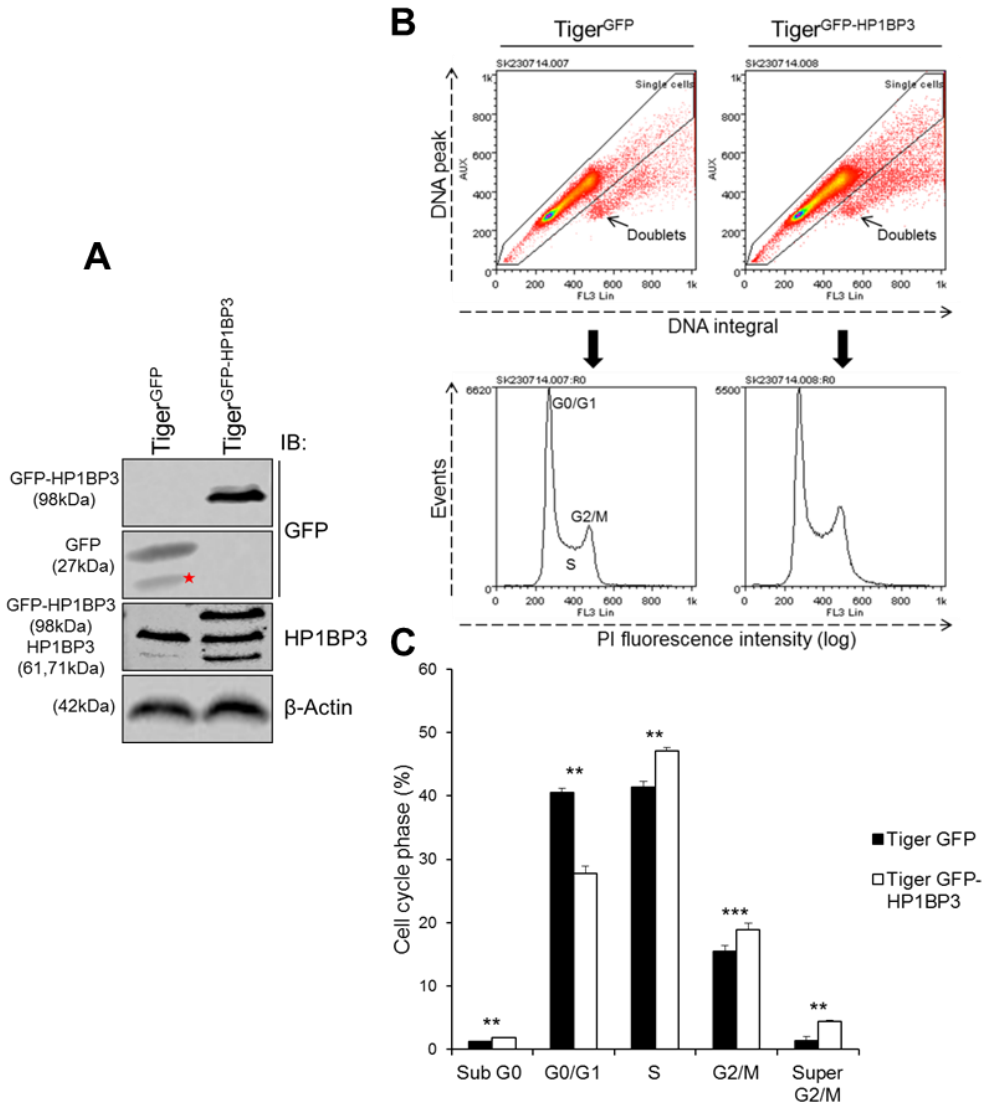


Figure 5-1: HP1BP3 overexpression induced cell cycle progression in fibroblasts (Tiger cells). (A) Western blotting analysis with anti-GFP, -HP1BP3, and -β-Actin (loading control) antibodies for cell lysates of Tiger$^{GFP-HP1BP3}$ or Tiger^{GFP} (control cells). The red stars indicate unspecific bands. After two days in culture, cells stained with PI as outlined in Materials & Methods chapter. Then, the cells were prepared for FACS analysis, to analyse cell cycle phases. (B) Histograms of cell cycle data were generated by WEASEL software for Tiger^{GFP} or Tiger$^{GFP-HP1BP3}$. (C) Statistical analysis of the cell cycle for Tiger^{GFP} or Tiger$^{GFP-HP1BP3}$ cells in which statistical differences resulted with stably expressing HP1BP3 are compared to control (GFP expressing cells). Statistical significant values were calculated using student's *t* test. *P= 0.01 to 0.05, **p= 0.001 to 0.01, ***p<0.001. Error bars show the STDEV of seeded cells in triplicate wells for each cell line. The percentage of sub G0 or super G2/M represents a small negative numbers of cells that are added to a little more or a little less than 100 %.

In Addition, flow-cytometric analysis showed the HCT116$^{GFP\text{-}HP1BP3}$ G0/G1 phase population was decreased; from 39.3 % to 31.0 %, while the S and the G2/M phase populations were increased respectively; from 33.0 % to 35.5 % in S phase and from 12.3 % to 17.8 % in G2/M phase (Figure 5-2 C). These results demonstrate that ectopic HP1BP3 expression induces mammalian cell division.

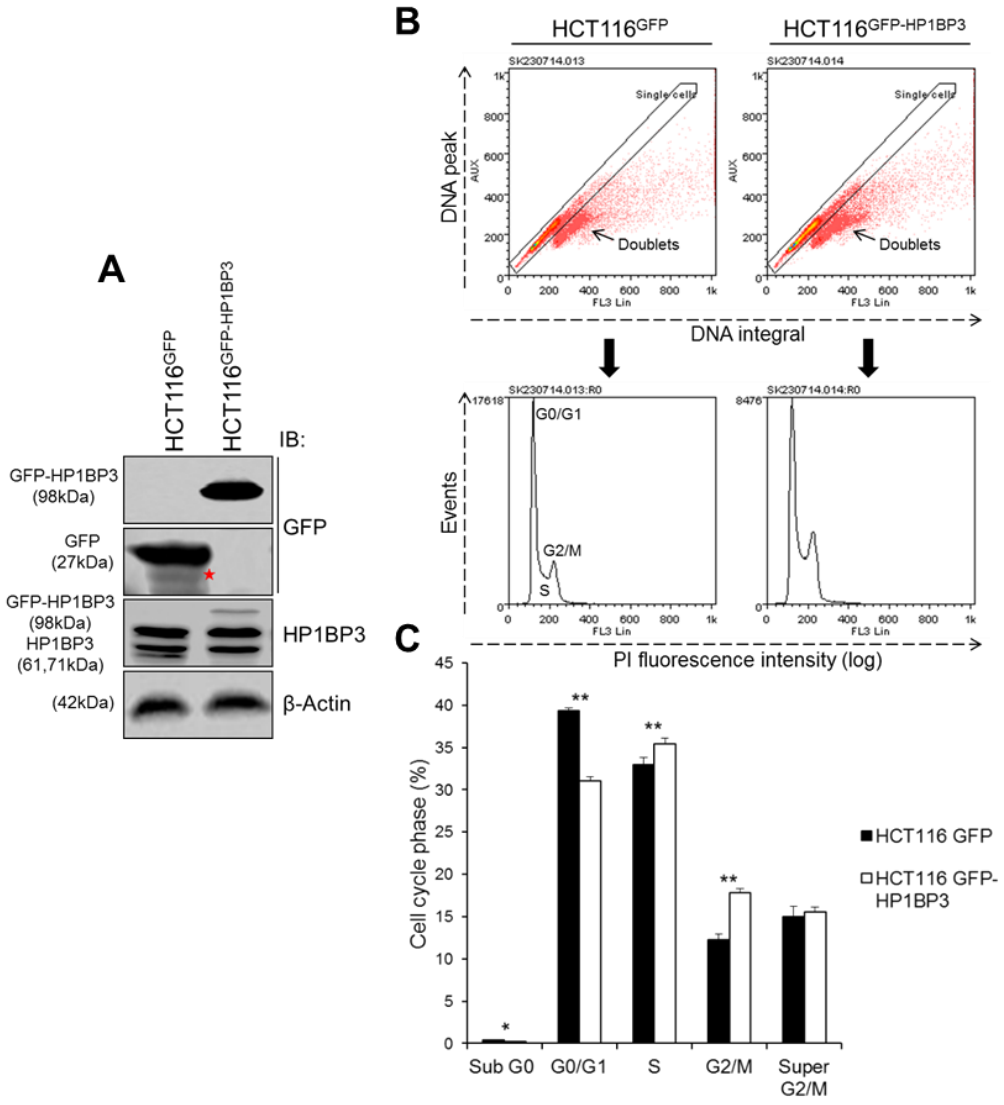


Figure 5-2: HP1BP3 overexpression induced cell cycle progression in HCT116 cells. (A) Western blotting analysis with anti-GFP, -HP1BP3, and -β-Actin (loading control) antibodies for cell lysates of HCT116^{GFP} (control cells) or HCT116$^{GFP\text{-}HP1BP3}$. The red stars indicate unspecific bands. After two days in culture, cells stained with PI as outlined in Materials & Methods chapter. Then, the cells were prepared for FACS analysis, to analyse cell cycle phases. (B) Histograms of cell cycle data were generated by WEASEL software for HCT116^{GFP} or HCT116$^{GFP\text{-}HP1BP3}$. (C) Statistical analysis of the cell cycle for HCT116^{GFP} or HCT116$^{GFP\text{-}HP1BP3}$ cells in which statistical differences resulted with stably expressing HP1BP3 are compared to control (GFP expressing cells). Statistical significant values were calculated using student's *t* test. *P= 0.01 to 0.05, **p= 0.001 to 0.01, ***p<0.001. Error bars show the STDEV of seeded cells in triplicate wells for each cell line.

5.2.1.2 Endogenous upregulation of HP1BP3 induces S and G2/M phases in HCT116 cells with *FBXW7* deletion

We showed exogenous overexpression of HP1BP3 (Figure 5-2 C) induced cell cycle progression in HCT116 cells. Our earlier data also showed that an endogenous HP1BP3 upregulation associated with loss of *FBXW7* in HCT116 cells (Chapter 3; Figure 3-1 B). We have therefore examined the cell cycle progression related to loss of *FBXW7*, where there is endogenous accumulation of HP1BP3 in HCT116$^{FBXW7(-/-)}$ cells.

The western blotting verified the accumulation of HP1BP3 proteins in the HCT116$^{FBXW7(-/-)}$ cells (Figure 5-3 A). The PI staining and the following FACS analysis (Figure 5-3 B and C) showed that, compared to the control HCT116$^{FBXW7(+/+)}$ cells, the HCT116$^{FBXW7(-/-)}$ population in G0/G1 was decreased from 68.6 % to 42.0 %, while the S phase population was increased from 17.6 % to 37.8 % and the G2/M population was increased from 10.7 % to 16 % (Figure 5-3 C). This finding suggests that HP1BP3 upregulation due to mutation of *FBXW7* (Figure 5-3 A), induces entry into S and G2/M phases in human colorectal cancer cells.

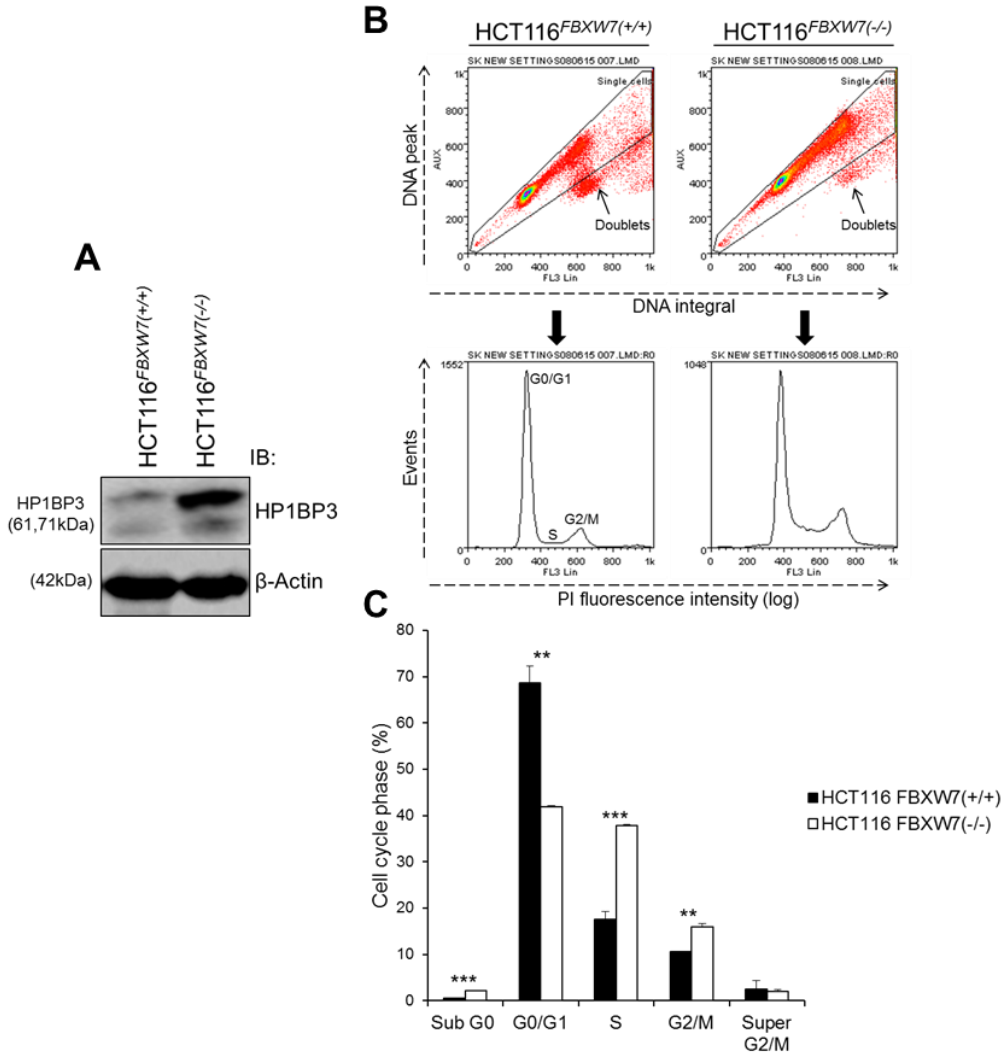


Figure 5-3: HP1BP3 accumulation induced cell cycle progression in HCT116$^{FBXW7(-/-)}$ cells. (A) Western blotting analysis with anti-HP1BP3 and -β-Actin (loading control) antibodies for cell lysates of HCT116$^{FBXW7(+/+)}$ (control cells) or HCT116$^{FBXW7(-/-)}$. The red stars indicate unspecific bands. After two days in culture, cells stained with PI as outlined in Materials & Methods chapter. Then, the cells were prepared for FACS analysis, to analyse cell cycle phases. (B) Histograms of cell cycle data were generated by WEASEL software for HCT116$^{FBXW7(+/+)}$ or HCT116$^{FBXW7(-/-)}$. (C) Statistical analysis of the cell cycle for HCT116$^{FBXW7(+/+)}$ or HCT116$^{FBXW7(-/-)}$ cells. Statistical significant values were calculated using student's *t* test. *P= 0.01 to 0.05, **p= 0.001 to 0.01, ***p<0.001. Error bars show the STDEV of seeded cells in triplicate wells for each cell line.

5.2.1.3 Inhibition and/or inactivation of HP1BP3 increases G0/G1 and consequently decreases HCT116$^{FBXW7(-/-)}$ cell populations in S phase

The HP1BP3 gain-of-function experiment revealed induced cell progression in HCT116$^{FBXW7(+/+)}$ cells (Figure 5-2 C). Moreover, the HP1BP3 upregulation associated with *FBXW7* loss caused cell cycle induction (Figure 5-3 C). These findings led us to validate the specificity of cell cycle activity modulated by HP1BP3 by downregulating and knockout of *HP1BP3* gene (loss-of-function) in HCT116$^{FBXW7(-/-)}$ cells.

This was initially achieved by using the *HP1BP3*-knockdown (shRNA-HP1BP3) versus control (Scramble-shRNA) in HCT116$^{FBXW7(-/-)}$ cells. Dr Normatova and Dr Babaei-Jadidi have initially generated and characterised the stable cell lines that are expressing the shRNA-HP1BP3, the Scramble-shRNA-GFP expressing cells (control) and the *HP1BP3* knockout cells using CRISPR-Cas9 methodology, respectively in Dr Nateri's laboratory. Prior to cell cycle analysis, HP1BP3 expression levels were confirmed again, by western blotting in the Scramble-shRNA and shRNA-HP1BP3 HCT116$^{FBXW7(-/-)}$ cells. There was considerable downregulation of both HP1BP3 isoforms (a and b isoforms at 71 and 61 kDa, respectively) in the *HP1BP3* knockdown cells as compared to the control cells (Figure 5-4 A). Both cell lines were PI-stained followed by FACS analysis. Interestingly, *HP1BP3* knockdown led to a substantial increase of cells in G0/G1, from 28.9 % to 32.6 % in comparison to the control, while reduced cells in S phase, from 49.8 % to 45.3 % (Figure 5-4 C). However, there was no significant

change in the G2/M population between *HP1BP3* knockdown and the control cells. There were 16.4 % and 17.0 % G2/M cells in the control and *HP1BP3* knockdown cells, respectively (Figure 5-4 C).

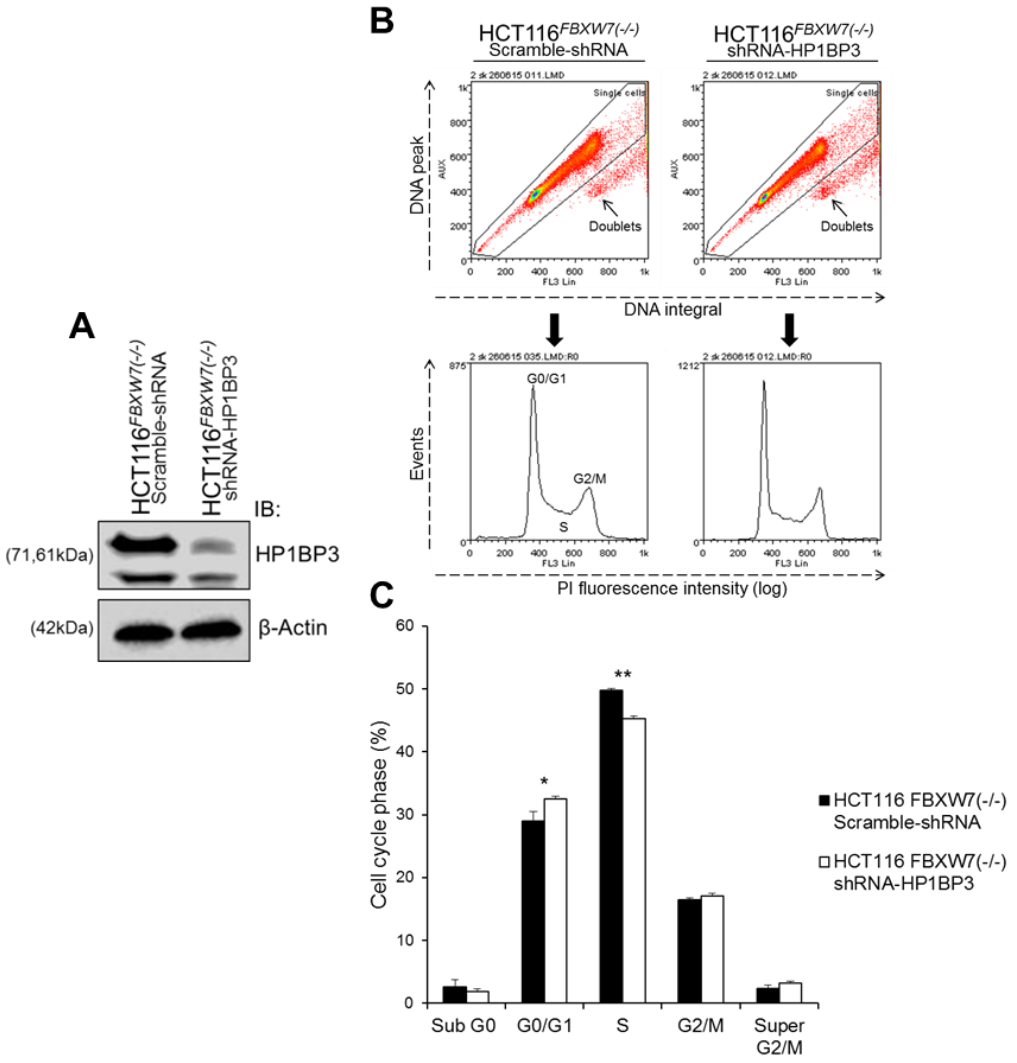


Figure 5-4: *HP1BP3* knockdown induced G0/G1 phase arrest in HCT116$^{FBXW7(-/-)}$ stably expressing shRNA-HP1BP3 cells. (A) Western blotting analysis with anti-HP1BP3 and -β-Actin (loading control) antibodies for cell lysates of HCT116$^{FBXW7(-/-)}$ cells that were stably expressing scramble-shRNA or scrambled control shRNA for HP1BP3. After two days in culture, cells stained with PI as outlined in Materials & Methods chapter. Then, the cells were prepared for FACS analysis, to analyse cell cycle phases. (B) Histograms of cell cycle data were generated by WEASEL software for HCT116$^{FBXW7(-/-)}$ Scramble-shRNA or HCT116$^{FBXW7(-/-)}$ shRNA-HP1BP3. (C) Statistical analysis of the cell cycle in the indicated stable cell lines in which statistical differences resulted with stably knockdown *HP1BP3* are compared to control (HCT116$^{FBXW7(-/-)}$ Scramble-shRNA) cell line, as presented. Statistical significant values were calculated using student's t test. *P= 0.01 to 0.05, **p= 0.001 to 0.01, ***p<0.001. Error bars show the STDEV of seeded cells in triplicate wells for each cell line.

We performed further experiments to confirm this finding using of *HP1BP3* knockout HCT116$^{FBXW7(-/-)}$ [HCT116$^{FBXW7(-/-):HP1BP3(-/-)}$] cells compared to the *HP1BP3* wild-type HCT116$^{FBXW7(-/-)}$ control cells [HCT116$^{FBXW7(-/-):HP1BP3(+/+)}$]. Knockout HCT116$^{FBXW7(-/-):HP1BP3(-/-)}$ cells were further confirmed that HP1BP3 was only expressed in the HCT116$^{FBXW7(-/-):HP1BP3(+/+)}$ control cells (Figure 5-5 A). The HCT116$^{FBXW7(-/-):HP1BP3(-/-)}$ population in G0/G1 was increased significantly from 17.5 % to 28.0 %, while the S-phase population was decreased greatly from 50.6 % to 41.7 %, (Figure 5-5, C). Consistent with *HP1BP3* knockdown cells however the G2/M population was unchanged [HCT116$^{FBXW7(-/-):HP1BP3(+/+)}$ control cells versus HCT116$^{FBXW7(-/-):HP1BP3(-/-)}$ cells] (Figure 5-5 C), where there was 26.8 % and 27.7 % G2/M cells in the control and *HP1BP3* knockdown cells, respectively (Figure 5-5 C). In summary, the cell population in G0/G1 phase after the knockdown or knockout of *HP1BP3* increased significantly as compared with that for S-phase cells. It appears that loss of *HP1BP3* blocks the G1 to S transition. The data support our initial hypothesis that HP1BP3 can regulate the cell cycle progression in colorectal cancer cells.

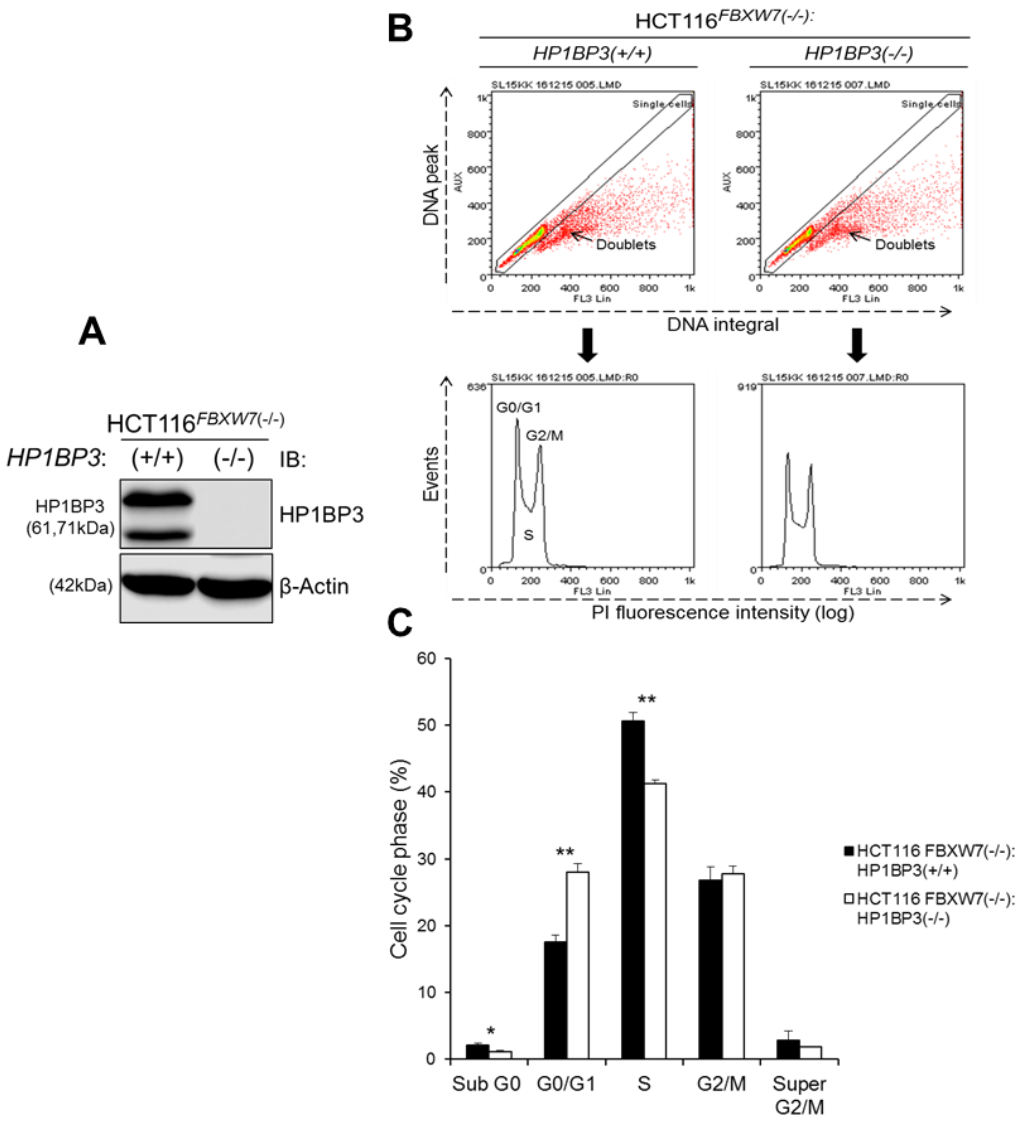


Figure 5-5: *HP1BP3* knockout arrested the cells at G0/G1-phase. (A) Western blotting analysis with anti-HP1BP3 and -β-Actin (loading control) antibodies for cell lysates of stable *HP1BP3* knockout HCT116$^{FBXW7(-/-)}$ and the control cell (HCT116$^{FBXW7(-/-):HP1BP3(+/+)}$). After two days in culture, cells stained with PI as outlined in Materials & Methods chapter. Then, the cells were prepared for FACS analysis, to analyse cell cycle phases. Histogram analysis was generated for (A) HCT116$^{FBXW7(-/-):HP1BP3(+/+)}$ control or HCT116$^{FBXW7(-/-):HP1BP3(-/-)}$ knockout cells. (B) Histograms of cell cycle data were generated by WEASEL software for HCT116$^{FBXW7(-/-):HP1BP3(+/+)}$ or HCT116$^{FBXW7(-/-):HP1BP3(-/-)}$. (C) Statistical analysis for cell cycle in the indicated cell lines in which statistical differences resulted with *HP1BP3* knockout are compared to control (HCT116$^{FBXW7(-/-):HP1BP3(+/+)}$) cell line, as presented. Statistical significant values were calculated using student's *t* test. *P= 0.01 to 0.05, **p= 0.001 to 0.01, ***p<0.001. Error bars show the STDEV of seeded cells in triplicate wells for each cell line.

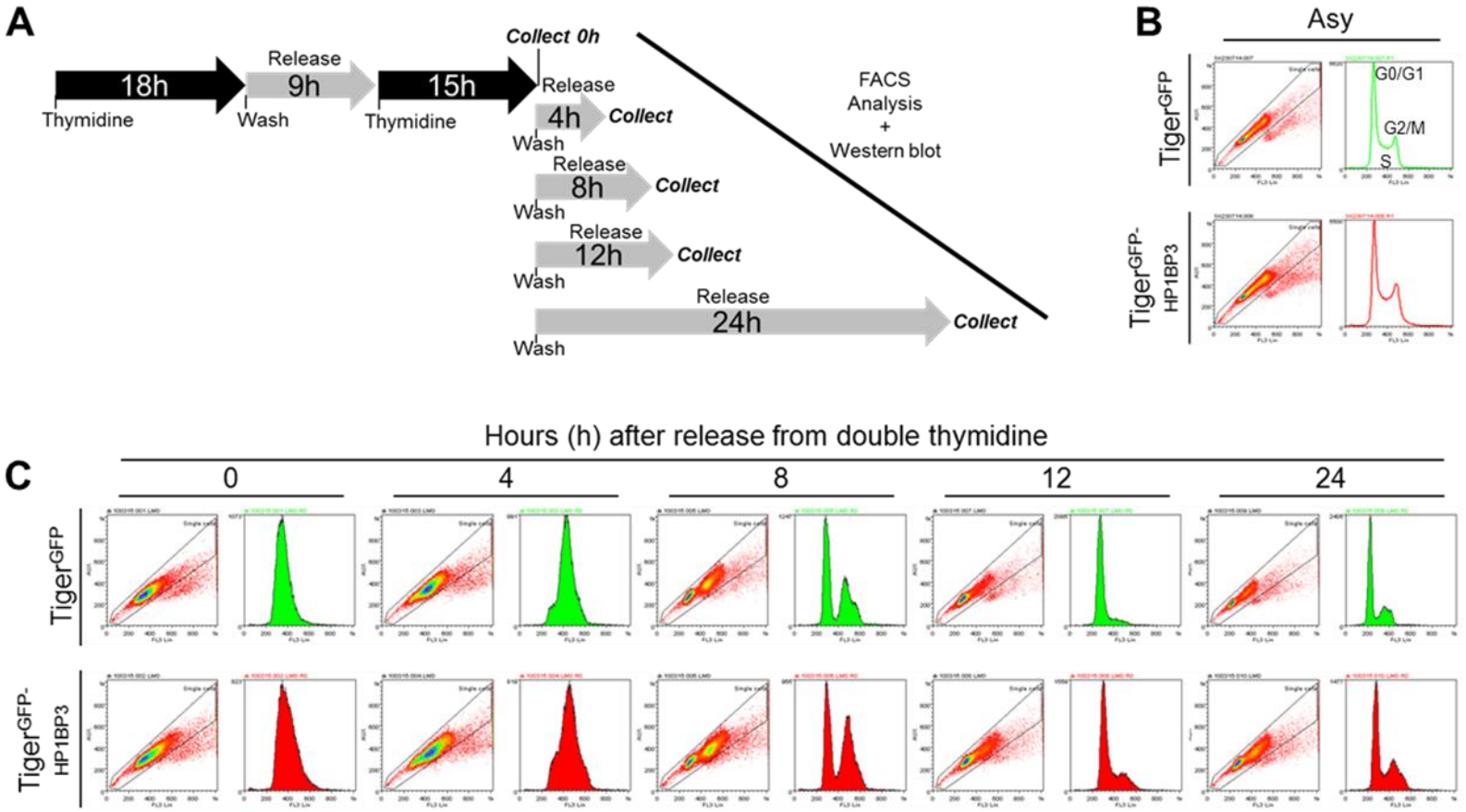
5.2.2 HP1BP3 epigenetically controls the transition between cell cycle phases in fibroblast (Tiger) cells

5.2.2.1 The HP1BP3 overexpression arrests Tiger cells in G2/M while inducing G1 to S phases transition

Chromatin binding proteins and chromatin modifications are highly dynamic and controlled during cell cycle progression. Earlier, we demonstrated correlation between H3K9me3 and H3K9ac levels, and cell cycle progression controlled by HP1BP3 over-expression (Chapter 4; Figure 4.3). Accordingly, we postulated that HP1BP3 upregulation might deregulate heterochromatin–euchromatin inversion within the context of the cell cycle. To address this possibility, we treated Tiger^{GFP} versus Tiger$^{GFP\text{-}HP1BP3}$ cells with a double thymidine block (an inhibitor of DNA synthesis) (Figure 5-6 A) and/or followed by treatment of cells with nocodazole (a mitotic inhibitor) (Figure 5-7 A) to obtain large cell populations at distinct phases of the cell cycle.

The cell cycle distributions and profiles of Tiger^{GFP} and Tiger$^{GFP\text{-}HP1BP3}$ cells treated with double thymidine block were evaluated via flow-cytometric analysis of PI-stained cells at different time points after release from the cell-cycle block (Figure 5-6, C-E, G, H, J and K) (Materials & Methods; Section 2.2.7). An untreated Tiger^{GFP} and Tiger$^{GFP\text{-}HP1BP3}$ cells used as an asynchronous (Asy) population (Figure 5-6 B). Tiger cells were synchronized at the G1/S phase border by double thymidine block (Figure 5-6 C; 0 h). At 8 h after release from double thymidine block, the

Tiger$^{GFP\text{-}HP1BP3}$ population in G0/G1 was decreased from 51.6 % to 37.5 %, while the S phase population was increased from 14.3 % to 20.5 %, and the G2/M population was increased from 23.3 % to 31.8 % when compared to the control (Figure 5-6 F). At 12 h after release, the Tiger$^{GFP\text{-}HP1BP3}$ G0/G1 population was decreased from 76.6 % to 56.0 %, while the S phase population was increased from 15.9 % to 33.2 % and the G2/M population was increased from 3.8 % to 6.7 % as compared to the control (Figure 5-6 I). However, at 24 h after release, ectopic HP1BP3 reduced the G0/G1 population from 61.25 % to 51.2 % and increased the S phase population from 12.3 % to 21.5 % (Figure 5-6 L). Surprisingly, the Tiger^{GFP} versus Tiger$^{GFP\text{-}HP1BP3}$ G2/M population from 15.6 % to 17.6 %, which was not statistically significant (Figure 5-6 L). These data suggest that overexpression of HP1BP3 is sufficient to induce the transition from G1 to S phase while extended G2/M arrest.


A
18h
Thymidine
Release
9h
Wash
15h
Thymidine
Collect 0h
Release
4h
Collect
Wash
Release
8h
Collect
Wash
Release
12h
Collect
Wash
Release
24h
Collect
Wash
FACS
Analysis
+
Western blot
B
Asy
TigerGFP
TigerGFP-HP1BP3
G0/G1
G2/M
S
C
Hours (h) after release from double thymidine
0
4
8
12
24
TigerGFP
TigerGFP-HP1BP3

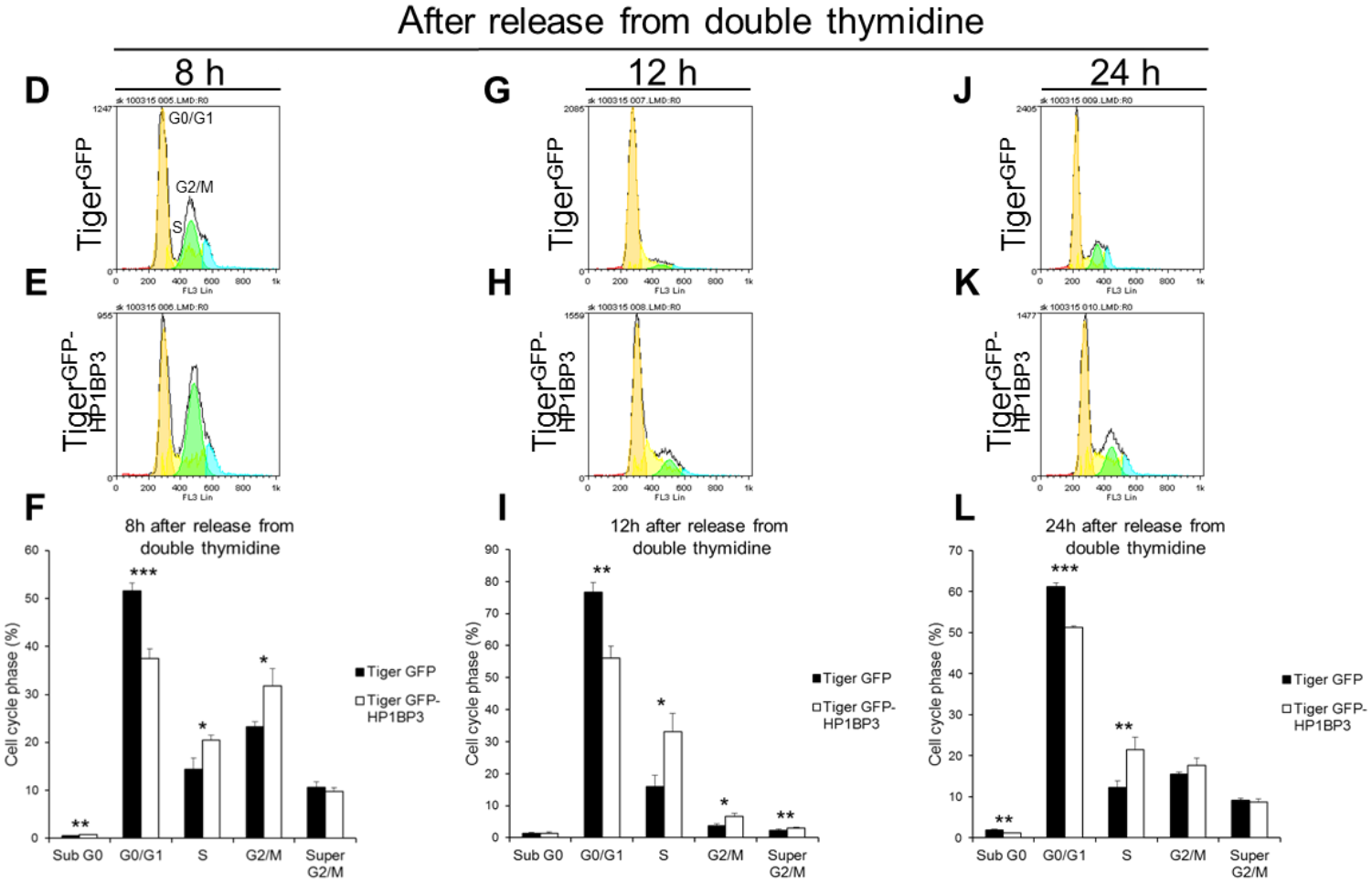
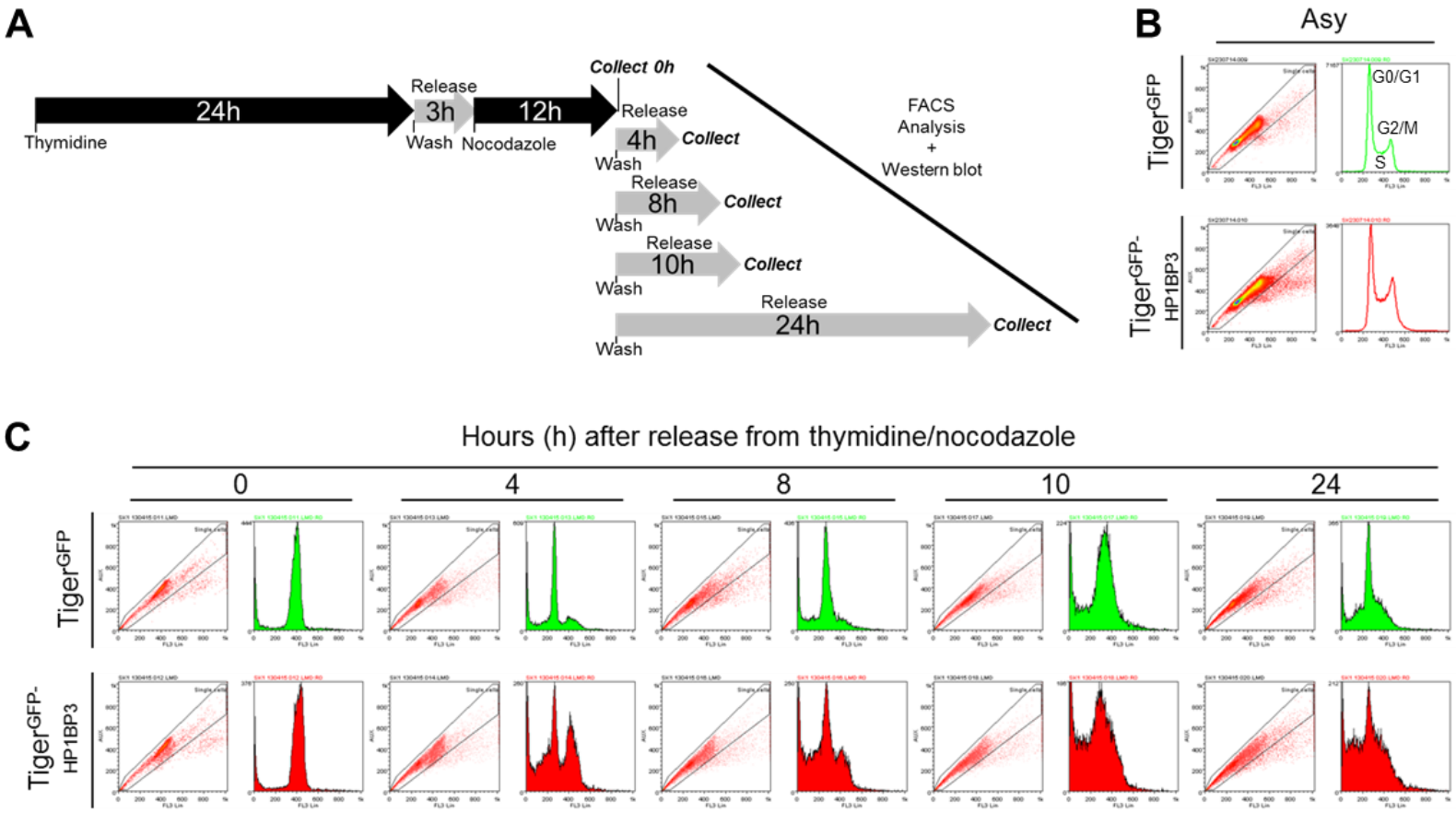

After release from double thymidine
8 h
12 h
24 h
D
E
G
H
J
K
TigerGFP
TigerGFP-HP1BP3
G0/G1
G2/M
S
FL3 Lin
F
I
L
8h after release from double thymidine
12h after release from double thymidine
24h after release from double thymidine
Cell cycle phase (%)
Tiger GFP
Tiger GFP-HP1BP3
Sub G0
G0/G1
S
G2/M
Super G2/M

Figure 5-6: HP1BP3 overexpression increases G1 to S transitioned cells while arresting another population of cells at G2/M phase, in G1/S-arrested Tiger cells. (A) Schematic shows the double-thymidine block protocol used to synchronise Tiger^{GFP} (control) and Tiger$^{GFP\text{-}HP1BP3}$ cell lines in G1/S border. (B) FACS profile of an asynchronous (Asy) population of cells was used as an untreated control for double-thymidine treated cells. Both cell lines were released into normal medium from the double-thymidine block for the indicated time points. Then, cell cycle profile (C-E, G, H, J, and K) was determined by FACS analysis of PI-stained cells collected at these time points. At 8 h (F), 12 h (I), and 24 h (L), cells were statistically analysed for their cell cycle distribution using WEASEL software. Statistical significant values were calculated for Tiger^{GFP} versus Tiger$^{GFP\text{-}HP1BP3}$ using student's *t* test. *P= 0.01 to 0.05, **p= 0.001 to 0.01, ***p<0.001. Error bars show the STDEV of seeded cells in triplicate wells for each cell line.

To further explore the mechanism of action of HP1BP3 in arresting Tiger cells at G2/M, the Tiger cells were synchronized and released in presence of thymidine/nocodazole, to examine cell cycle progression from mitosis to G0/G1 and from G0/G1 to S phase. Thymidine/nocodazole-induced synchronization was performed as presented in Figure 5-7 A and details described in Materials & Methods chapter; Section 2.2.7. Then, the percentage of cells were estimated in different cell cycle phases and their distribution were assessed by PI and flow-cytometric analysis (Figure 5-7 C-E, G, H, J, and K). An untreated asynchronous cell populations were used as a control for normal cell cycle progression (Figure 5-7 B).

The findings at 0 h after release from thymidine/nocodazole represents mitotic arrest in both cell lines (Figure 5-7 C; 0 h). At 4 h after release from treatment, ectopic HP1BP3 expressing cells was significantly decreased from 47.2 % to 17.7 % in the G1/G0 population, and was increased from 12.1 % to 19.3 % in the S phase population and from 7.9 % to 19.5 % in the G2/M population when compared to the control (Figure 5-7 F). At 8 h after release, HP1BP3 over-expression further decreased the G0/G1 population from 50.3 % to 32.9 % and increased the S phase population from 20.1 % to 23.8 % and the G2/M population from 5.0 % to 14.4 % in comparison to the control (Figure 5-7 I). Furthermore, at 24 h after release, HP1BP3 over-expression decreased the G1/G0 population from 43.5 % to 25.8 % and increased the S phase population from 24.8 % to 29.3 % and the G2/M population from 6.1 % to 11.9 % as compared to the control (Figure 5-7 L). Consistent with above findings (Figure 5-6 F, I, and L), these results demonstrated that HP1BP3

upregulation causes a delayed progression through the G2/M to G0/G1 while inducing G1 to S transitions in Tiger cells.


A
24h
Thymidine
Release
3h
Wash
12h
Nocodazole
Collect 0h
Release
4h
Collect
Wash
Release
8h
Collect
Wash
Release
10h
Collect
Wash
Release
24h
Collect
Wash
FACS
Analysis
+
Western blot
B
Asy
TigerGFP
TigerGFP-HP1BP3
G0/G1
G2/M
S
C
Hours (h) after release from thymidine/nocodazole
0
4
8
10
24
TigerGFP
TigerGFP-HP1BP3

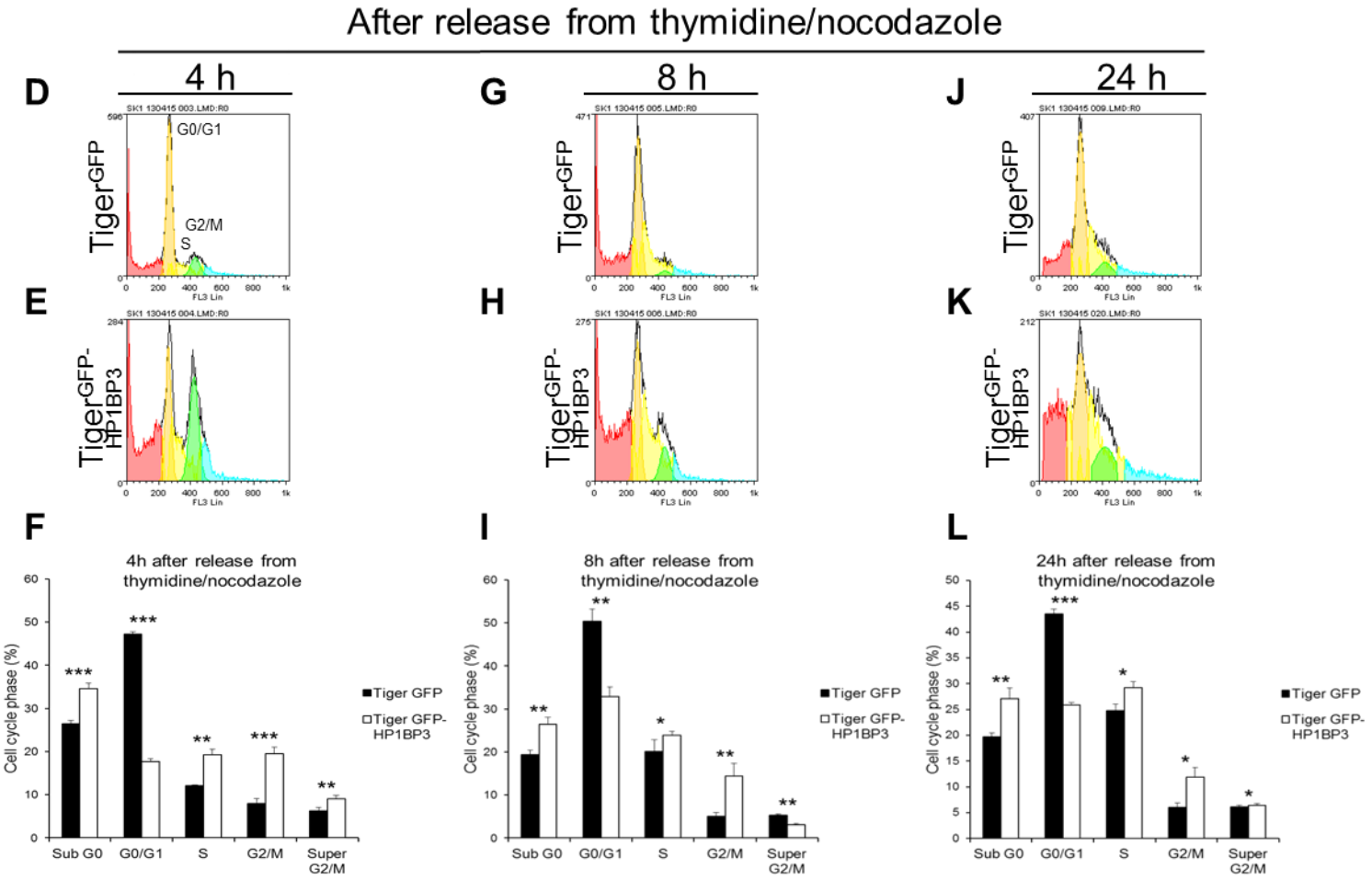

After release from thymidine/nocodazole
4 h
8 h
24 h
D
E
F
G
H
I
J
K
L
TigerGFP
TigerGFP-HP1BP3
G0/G1
G2/M
S
FL3 Lin
4h after release from thymidine/nocodazole
8h after release from thymidine/nocodazole
24h after release from thymidine/nocodazole
Cell cycle phase (%)
Sub G0
G0/G1
S
G2/M
Super G2/M
Tiger GFP
Tiger GFP-HP1BP3

Figure 5-7: HP1BP3 upregulation delayed G2/M-G0/G1 transition but induced G0/G1 to S transition, in mitotic-arrested Tiger cells. (A) Schematic shows the thymidine-nocodazole block protocol used to synchronise Tiger^{GFP} (control) and Tiger$^{GFP\text{-}HP1BP3}$ cell lines in mitosis. (B) FACS profile of an asynchronous (Asy) population of cells was used as an untreated control for thymidine/nocodazole treated cells. Both cell lines were released into normal medium from the thymidine/nocodazole block for the indicated time points. Then, cell cycle profile (C-E, G, H, J, and K) was determined by FACS analysis of Propidium iodide (PI)-stained cells collected at these time points. At 4 h (F), 8 h (I), and 24 h (L), cells were statistically analysed for their cell cycle distribution using WEASEL software. Statistical significant values were calculated for Tiger^{GFP} versus Tiger$^{GFP\text{-}HP1BP3}$ using student's *t* test. *P= 0.01 to 0.05, **p= 0.001 to 0.01, ***p<0.001. Error bars show the STDEV of seeded cells in triplicate wells for each cell line.

5.2.2.2 Overexpression of HP1BP3 in Tiger cells, decreases SUV39H1/H3K9me3 during G1/S and G2/M, increases H3K9ac especially in G1 to S-transited cells and G2/M, and reduces Cyclin B1 during S and G2/M phase

We demonstrated early S phase entry and delayed mitosis entry/exit in Tiger cells over-expressing HP1BP3. Mechanisms of epigenetic regulation by HP1BP3 in cell cycle was not fully known. Therefore, to investigate the epigenetic mechanism underlying cell cycle deregulation caused by HP1BP3 upregulation, here we examined the levels of chromatin repressive marker H3K9me3, and the active chromatin histone acetylation marker H3K9ac and also histone methyltransferase SUV39H1, at different cell cycle phases using western blotting analysis.

Tiger^{GFP} (control) and Tiger$^{GFP\text{-}HP1BP3}$ cell lines were synchronised with double thymidine block and released at different time points (Figure 5-6 A). Then, cell lysates were extracted at each time point after validating their cell cycle profiles as described in (Figure 5-6 C). H3 and β-actin served as the loading control. Cyclin B1 was used as the control for cell cycle progression, where its levels were repressed at G1, increased as the cells progressed to S phase and G2, and peaked at G2/M (Cogswell et al., 1995; Hwang et al., 1995; Jackman and Pines, 1996).

In Tiger$^{GFP\text{-}HP1BP3}$ cells, the exogenous expression of HP1BP3 (98 kDa) peaked at 0 h, when the cells were at the G1/S checkpoint (Figure 5-8 A). In the Tiger^{GFP} cells, endogenous expression of the HP1BP3 a isoform peaked at the G1/S checkpoint, and then decreased gradually during cell cycle progression (Figure 5-8 A). Interestingly, the HP1BP3 b isoform peaked at the G1/S checkpoint, decreased when the cells transitioned from G1/S to G2/M, and then increased again when all G2/M cells reached G0/G1 (Figure 5-8 A). In fact, the finding may lead to further questions and speculation whether the long and short isoforms display a differential regulation in cell cycle checkpoint control. Further study requires pursuing in future. However, there were no significant differences in the endogenous expression of the HP1BP3 in HP1BP3 overexpressing Tiger cells (Figure 5-8 A).

Additionally, SUV39H1 expression levels and H3K9me3 levels were significantly decreased at all cell cycle phases when HP1BP3 was over-expressed in the Tiger cells as compared to the control (Figure 5-8 B and C). However, in Tiger^{GFP} cells, SUV39H1 expression levels and H3K9me3 levels were maintained at 0 h and 4 h after release from double thymidine block (where cells are in G1/S and G2/M), and then decreased while the cell cycle progressed (Figure 5-8 B and C). On the contrary, the euchromatin marker H3K9ac was upregulated significantly from 0 h to 12 h after release in Tiger$^{GFP\text{-}HP1BP3}$ cells as compared to the control (Figure 5-8 D). However, H3K9ac levels decreased significantly when the cells progressed from G1/S to G2/M (Figure 5-8 D; 4 h), and then increased gradually until all G2/M

cells reached G1/S transition (Figure 5-8 D; 12 h). Further studies are required to identify the activation or inhibition of certain and specific gene associated with specific phase(s) in cell cycle, and potential underlying biological mechanisms. In addition, Cyclin B1 (G2/mitotic-specific cyclin) was significantly decreased in Tiger$^{GFP\text{-}HP1BP3}$ versus Tiger^{GFP} cells from 0 h to 12 h after release (Figure 5-8 E), which may further confirm of delayed G2/M-G0/G1 transition for HP1BP3 overexpressing cells (Figure 5-7 E, F, H, and I). In contrast, in Tiger^{GFP} cells the Cyclin B1 level was maintained in S phase and G2 (Figure 5-8 E; 0 h and 4 h), peaked in mitosis (Figure 5-8 E; 8 h), and then declined after all cells had shifted from G2/M to G0/G1 and as it was expected (Figure 5-8 E; 12 h).

These data, together suggest that HP1BP3 upregulation is an important cell cycle regulator that may modulate the expression/levels of SUV39H1/H3K9me3 and H3K9ac in specific cell cycle phases. It also appears that HP1BP3 upregulation–mediated Cyclin B1 repression is responsible for the G2 delay and slower mitotic transition reported earlier (Section 5.2.2.1).

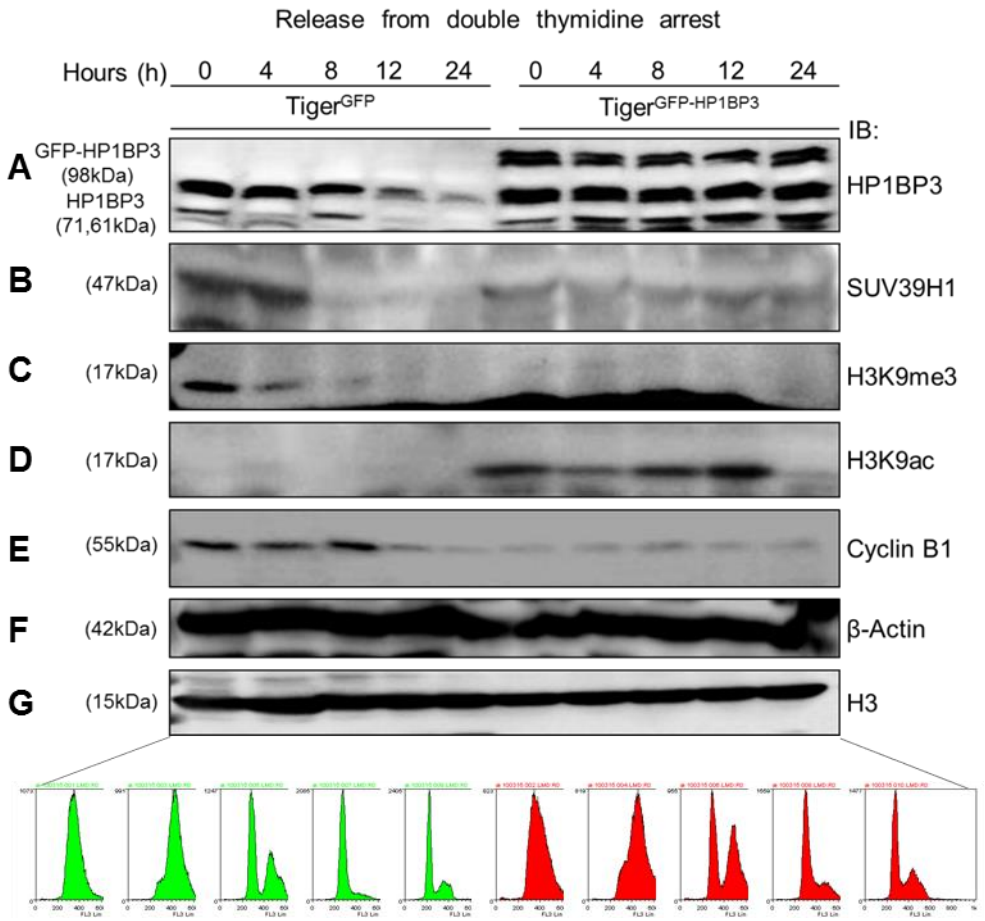


Figure 5-8: HP1BP3 modulate the expression/levels of SUV39H1/H3K9me3, H3K9ac and Cyclin B1 in specific cell cycle phases in Tiger cells. Both Tiger^{GFP} (control cell line) and Tiger$^{GFP\text{-}HP1BP3}$ were released from double-thymidine block. Cell lysates were prepared for western blot analysis using antibody against (A) HP1BP3, (B) SUV39H1, (C) H3K9me3, or (D) H3K9ac. (E) Cell cycle progression was verified by anti-Cyclin B1. (F + G) β-Actin and H3 were used as loading control. WB experiment was repeated in two different occasions.

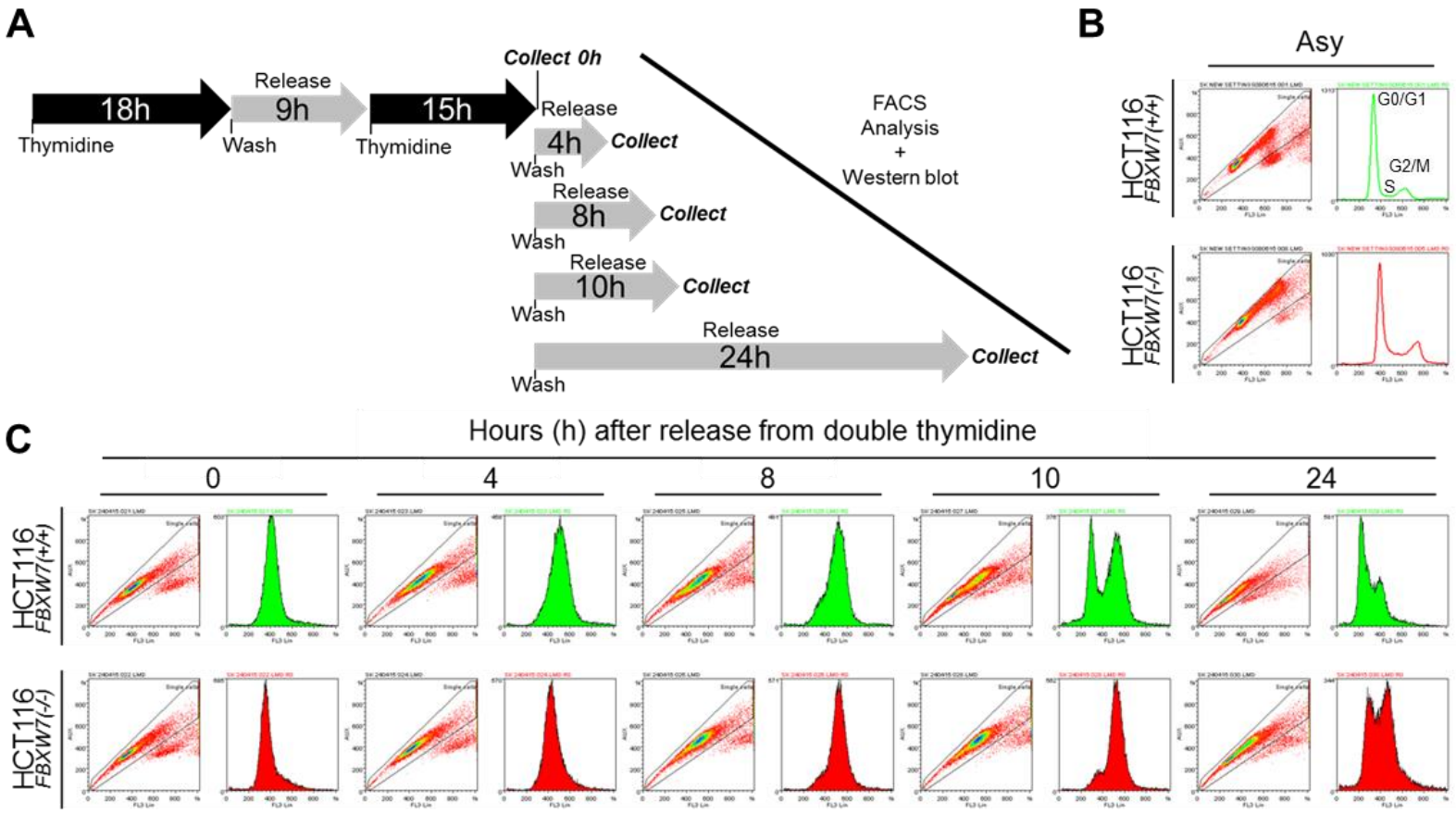
5.2.3 Differential expression of HP1BP3 regulates-specific cell cycle phases in HCT116$^{FBXW7(-/-)}$ CRC cells

5.2.3.1 Loss of *FBXW7*-mediated HP1BP3 upregulation may arrest HCT116 cells in G2/M while accelerating G1 to S transition

As the HCT116$^{FBXW7(-/-)}$ cell line maintains high levels of HP1BP3 endogenously (Chapter 3, Figure 3.1), we investigated the possible influence of the loss of *FBXW7*-mediated HP1BP3 accumulation on cell cycle progression. To achieve this, the *FBXW7*-wildtype control [HCT116$^{FBXW7(+/+)}$] and the *FBXW7*-deleted [HCT116$^{FBXW7(-/-)}$] cell lines were treated with G1/S-arresting agent (double thymidine block) (Figure 5-9 A and Materials & Methods; Section 2.2.7). Then, the cells were released into specific cell cycle phases and the cell cycle was analysed (Figure 5-9 C, F, and I) as described earlier in this chapter (Section 5.2.2.1). An asynchronous untreated population was used as the control (Figure 5-9 B).

At 10 h after release from double thymidine treatment, the HCT116$^{FBXW7(-/-)}$ G0/G1 population cells were significantly decreased from 32.5 % to 0.2 %, while the S phase population decreased from 35.9 % to 14.25 % and the G2/M population increased from 4.8 % to 84.4 % when compared to the control (Figure 5-9 F). Moreover, at 24 h after release, the HCT116$^{FBXW7(-/-)}$ G0/G1 population substantially decreased from 53.9 % to 5.3 %, while the S phase population increased from 5.4 % to 50.9 % and the G2/M population increased from 7.8 % to 30.0 % in comparison to the control (Figure 5-9 I).

Consistent with Tiger$^{GFP\text{-}HP1BP3}$ overexpressing cells, the endogenous HP1BP3 accumulation, which is mediated by *FBXW7* mutation in colon cancer, caused early G0/G1- and S- phases entry and for G2/M arrest in HCT116$^{FBXW7(-/-)}$ cancer cells.


A
18h
Thymidine
Release
9h
Wash
15h
Thymidine
Collect 0h
Release
4h
Collect
Wash
Release
8h
Collect
Wash
Release
10h
Collect
Wash
Release
24h
Collect
Wash
FACS
Analysis
+
Western blot
B
Asy
HCT116
FBXW7(+/+)
HCT116
FBXW7(-/-)
G0/G1
G2/M
S
C
Hours (h) after release from double thymidine
0
4
8
10
24
HCT116
FBXW7(+/+)
HCT116
FBXW7(-/-)

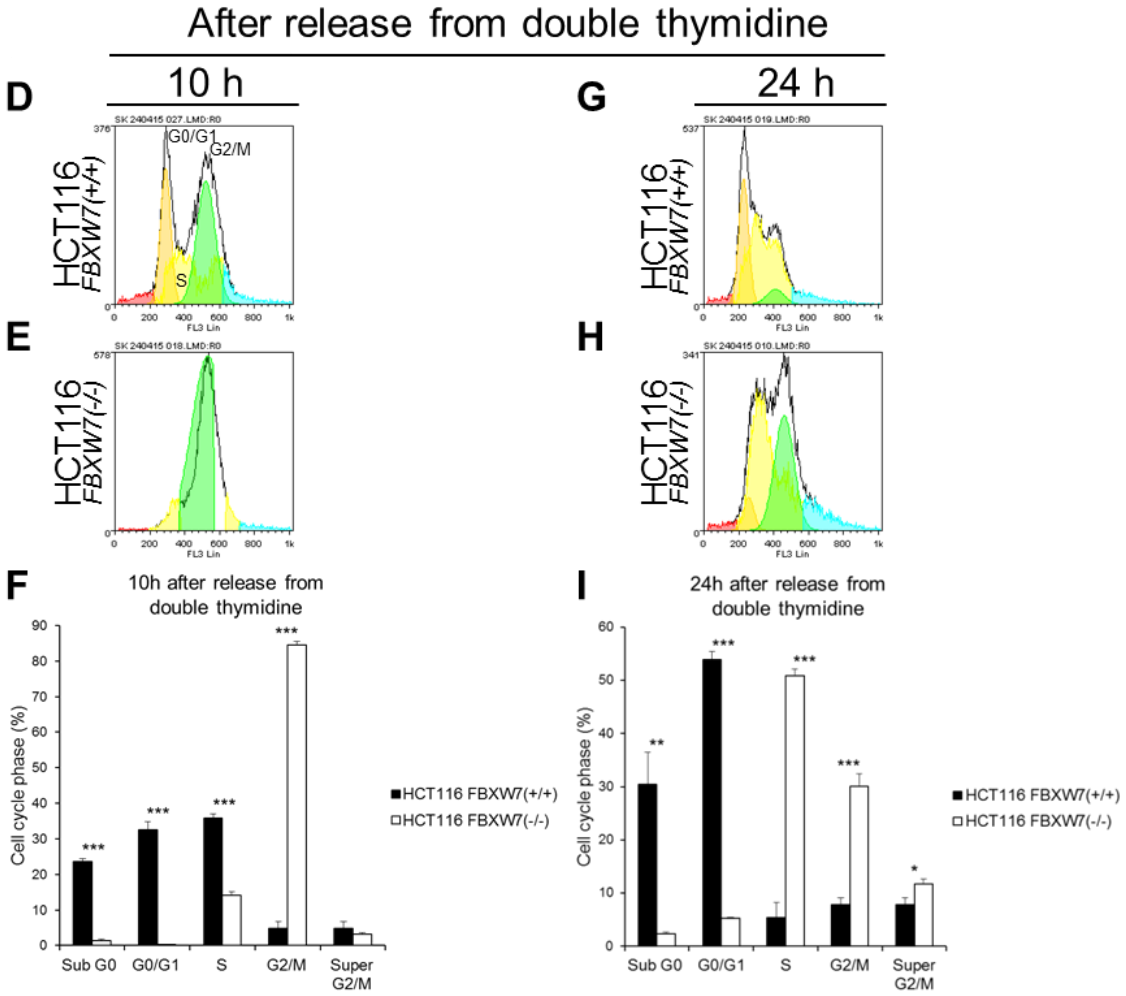


Figure 5-9: FBXW7 loss arrests cells at G2/M phase and induces G1 to S transitioned cells, in HCT116 cells. (A) Schematic shows the double-thymidine block protocol used to synchronise HCT116$^{FBXW7(+/+)}$ (control) and HCT116$^{FBXW7(-/-)}$ cell lines in G1/S boundary. (B) FACS profile of an asynchronous (Asy) population of cells was used as an untreated control for double-thymidine treated cells. Both cell lines were released into normal medium from the double-thymidine block for the indicated time points. Then, cell cycle profile (C-E and G-H) was determined by FACS analysis of Propidium iodide (PI)-stained cells collected at these time points. At 10 h (F) and 24 h (I), cells were statistically analysed for their cell cycle distribution using WEASEL software. Statistical significant values were calculated for HCT116$^{FBXW7(+/+)}$ versus HCT116$^{FBXW7(-/-)}$ using student's *t* test. *P= 0.01 to 0.05, **p= 0.001 to 0.01, ***p<0.001. Error bars show the STDEV of seeded cells in triplicate wells for each cell line.

5.2.3.2 Loss of *HP1BP3* in HCT116$^{FBXW7(-/-)}$ cells reversed the *FBXW7*-knockout associated cell cycle effects; induced the G2/M to G0/G1 transition, while arrested cells in G0/G1, and decreased cells in S phase

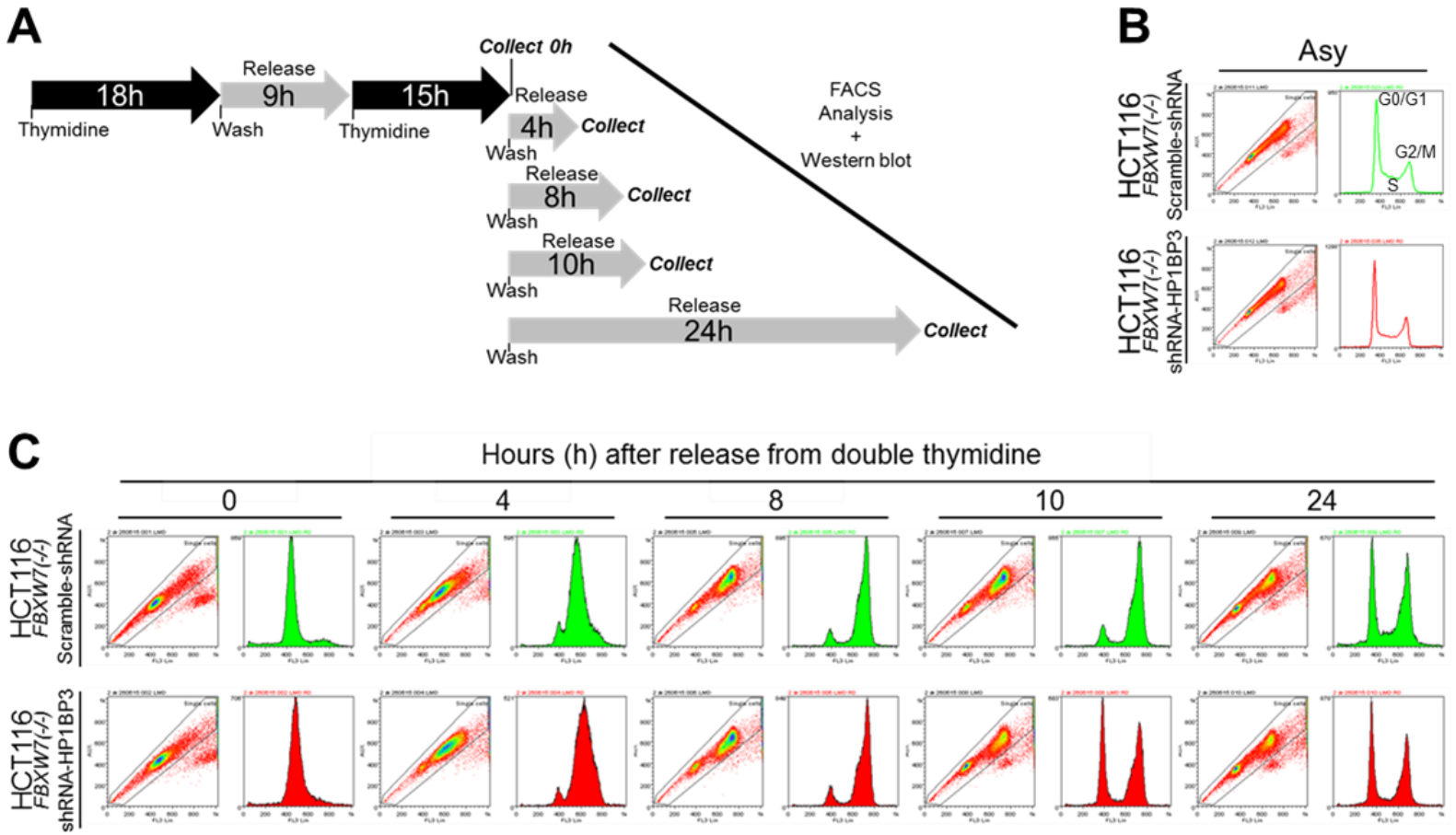
Our earlier results show that loss of *FBXW7* accelerates G1 to S transition and arrests cells in G2/M phase. As HP1BP3 protein level was enhanced due to lack of FBXW7 (Chapter 3; Figure 3.1), we hypothesised that the HP1BP3 upregulation in HCT116$^{FBXW7(-/-)}$ cells could mediate the deregulation of cell cycle phases described in Figure 5-9.

Therefore, a double thymidine treatment and (Figure 5-10 A, Materials & Methods; Section 2.2.7) was applied to stable *HP1BP3* knockdown (HP1BP3-shRNA)-HCT116$^{FBXW7(-/-)}$ cells and Scramble-shRNA-HCT116$^{FBXW7(-/-)}$ control cells to explore the specificity role of HP1BP3 in deregulating specific cell cycle phases. Both cell lines were released to different time points (Figure 5-10 C-E, G, and H) and cell cycle phases were analysed using PI staining and FACS (Figure 5-10 F and I). An asynchronous untreated population was used as the control (Figure 5-10 B).

Cell cycle analysis at 10 h after double thymidine release showed that the HP1BP3-shRNA-HCT116$^{FBXW7(-/-)}$ G2/M population substantially decreased from 80.3 % to 54.1 % and that the G0/G1 population was increased from 9.45 % to 35.7 % compared to the control (Figure 5-10 F). The percentage of cell in S- phase was however unchanged at 10 h after double thymidine

release (Figure 5-10 F). The changes indicate a quick transition from G2/M to G0/G1 when *HP1BP3* is knocked down in HCT116$^{FBXW7(-/-)}$ *cells*. Moreover, the HP1BP3-shRNA-HCT116$^{FBXW7(-/-)}$ G0/G1 population was significantly increased by statistical analysis, from 26.9 % to 30.2 % and the S phase population was decreased from 29.3 % to 24.8 % at 24 h after release from the G1 to S checkpoint in comparison to the Scramble-shRNA-HCT116$^{FBXW7(-/-)}$ control cells (Figure 5-10 I). This change represents G0/G1 arrest and delayed G1 to S transition.

These data suggest that the loss of *HP1BP3* is implicated in cell cycle disruption by stimulating quick G2/M exit followed by G0/G1 arrest and consequent reduction of the time that normal cells spent in S phase. Whether it is associated with the shearing of mitotic spindle caused by the premature mitotic exit and/or the inhibition/disruption of DNA synthesis, further experiments are needed to confirm.


A
18h
Thymidine
Release
9h
Wash
15h
Thymidine
Collect 0h
Release
4h
Collect
Wash
Release
8h
Collect
Wash
Release
10h
Collect
Wash
Release
24h
Collect
Wash
FACS
Analysis
+
Western blot
B
Asy
HCT116
FBXW7(-/-)
Scramble-shRNA
HCT116
FBXW7(-/-)
shRNA-HP1BP3
G0/G1
G2/M
S
C
Hours (h) after release from double thymidine
0
4
8
10
24
HCT116
FBXW7(-/-)
Scramble-shRNA
HCT116
FBXW7(-/-)
shRNA-HP1BP3

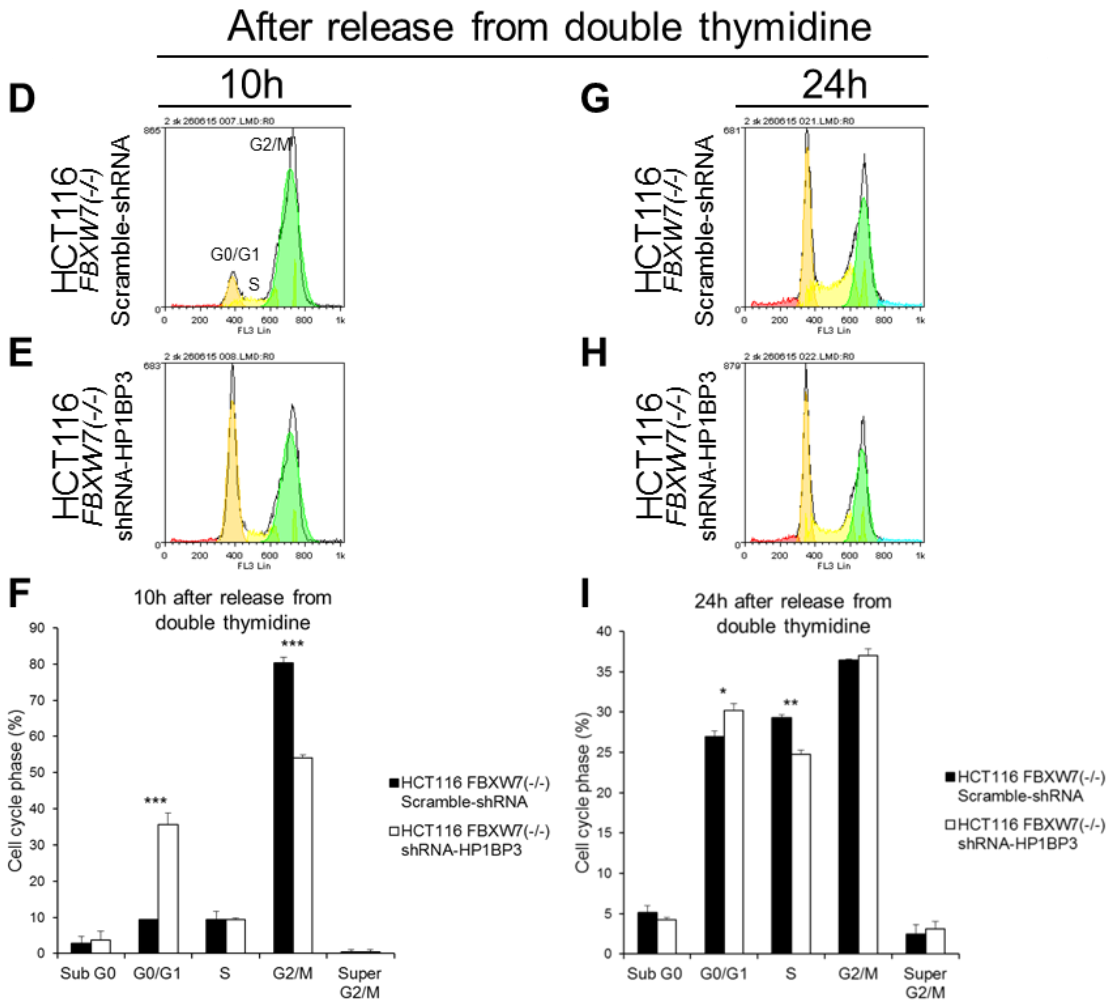


Figure 5-10: *HP1BP3* loss induces G2/M to G0/G1 transition and arrests cells at G0/G1 phase, in HCT116$^{FBXW7(-/-)}$ cells. (A) Schematic shows the double-thymidine block protocol used to synchronise HCT116$^{FBXW7(-/-)}$ Scramble-shRNA (control) or HCT116$^{FBXW7(-/-)}$ HP1BP3-shRNA at G1/S boundary. (B) FACS profile of an asynchronous (Asy) population of cells was used as an untreated control for double-thymidine treated cells. Both cell lines were released into normal medium from the double-thymidine block for the indicated time points. Then, cell cycle profile (C-E and G-H) was determined by FACS analysis of PI-stained cells collected at these time points. At 10 h (F) and 24 h (I), cells were statistically analysed for their cell cycle distribution using WEASEL software. Statistical significant values were calculated for the indicated cell lines using student's t test. *P= 0.01 to 0.05, **p= 0.001 to 0.01, ***p<0.001. Error bars show the STDEV of seeded cells in triplicate wells for each cell line.

5.3 Discussion

Histone and nuclear proteins are responsible for modulating chromatin structure (Soshnev et al., 2016). This epigenetic modulation between heterochromatin and euchromatin is highly dynamic and tightly regulated throughout the cell cycle (Becker and Workman, 2013; Ma et al., 2014). Recently, HP1BP3 was identified as a regulator of cell cycle progression (Dutta et al., 2014a). It plays a vital role in maintaining heterochromatin integrity during G1 to S transition, thereby regulating G1 duration (Dutta et al., 2014a), and it possibly mediates chromosome organisation and condensation during mitosis (Hayashihara et al., 2010a). However, HP1BP3 is highly expressed in G1 and G1 to S transition in comparison to its expression in G2/M phase (Dutta et al., 2014a). Another study identified the importance of HP1BP3 in cell growth and viability (Garfinkel et al., 2015a; Garfinkel et al., 2015b). Therefore, it is believed that HP1BP3 can control the cell division capacity. However, the mechanisms underlying epigenetics regulation mediated by HP1BP3 have yet to be explored in normal fibroblast and colon cancer cells.

Here, we show that HP1BP3 upregulation induces cell cycle progression by promoting G1 to S transition. This was observed in Tiger and HCT116 cell lines over-expressing HP1BP3 (Figure 5-1, Figure 5-2, Figure 5-6, and Figure 5-7) and in HCT116$^{FBXW7(-/-)}$ cells with accumulated HP1BP3 expression endogenously (Figure 5-3 and Figure 5-9). In addition, *HP1BP3* loss in the HCT116$^{FBXW7(-/-)}$ cell line caused significant acceleration in G2/M to G0/G1 transition and subsequent G0/G1 arrest (Figure 5-4, Figure 5-5, and

Figure 5-10). These findings indicate that the cell cycle deregulation in colorectal cancer with *FBXW7* mutation could mainly be caused by the irregular accumulation of HP1BP3.

We further investigated the irregular cell cycle patterns forced by ectopic HP1BP3 expression following cell synchronisation and release to specific cell cycle phases. The expression/levels of heterochromatin components (HP1BP3, SUV39H1, H3K9me3), H3K9ac, and Cyclin B1 were also explored (Figure 5-8). SUV39H1 is maximally phosphorylated by Cyclin-dependent kinase 2 (CDK2) at G1 to S transition to reduce its activity and to allow proper cell cycle progression while its phosphorylation is maintained during S-G2-M phase (Park et al., 2014). Also phosphorylation of SUV39H1 occurs specifically during metaphase in mitosis, when chromosomes are aligned on the spindle with sister kinetochores facing toward the opposite poles (Aagaard et al., 2000). Moreover, it has been reported that SUV39H1 is highly enriched in centromeric region during prometa- to metaphase with weaker affinity for the chromosomal arms, while its expression tends to be significantly weakened in ana- to telo -phases when the two sister chromatids pulled apart at opposite poles and their DNA starts to decondense (Aagaard et al., 2000). The CDK2-mediated phosphorylation of SUV39H1 resulted in favoured detachment from chromatin (Park et al., 2014). This detachment stimulated KDM4A histone lysine demethylase occupancy on heterochromatin and consequently altered heterochromatin markers (Park et al., 2014). This phosphorylation process is vital for controlling the replication timing of heterochromatin during the cell cycle (Park et al., 2014; Zhang et

al., 2002). When HP1BP3 was upregulated, we observed quick G1 to S transition in cells with G2/M arrest (Figure 5-1, Figure 5-2, Figure 5-3, Figure 5-6, Figure 5-7, and Figure 5-9). In cells with induced G1 to S transition, SUV39H1 and H3K9me3 levels tended to be downregulated (Figure 5-8 B and C), while H3K9ac was upregulated (Figure 5-8 D). These findings suggest the existence of a phosphorylation hyperactive mechanism that can inhibit the SUV39H1 histone methyltransferase activity or other mechanism that downregulates its expression and consequently stimulates active H3K9 acetylation. Here we showed that HP1BP3 upregulation inhibits SUV39H1 expression and its activity, mediated either by CDK2 stimulation and/or by unknown mechanism(s), consequently increased H3K9ac levels. However, further experiments need to be done to uncover the underlying mechanisms of HP1BP3 modulating SUV39H1 activity. Furthermore, our results indicated that elevated level of HP1BP3 causes G2/M arrest and abnormal mitotic progression through suppression of Cyclin B1 (Figure 5-8 E). The Cyclin B1 which is required for the G2 checkpoint and normal mitotic transition (Cogswell et al., 1995; Hwang et al., 1995; Jackman and Pines, 1996).

These findings highlight the regulatory role of HP1BP3 in cell cycle progression, as the over-expression of HB1BP3 could lead to induced proliferation and/or apoptosis in cancers with *FBXW7* mutation.

CHAPTER 6

General Discussion

6.1 Introduction

Chromatin-mediated epigenetic regulation and its association with various nuclear activities point towards the existence of chromatin assembly activity with chromatin remodelling complexes. Currently, most of studies focused on posttranslational modifications of histone proteins in the chromosome and their influence on chromatin structure and gene transcription. These post-translational modifications regulate a variety of normal and tumour-related processes by modulating the euchromatin/heterochromatin transition (Carlberg and Molnár, 2016; Soshnev et al., 2016; Vaiopoulos et al., 2014). The underlying complexity of this chromatin transition is determined through direct interactions between histone and DNA (Kornberg, 1977) and DNA-associated protein (Li and Reinberg, 2011; Probst et al., 2009). However, the heterochromatin proteins and their partners' identity remained largely unclear. Moreover, the heterochromatin-associated proteins are also exposed to post-translational modifications to modulate their activity (Carlberg and Molnár, 2016; Hiragami-Hamada et al., 2011; Minc et al., 1999; Soshnev et al., 2016). Therefore, their protein level must be tightly controlled to avoid alterations that deregulate cell biology that may lead to cell transformation and tumour formation.

One of the most common ways that limits the expression of many proteins is to destroy them via the ubiquitin/proteasome pathway (Lecker et al., 2006; Tu et al., 2012). FBXW7 is an E3-ligase which targets several proto-oncogenes and transcriptional modulators for degradation, and it plays crucial roles in tumorigenesis (Babaei-Jadidi et al., 2011b; Wang et al.,

2012a; Welcker and Clurman, 2008). Our lab identified proteins which are targeted by the *FBXW7* tumour-suppressor gene for the ubiquitin-mediated degradation [(Babaei-Jadidi et al., 2011b) & Li et al., in publication]. Among these proteins, HP1BP3 modulates the entry/exit point of nucleosomal DNA through binding to HP1α protein and this binding is associated with chromatin condensation (Garfinkel et al., 2015b; Hayashihara et al., 2010b). However, the biochemical/biological mechanisms and consequences of HP1BP3 binding to FBXW7 and HP1a are remained largely unclear.

HP1α protein interacts with tri-methylated H3 (H3K9me3) (Lachner et al., 2001) which is correlated with SUV39H1/2 methyltransferases (Bártová et al., 2008; Lachner et al., 2001; Rea, 2000). This complex is required for constitutive heterochromatin formation and gene silencing (Canzio et al., 2014; Maison et al., 2002; Maison et al., 2011). Others have demonstrated that HP1α can also activate gene expression in certain contexts (Cryderman et al., 2011; Kwon and Workman, 2011; Piacentini et al., 2009; Sdek et al., 2013; Shoji et al., 2014). It seems that H3K9 methylation may also protect cells from genome instability (Peng and Karpen, 2009; Peters et al., 2001). In addition, HP1α modulation at chromatin inversion is important in the normal homeostasis and cancer (De Koning et al., 2009; Kwon and Workman, 2011; Maison et al., 2002; Vad-Nielsen and Nielsen, 2015). In contrast to H3K9 trimethylation, the acetylation of H3K9, which build-up by the action of histone acetyltransferase, is a well-known epigenetic marker enriched in the euchromatic promoter region of activated genes (Bannister and Kouzarides, 2011; Bártová et al., 2008; Wang et al., 2008). Deregulation

of other non-histone cofactor molecules and enzyme activity responsible for tri-methylating or acetylating H3K9 plays a prominent role in carcinogenesis (Hamamoto et al., 2015; Hayami et al., 2011; Hu et al., 2014; Khanal et al., 2013; Kogure et al., 2013; Wang et al., 2013b; Yin et al., 2015). Consequently, anomalous of H3K9me3 or H3K9ac level has been considered as a hallmark of many cancers, including CRC (Benard et al., 2014; Benard et al., 2013; Deligezer et al., 2010; Hamamoto et al., 2015; Leszinski et al., 2012; Vaiopoulos et al., 2014). Moreover, low H3K9me3 levels contribute to elevated self-renewal capability of differentiated melanoma cells (Tan et al., 2014). Additionally, any epigenetic abnormalities may cause cancer via the exhibition of wrong transcription pattern that can be resulted from permanent activation or inhibition of oncogenes or tumour suppressor genes, respectively.

Moreover, cell cycle abnormalities have also been detected in many cancers, including CRC. Cell cycle progression depends on several epigenetic mechanisms that regulate chromatin folding at different stages of the cell cycle (Aagaard et al., 2000; Fischle et al., 2005; Minc et al., 1999; Park et al., 2014). Over the past decades, many lines of scientific evidence supported the idea that the histone tail modifications, which contributes to the conversion of euchromatin into heterochromatin and vice versa, are vital for proper DNA replication and chromosomes segregation throughout the cell cycle (Fischle et al., 2005; Ma et al., 2014; Park et al., 2014; Zhang et al., 2002). However, a full understanding of the mechanisms underlying the effect of epigenetic

modifications and the major effectors of these modifications in the cell cycle remain indefinable.

Moreover, histone modifications has been associated with EMT-mediated metastasis in CRC (Bedi et al., 2014; Gargalionis et al., 2012; Lin et al., 2010; Liu et al., 2008; Weyemi et al., 2016; Zha et al., 2016). Although extensive epigenetic reprogramming (Tam and Weinberg, 2013; Wu et al., 2012) occurs in EMT during cell differentiation and malignant transformation (Meissner, 2010; Mohn and Schübeler, 2009), how epigenetic regulates EMT via heterochromatin-associated proteins is still unknown. However, there are strong evidences about the correlation of FBXW7 substrates and their involvement in promoting tumour formation and progression, including EMT.

Up to date, many of FBXW7 substrates have been identified and characterised. These substrates play fundamental roles in cell growth, division, differentiation, and/or tissue development (Babaei-Jadidi et al., 2011a; Bialkowska et al., 2014; Busino et al., 2012; Davis et al., 2013b; Finkin et al., 2008; Fukushima et al., 2012; Inuzuka et al., 2011; Kitagawa et al., 2009; Kourtis et al., 2015; Mao et al., 2008; Nateri et al., 2004; Sancho et al., 2013; Yada et al., 2004; Ye et al., 2004; Zhan et al., 2015). Also, *FBXW7* is found to be mutated in a variety of human cancers, including T cell acute lymphoblastic leukaemia, breast, and colon cancers (Davis et al., 2014; Kuipers et al., 2015; Welcker and Clurman, 2008; Xu et al., 2016). Therefore, as HP1BP3 is a substrate of FBXW7, the main purpose of this

study is to explore the role of HP1BP3 underlining epigenetic-reprogramming mechanisms in normal and cancer cells, especially during EMT and cell cycle progression.

This study provided evidences that:

1. HP1BP3 is a strictly nuclear protein.
2. HP1BP3 protein regulation by FBXW7-mediated degradation, possibly associated GSK-3β protein kinase phosphorylation.
3. HP1BP3 protein expression play an important role in heterochromatin to euchromatin conversion.
4. FBXW7 and Suv39h1/2 mediates chromatin dynamics modulated by HP1BP3.
5. HP1BP3 underlay above mechanisms to modulate the epithelial-mesenchymal transition (EMT) pathway and cell cycle phase transitions.

6.2 FBXW7 and SUV39H1 mediates chromatin dynamics in HP1BP3 dependant manners

Recently, it has been found that HP1BP3 interacts with HP1α chromo shadow domain through a novel PXVXL-binding motif at proline 255–leucine 259 (Hayashihara et al., 2010a). However, the mechanisms and regulations of HP1α-mediated genes activation are yet to be investigated.

I showed that FBXW7 regulated HP1BP3 protein level (Figure 3-1 B) in a GSK-3β-dependent manner (Figure 3-3 and Figure 3-4). Moreover, the

accumulation of HP1BP3 protein caused by *FBXW7* mutation in HCT116 CRC cells did not affect HP1α expression levels (Figure 3-1 B) but it did induce the binding of HP1BP3 to HP1α (Figure 3-8 B and Figure 3-9 C) while decreasing the levels of H3K9me3 and increasing H3K9ac, respectively (Figure 3-10 B). Moreover, the loss of H3K9me3 mediated via *Suv39h1/2* knockout in mouse fibroblasts (Figure 3-13) did not change the co-localisation of HP1BP3 to HP1α (Figure 3-12) and the expression levels of both proteins (Figure 3-11). However, it did alter the distribution of both proteins in the nucleus. The depletion of H3K9me3/Suv39h1/2 complex resulted in the enrichment of HP1BP3 and HP1α in the euchromatic region (Figure 3-12). It seems that HP1BP3 upregulation rescues the repression activity of HP1α by decreasing H3K9me3 levels and consequently leads to more transcriptional active chromatin by stimulating the acetylated form of the same lysine 9 residue in histone H3 (H3K9ac). Thus, the accumulation of HP1BP3 in about 20 % of CRC cases that acquire *FBXW7* mutation and consequent alteration of the chromatin structure and gene expression could represent one of the leading causes for the development of sporadic CRC. These findings indicate that the chromatin association of HP1BP3 and HP1α is dependant to FBXW7 and SUV39H1 activities in mammalian cells.

H3K9me3 found to be decreased in CRC patients when compared to healthy controls (Gezer et al., 2013). In contrast, despite H3K9me3 association with the transcriptional repression and hence involvement in abnormal silencing of tumour suppressor genes [i.e. DCC (Derks et al., 2009)], it has been reported that SUV39H/H3K9me3 is increased in invasive and lymph node

metastatic regions of CRC tissues (Yokoyama et al., 2013). Also, Bernad and colleagues revealed that elevated levels of H3K9me3 mark in early-stage CRC patients which correlated to good prognosis groups (Benard et al., 2014). Taken together, in contrast to the H3K9me3/HP1α complex, the HP1BP3/HP1α complex might function by regulating heterochromatin–euchromatin inversion, which could lead to the transcriptional activation of many genes, including tumour suppressors and/or oncogenes, in normal cells versus early stage of cancer cells with *FBXW7* mutation. Therefore, I further focused on exploring the mechanisms by which *FBXW7* is mutated, leading to HP1BP3 accumulation, H3K9me3 repression and H3K9ac stimulation in CRC cells, as well as the possible oncogenic activity of HP1BP3.

6.3 HP1BP3 induces EMT in HCT116 CRC cells

Induced mRNA levels of SUV39H1 (a H3K9 methyltransferase) were detected in primary CRC tissues (Kang et al., 2007), suggesting the possible involvement of SUV39H1 in regulating the expression of EMT related genes. It seems that the alteration of SUV39H1/H3K9me3 expression/levels and the involvement other histone modifiers may play central role in human CRC development and metastasis through mechanisms that are not fully understood.

I found that the stably overexpressed HP1BP3 protein in Tiger fibroblast and HCT116 cells decreases the expression/levels of both SUV39H1 and H3K9me3, increases H3K9ac, and does not affect the expression of HP1α (Figure 4-3). Moreover, this induction causes morphological changes in both

stable cell lines (Figure 4-5). It was reported that HP1BP3 and Drosha co-binding to 42 highly transcribed miRNA loci, indicating the role of HP1BP3 in global human miRNA biogenesis (Liu et al., 2016a). These findings pulse the findings of the loss-of-function experiment (Figure 4-4 and Figure 4-7) strongly suggest that HP1BP3 upregulation might induce microRNAs that target *SUV39H1* gene. Then, the suppression of SUV39H1 could subsequently recruit chromatin-remodelling complexes and causes changes in cell morphologies and possibly the expression of cell polarity and EMT-related genes.

During investigating the role of HP1BP3 in EMT pathway activation, I found that the stable HP1BP3 overexpression causes upregulation of ZEB-1, Vimentin, and Snail1 proteins level in Tiger and HCT116 cell lines (Figure 4-6). In addition, induced N-cadherin and decreased E-cadherin were found in Tiger and HCT116 cells, respectively, that stably expressing HP1BP3 (Figure 4-6).

Microarray analysis of HeLa cells revealed that *HP1BP3* loss affected the transcription of 383 genes, where the transcription of 271 genes was up-regulated and that of the remaining genes was down-regulated (Garfinkel et al., 2015b). Mass spectrometry–based quantitative proteomic analysis identified 384 proteins with differential expression in *HP1BP3*-deficient 293T cells than in the experimental control, where 176 and 208 proteins were up- and down-regulated, respectively (Dutta et al., 2014a). Moreover, increased expression of LSD1 (a H3K9me3 demethylase) and decreased

expression of E-cadherin has been correlated with metastasis and poor prognosis of CRC (Jie et al., 2013). Similarly, it appears that FBXW7-mediated HP1BP3 accumulation may lead to SUV39H1 repression and H3K9me3 inhibition and/or disassociation from the Snail1, Vimentin, and ZEB-1 promoters, leading to their transcriptional activation and E-cadherin repression, which could be consequential hallmarks of cancer in colon mutated for *FBXW7* gene (Kuipers et al., 2015; Wang et al., 2013d; Yang et al., 2015; Yu et al., 2014). Overall, HP1BP3 might be epigenetically involved in the EMT/MET mechanisms. The upregulation of HP1BP3 also provides hints to facilitate understanding of the epigenetic alterations that lead to epithelial cell invasion in colon cancer. In principle, the HP1BP3 could be a potential target for reversing EMT and intervention in the progression of about 20 % of colorectal cancer cases that acquire *FBXW7* mutation, however further studies require to explore these possibilities.

6.4 HP1BP3 induces the transition from G1 to S phase and mitotic arrest

Dutta and colleges have reported the association between the non-histone HP1BP3 protein and chromatin remodelling during the different stages of cell cycle progression by applying applied proteomic approaches (Dutta et al., 2014a). Interestingly, two studies had strong evidence that HP1BP3 localises in the nuclei but is excluded from the nucleoli and chromosomes in interphase and mitosis, respectively (Garfinkel et al., 2015b; Hayashihara et al., 2010a). Such localisation patterns have also been found for proteins associated with high-order chromatin structure formation (Cherukuri et al.,

2008). Moreover, HP1BP3–chromatin association is increased during G1–S transition to control cell proliferation (Dutta et al., 2014a). Maintenance of the proper duration of each cell cycle phase is important; dysregulation of the duration of any cell cycle phase can lead to uncontrolled cell proliferation and therefore cancer development. As cell cycle progression is regulated by protein kinases [known as cyclin-dependent kinases (CDKs)], checkpoint regulatory proteins and chromatin-associated proteins, these proteins must be expressed properly at the correct interval. Accurate G1 to S transition plays a pivotal role in regulating cell proliferative capacity (Bertoli et al., 2013; Liu et al., 2016b; Nielsen et al., 1999; Wang et al., 2014). Furthermore, *HP1BP3*-null mice exhibited partial post-natal lethality and adult growth retardation (Garfinkel et al., 2015a; Garfinkel et al., 2015b). Thus, consistent with above studies my observation further highlighted the impact of HP1BP3 in regulating G1 to S transition and cell proliferation.

I showed that HP1BP3 regulates cell cycle in Tiger fibroblasts and HCT116 CRC cells. The induction of HP1BP3 caused by either *FBXW7* mutation in HCT116 or over-expressing HP1BP3 in Tiger and HCT116 alters the cell cycle progression by induction of the early S-phase entry, while causes delays in mitotic entry and its exit (Figure 5-1 C, Figure 5-2 C, Figure 5-3 C, Figure 5-6 D-I, Figure 5-7 D-I, and Figure 5-9 D-I). Moreover, the expression/levels of SUV39H1/H3K9me3 and H3K9ac were stimulated and attenuated, respectively (Figure 5-8 B-D), at all cell cycle stages because of HP1BP3 upregulation in Tiger cells. Additionally, HP1BP3 upregulation decreases the expression of the G2/mitotic-specific cyclin, Cyclin B1 (Figure

5-8 E). This decrease of Cyclin B1 supports the finding that HP1BP3 caused delayed G2/M to G0/G1 transition by arresting the cells in G2/M phase.

Furthermore, loss of *HP1BP3* in HCT116 CRC cells induced G2/M to G0/G1 transition, while arrested cells in G0/G1, and decreased cells in S- phase (Figure 5-4 C, Figure 5-5 C, and Figure 5-10 D-I). Together, these findings may imply that HP1BP3 upregulation can generally stimulate tumour growth in the colon by accelerating G1 to S transition and promote more open chromatin structure via SUV39H1/H3K9me3 inhibition and H3K9ac stimulation during DNA replication and/or mitosis. Additionally, it seems that HP1BP3 upregulation-mediated Cyclin B1 inhibition is responsible for the G2 delay and slow mitotic transition.

In addition, HP1α is enriched at both centromeric and pericentromeric heterochromatin regions during G1 and early S phase and is required for maintaining the late replication of pericentric heterochromatin during S phase (Prasanth et al., 2004; Quivy et al., 2008). Interestingly, a study conducted on *Drosophila* embryonic cells revealed an increased mid-S phase population in HP1α depleted cells (Schwaiger et al., 2010). Suggesting the important regulatory mechanisms of HP1α during the cell cycle, particularly at the S- and G2/M- phase (Schwaiger et al., 2010). However, its dissociation from heterochromatin is required during late G2- phase and G2 to M transition (Fischle et al., 2005; Terada, 2006). Regardless of that, HP1α is essential for protecting the integrity of chromosomes during cell division (Fanti et al., 1998; Kellum and Alberts, 1995). Moreover, despite the well-known role of

HP1α in gene silencing and maintaining heterochromatin (Canzio et al., 2014; Chevillard et al., 1993; Muchardt et al., 2002), emerging evidences show that the HP1α located in *Drosophila*'s chromosomes was found at many euchromatic/gene active sites (Kwon and Workman, 2011; Piacentini et al., 2009; Sdek et al., 2013). Thus, it seems that HP1BP3 over-expression could mediates decreased HP1α binding to pericentromeric heterochromatin during interphase. This may be associated with increased H3K9 acetylation levels in pericentromeric heterochromatin, which consequently give rise to induced G1 to S phase and/or mitotic arrest resulting from the inhibition of histone deacetylation.

Moreover, HP1α association to pericentric heterochromatin occurs through the chromo domain of HP1α and the N-terminal tail of H3K9me3 (Bannister et al., 2001b; Lachner et al., 2001), produced by SUV39H1-mediated HP1α (chromo shadow) interaction (Bannister et al., 2001b; Lachner et al., 2001; Smothers and Henikoff, 2000; Yamamoto and Sonoda, 2003). Nevertheless, chromosomal studies of HP1α distribution pattern presented that HP1α does not constantly co-localise with H3K9me3 or SUV39H1, particularly in euchromatic regions of chromosomes (Cowell et al., 2002; Greil et al., 2003; Kwon and Workman, 2011); in some cases, HP1 is found to directly bind DNA (Kwon and Workman, 2011; Zhao et al., 2000). All these features indicate the distinct regulatory roles for HP1α in chromatin remodelling and in epigenetic gene regulation. Furthermore, the phosphorylation-mediated SUV39H1 dissociation from chromatin by CDK2 leads to early replication of heterochromatin in S phase (Park et al., 2014). Therefore, we may

conclude that HP1BP3 and SUV39H1/HP1α complex could be mutually antagonistic in chromatin binding during DNA replication and/or cell division, which indicates a potential mechanism for how HP1BP3 stimulates DNA replication. Moreover, the induction observed for H3K9ac in response to HP1BP3 upregulation might reflect a direct effect of transcriptional activation, which could influence cell cycle proliferation and/or invasion in colorectal cancer cells lacking the *FBXW7* gene.

6.5 Experimental limitations

To reach the determined goals of my current study a variety of related experimental plans has been adjusted. Nevertheless, my research has encountered several obstacles, such as:

- Due to time limitation, we could not complete the validation of HP1BP3 phosphorylation mediated by GSK-3β activity using the site-directed mutagenesis based on overlapping PCR, to confirm the existence of amino acid residues in HP1BP3 that could be phosphorylated by GSK-3β (*Appendix* 1 and 2).
- Additional investigation is required to discover how GSK-3β activity could promote the degradation of phospho-HP1BP3 by the FBXW7 E3 ligase.
- Absence of anti-phospho-Ser/Thr HP1BP3 antibodies that could detect the endogenous expression level of phospho-HP1BP3 in different cell cycle phases and in response to GSK-3β activation and/or inhibition.
- To functionally validate the metastatic potential of HP1BP3 *in vivo*, Dr Nateri's laboratory has recently planned a project to develop metastatic xenograft models using immuno-deficient mice using stably over expressing and knockout *HP1BP3* for HCT116 cell lines and with and without of *FBXW7* deletion background.
- Due to time limitation, I could not specify the exact site/s in HP1BP3 that is/are responsible to stimulate euchromatin formation, activate the EMT pathway, and to alter the cell cycle progression, using different HP1BP3 deletions (generated in collaboration with my

colleague, Dr Normatova in our laboratory) in HCT116 (Figure 6-1) and Tiger fibroblast cell lines. These deletions could also be used to map the interaction region between FBXW7 and HP1BP3.

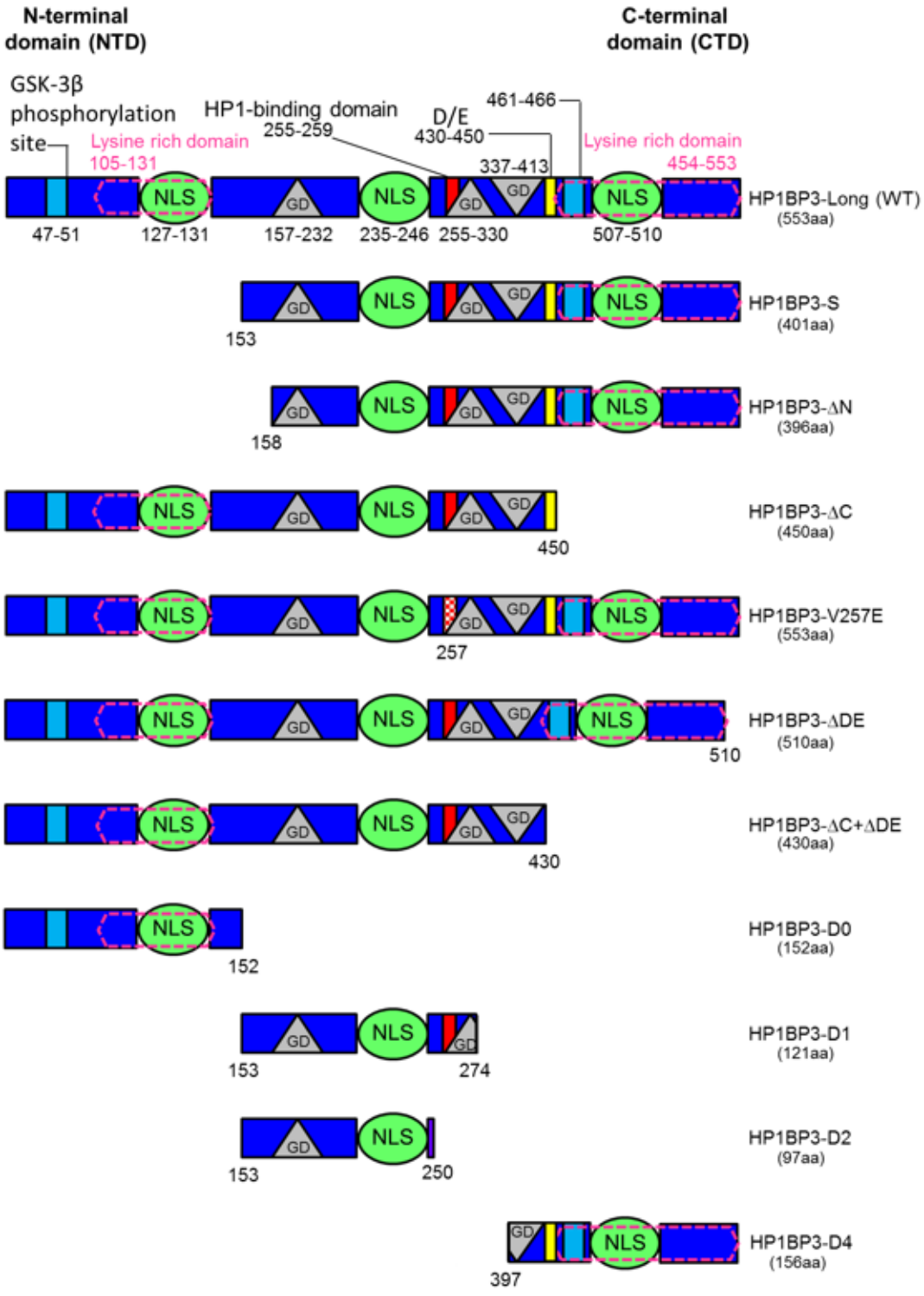


Figure 6-1: Schematic representations of each HP1BP3 recombinant construct sequence with amino acid start and stop numbers. Pink dashed boxes represent lysine-rich domain (ubiquitin-binding domain). Green ovals represent nuclear localisation signals (NLS). Grey triangles represent H15 globular domains (GD). Red box represents HP1α-binding domain. White dotted box represents a valine (V257) to glutamic acid (E) substitution. Light blue boxes represent GSK-3β phosphorylation site. Yellow represents DE (poly aspartate/glutamate) domain.

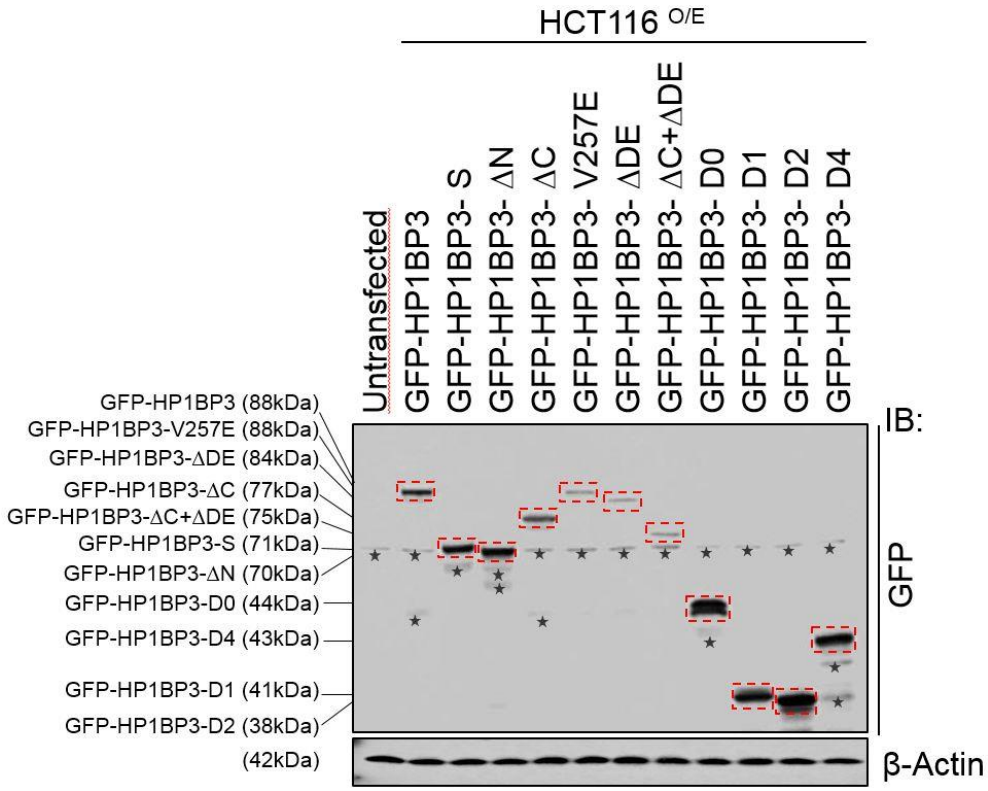


Figure 6-2: Validation of HP1BP3 recombinant constructs. Evaluation of GFP-fused HP1BP3 protein expression of HP1BP3 mutations (deletion/point mutation) in cells was performed by western blotting analysis. HCT116 cells were transiently transfected with HP1BP3 mutant constructs. The protein lysates were immunoblotted against GFP antibody. Expected bands were boxed on the blot as demonstrated. β-Actin is used as a loading control in western blotting analysis. The first line represents negative control (untransfected HCT116 cells). Stars indicate non-specific binding.

6.6 Conclusions and perspectives

In conclusion**,** we successfully identified HP1BP3 as a key regulator of chromatin dynamics, EMT pathway, and cell cycle progression. Hence, the obtained data provide valuable new evidence that loss of HP1BP3/FBXW7 complex plays a substantial role in colorectal cancer development via the dynamics of chromatin re-modelling. In longer term, the functions and mapping the interactions between HP1BP3 and FBXW7 and their consequences in epigenetics-mediated regulation might represent a novel therapeutic target for drug discovery. For example, in epithelial derived cancer cells mutated for FBXW7, histone acetyltransferase (HAT) inhibitors can reduce the Snail1 activity and consequently enhancing the E-cadherin expression. Given that, discovering how epigenetic therapy could make cancer cells more sensitive to the effects of radiotherapy and chemotherapy is currently become a great interest in this area of research. HP1BP3 could allow future studies to better anticipate the influence of chromatin biology on several disease pathogenesis and cellular processes.

Several other considerations that can be taken into account in the future are:

- Generating phosphorylation site-specific antibodies for HP1BP3 that could detect the phosphorylated form of HP1BP3 protein.
- The pathological significance of the negative correlation between HP1BP3 and H3K9me3/H3K9ac expression/levels can be examined using human colorectal cancer tissues microarray (TMA).
- Further study of FBXW7/HP1BP3/SUV39H1/HP1α interplay in cancer biology using *in vivo* models. Using a *Hp1bp3* conditional

knockout, has recently been conducted a full programme in Dr Nateri's laboratory.

- Last but not least, further studies will be needed to identify post-transcriptional and/or other type of post-translational factors regulating HP1BP3 activity and/or its expression and also to determine downstream targets using the bioinformatics approaches and eventually the implications of these regulatory mechanisms/pathways in different cellular processes.

Taken together, here we demonstrated the roles of HP1BP3-mediated the epigenetic reprogramming in regulation of EMT and cell cycle control of normal and cancer cells for the first time. Thus, the future explosion in our knowledge of how HP1BP3 modulates chromatin organization and gene transcription will further highlight the importance of aberrant HP1BP3-mediated epigenetic mechanisms in the initiation and progression of human cancer.

References

Aagaard, L., Schmid, M., Warburton, P., and Jenuwein, T. (2000). Mitotic phosphorylation of SUV39H1, a novel component of active centromeres, coincides with transient accumulation at mammalian centromeres. J Cell Sci 113, 817-829.

Akhoondi, S., Sun, D., von der Lehr, N., Apostolidou, S., Klotz, K., Maljukova, A., Cepeda, D., Fiegl, H., Dofou, D., Marth, C., et al. (2007). FBXW7/hCDC4 is a general tumor suppressor in human cancer. Cancer Research 67, 9006-9012.

Alexandrow, M.G., and Hamlin, J.L. (2005). Chromatin decondensation in S-phase involves recruitment of Cdk2 by Cdc45 and histone H1 phosphorylation. The Journal of Cell Biology 168, 875-886.

Allfrey, V.G., Faulkner, R., and Mirsky, A.E. (1964). Acetylation and methylation of histones and their possible role in the regulation of RNA synthesis. Proceedings of the National Academy of Sciences of the United States of America 51, 786-794.

Antonin, W., and Neumann, H. (2016). Chromosome condensation and decondensation during mitosis. Current Opinion in Cell Biology 40, 15-22.

Ayyanathan, K., Lechner, M.S., Bell, P., Maul, G.G., Schultz, D.C., Yamada, Y., Tanaka, K., Torigoe, K., and Rauscher, F.J. (2003). Regulated recruitment of HP1 to a euchromatic gene induces mitotically heritable, epigenetic gene silencing: a mammalian cell culture model of gene variegation. Genes & Development 17, 1855-1869.

Babaei-Jadidi, R., Li, N., Saadeddin, A., Spencer-Dene, B., Jandke, A., Muhammad, B., Ibrahim, E.E., Muraleedharan, R., Abuzinadah, M., Davis, H., et al. (2011). FBXW7 influences murine intestinal homeostasis and cancer, targeting Notch, Jun, and DEK for degradation. The Journal of Experimental Medicine 208, 295-312.

Balamurugan, K., Sharan, S., Klarmann, K.D., Zhang, Y., Coppola, V., Summers, G.H., Roger, T., Morrison, D.K., Keller, J.R., and Sterneck, E. (2013). FBXW7α attenuates inflammatory signalling by downregulating C/EBPδ and its target gene Tlr4. Nature Communications 4, 1662.

Bannister, A.J., and Kouzarides, T. (2011). Regulation of chromatin by histone modifications. Cell Research 21, 381-395.

Bannister, A.J., Zegerman, P., Partridge, J.F., Miska, E.A., Thomas, J.O., Allshire, R.C., and Kouzarides, T. (2001). Selective recognition of methylated lysine 9 on histone H3 by the HP1 chromo domain. Nature 410, 120-124.

Barlev, N.A., Liu, L., Chehab, N.H., Mansfield, K., Harris, K.G., Halazonetis, T.D., and Berger, S.L. (2001). Acetylation of p53 activates transcription through recruitment of coactivators/histone acetyltransferases. Molecular Cell 8, 1243-1254.

Barski, A., Cuddapah, S., Cui, K., Roh, T.-Y., Schones, D.E., Wang, Z., Wei, G., Chepelev, I., and Zhao, K. (2007). High-resolution profiling of histone methylations in the human genome. Cell 129, 823-837.

Bártová, E., Krejčí, J., Harničarová, A., Galiová, G., and Kozubek, S. (2008). Histone modifications and nuclear architecture: a review. Journal of Histochemistry and Cytochemistry 56, 711-721.

Bassermann, F., Eichner, R., and Pagano, M. (2014). The ubiquitin proteasome system—implications for cell cycle control and the targeted treatment of cancer. Biochimica et Biophysica Acta (BBA)-Molecular Cell Research 1843, 150-162.

Batlle, E., Sancho, E., Franci, C., Dominguez, D., Monfar, M., Baulida, J., and Garcia de Herreros, A. (2000). The transcription factor Snail is a repressor of E-cadherin gene expression in epithelial tumour cells. Nat Cell Biol 2, 84-89.

Becker, P.B., and Workman, J.L. (2013). Nucleosome remodeling and epigenetics. Cold Spring Harbor perspectives in biology 5, a017905.

Bedi, U., Mishra, V.K., Wasilewski, D., Scheel, C., and Johnsen, S.A. (2014). Epigenetic plasticity: a central regulator of epithelial-to-mesenchymal transition in cancer. Oncotarget 5, 2016-2029.

Benard, A., Goossens-Beumer, I.J., van Hoesel, A.Q., de Graaf, W., Horati, H., Putter, H., Zeestraten, E.C., van de Velde, C.J., and Kuppen, P.J. (2014). Histone trimethylation at H3K4, H3K9 and H4K20 correlates with patient survival and tumor recurrence in early-stage colon cancer. BMC Cancer 14, 1.

Benard, A., van de Velde, C.J.H., Lessard, L., Putter, H., Takeshima, L., Kuppen, P.J.K., and Hoon, D.S.B. (2013). Epigenetic status of LINE-1 predicts clinical outcome in early-stage rectal cancer. Br J Cancer 109, 3073-3083.

Bertoli, C., Skotheim, J.M., and de Bruin, R.A. (2013). Control of cell cycle transcription during G1 and S phases. Nature Reviews Molecular Cell Biology 14, 518-528.

Bhaskara, S., Jacques, V., Rusche, J.R., Olson, E.N., Cairns, B.R., and Chandrasekharan, M.B. (2013). Histone deacetylases 1 and 2 maintain S-phase chromatin and DNA replication fork progression. Epigenetics and Chromatin 6, 1.

Bialkowska, A.B., Liu, Y., Nandan, M.O., and Yang, V.W. (2014). A colon cancer-derived mutant of Krüppel-like factor 5 (KLF5) is resistant to degradation by glycogen synthase kinase 3β (GSK3β) and the E3 ubiquitin ligase F-box and WD repeat domain-containing 7α (FBW7α). Journal of Biological Chemistry 289, 5997-6005.

Bonetti, P., Davoli, T., Sironi, C., Amati, B., Pelicci, P.G., and Colombo, E. (2008). Nucleophosmin and its AML-associated mutant regulate c-Myc turnover through Fbw7γ. The Journal of Cell Biology 182, 19-26.

Brownell, J.E., Zhou, J., Ranalli, T., Kobayashi, R., Edmondson, D.G., Roth, S.Y., and Allis, C.D. (1996). Tetrahymena histone acetyltransferase A: a homolog to yeast Gcn5p linking histone acetylation to gene activation. Cell 84, 843-851.

Busino, L., Millman, S.E., Scotto, L., Kyratsous, C.A., Basrur, V., O'Connor, O., Hoffmann, A., Elenitoba-Johnson, K.S., and Pagano, M. (2012). Fbxw7 [alpha]-and GSK3-mediated degradation of p100 is a pro-survival mechanism in multiple myeloma. Nature Cell Biology 14, 375-385.

Büssow, K. (2015). Stable mammalian producer cell lines for structural biology. Current Opinion in Structural Biology 32, 81-90.

Cai, Z., Tang, X., Gao, H., Tang, C., Nandakumar, V., Jones, L., Ye, H., Lou, F., Zhang, D., and Sun, H. (2014). APC, FBXW7, KRAS, PIK3CA, and TP53 gene mutations in human colorectal cancer tumors frequently detected by Next-Generation DNA sequencing. Journal of Molecular and Genetic Medicine 8, 145.

Canzio, D., Larson, A., and Narlikar, G.J. (2014). Mechanisms of functional promiscuity by HP1 proteins. Trends in Cell Biology 24, 377-386.

Cao, J., Ge, M.-H., and Ling, Z.-Q. (2016). Fbxw7 tumor suppressor: a vital regulator contributes to human tumorigenesis. Medicine 95, e2496.

Carlberg, C., and Molnár, F. (2016). The Impact of Chromatin. In Mechanisms of Gene Regulation. Springer. pp. 17-34.

Chau, V., Tobias, J.W., Bachmair, A., Marriott, D., Ecker, D.J., Gonda, D.K., and Varshavsky, A. (1989). A multiubiquitin chain is confined to specific lysine in a targeted short-lived protein. Science 243, 1576-1584.

Chaudhary, S., Pak, J.E., Gruswitz, F., Sharma, V., and Stroud, R.M. (2012). Overexpressing human membrane proteins in stably transfected and clonal human embryonic kidney 293S cells. Nature Protocols 7, 453-466.

Chen, J., Liu, H., Liu, J., Qi, J., Wei, B., Yang, J., Liang, H., Chen, Y., Chen, J., Wu, Y., et al. (2013). H3K9 methylation is a barrier during somatic cell reprogramming into iPSCs. Nature Genetics 45, 34-42.

Chen, S., Yao, X., Li, Y., Saifudeen, Z., Bachvarov, D., and El-Dahr, S.S. (2015). Histone deacetylase 1 and 2 regulate Wnt and p53 pathways in the ureteric bud epithelium. Development 142, 1180-1192.

Cheng, Y., and Li, G. (2012). Role of the ubiquitin ligase Fbw7 in cancer progression. Cancer and Metastasis Reviews 31, 75-87.

Cherukuri, S., Hock, R., Ueda, T., Catez, F., Rochman, M., and Bustin, M. (2008). Cell cycle-dependent binding of HMGN proteins to chromatin. Molecular Biology of The Cell 19, 1816-1824.

Chevillard, C., Reik, W., McDermott, M., Fontes, M., Mattei, M.G., and Singh, P.B. (1993). Chromosomal localization of human homologs of the Drosophila heterochromatin protein 1 (HP1) gene. Mammalian Genome 4, 124-126.

Chin, H.G., Patnaik, D., Esteve, P.-O., Jacobsen, S.E., and Pradhan, S. (2006). Catalytic properties and kinetic mechanism of human recombinant Lys-9 histone H3 methyltransferase SUV39H1: participation of the chromodomain in enzymatic catalysis. Biochemistry 45, 3272-3284.

Cho, S.W., Kim, S., Kim, J.M., and Kim, J.-S. (2013). Targeted genome engineering in human cells with the Cas9 RNA-guided endonuclease. Nature Biotechnology 31, 230-232.

Ciechanover, A. (1998). The ubiquitin–proteasome pathway: on protein death and cell life. The EMBO Journal 17, 7151-7160.

Chung, D.C. (2000). The genetic basis of colorectal cancer: Insights into critical pathways of tumorigenesis. Gastroenterology 119, 854-865.

Cimini, D., Mattiuzzo, M., Torosantucci, L., and Degrassi, F. (2003). Histone hyperacetylation in mitosis prevents sister chromatid separation and produces chromosome segregation defects. Molecular Biology of The Cell 14, 3821-3833.

Cogswell, J.P., Godlevski, M.M., Bonham, M., Bisi, J., and Babiss, L. (1995). Upstream stimulatory factor regulates expression of the cell cycle-dependent cyclin B1 gene promoter. Molecular and Cellular Biology 15, 2782-2790.

Cooper, G.M. (2000). The eukaryotic cell cycle. The Cell; A molecular approach. 2nd edition. Sunderland (MA); Sinauer Associates.

Cooper, J.A. (1987). Effects of cytochalasin and phalloidin on actin. The Journal of Cell Biology 105, 1473-1478.

Costes, S.V., Daelemans, D., Cho, E.H., Dobbin, Z., Pavlakis, G., and Lockett, S. (2004). Automatic and quantitative measurement of protein-protein colocalization in live cells. Biophysical Journal 86, 3993-4003.

Cowell, I.G., Aucott, R., Mahadevaiah, S.K., Burgoyne, P.S., Huskisson, N., Bongiorni, S., Prantera, G., Fanti, L., Pimpinelli, S., and Wu, R. (2002). Heterochromatin, HP1 and methylation at lysine 9 of histone H3 in animals. Chromosoma 111, 22-36.

Cremona, C.A., Sancho, R., Diefenbacher, M.E., and Behrens, A. (2016). Fbw7 and its counteracting forces in stem cells and cancer: oncoproteins in the balance. Seminars in Cancer Biology 36, 52-61.

Cross, D.A., Culbert, A.A., Chalmers, K.A., Facci, L., Skaper, S.D., and Reith, A.D. (2001). Selective small-molecule inhibitors of glycogen synthase kinase-3 activity protect primary neurones from death. Journal of Neurochemistry 77, 94-102.

Cryderman, D.E., Vitalini, M.W., and Wallrath, L.L. (2011). Heterochromatin protein 1a is required for an open chromatin structure. Transcription 2, 95-99.

Czvitkovich, S., Sauer, S., Peters, A.H., Deiner, E., Wolf, A., Laible, G., Opravil, S., Beug, H., and Jenuwein, T. (2001). Over-expression of the SUV39H1 histone methyltransferase induces altered proliferation and differentiation in transgenic mice. Mechanisms of Development 107, 141-153.

Dash, P.K., Johnson, D., Clark, J., Orsi, S.A., Zhang, M., Zhao, J., Grill, R.J., Moore, A.N., and Pati, S. (2011). Involvement of the glycogen synthase kinase-3 signalling pathway in TBI pathology and neurocognitive outcome. PloS One 6, e24648.

Davie, J.R. (1998). Covalent modifications of histones: expression from chromatin templates. Current Opinion in Genetics and Development 8, 173-178.

Davie, J.R., and Spencer, V.A. (1999). Control of histone modifications. Journal of Cellular Biochemistry 33, 141-148.

Davies, R.J., Miller, R., and Coleman, N. (2005). Colorectal cancer screening: prospects for molecular stool analysis. Nature Reviews Cancer 5, 199-209.

Davis, H., Lewis, A., Behrens, A., and Tomlinson, I. (2013a). Investigation of the atypical FBXW7 mutation spectrum in human tumours by conditional expression of a heterozygous propellor tip missense allele in the mouse intestines. Gut 63, 792-799.

Davis, H., Lewis, A., Spencer-Dene, B., Tateossian, H., Stamp, G., Behrens, A., and Tomlinson, I. (2011). FBXW7 mutations typically found in human cancers are distinct from null alleles and disrupt lung development. The Journal of Pathology 224, 180-189.

Davis, M.A., Larimore, E.A., Fissel, B.M., Swanger, J., Taatjes, D.J., and Clurman, B.E. (2013b). The SCF–Fbw7 ubiquitin ligase degrades MED13 and MED13L and regulates CDK8 module association with Mediator. Genes and Development 27, 151-156.

Davis, R.J., Welcker, M., and Clurman, B.E. (2014). Tumor suppression by the Fbw7 ubiquitin ligase: mechanisms and opportunities. Cancer Cell 26, 455-464.

Dawson, M.A., Bannister, A.J., Göttgens, B., Foster, S.D., Bartke, T., Green, A.R., and Kouzarides, T. (2009). JAK2 phosphorylates histone H3Y41 and excludes HP1α from chromatin. Nature 461, 819-822.

Dawson, Mark A., and Kouzarides, T. (2012). Cancer epigenetics: from mechanism to therapy. Cell 150, 12-27.

De Koning, L., Savignoni, A., Boumendil, C., Rehman, H., Asselain, B., Sastre-Garau, X., and Almouzni, G. (2009). Heterochromatin protein 1α: a hallmark of cell proliferation relevant to clinical oncology. EMBO Molecular Medicine 1, 178-191.

De Lange, R., Burtscher, H., Jarsch, M., and Weidle, U.H. (2000). Identification of metastasis-associated genes by transcriptional profiling of metastatic versus non-metastatic colon cancer cell lines. Anticancer Research 21, 2329-2339.

De Mesquita, D.D., Zhan, Q., Crossley, L., and Badwey, J.A. (2001). p90-RSK and Akt may promote rapid phosphorylation/inactivation of glycogen synthase kinase 3 in chemoattractant-stimulated neutrophils. FEBS letters 502, 84-88.

Deligezer, U., Akisik, E.Z., Akisik, E.E., Kovancilar, M., Bugra, D., Erten, N., Holdenrieder, S., and Dalay, N. (2010). H3K9me3/H4K20me3 ratio in circulating nucleosomes as potential biomarker for colorectal cancer. In Circulating nucleic acids in plasma and serum (Springer), pp. 97-103.

Derks, S., Bosch, L.J., Niessen, H.E., Moerkerk, P.T., van den Bosch, S.M., Carvalho, B., Mongera, S., Voncken, J.W., Meijer, G.A., and de Bruïne, A.P. (2009). Promoter CpG island hypermethylation-and H3K9me3 and H3K27me3-mediated epigenetic silencing targets the deleted in colon cancer (DCC) gene in colorectal carcinogenesis without affecting neighboring genes on chromosomal region 18q21. Carcinogenesis 30, 1041-1048.

Di Paola, D., Rampakakis, E., Chan, M.K., and Zannis-Hadjopoulos, M. (2012). Differential chromatin structure encompassing replication origins in transformed and normal cells. Genes and Cancer 3, 152-176.

Dialynas, G.K., Makatsori, D., Kourmouli, N., Theodoropoulos, P.A., McLean, K., Terjung, S., Singh, P.B., and Georgatos, S.D. (2006). Methylation-independent binding to histone H3 and cell cycle-dependent

incorporation of HP1β into heterochromatin. Journal of Biological Chemistry 281, 14350-14360.

Dialynas, G.K., Vitalini, M.W., and Wallrath, L.L. (2008). Linking Heterochromatin protein 1 (HP1) to cancer progression. Mutation Research/Fundamental and Molecular Mechanisms of Mutagenesis 647, 13-20.

Dillon, N., and Festenstein, R. (2002). Unravelling heterochromatin: competition between positive and negative factors regulates accessibility. Trends in Genetics 18, 252-258.

Du, B., and Shim, J.S. (2016). Targeting Epithelial–Mesenchymal Transition (EMT) to Overcome Drug Resistance in Cancer. Molecules 21, 965.

Dunican, D.S., McWilliam, P., Tighe, O., Parle-McDermott, A., and Croke, D.T. (2002). Gene expression differences between the microsatellite instability (MIN) and chromosomal instability (CIN) phenotypes in colorectal cancer revealed by high-density cDNA array hybridization. Oncogene 21, 3253-3257.

Dutta, B., Ren, Y., Hao, P., Sim, K.H., Cheow, E., Adav, S., Tam, J.P., and Sze, S.K. (2014a). Profiling of the chromatin-associated proteome identifies HP1BP3 as a novel regulator of cell cycle progression. Molecular and Cellular Proteomics 13, 2183-2197.

Dutta, B., Yan, R., Lim, S.K., Tam, J.P., and Sze, S.K. (2014b). Quantitative profiling of chromatome dynamics reveals a novel role for HP1BP3 in hypoxia-induced oncogenesis. Molecular and Cellular Proteomics 13, 3236-3249.

Eissenberg, J.C., and Elgin, S.C.R. (2000). The HP1 protein family: getting a grip on chromatin. Current Opinion in Genetics and Development 10, 204-210.

Ekholm-Reed, S., Goldberg, M.S., Schlossmacher, M.G., and Reed, S.I. (2013). Parkin-dependent degradation of the F-box protein Fbw7β promotes neuronal survival in response to oxidative stress by stabilizing Mcl-1. Molecular and Cellular Biology 33, 3627-3643.

Elgin, S.C.R., and Reuter, G. (2007). Epigenetics, pp. 81-100.

Eliana, K., Federica, L., Roya, B., and Abdolrahman, N. (2013). Colorectal cancer: a pathology of the colon-rectum and a disease of the genome. Intern Med 3, 2.

Enroth, S., Rada-Iglesisas, A., Andersson, R., Wallerman, O., Wanders, A., Pahlman, L., Komorowski, J., and Wadelius, C. (2011). Cancer associated epigenetic transitions identified by genome-wide histone methylation

binding profiles in human colorectal cancer samples and paired normal mucosa. Bmc Cancer 11, 450.

Fan, Y., Nikitina, T., Morin-Kensicki, E.M., Zhao, J., Magnuson, T.R., Woodcock, C.L., and Skoultchi, A.I. (2003). H1 linker histones are essential for mouse development and affect nucleosome spacing in vivo. Molecular and Cellular Biology 23, 4559-4572.

Fan, Y., Nikitina, T., Zhao, J., Fleury, T.J., Bhattacharyya, R., Bouhassira, E.E., Stein, A., Woodcock, C.L., and Skoultchi, A.I. (2005). Histone H1 depletion in mammals alters global chromatin structure but causes specific changes in gene regulation. Cell 123, 1199-1212.

Fanti, L., Giovinazzo, G., Berloco, M., and Pimpinelli, S. (1998). The heterochromatin protein 1 prevents telomere fusions in Drosophila. Molecular Cell 2, 527-538.

Favoriti, P., Carbone, G., Greco, M., Pirozzi, F., Pirozzi, R.E.M., and Corcione, F. (2016). Worldwide burden of colorectal cancer: a review. Updates in Surgery 68, 7-11.

Felsenfeld, G., and Groudine, M. (2003). Controlling the double helix. Nature 421, 448-453.

Feng, J., Cen, J., Li, J., Zhao, R., Zhu, C., Wang, Z., Xie, J., and Tang, W. (2015). Histone deacetylase inhibitor valproic acid (VPA) promotes the epithelial mesenchymal transition of colorectal cancer cells via up regulation of Snail. Cell Adhesion and Migration 9, 495-501.

Finkin, S., Aylon, Y., Anzi, S., Oren, M., and Shaulian, E. (2008). Fbw7 regulates the activity of endoreduplication mediators and the p53 pathway to prevent drug-induced polyploidy. Oncogene 27, 4411-4421.

Finley, D. (2009). Recognition and processing of ubiquitin-protein conjugates by the proteasome. Annual review of biochemistry 78, 477-513.

Fischle, W., Tseng, B.S., Dormann, H.L., Ueberheide, B.M., Garcia, B.A., Shabanowitz, J., Hunt, D.F., Funabiki, H., and Allis, C.D. (2005). Regulation of HP1–chromatin binding by histone H3 methylation and phosphorylation. Nature 438, 1116-1122.

Flügel, D., Görlach, A., and Kietzmann, T. (2012). GSK-3β regulates cell growth, migration, and angiogenesis via Fbw7 and USP28-dependent degradation of HIF-1α. Blood 119, 1292-1301.

Fukushima, H., Matsumoto, A., Inuzuka, H., Zhai, B., Lau, A.W., Wan, L., Gao, D., Shaik, S., Yuan, M., and Gygi, S.P. (2012). SCF Fbw7 modulates the NFκB signaling pathway by targeting NFκB2 for ubiquitination and destruction. Cell Reports 1, 434-443.

García-Giménez, J.L. (2015). Epigenetic biomarkers and diagnostics (Elsevier Science). In: Garcia-Giménez JL ed.

Garfinkel, B.P., Arad, S., Le, P.T., Bustin, M., Rosen, C.J., Gabet, Y., and Orly, J. (2015a). Proportionate dwarfism in mice lacking Heterochromatin Protein 1 Binding Protein 3 (HP1BP3) is associated with alterations in the endocrine IGF-1 pathway. Endocrinology 156, 4558-4570.

Garfinkel, B.P., Arad, S., Neuner, S., Netser, S., Wagner, S., Kaczorowski, C.C., Rosen, C.J., Gal, M., Soreq, H., and Orly, J. (2016). HP1BP3 expression determines maternal behavior and offspring survival. Genes, Brain and Behavior 15, 678-688.

Garfinkel, B.P., Melamed-Book, N., Anuka, E., Bustin, M., and Orly, J. (2015b). HP1BP3 is a novel histone H1 related protein with essential roles in viability and growth. Nucleic Acids Research 43, 2074-2090.

Gargalionis, A.N., Piperi, C., Adamopoulos, C., and Papavassiliou, A.G. (2012). Histone modifications as a pathogenic mechanism of colorectal tumorigenesis. The International Journal of Biochemistry and Cell Biology 44, 1276-1289.

Gezer, U., Ustek, D., Yoruker, E.E., Cakiris, A., Abaci, N., Leszinski, G., Dalay, N., and Holdenrieder, S. (2013). Characterization of H3K9me3- and H4K20me3-associated circulating nucleosomal DNA by high-throughput sequencing in colorectal cancer. Tumour Biology: The Journal of The International Society for Oncodevelopmental Biology and Medicine 34, 329-336.

Ghattass, K., Assah, R., El-Sabban, M., and Gali-Muhtasib, H. (2013). Targeting hypoxia for sensitization of tumors to radio-and chemotherapy. Current Cancer Drug Targets 13, 670-685.

Grady, W.M., and Carethers, J.M. (2008). Genomic and epigenetic instability in colorectal cancer pathogenesis. Gastroenterology 135, 1079-1099.

Greene, F.L., Page, D., Fleming, I., Fritz, A., Balch, C., Haller, D., and Morrow, M. (2002). American Joint Committee on Cancer. AJCC cancer staging manual, xiv.

Gregory, P.D., Wagner, K., and Horz, W. (2001). Histone acetylation and chromatin remodeling. Experimental Cell Research 265, 195-202.

Greil, F., van der Kraan, I., Delrow, J., Smothers, J.F., de Wit, E., Bussemaker, H.J., van Driel, R., Henikoff, S., and van Steensel, B. (2003). Distinct HP1 and Su (var) 3-9 complexes bind to sets of developmentally coexpressed genes depending on chromosomal location. Genes and Development 17, 2825-2838.

Grewal, S.I.S., and Elgin, S.C.R. (2007). Transcription and RNA interference in the formation of heterochromatin. Nature 447, 399-406.

Grim, J.E., Knoblaugh, S.E., Guthrie, K.A., Hagar, A., Swanger, J., Hespelt, J., Delrow, J.J., Small, T., Grady, W.M., and Nakayama, K.I. (2012). Fbw7 and p53 cooperatively suppress advanced and chromosomally unstable intestinal cancer. Molecular and Cellular Biology 32, 2160-2167.

Grunstein, M., Hecht, A., Fisher-Adams, G., Wan, J., Mann, R.K., Strahl-Bolsinger, S., Laroche, T., and Gasser, S. (1995). The regulation of euchromatin and heterochromatin by histones in yeast. Journal of Cell Science 19, 29-36.

Guha, S., Cullen, J.P., Morrow, D., Colombo, A., Lally, C., Walls, D., Redmond, E.M., and Cahill, P.A. (2011). Glycogen synthase kinase 3 beta positively regulates Notch signaling in vascular smooth muscle cells: role in cell proliferation and survival. Basic research in cardiology 106, 773.

Hadac, J.N., Miller, D.D., Grimes, I.C., Clipson, L., Newton, M.A., Schelman, W.R., and Halberg, R.B. (2016). Heterochromatin Protein 1 Binding Protein 3 expression as a candidate marker of intrinsic 5-fluorouracil resistance. Anticancer Research 36, 845-852.

Hagedorn, M., Delugin, M., Abraldes, I., Allain, N., Belaud-Rotureau, M.-A., Turmo, M., Prigent, C., Loiseau, H., Bikfalvi, A., and Javerzat, S. (2007). FBXW7/hCDC4 controls glioma cell proliferation in vitro and is a prognostic marker for survival in glioblastoma patients. Cell Division 2, 1.

Haggar, F.A., and Boushey, R.P. (2009). Colorectal cancer epidemiology: incidence, mortality, survival, and risk factors. Clinics in Colon and Rectal Surgery 22, 191-197.

Hamamoto, R., Saloura, V., and Nakamura, Y. (2015). Critical roles of non-histone protein lysine methylation in human tumorigenesis. Nature Reviews Cancer 15, 110-124.

Hanahan, D., and Weinberg, R.A. (2000). The Hallmarks of Cancer. Cell 100, 57-70.

Hanahan, D., and Weinberg, R.A. (2011). Hallmarks of cancer: the next generation. Cell 144, 646-674.

Hayakawa, T., Haraguchi, T., Masumoto, H., and Hiraoka, Y. (2003). Cell cycle behavior of human HP1 subtypes: distinct molecular domains of HP1 are required for their centromeric localization during interphase and metaphase. Journal of Cell Science 116, 3327-3338.

Hayami, S., Kelly, J.D., Cho, H.S., Yoshimatsu, M., Unoki, M., Tsunoda, T., Field, H.I., Neal, D.E., Yamaue, H., and Ponder, B.A. (2011). Overexpression of LSD1 contributes to human carcinogenesis through

chromatin regulation in various cancers. International Journal of Cancer 128, 574-586.

Hayashihara, K., Uchiyama, S., Shimamoto, S., Kobayashi, S., Tomschik, M., Wakamatsu, H., No, D., Sugahara, H., Hori, N., Noda, M., et al. (2010). The middle region of an HP1-binding protein, HP1-BP74, associates with linker DNA at the entry/exit site of nucleosomal DNA. Journal of Biological Chemistry 285, 6498–6507.

He, L., and Hannon, G.J. (2004). MicroRNAs: small RNAs with a big role in gene regulation. Nature Reviews Genetics 5, 522-531.

Hebbes, T.R., Thorne, A.W., and Cranerobinson, C. (1988). A direct link between core histone acetylation and transcriptionally active chromatin. Embo Journal 7, 1395-1402.

Heckman, K.L., and Pease, L.R. (2007). Gene splicing and mutagenesis by PCR-driven overlap extension. Nature Protocols 2, 924-932.

Heitz, E. (1928). Das Heterochromatin der Moose (Bornträger). Jahrb Wiss Botanik 69, 762–818.

Henikoff, S., Ahmad, K., and Malik, H.S. (2001). The centromere paradox: stable inheritance with rapidly evolving DNA. Science 293, 1098-1102.

Hermsen, M., Postma, C., Baak, J., Weiss, M., Rapallo, A., Sciutto, A., Roemen, G., Arends, J.W., Williams, R., Giaretti, W., et al. (2002). Colorectal adenoma to carcinoma progression follows multiple pathways of chromosomal instability. Gastroenterology 123, 1109-1119.

Hiragami-Hamada, K., Shinmyozu, K., Hamada, D., Tatsu, Y., Uegaki, K., Fujiwara, S., and Nakayama, J.-i. (2011). N-terminal phosphorylation of HP1α promotes its chromatin binding. Molecular and cellular biology 31, 1186-1200.

Hu, C.-E., Liu, Y.-C., Zhang, H.-D., and Huang, G.-J. (2014). JMJD2A predicts prognosis and regulates cell growth in human gastric cancer. Biochemical and Biophysical Research Communications 449, 1-7.

Huzil, J.T., Pannu, R., Ptak, C., Garen, G., and Ellison, M.J. (2007). Direct catalysis of lysine 48-linked polyubiquitin chains by the ubiquitin-activating enzyme. Journal of Biological Chemistry 282, 37454-37460.
Hwang, A., Maity, A., McKenna, W.G., and Muschel, R.J. (1995). Cell cycle-dependent regulation of the cyclin B1 promoter. Journal of Biological Chemistry 270, 28419-28424.

Ibrahim, E.E., Babaei-Jadidi, R., Saadeddin, A., Spencer-Dene, B., Hossaini, S., Abuzinadah, M., Li, N., Fadhil, W., Ilyas, M., and Bonnet, D. (2012). Embryonic NANOG activity defines colorectal cancer stem cells and

modulates through AP1-and TCF-dependent mechanisms. Stem Cells 30, 2076-2087.

Inuzuka, H., Shaik, S., Onoyama, I., Gao, D., Tseng, A., Maser, R.S., Zhai, B., Wan, L., Gutierrez, A., and Lau, A.W. (2011). SCFFBW7 regulates cellular apoptosis by targeting MCL1 for ubiquitylation and destruction. Nature 471, 104-109.

Issa, J.-P. (2004). CpG island methylator phenotype in cancer. Nat Rev Cancer 4, 988-993.

Jackman, M., and Pines, J. (1996). Cyclins and the G2/M transition. Cancer Surveys 29, 47-73.

James, T.C., Eissenberg, J.C., Craig, C., Dietrich, V., Hobson, A., and Elgin, S.C.R. (1989). Distribution patterns of HP1, a heterochromatin-associated nonhistone chromosomal protein of Drosophila. European Journal of Cell Biology 50, 170-180.

Jayani, R.S., Ramanujam, P.L., and Galande, S. (2010). Chapter 2 - Studying Histone Modifications and Their Genomic Functions by Employing Chromatin Immunoprecipitation and Immunoblotting. In Methods in Cell Biology, G.V. Shivashankar, ed. (Academic Press), pp. 35-56.

Ji, M., Lee, E.J., Kim, K.B., Kim, Y., Sung, R., Lee, S.-J., Kim, D.S., and Park, S.M. (2015). HDAC inhibitors induce epithelial-mesenchymal transition in colon carcinoma cells. Oncology Reports 33, 2299-2308.

Jie, D., Zhongmin, Z., Guoqing, L., Sheng, L., Yi, Z., Jing, W., and Liang, Z. (2013). Positive expression of LSD1 and negative expression of E-cadherin correlate with metastasis and poor prognosis of colon cancer. Digestive Diseases and Sciences 58, 1581-1589.

Kang, M.Y., Lee, B.B., Kim, Y.H., Chang, D.K., Kyu Park, S., Chun, H.K., Song, S.Y., Park, J., and Kim, D.H. (2007). Association of the SUV39H1 histone methyltransferase with the DNA methyltransferase 1 at mRNA expression level in primary colorectal cancer. International Journal of Cancer 121, 2192-2197.

Kellum, R., and Alberts, B.M. (1995). Heterochromatin protein 1 is required for correct chromosome segregation in Drosophila embryos. Journal of Cell Science 108, 1419-1431.

Khanal, P., Kim, G., Lim, S.-C., Yun, H.-J., Lee, K.Y., Choi, H.-K., and Choi, H.S. (2013). Prolyl isomerase Pin1 negatively regulates the stability of SUV39H1 to promote tumorigenesis in breast cancer. The FASEB Journal 27, 4606-4618.

Kiesslich, T., Pichler, M., and Neureiter, D. (2013). Epigenetic control of epithelial-mesenchymal-transition in human cancer (Review). Molecular and Clinical Oncology 1, 3-11.

Kim, M.S., Lee, J., and Sidransky, D. (2010). DNA methylation markers in colorectal cancer. Cancer and Metastasis Reviews 29, 181-206.

Kimura, T., Gotoh, M., Nakamura, Y., and Arakawa, H. (2003). hCDC4b, a regulator of cyclin E, as a direct transcriptional target of p53. Cancer Science 94, 431-436.

King, B., Trimarchi, T., Reavie, L., Xu, L., Mullenders, J., Ntziachristos, P., Aranda-Orgilles, B., Perez-Garcia, A., Shi, J., and Vakoc, C. (2013). The ubiquitin ligase FBXW7 modulates leukemia-initiating cell activity by regulating MYC stability. Cell 153, 1552-1566.

Kitagawa, K., Hiramatsu, Y., Uchida, C., Isobe, T., Hattori, T., Oda, T., Shibata, K., Nakamura, S., Kikuchi, A., and Kitagawa, M. (2009). Fbw7 promotes ubiquitin-dependent degradation of c-Myb: involvement of GSK3-mediated phosphorylation of Thr-572 in mouse c-Myb. Oncogene 28, 2393-2405.

Kogure, M., Takawa, M., Cho, H.-S., Toyokawa, G., Hayashi, K., Tsunoda, T., Kobayashi, T., Daigo, Y., Sugiyama, M., and Atomi, Y. (2013). Deregulation of the histone demethylase JMJD2A is involved in human carcinogenesis through regulation of the G 1/S transition. Cancer Letters 336, 76-84.

Komander, D., and Rape, M. (2012). The ubiquitin code. Annual review of biochemistry 81, 203-229.

Kornberg, R.D. (1977). Structure of chromatin. Annual Review of Biochemistry 46, 931-954.

Kourtis, N., Moubarak, R.S., Aranda-Orgilles, B., Lui, K., Aydin, I.T., Trimarchi, T., Darvishian, F., Salvaggio, C., Zhong, J., and Bhatt, K. (2015). FBXW7 modulates cellular stress response and metastatic potential through HSF1 post-translational modification. Nature Cell Biology 17, 322-332.

Kouzarides, T. (2007). Chromatin modifications and their function. Cell 128, 693-705.

Krouwels, I.M., Wiesmeijer, K., Abraham, T.E., Molenaar, C., Verwoerd, N.P., Tanke, H.J., and Dirks, R.W. (2005). A glue for heterochromatin maintenance stable SUV39H1 binding to heterochromatin is reinforced by the SET domain. The Journal of Cell Biology 170, 537-549.

Kuipers, E.J., Grady, W.M., Lieberman, D., Seufferlein, T., Sung, J.J., Boelens, P.G., van de Velde, C.J., and Watanabe, T. (2015). Colorectal cancer. Nature Reviews Disease Primers 1, 15065.

Kwon, S.H., and Workman, J.L. (2011). The changing faces of HP1: From heterochromatin formation and gene silencing to euchromatic gene expression. BioEssays 33, 280-289.

Labianca, R., Nordlinger, B., Beretta, G., Mosconi, S., Mandalà, M., Cervantes, A., Arnold, D., and Group, E.G.W. (2013). Early colon cancer: ESMO clinical practice guidelines for diagnosis, treatment and follow-up. Annals of Oncology 24, 64-72.

Lachner, M., O'Carroll, D., Rea, S., Mechtler, K., and Jenuwein, T. (2001). Methylation of histone H3 lysine 9 creates a binding site for HP1 proteins. Nature 410, 116-120.

Lai, T., Yang, Y., and Ng, S.K. (2013). Advances in mammalian cell line development technologies for recombinant protein production. Pharmaceuticals 6, 579-603.

Lamouille, S., Xu, J., and Derynck, R. (2014). Molecular mechanisms of epithelial–mesenchymal transition. Nat Rev Mol Cell Biol 15, 178-196.

Le Bras, G.F., Taubenslag, K.J., and Andl, C.D. (2012). The regulation of cell-cell adhesion during epithelial-mesenchymal transition, motility and tumor progression. Cell Adhesion and Migration 6, 365-373.

Lecker, S.H., Goldberg, A.L., and Mitch, W.E. (2006). Protein degradation by the ubiquitin–proteasome pathway in normal and disease states. Journal of the American Society of Nephrology 17, 1807-1819.

Lee, Y.-H., and Ann, D.K. (2015). Bi-phasic expression of Heterochromatin Protein 1 (HP1) during breast cancer progression: Potential roles of HP1 and chromatin structure in tumorigenesis. Journal of Nature and Science 1, 127.

Leszinski, G., Gezer, U., Siegele, B., Stoetzer, O., and Holdenrieder, S. (2012). Relevance of histone marks H3K9me3 and H4K20me3 in cancer. Anticancer Research 32, 2199-2205.

Li, A., Dawson, J.C., Forero-Vargas, M., Spence, H.J., Yu, X., König, I., Anderson, K., and Machesky, L.M. (2010). The actin-bundling protein fascin stabilizes actin in invadopodia and potentiates protrusive invasion. Current Biology 20, 339-345.

Li, G., and Reinberg, D. (2011). Chromatin higher-order structures and gene regulation. Current Opinion in Genetics and Development 21, 175-186.

Li, N., Lorenzi, F., Kalakouti, E., Normatova, M., Babaei-Jadidi, R., Tomlinson, I., and Nateri, A.S. (2015). FBXW7-mutated colorectal cancer cells exhibit aberrant expression of phosphorylated-p53 at serine-15. Oncotarget 6, 9240- 9256.

Li, Q., Li, Z., Sun, C.-X., and Yu, A.C.-H. (2002). Identification of transcripts expressed under functional differentiation in primary culture of cerebral cortical neurons. Neurochemical Research 27, 147-154.

Lieberthal, J.G., Kaminsky, M., Parkhurst, C.N., and Tanese, N. (2009). The role of YY1 in reduced HP1α gene expression in invasive human breast cancer cells. Breast Cancer Research 11,601-613.

Lin, T., Ponn, A., Hu, X., Law, B.K., and Lu, J. (2010). Requirement of the histone demethylase LSD1 in Snai1-mediated transcriptional repression during epithelial-mesenchymal transition. Oncogene 29, 4896-4904.

Liu, H., Liang, C., Kollipara, R.K., Matsui, M., Ke, X., Jeong, B.-C., Wang, Z., Yoo, K.S., Yadav, G.P., and Kinch, L.N. (2016a). HP1BP3, a chromatin retention factor for co-transcriptional MicroRNA processing. Molecular Cell 63, 420-432.

Liu, J., Yin, X., Liu, B., Zheng, H., Zhou, G., Gong, L., Li, M., Li, X., Wang, Y., and Hu, J. (2014). HP1α mediates defective heterochromatin repair and accelerates senescence in Zmpste24-deficient cells. Cell cycle 13, 1237-1247.

Liu, M., Huang, F., Zhang, D., Ju, J., Wu, X.-B., Wang, Y., Wang, Y., Wu, Y., Nie, M., and Li, Z. (2015). Heterochromatin protein HP1γ promotes colorectal cancer progression and is regulated by miR-30a. Cancer Research 75, 4593-4604.

Liu, T.F., and McCall, C.E. (2013). Deacetylation by SIRT1 reprograms inflammation and cancer. Genes and Cancer 4, 135-147.

Liu, X., Liao, W., Peng, H., Luo, X., Luo, Z., Jiang, H., and Xu, L. (2016b). miR-181a promotes G1/S transition and cell proliferation in paediatric acute myeloid leukemia by targeting ATM. Journal of Cancer Research and Clinical Oncology 142, 77-87.

Liu, Y., Hong, Y., Zhao, Y., Ismail, T.M., Wong, Y., and Eu, K.W. (2008). Histone H3 (lys-9) deacetylation is associated with transcriptional silencing of E-cadherin in colorectal cancer cell lines. Cancer Investigation 26, 575-582.

Lorenzi, F., Babaei-Jadidi, R., Sheard, J., Spencer-Dene, B., and Nateri, A.S. (2016). Fbxw7-associated drug resistance is reversed by induction of terminal differentiation in murine intestinal organoid culture. Molecular Therapy Methods and Clinical Development 3, 16024.

Lu, B.Y., Emtage, P.C.R., Duyf, B.J., Hilliker, A.J., and Eissenberg, J.C. (2000). Heterochromatin protein 1 is required for the normal expression of two heterochromatin genes in Drosophila. Genetics 155, 699-708.

Luo, J., Su, F., Chen, D., Shiloh, A., and Gu, W. (2000). Deacetylation of p53 modulates its effect on cell growth and apoptosis. Nature 408, 377-381.

Ma, Y., Kanakousaki, K., and Buttitta, L. (2014). How the cell cycle impacts chromatin architecture and influences cell fate. Frontiers in Genetics 6, 19-19.

Maeda, M., Johnson, K.R., and Wheelock, M.J. (2005). Cadherin switching: essential for behavioral but not morphological changes during an epithelium-to-mesenchyme transition. J Cell Sci 118, 873-887.

Maison, C., Bailly, D., Peters, A., Quivy, J.P., Roche, D., Taddei, A., Lachner, M., Jenuwein, T., and Almouzni, G. (2002). Higher-order structure in pericentric heterochromatin involves a distinct pattern of histone modification and an RNA component. Nature Genetics 30, 329-334.

Maison, C., Bailly, D., Roche, D., de Oca, R.M., Probst, A.V., Vassias, I., Dingli, F., Lombard, B., Loew, D., Quivy, J.-P., et al. (2011). SUMOylation promotes de novo targeting of HP1 alpha to pericentric heterochromatin. Nature Genetics 43, 719 - 727.

Mani, S.A., Guo, W., Liao, M.-J., Eaton, E.N., Ayyanan, A., Zhou, A.Y., Brooks, M., Reinhard, F., Zhang, C.C., and Shipitsin, M. (2008). The epithelial-mesenchymal transition generates cells with properties of stem cells. Cell 133, 704-715.

Mao, J.-H., Kim, I.-J., Wu, D., Climent, J., Kang, H.C., DelRosario, R., and Balmain, A. (2008). FBXW7 targets mTOR for degradation and cooperates with PTEN in tumor suppression. Science 321, 1499-1502.

Mao, J.H., Perez-Losada, J., Wu, D., Delrosario, R., Tsunematsu, R., Nakayama, K.I., Brown, K., Bryson, S., and Balmain, A. (2004). Fbxw7/Cdc4 is a p53-dependent, haploinsufficient tumour suppressor gene. Nature 432, 775-779.

Maresca, T.J., Freedman, B.S., and Heald, R. (2005). Histone H1 is essential for mitotic chromosome architecture and segregation in Xenopus laevis egg extracts. The Journal of Cell Biology 169, 859-869.

Marks, P.A. (2010). Histone deacetylase inhibitors: A chemical genetics approach to understanding cellular functions. Biochimica Et Biophysica Acta-Gene Regulatory Mechanisms 1799, 717-725.

Mateescu, B., Bourachot, B., Rachez, C., Ogryzko, V., and Muchardt, C. (2008). Regulation of an inducible promoter by an HP1 beta-HP1 gamma switch. Embo Reports 9, 267–272.

Matsumoto, A., Onoyama, I., Sunabori, T., Kageyama, R., Okano, H., and Nakayama, K.I. (2011). Fbxw7-dependent degradation of Notch is required

for control of "stemness" and neuronal-glial differentiation in neural stem cells. Journal of Biological Chemistry 286, 13754-13764.

Meehan, R.R., Kao, C.F., and Pennings, S. (2003). HP1 binding to native chromatin in vitro is determined by the hinge region and not by the chromodomain. The EMBO Journal 22, 3164-3174.

Meissner, A. (2010). Epigenetic modifications in pluripotent and differentiated cells. Nat Biotech 28, 1079-1088.

Minc, E., Allory, Y., Worman, H.J., Courvalin, J.-C., and Buendia, B. (1999). Localization and phosphorylation of HP1 proteins during the cell cycle in mammalian cells. Chromosoma 108, 220-234.

Mohn, F., and Schübeler, D. (2009). Genetics and epigenetics: stability and plasticity during cellular differentiation. Trends in Genetics 25, 129-136.

Moreno-Bueno, G., Peinado, H., Molina, P., Olmeda, D., Cubillo, E., Santos, V., Palacios, J., Portillo, F., and Cano, A. (2009). The morphological and molecular features of the epithelial-to-mesenchymal transition. Nature Protocols 4, 1591-1613.

Mounia, G., Delphine, B., Christèle, M., and Geneviève, A. (2004). Mouse centric and pericentric satellite repeats form distinct functional heterochromatin. The Journal of Cell Biology 166, 493-505.

Muchardt, C., Guilleme, M., Seeler, J.S., Trouche, D., Dejean, A., and Yaniv, M. (2002). Coordinated methyl and RNA binding is required for heterochromatin localization of mammalian HP1 alpha. Embo Reports 3, 975–981.

Mungamuri, S.K., Benson, E.K., Wang, S., Gu, W., Lee, S.W., and Aaronson, S.A. (2012). p53-mediated heterochromatin reorganization regulates its cell fate decisions. Nature Structural and Molecular Biology 19, 478-484.

Murphy, M., Ahn, J., Walker, K.K., Hoffman, W.H., Evans, R.M., Levine, A.J., and George, D.L. (1999). Transcriptional repression by wild-type p53 utilizes histone deacetylases, mediated by interaction with mSin3a. Genes and Development 13, 2490-2501.

Nakayama, J., Rice, J.C., Strahl, B.D., Allis, C.D., and Grewal, S.I. (2001). Role of histone H3 lysine 9 methylation in epigenetic control of heterochromatin assembly. Science 292, 110-113.

Nateri, A.S., Riera-Sans, L., Da Costa, C., and Behrens, A. (2004). The ubiquitin ligase SCFFbw7 antagonizes apoptotic JNK signaling. Science 303, 1374-1378.

Nateri, A.S., Spencer-Dene, B., and Behrens, A. (2005). Interaction of phosphorylated c-Jun with TCF4 regulates intestinal cancer development. Nature 437, 281-285.

Neuner, S.M., Garfinkel, B.P., Wilmott, L.A., Ignatowska-Jankowska, B.M., Citri, A., Orly, J., Lu, L., Overall, R.W., Mulligan, M.K., and Kempermann, G. (2016). Systems genetics identifies Hp1bp3 as a novel modulator of cognitive aging. Neurobiology of Aging 46, 58-67.

Nielsen, N.H., Lodén, M., Cajander, J., Emdin, S.O., and Landberg, G. (1999). G1-S transition defects occur in most breast cancers and predict outcome. Breast Cancer Research and Treatment 56, 103-110.

Nieto, M.A., and Cano, A. (2012). The epithelial–mesenchymal transition under control: global programs to regulate epithelial plasticity. Seminars in Cancer Biology (Elsevier) 22, 359-488..

Onoyama, I., Tsunematsu, R., Matsumoto, A., Kimura, T., de Alborán, I.M., Nakayama, K., and Nakayama, K.I. (2007). Conditional inactivation of Fbxw7 impairs cell-cycle exit during T cell differentiation and results in lymphomatogenesis. The Journal of Experimental Medicine 204, 2875-2888.

Pan, C., and Fan, Y. (2016). Role of H1 linker histones in mammalian development and stem cell differentiation. Biochimica et Biophysica Acta (BBA)-Gene Regulatory Mechanisms 1859, 496-509.

Park, H.-J., Kim, H.-J., Bae, G.-S., Seo, S.-W., Kim, D.-Y., Jung, W.-S., Kim, M.-S., Song, M.-Y., Kim, E.-K., and Kwon, K.-B. (2009). Selective GSK-3β inhibitors attenuate the cisplatin-induced cytotoxicity of auditory cells. Hearing research 257, 53-62.

Park, J.-A., Kim, A.-J., Kang, Y., Jung, Y.-J., Kim, H.K., and Kim, K.-C. (2011). Deacetylation and methylation at histone H3 lysine 9 (H3K9) coordinate chromosome condensation during cell cycle progression. Molecules and Cells 31, 343-349.

Park, S.H., Yu, S.E., Chai, Y.G., and Jang, Y.K. (2014). CDK2-dependent phosphorylation of Suv39H1 is involved in control of heterochromatin replication during cell cycle progression. Nucleic Acids Research 42, 6196-6207.

Peng, J.C., and Karpen, G.H. (2009). Heterochromatic genome stability requires regulators of histone H3 K9 methylation. PLoS Genet 5, e1000435.

Pereira, F., Barbáchano, A., Silva, J., Bonilla, F., Campbell, M.J., Muñoz, A., and Larriba, M.J. (2011). KDM6B/JMJD3 histone demethylase is induced by vitamin D and modulates its effects in colon cancer cells. Human molecular genetics, ddr399.

Peserico, A., and Simone, C. (2010). Physical and functional HAT/HDAC interplay regulates protein acetylation balance. BioMed Research International 2011, 20-34.

Peters, A., O'Carroll, D., Scherthan, H., Mechtler, K., Sauer, S., Schofer, C., Weipoltshammer, K., Pagani, M., Lachner, M., Kohlmaier, A., et al. (2001). Loss of the Suv39h histone methyltransferases impairs mammalian heterochromatin and genome stability. Cell 107, 323-337.

Petti, E., Jordi, F., Buemi, V., Dinami, R., Benetti, R., Blasco, M.A., and Schoeftner, S. (2015). Altered telomere homeostasis and resistance to skin carcinogenesis in Suv39h1 transgenic mice. Cell Cycle 14, 1438-1446.

Piacentini, L., Fanti, L., Negri, R., Del Vescovo, V., Fatica, A., Altieri, F., and Pimpinelli, S. (2009). Heterochromatin protein 1 (HP1a) positively regulates euchromatic gene expression through RNA transcript association and interaction with hnRNPs in Drosophila. PLoS Genet 5, e1000670.

Pickart, C. (1997). Targeting of substrates to the 26S proteasome. The FASEB Journal 11, 1055-1066.

Popov, N., Schülein, C., Jaenicke, L.A., and Eilers, M. (2010). Ubiquitylation of the amino terminus of Myc by SCF [beta]-TrCP antagonizes SCFFbw7-mediated turnover. Nature Cell Biology 12, 973-981.

Prasanth, S.G., Prasanth, K.V., Siddiqui, K., Spector, D.L., and Stillman, B. (2004). Human Orc2 localizes to centrosomes, centromeres and heterochromatin during chromosome inheritance. The EMBO Journal 23, 2651-2663.

Probst, A.V., and Almouzni, G. (2008). Pericentric heterochromatin: dynamic organization during early development in mammals. Differentiation 76, 15-23.

Probst, A.V., Dunleavy, E., and Almouzni, G. (2009). Epigenetic inheritance during the cell cycle. Nature Reviews Molecular Cell Biology 10, 192-206.

Quivy, J.-P., Gérard, A., Cook, A.J., Roche, D., and Almouzni, G. (2008). The HP1–p150/CAF-1 interaction is required for pericentric heterochromatin replication and S-phase progression in mouse cells. Nature Structural and Molecular Biology 15, 972-979.

Rajagopalan, H., Jallepalli, P.V., Rago, C., Velculescu, V.E., Kinzler, K.W., Vogelstein, B., and Lengauer, C. (2004). Inactivation of hCDC4 can cause chromosomal instability. Nature 428, 77-81.

Ramadoss, S., Chen, X., and Wang, C.-Y. (2012). Histone demethylase KDM6B promotes epithelial-mesenchymal transition. Journal of Biological Chemistry 287, 44508-44517.

Ran, F.A., Hsu, P.D., Wright, J., Agarwala, V., Scott, D.A., and Zhang, F. (2013). Genome engineering using the CRISPR-Cas9 system. Nature Protocols 8, 2281-2308.

Rao, C.V., and Yamada, H.Y. (2013). Genomic instability and colon carcinogenesis: from the perspective of genes. Frontiers in Oncology 3, 130.

Rea, S. (2000). Regulation of chromatin structure by site-specific histone H3 methyltransferases. Nature 406, 593-599.

Richards, E.J., and Elgin, S.C. (2002). Epigenetic codes for heterochromatin formation and silencing: rounding up the usual suspects. Cell 108, 489-500.

Romero-Pérez, L., López-García, M.Á., Díaz-Martín, J., Biscuola, M., Castilla, M.Á., Tafe, L.J., Garg, K., Oliva, E., Matias-Guiu, X., and Soslow, R.A. (2013). ZEB1 overexpression associated with E-cadherin and microRNA-200 downregulation is characteristic of undifferentiated endometrial carcinoma. Modern Pathology 26, 1514-1524.

Sanchez-Tillo, E., Lazaro, A., Torrent, R., Cuatrecasas, M., Vaquero, E., Castells, A., Engel, P., and Postigo, A. (2010). ZEB1 represses E-cadherin and induces an EMT by recruiting the SWI/SNF chromatin-remodeling protein BRG1. Oncogene 29, 3490-3500.

Sancho, R., Blake, S.M., Tendeng, C., Clurman, B.E., Lewis, J., and Behrens, A. (2013). Fbw7 repression by hes5 creates a feedback loop that modulates Notch-mediated intestinal and neural stem cell fate decisions. PLoS Biol 11, e1001586.

Sancho, R., Jandke, A., Davis, H., Diefenbacher, M.E., Tomlinson, I., and Behrens, A. (2010). F-box and WD repeat domain-containing 7 regulates intestinal cell lineage commitment and is a haploinsufficient tumor suppressor. Gastroenterology 139, 929-941.

Schafer, S., and Jung, M. (2005). Chromatin modifications as targets for new anticancer drugs. Archiv der Pharmazie 8, 347-357.

Schiessel, R., and Metzger, P. (2012). Intersphincteric resection for low rectal tumors. Springer Vienna, 159-163.

Schuhmacher, M.K., Kudithipudi, S., Kusevic, D., Weirich, S., and Jeltsch, A. (2015). Activity and specificity of the human SUV39H2 protein lysine methyltransferase. Biochimica et Biophysica Acta (BBA)-Gene Regulatory Mechanisms 1849, 55-63.

Schwaiger, M., Kohler, H., Oakeley, E.J., Stadler, M.B., and Schübeler, D. (2010). Heterochromatin protein 1 (HP1) modulates replication timing of the Drosophila genome. Genome Research 20, 771-780.

Sdek, P., Oyama, K., Angelis, E., Chan, S.S., Schenke-Layland, K., and MacLellan, W.R. (2013). Epigenetic regulation of myogenic gene expression by Heterochromatin protein 1 alpha. PLoS ONE 8, e58319.

Shoji, K., Hara, K., Kawamoto, M., Kiuchi, T., Kawaoka, S., Sugano, S., Shimada, T., Suzuki, Y., and Katsuma, S. (2014). Silkworm HP1a transcriptionally enhances highly expressed euchromatic genes via association with their transcription start sites. Nucleic Acids Research 42, 11462-11471.

Singh, P. (2010). HP1 proteins—What is the essential interaction? Russian Journal of Genetics 46, 1257-1262.

Skaar, J.R., Pagan, J.K., and Pagano, M. (2013). Mechanisms and function of substrate recruitment by F-box proteins. Nature Reviews Molecular Cell Biology 14, 369-381.

Skaar, J.R., Pagan, J.K., and Pagano, M. (2014). SCF ubiquitin ligase-targeted therapies. Nature Reviews Drug Discovery 13, 889-903.

Smith, D.G., Buffet, M., Fenwick, A.E., Haigh, D., Ife, R.J., Saunders, M., Slingsby, B.P., Stacey, R., and Ward, R.W. (2001). 3-Anilino-4-arylmaleimides: potent and selective inhibitors of glycogen synthase kinase-3 (GSK-3). Bioorganic & Medicinal Chemistry Letters 11, 635-639.

Smothers, J.F., and Henikoff, S. (2000). The HP1 chromo shadow domain binds a consensus peptide pentamer. Current Biology 10, 27-30.

Soshnev, Alexey A., Josefowicz, Steven Z., and Allis, C.D. (2016). Greater than the sum of parts: Complexity of the dynamic epigenome. Molecular Cell 62, 681-694.

Stintzing, S. (2014). Management of colorectal cancer. F1000 Prime Reports 6, 108.

Stoeber, K., Tlsty, T.D., Happerfield, L., Thomas, G.A., Romanov, S., Bobrow, L., Williams, E.D., and Williams, G.H. (2001). DNA replication licensing and human cell proliferation. Journal of Cell Science 114, 2027-2041.

Stypula-Cyrus, Y., Damania, D., Kunte, D.P., Cruz, M.D., Subramanian, H., Roy, H.K., and Backman, V. (2013). HDAC up-regulation in early colon field carcinogenesis is involved in cell tumorigenicity through regulation of chromatin structure. PLoS One 8, e64600.

Sundqvist, A., Bengoechea-Alonso, M.T., Ye, X., Lukiyanchuk, V., Jin, J., Harper, J.W., and Ericsson, J. (2005). Control of lipid metabolism by phosphorylation-dependent degradation of the SREBP family of transcription factors by SCF Fbw7. Cell Metabolism 1, 379-391.

Sutherland, C., Leighton, I.A., and Cohen, P. (1993). Inactivation of glycogen synthase kinase-3β by phosphorylation: new kinase connections in insulin and growth-factor signalling. Biochemical Journal 296, 15-19.

Tam, W.L., and Weinberg, R.A. (2013). The epigenetics of epithelial-mesenchymal plasticity in cancer. Nat Med 19, 1438-1449.

Tan, Y., Tajik, A., Chen, J., Jia, Q., Chowdhury, F., Wang, L., Chen, J., Zhang, S., Hong, Y., and Yi, H. (2014). Matrix softness regulates plasticity of tumour-repopulating cells via H3K9 demethylation and Sox2 expression. Nature communications 5, 4619.

Tell, R., Rivera, C.A., Eskra, J., Taglia, L.N., Blunier, A., Tian Wang, Q., and Benya, R.V. (2011). Gastrin-releasing peptide signaling alters colon cancer invasiveness via Heterochromatin protein 1Hsβ. The American Journal of Pathology 178, 672-678.

Terada, Y. (2006). Aurora-B/AIM-1 regulates the dynamic behavior of HP1α at the G2–M transition. Molecular Biology of The Cell 17, 3232-3241.

Thoma, F. (1992). Nucleosome positioning. Biochimica et Biophysica Acta (BBA) - Gene Structure and Expression 1130, 1-19.

Thoma, F., and Koller, T. (1977). Influence of histone H1 on chromatin structure. Cell 12, 101-107.

Thomsen, R., Christensen, D.B., Rosborg, S., Linnet, T.E., Blechingberg, J., and Nielsen, A.L. (2011). Analysis of HP1α regulation in human breast cancer cells. Molecular Carcinogenesis 50, 601-613.

Torre, L.A., Bray, F., Siegel, R.L., Ferlay, J., Lortet-Tieulent, J., and Jemal, A. (2015). Global cancer statistics, 2012. CA: a cancer journal for clinicians 65, 87-108.

Tretiakova, M.S., Bond, S.D., Wheeler, D., Contreras, A., Kocherginsky, M., Kroll, T.G., and Hale, T.K. (2014). Heterochromatin protein 1 expression is reduced in human thyroid malignancy. Laboratory Investigation 94, 788-795.

Tsunematsu, R., Nakayama, K., Oike, Y., Nishiyama, M., Ishida, N., Hatakeyama, S., Bessho, Y., Kageyama, R., Suda, T., and Nakayama, K.I. (2004). Mouse Fbw7/Sel-10/Cdc4 Is Required for Notch Degradation during Vascular Development. Journal of Biological Chemistry 279, 9417-9423.

Tu, Y., Chen, C., Pan, J., Xu, J., Zhou, Z.-G., and Wang, C.-Y. (2012). The Ubiquitin Proteasome Pathway (UPP) in the regulation of cell cycle control and DNA damage repair and its implication in tumorigenesis. Int J Clin Exp Pathol 5, 726-738.

Vad-Nielsen, J., and Nielsen, A.L. (2015). Beyond the histone tale: HP1α deregulation in breast cancer epigenetics. Cancer Biology and Therapy 16, 189-200.

Vaiopoulos, A.G., Athanasoula, K.C., and Papavassiliou, A.G. (2014). Epigenetic modifications in colorectal cancer: molecular insights and therapeutic challenges. Biochimica et Biophysica Acta (BBA)-Molecular Basis of Disease 1842, 971-980.

Vakoc, C.R., Mandat, S.A., Olenchock, B.A., and Blobel, G.A. (2005). Histone H3 lysine 9 methylation and HP1γ are associated with transcription elongation through mammalian chromatin. Molecular Cell 19, 381-391.

van Drogen, F., Sangfelt, O., Malyukova, A., Matskova, L., Yeh, E., Means, A.R., and Reed, S.I. (2006). Ubiquitylation of cyclin E requires the sequential function of SCF complexes containing distinct hCdc4 isoforms. Molecular Cell 23, 37-48.

van Engeland, M., Derks, S., Smits, K.M., Meijer, G.A., and Herman, J.G. (2011). Colorectal cancer epigenetics: complex simplicity. Journal of Clinical Oncology 29, 1382-1391.

Vaquero, A., Scher, M., Erdjument-Bromage, H., Tempst, P., Serrano, L., and Reinberg, D. (2007). SIRT1 regulates the histone methyl-transferase SUV39H1 during heterochromatin formation. Nature 450, 440-444.

Vaute, O., Nicolas, E., Vandel, L., and Trouche, D. (2002). Functional and physical interaction between the histone methyl transferase Suv39H1 and histone deacetylases. Nucleic Acids Research 30, 475-481.

Vermaak, D., Henikoff, S., and Malik, H.S. (2005). Positive selection drives the evolution of rhino, a member of the Heterochromatin protein 1 family in Drosophila. Plos Genetics 1, 96–108.

Vignjevic, D., Kojima, S.-i., Aratyn, Y., Danciu, O., Svitkina, T., and Borisy, G.G. (2006). Role of fascin in filopodial protrusion. The Journal of Cell Biology 174, 863-875.

Wang, D., Zhou, J., Liu, X., Lu, D., Shen, C., Du, Y., Wei, F.-Z., Song, B., Lu, X., and Yu, Y. (2013a). Methylation of SUV39H1 by SET7/9 results in heterochromatin relaxation and genome instability. Proceedings of the National Academy of Sciences 110, 5516-5521.

Wang, H.-L., Liu, M.-M., Ma, X., Fang, L., Zhang, Z.-F., Song, T.-F., Gao, J.-Y., Kuang, Y., Jiang, J., and Li, L. (2013b). Expression and effects of JMJD2A histone demethylase in endometrial carcinoma. Asian Pacific Journal of Cancer Prevention: APJCP 15, 3051-3056.

Wang, Q., Zhai, Y.-Y., Dai, J.-H., Li, K.-Y., Deng, Q., and Han, Z.-G. (2014). SAMD9L inactivation promotes cell proliferation via facilitating G1-

S transition in hepatitis B Virus-associated hepatocellular carcinoma. International journal of biological sciences 10, 807.

Wang, R., Wang, Y., Liu, N., Ren, C., Jiang, C., Zhang, K., Yu, S., Chen, Y., Tang, H., and Deng, Q. (2013c). FBW7 regulates endothelial functions by targeting KLF2 for ubiquitination and degradation. Cell Research 23, 803-819.

Wang, Y., Liu, Y., Lu, J., Zhang, P., Wang, Y., Xu, Y., Wang, Z., Mao, J.-H., and Wei, G. (2013d). Rapamycin inhibits FBXW7 loss-induced epithelial–mesenchymal transition and cancer stem cell-like characteristics in colorectal cancer cells. Biochemical and Biophysical Research Communications 434, 352-356.

Wang, Z., Inuzuka, H., Fukushima, H., Wan, L., Gao, D., Shaik, S., Sarkar, F.H., and Wei, W. (2012a). Emerging roles of the FBW7 tumour suppressor in stem cell differentiation. Embo Reports 13, 36-43.

Wang, Z., Inuzuka, H., Zhong, J., Wan, L., Fukushima, H., Sarkar, F.H., and Wei, W. (2012b). Tumor suppressor functions of FBW7 in cancer development and progression. FEBS Letters 586, 1409-1418.

Wang, Z., Zang, C., Rosenfeld, J.A., Schones, D.E., Barski, A., Cuddapah, S., Cui, K., Roh, T.-Y., Peng, W., and Zhang, M.Q. (2008). Combinatorial patterns of histone acetylations and methylations in the human genome. Nature Genetics 40, 897-903.

Weber, K., Bibring, T., and Osborn, M. (1975). Specific visualization of tubulin-containing structures in tissue culture cells by immunofluorescence: cytoplasmic microtubules, vinblastine-induced paracrystals, and mitotic figures. Experimental Cell Research 95, 111-120.

Weichert, W., Röske, A., Niesporek, S., Noske, A., Buckendahl, A.-C., Dietel, M., Gekeler, V., Boehm, M., Beckers, T., and Denkert, C. (2008). Class I histone deacetylase expression has independent prognostic impact in human colorectal cancer: specific role of class I histone deacetylases in vitro and in vivo. Clinical Cancer Research 14, 1669-1677.

Welcker, M., and Clurman, B.E. (2008). FBW7 ubiquitin ligase: a tumour suppressor at the crossroads of cell division, growth and differentiation. Nat Rev Cancer 8, 83-93.

Weyemi, U., Redon, C.E., Choudhuri, R., Aziz, T., Maeda, D., Boufraqech, M., Parekh, P.R., Sethi, T.K., Kasoji, M., and Abrams, N. (2016). The histone variant H2A. X is a regulator of the epithelial-mesenchymal transition. Nature Communications 7, 10711.

Whitfield, M.L., Sherlock, G., Saldanha, A.J., Murray, J.I., Ball, C.A., Alexander, K.E., Matese, J.C., Perou, C.M., Hurt, M.M., and Brown, P.O. (2002). Identification of genes periodically expressed in the human cell cycle

and their expression in tumors. Molecular Biology of The Cell 13, 1977-2000.

Whitfield, M.L., Zheng, L.-X., Baldwin, A., Ohta, T., Hurt, M.M., and Marzluff, W.F. (2000). Stem-loop binding protein, the protein that binds the 3′ end of histone mRNA, is cell cycle regulated by both translational and posttranslational mechanisms. Molecular and Cellular Biology 20, 4188-4198.

Wood, L.D., Parsons, D.W., Jones, S., Lin, J., Sjöblom, T., Leary, R.J., Shen, D., Boca, S.M., Barber, T., Ptak, J., et al. (2007). The genomic landscapes of human breast and colorectal cancers. Science 318, 1108-1113.

Wu, C.-Y., Tsai, Y.-P., Wu, M.-Z., Teng, S.-C., and Wu, K.-J. (2012). Epigenetic reprogramming and post-transcriptional regulation during the epithelial–mesenchymal transition. Trends in Genetics 28, 454-463.

Wu, Z.-H., and Pfeffer, L.M. (2016). MicroRNA regulation of F-box proteins and its role in cancer. Paper presented at: Seminars in Cancer Biology (Elsevier) 36.

Xiao, X., Shi, X., Fan, Y., Wu, C., Zhang, X., Minze, L., Liu, W., Ghobrial, R.M., Lan, P., and Li, X.C. (2016). The costimulatory receptor OX40 inhibits interleukin-17 expression through activation of repressive chromatin remodeling pathways. Immunity 44, 1271-1283.

Xu, W., Taranets, L., and Popov, N. (2016). Regulating Fbw7 on the road to cancer. Paper presented at: Seminars in Cancer Biology (Elsevier) 36:62-70.

Yada, M., Hatakeyama, S., Kamura, T., Nishiyama, M., Tsunematsu, R., Imaki, H., Ishida, N., Okumura, F., Nakayama, K., and Nakayama, K.I. (2004). Phosphorylation-dependent degradation of c-Myc is mediated by the F-box protein Fbw7. The EMBO Journal 23, 2116-2125.

Yamagishi, H., Kuroda, H., Imai, Y., and Hiraishi, H. (2016). Molecular pathogenesis of sporadic colorectal cancers. Chinese Journal of Cancer 35, 1.

Yamamoto, K., and Sonoda, M. (2003). Self-interaction of heterochromatin protein 1 is required for direct binding to histone methyltransferase, SUV39H1. Biochemical and Biophysical Research Communications 301, 287-292.

Yan, Q., Cho, E., Lockett, S., and Muegge, K. (2003). Association of Lsh, a regulator of DNA methylation, with pericentromeric heterochromatin is dependent on intact heterochromatin. Molecular and Cellular Biology 23, 8416-8428.

Yang, H., Lu, X., Liu, Z., Chen, L., Xu, Y., Wang, Y., Wei, G., and Chen, Y. (2015). FBXW7 suppresses epithelial-mesenchymal transition, stemness and metastatic potential of cholangiocarcinoma cells. Oncotarget 6, 6310.

Ye, X., Nalepa, G., Welcker, M., Kessler, B.M., Spooner, E., Qin, J., Elledge, S.J., Clurman, B.E., and Harper, J.W. (2004). Recognition of phosphodegron motifs in human cyclin E by the SCFFbw7 ubiquitin ligase. Journal of Biological Chemistry 279, 50110-50119.

Yin, Y.-W., Jin, H.-J., Zhao, W., Gao, B., Fang, J., Wei, J., Zhang, D.D., Zhang, J., and Fang, D. (2015). The histone acetyltransferase GCN5 expression is elevated and regulated by c-Myc and E2F1 transcription factors in human colon cancer. Gene Expression 16, 187-196.

Yokoyama, Y., Hieda, M., Nishioka, Y., Matsumoto, A., Higashi, S., Kimura, H., Yamamoto, H., Mori, M., Matsuura, S., and Matsuura, N. (2013). Cancer associated up-regulation of H3K9 trimethylation. Increased H3K9me3 levels in the invasive region of colorectal cancer tissue. Cancer Science 104.

Young, A., Hobbs, R., and Kerr, D. (2011). ABC of colorectal cancer. Wiley-Blackwell. pp. 63-68.

Yu, J., Zhang, W., Gao, F., Liu, Y.-X., Chen, Z.-Y., Cheng, L.-Y., Xie, S.-F., and Zheng, S.-S. (2014). FBW7 increases chemosensitivity in hepatocellular carcinoma cells through suppression of epithelial-mesenchymal transition. Hepatobiliary and Pancreatic Diseases International 13, 184-191.

Zeng, A., Li, Y.-Q., Wang, C., Han, X.-S., Li, G., Wang, J.-Y., Li, D.-S., Qin, Y.-W., Shi, Y., Brewer, G., et al. (2013). Heterochromatin protein 1 promotes self-renewal and triggers regenerative proliferation in adult stem cells. The Journal of Cell Biology 201, 409-425.

Zha, L., Cao, Q., Cui, X., Li, F., Liang, H., Xue, B., and Shi, H. (2016). Epigenetic regulation of E-cadherin expression by the histone demethylase UTX in colon cancer cells. Medical Oncology 33, 1-11.

Zhan, P., Wang, Y., Zhao, S., Liu, C., Wang, Y., Wen, M., Mao, J.-H., Wei, G., and Zhang, P. (2015). FBXW7 negatively regulates ENO1 expression and function in colorectal cancer. Laboratory Investigation 95, 995–1004.

Zhang, J., Xu, F., Hashimshony, T., Keshet, I., and Cedar, H. (2002). Establishment of transcriptional competence in early and late S phase. Nature 420, 198-202.

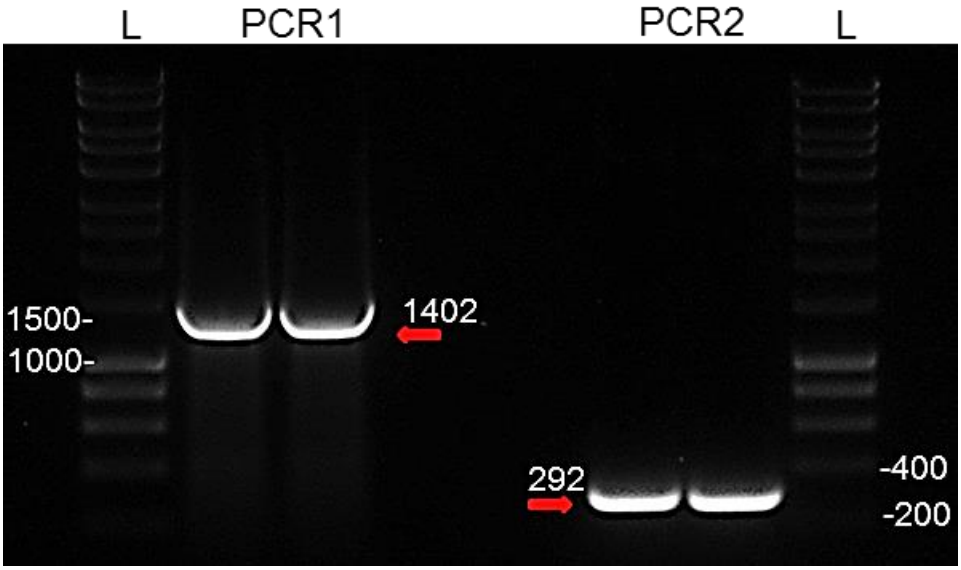
Zhang, Y., Cooke, M., Panjwani, S., Cao, K., Krauth, B., Ho, P.-Y., Medrzycki, M., Berhe, D.T., Pan, C., and McDevitt, T.C. (2012). Histone h1 depletion impairs embryonic stem cell differentiation. PLoS Genet 8, e1002691.

Zhao, T., Heyduk, T., Allis, C.D., and Eissenberg, J.C. (2000). Heterochromatin protein 1 binds to nucleosomes and DNA in vitro. Journal of Biological Chemistry 275, 28332-28338.

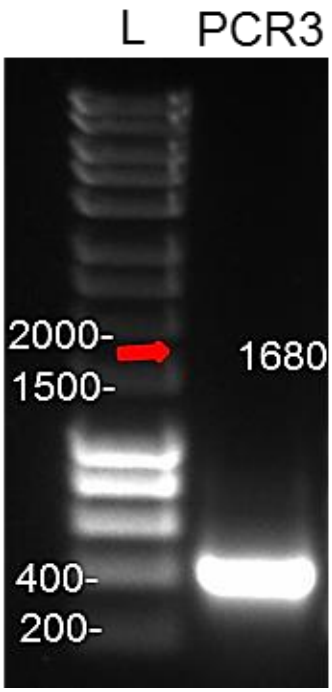
Zhou, X.Z., and Lu, K.P. (2016). The isomerase PIN1 controls numerous cancer-driving pathways and is a unique drug target. Nature Reviews Cancer 7, 463-78.

Appendices

Appendix 1: Site directed mutagenesis for creating point mutation [Threonine (ACC) and Serine (TCC) are substituted with Alanine (GCC)] in *HP1BP3*.

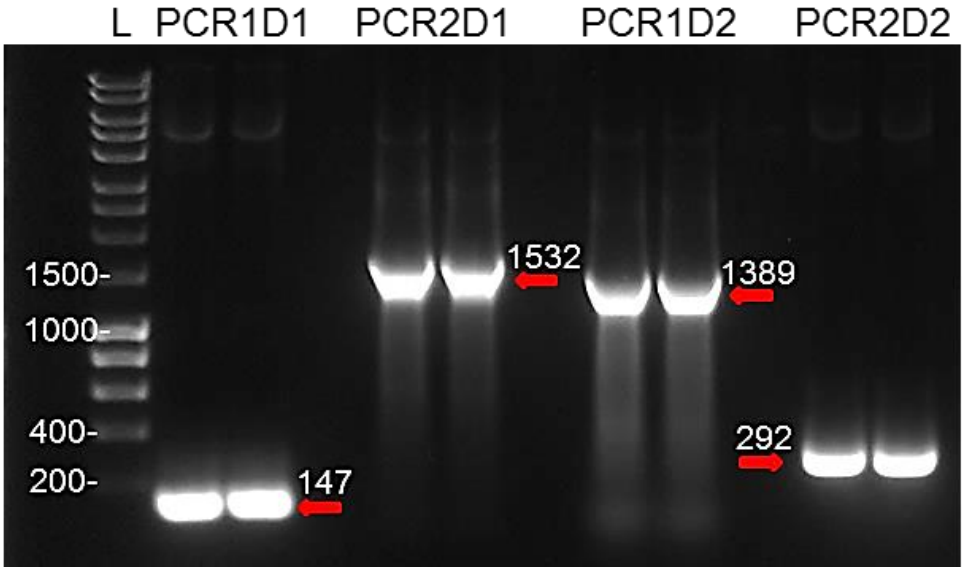


Validation of generated fragment A and B which resulted from PCR1 and PCR2 reactions by gel electrophoresis (Materials and Methods; Section 2.2.2.5, Figure 2-5). PCR1 and PCR2 products were run on 1 % agarose gel. In Step 1, Fragment A and B (N- and C-terminal domains) are amplified by PCR1 and PCR2, respectively, and used as a template for Step 2, i.e. PCR3, to create the mutated DNA fragment (Fragment C) with a distinct point mutation. Red arrows pointed toward the expected bands. L: Ladder, DNA HyperLadder™ 1kb (Bioline).

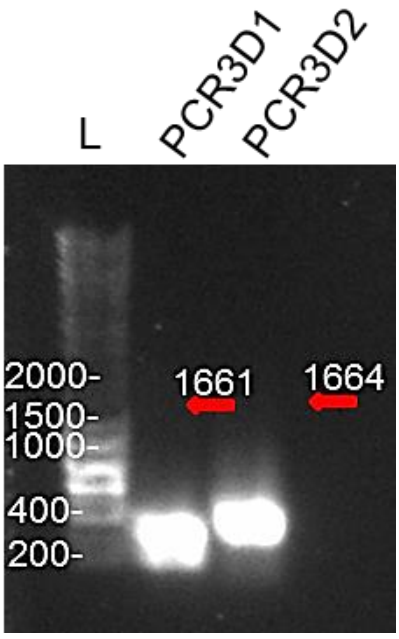


Validation of fragment C that uses the product of PCR1 and PCR2 as a templet to generate PCR3 product with the desired point mutation. PCR3 product was run on 1 % agarose gel. PCR3 reaction was failure as expected band did not appear beside the red arrow, as demonstrated (Materials and Methods; Section 2.2.2.5, Figure 2-5). L: Ladder, DNA HyperLadder™ 1kb (Bioline).

Appendix 2: Site directed mutagenesis for creating deletion mutations (D1 and D2) in *HP1BP3*.



Validation of generated fragment A and B which resulted from PCR1 and PCR2 reactions by gel electrophoresis, for two different deletion mutations (D1 and D2) (Materials and Methods; Section 2.2.2.5, Figure 2-4). PCR1D1, PCR2D1, PCR1D2, and PCR2D2 products were run on 1 % agarose gel. In Step 1, Fragment A and B (N- and C-terminal domains) are amplified by PCR1 and PCR2, respectively, and used as a template for Step 2, i.e. PCR3, to create the mutated DNA fragment (Fragment C) with a distinct deletion mutation. Red arrows pointed toward the expected bands. L: Ladder, DNA HyperLadder™ 1kb (Bioline).



Validation of fragment C that uses the product of PCR1 and PCR2 as a templet to generate PCR3 product with the desired deletion mutations (D1 and D2). PCR3D1 and PCR3D2 product was run on 1 % agarose gel. PCR3 reaction was failure to generate the deleted recombinant DNA, as expected bands did not appear beside the red arrows, as demonstrated (Materials and Methods; Section 2.2.2.5, Figure 2-4). L: Ladder, DNA HyperLadder™ 1kb (Bioline).